



**HAL**  
open science

# The SWOT satellite mission: Contribution of the large swath altimetry for improving the hydrological and hydrodynamic processes of a large scale model

Vanessa Pedinotti

## ► To cite this version:

Vanessa Pedinotti. The SWOT satellite mission: Contribution of the large swath altimetry for improving the hydrological and hydrodynamic processes of a large scale model. Earth Sciences. Institut National Polytechnique de Toulouse - INPT, 2013. English. NNT: 2013INPT0014 . tel-04233731

**HAL Id: tel-04233731**

**<https://theses.hal.science/tel-04233731>**

Submitted on 9 Oct 2023

**HAL** is a multi-disciplinary open access archive for the deposit and dissemination of scientific research documents, whether they are published or not. The documents may come from teaching and research institutions in France or abroad, or from public or private research centers.

L'archive ouverte pluridisciplinaire **HAL**, est destinée au dépôt et à la diffusion de documents scientifiques de niveau recherche, publiés ou non, émanant des établissements d'enseignement et de recherche français ou étrangers, des laboratoires publics ou privés.



# THÈSE

En vue de l'obtention du

## DOCTORAT DE L'UNIVERSITÉ DE TOULOUSE

Délivré par l'Université Toulouse III - Paul Sabatier

Discipline ou spécialité : Océan, Atmosphère et Surfaces Continentales

---

Présentée et soutenue par *Vanessa PEDINOTTI*  
Le 21/02/2013

Titre :

***Préparation à la mission SWOT (Surface Water Ocean Topography) : Apport de l'altimétrie à large fauchée à la modélisation grande échelle des processus hydrologiques et hydrodynamiques en Afrique de l'Ouest.***

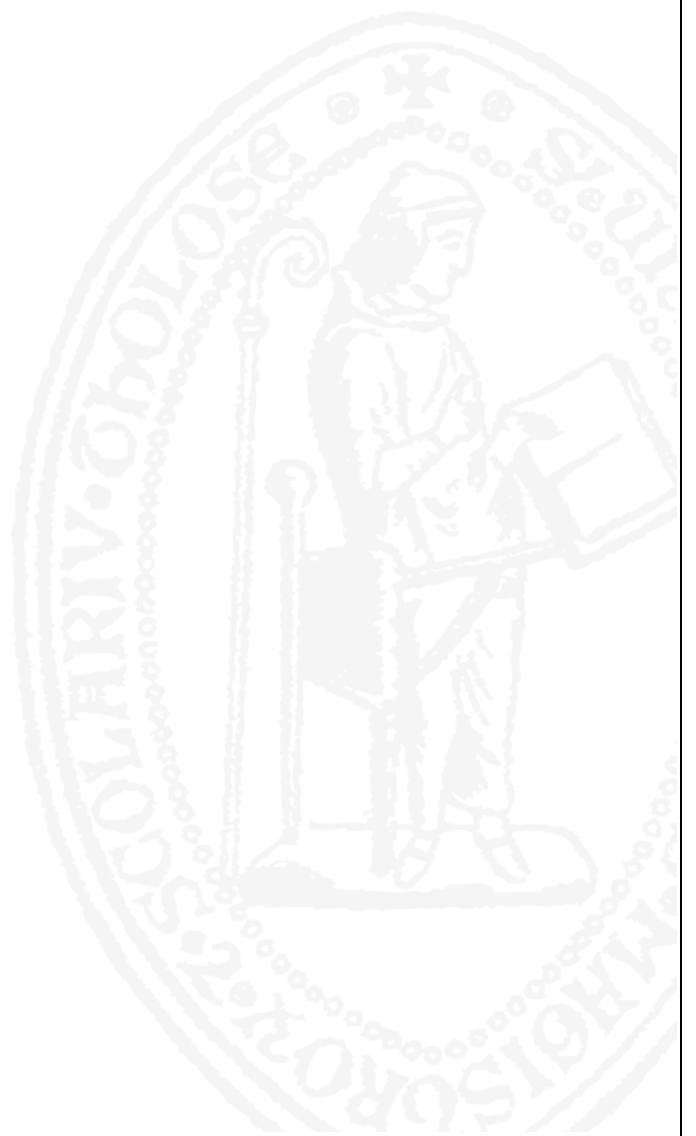
---

### JURY

**Benoît LAIGNEL**, Professeur, Université de Rouen, Président du jury.  
**Florence HABETS**, Directrice de recherche CNRS, Rapportrice.  
**Paul BATES**, Professeur, Université de Bristol, Rapporteur.  
**Sylvain BIANCAMARIA**, Chargé de recherche CNRS, Examineur.  
**Simon DADSON**, Professeur, Université d'Oxford, Examineur.  
**Sophie RICCI**, Chargée de recherche CERFACS, Examinatrice.  
**Aaron BOONE**, Chargé de recherche CNRS, Directeur de thèse.  
**Nelly MOGNARD**, Ingénieur CNES, Co-directrice de thèse.

---

**Ecole doctorale** : *Sciences de l'Univers, de l'Environnement et de l'Espace*  
**Unité de recherche** : *Centre National de Recherches Météorologiques*



## Aknowledgements

Cette partie liste de façon non exhaustive les personnes qui, de près ou de loin, ont rendu possible l'élaboration de cette thèse. Ma mémoire défaillante ne me permettra malheureusement pas de citer toutes les rencontres qui m'ont permis au fil du temps, de forger les idéaux, engouements et convictions qui m'ont menée jusqu'ici. Je pense cependant que chacun, bonne ou mauvaise rencontre, a eu son rôle à jouer dans cette (lente) progression.

Je remercie tout d'abord Aaron Boone, dit Aaron Man, l'homme multidisciplinaire qui allie comme personne la passion de son travail à l'humilité la plus déconcertante. Je te remercie pour ta patience, ton indulgence et ta bonne humeur quotidiennes. Merci surtout pour ta confiance et ta flexibilité, qui m'ont aidée à me sentir compétente et autonome dans les moments de doute. Tu as su partager ton savoir et ton expérience en prenant toujours en compte mon avis et mes envies, ce qui est je pense une qualité primordiale dans la direction d'une thèse. Enfin, un grand merci pour ton humour et ta dérision qui ont permis le partage de moments moins sérieux mais tout aussi importants.

Je remercie ma Co-Directrice de thèse, Nelly Mognard, de nous avoir accordé sa confiance et ses encouragements durant le déroulement de cette thèse. Merci de nous avoir communiqué votre enthousiasme quant au projet SWOT, qui ne cesse depuis de prendre de l'ampleur.

Ces travaux n'auraient pu aboutir sans la précieuse contribution de deux personnes que je tiens à remercier tout particulièrement. Dans un premier temps, merci à Bertrand Decharme pour les conseils et les connaissances partagées sur l'hydrologie et sur le modèle TRIP. Au départ intimidée, j'ai pu découvrir une personne réellement disponible et impliquée dont l'aide s'est avérée précieuse, en particulier durant la première partie de cette thèse. Merci ensuite à Sophie Ricci qui a accordé son temps, son énergie et surtout sa pédagogie afin de m'aiguiller dans les méandres des concepts de l'assimilation. Je te remercie chaudement d'avoir su me faire part de tes avis et conseils tout en me laissant une complète autonomie quant à mes choix. Je remercie aussi toutes les personnes avec lesquelles j'ai collaborées ou qui m'ont aidée, Sylvain, Christine, Fabrice, Jean-François C. et M., Bachir, Catherine, Patrick, Aurélien etc... Merci pour votre accessibilité et votre disponibilité.

Ces trois années n'auraient pas été les mêmes sans tous ceux qui ont contribué et/ou contribuent encore à maintenir le dynamisme et la convivialité propres à l'équipe MOANA. Je remercie les 'anciens', J-Philippe, Dominique, Florence, Mireille et Françoise pour leur accessibilité, qui m'a permis de prendre part à des débats animés durant les pauses café et les déjeuners. Un merci tout particulier à Florence pour son aide et sa disponibilité tout au long de ces trois années. J'ai une pensée pour mes tous premiers acolytes, mes aînés, Amanda, Cécile et

Romain. Nouvelle arrivée à Toulouse, j'ai pu trouver en vous des conseils avisés et des oreilles attentives. Merci pour les soirées et l'amitié partagées. Enfin, merci à mes acolytes de rire, Florent, Philippe, Olivier et Manu sans qui mes journées auraient été bien moins joyeuses. Un merci particulier à Philippe pour ta disponibilité, ton aide et ta patience même dans les 'très rares moments' où j'ai pu me montrer difficile.

Je remercie tous les auteurs de tous les livres qui quotidiennement, m'ont permis de m'évader intellectuellement et de relativiser.

Merci à ma colocataire préférée Anaïs, pour l'amitié sans faille qu'elle m'accorde depuis maintenant plus de six ans. Merci également à tous les amis qui ont partagé mes rires et mes pleurs durant ces trois années et avant. Merci à Pallavi pour sa présence et sa fraîcheur durant les derniers mois.

Je tiens à témoigner ma reconnaissance et mon admiration envers Maxime pour le soutien et la robustesse parfois surhumaine dont il a fait preuve face à mes humeurs les plus exécrables. Merci pour ton calme, ta sérénité et ton optimisme qui m'ont permis bien des fois de retrouver mon chemin dans le dédale de mes états d'âme. Merci d'être tous les jours ce roseau qui plie mais ne rompt pas.

Enfin, ma considération et ma gratitude les plus profondes s'adressent à ma mère qui a su m'inculquer sa détermination, sa force d'esprit et ses principes. Merci de m'avoir toujours laissé le choix, simplement. A ces remerciements, j'associe ma grand-mère ainsi que l'homme que je respecte le plus au monde, mon grand-père.

# Résumé

Le climat en Afrique de l'Ouest est fortement conditionné par sa mousson qui connaît depuis plusieurs décennies une forte variabilité inter et intra-annuelle, caractérisée par des conditions d'humidité ou de sécheresse intenses. Le bassin versant du fleuve Niger est directement influencé par ces fluctuations climatiques, qui impactent les ressources en eau et entraînent des événements extrêmes tels que des inondations. Le delta intérieur du Niger notamment est une large zone d'inondations, de laquelle une importante quantité d'eau est évaporée (environ 40 % de l'eau en entrée du delta). Cette évaporation impacte directement les basses couches de l'atmosphère et influence à son tour le climat, au moins à l'échelle régionale. Prenant sa source dans les hauteurs de Guinée, le fleuve Niger parcourt 4180km jusqu'au Nigeria où il se déverse dans l'océan à travers un très large delta. Il traverse 9 pays et est la principale ressource en eau des 100 millions de personnes qu'il approvisionne. En effet, dans ces régions rurales, l'économie repose majoritairement sur des activités telles que l'agriculture et l'élevage qui dépendent directement des conditions climatiques et de l'eau disponible. Afin de limiter les impacts des fluctuations climatiques, la surveillance et la gestion des ressources en eau sur ce bassin est donc nécessaire. Cependant, le contexte économique et politique de ces régions limite généralement le maintien d'un nombre suffisant de stations de mesures in-situ pour permettre une bonne connaissance des processus hydrologiques et hydrodynamiques du bassin du Niger.

La mission spatiale SWOT, née d'une collaboration entre la NASA/JPL (National Aeronautics and Space Administration/Jet Propulsory Laboratory), le CNES (Centre National d'Etudes Spatiales), et l'ASC-CSA (Agence Spatiale Canadienne), fournira des cartes globales de hauteur d'eau à une résolution encore jamais atteinte en altimétrie. Son lancement est prévu en 2019 et son principal avantage réside dans l'utilisation d'un interféromètre en bande Ka qui permet d'obtenir de larges fauchées au sol (environ 120km).

Dans le cadre de la préparation à la mission SWOT, cette thèse se propose d'offrir des perspectives d'utilisation des données SWOT pour l'hydrologie globale en se basant sur le cas d'étude complexe que représente le bassin du Niger. En effet, à des échelles spatiales importantes, la calibration des paramètres des modèles hydrologiques est rendue difficile par le manque d'observations. Dans un premier temps, le modèle d'hydrologie globale du Centre National de Recherches Météorologiques (CNRM), ISBA-TRIP, incluant un schéma d'inondations et un réservoir simple d'aquifères ajouté durant cette thèse est évalué à l'aide de multiples données issues soit de mesures in-situ, soit d'observations satellites. Cette première étude montre que le modèle, malgré sa relative simplicité, simule de façon cohérente la dynamique des eaux de surface et les zones inondées. Le

schéma d'inondations permet une forte amélioration du débit en aval du delta intérieur (-50 % de débit en période de mousson), et une augmentation non négligeable de l'évaporation (+30 % environ sur le delta en période de post-mousson). L'aquifère profond permet quant à lui une meilleure représentation des débits d'étiage. De plus, la comparaison avec les données GRACE montre que le modèle est capable de simuler correctement les anomalies de stock d'eau sur le bassin. Cette étude met aussi en évidence des paramètres sensibles du modèle sur lesquels reposent d'importantes incertitudes difficiles à estimer à cause du manque d'observations. Le coefficient de Manning, notamment, est un paramètre important contrôlant la dynamique des fleuves, mais difficile à estimer, en particulier sur une zone aussi large, où il peut varier considérablement en fonction de différents facteurs (sol, végétation ...).

La deuxième partie de la thèse consiste donc à mettre en place une méthode d'assimilation des hauteurs d'eau SWOT afin d'optimiser le coefficient de Manning. L'assimilation des données SWOT est appliquée dans le cadre d'une expérience jumelle, qui consiste à considérer une simulation de référence, appelée 'vérité', de laquelle sont issues les observations virtuelles de hauteur d'eau SWOT. Un run perturbé est ensuite généré en supposant que les incertitudes du modèle sont liées uniquement à une mauvaise estimation du paramètre à corriger. L'étude montre que l'assimilation permet l'optimisation d'un paramètre distribué spatialement, puisque l'on obtient une convergence globale du coefficient de Manning. De plus, l'assimilation permet une nette correction des biais de hauteur d'eau sur la rivière (30 % en moyenne sur la rivière), et dans une moindre mesure, des débits (7 %). L'assimilation permet aussi une meilleure représentation des inondations (occurrence, intensité) sur le Delta intérieur du Niger. Enfin, il est montré que le coefficient de Manning optimal issu de l'assimilation, peut être utilisé pour des prévisions hydrologiques sur une période plus longues que celle de la phase de calibration.

# Contents

<b>Introduction</b> . . . . .	<b>1</b>
<b>1 Land surface processes and continental hydrology : role in climate</b>	<b>17</b>
1.1 The water cycle . . . . .	18
1.2 Land surface hydrology . . . . .	19
1.3 Energy balance of continental surfaces . . . . .	22
1.4 Land-Climate interactions. . . . .	25
1.5 Modeling of hydrologic processes at regional and global scales . .	27
1.5.1 Land surface models . . . . .	27
1.5.2 River routing models . . . . .	34
1.6 Evaluation of CHSs : from local to global scale . . . . .	36
1.6.1 Local evaluation . . . . .	36
1.6.2 Regional and global evaluation : Classic methods. . . . .	37
1.6.3 The future SWOT satellite mission . . . . .	38
1.7 Modeling of the Niger river basin : A scientific, social and economic challenge. . . . .	43
1.7.1 Geo-demographical environment of the Niger river Basin .	43
1.7.2 Climatic conditions, rainfall variability and water resources availability . . . . .	45
1.7.3 The inland delta, a complex region for hydrologic modeling. . . . .	49
1.7.4 The African Monsoon Multidisciplinary Analysis (AMMA) program . . . . .	50
<b>2 The ISBA-TRIP Continental Hydrologic System</b>	<b>55</b>
2.1 The ISBA force restore land surface model . . . . .	55
2.1.1 Pronostic variables and atmospheric forcing . . . . .	56
2.1.2 ISBA input parameters . . . . .	59
2.1.3 Energy budget . . . . .	62
2.1.4 Water budget . . . . .	62
2.1.5 Evapotranspiration . . . . .	63
2.1.6 Hydrology . . . . .	63
2.2 The TRIP routing model . . . . .	66
2.2.1 Governing equations . . . . .	66
2.2.2 River discharge and groundwater outflow . . . . .	67
2.2.3 The flooding scheme . . . . .	69

<b>3</b>	<b>Evaluation of the ISBA-TRIP CHS over the Niger basin using in-situ and satellite derived data</b>	<b>73</b>
3.1	Domain . . . . .	74
3.2	Methodology . . . . .	76
3.3	TRIP specific parameters for the Niger river basin . . . . .	77
3.4	Atmospheric forcing dataset input for ISBA-TRIP . . . . .	78
3.5	Evaluation datasets . . . . .	81
3.5.1	Observed discharge . . . . .	83
3.5.2	Satellite-based flooded area . . . . .	83
3.5.3	Satellite-based Water Height . . . . .	85
3.5.4	Satellite-based total terrestrial water storage . . . . .	85
3.6	Results . . . . .	85
3.6.1	Improvement of LSMs simulated discharges due to river flooding . . . . .	85
3.6.2	The impact of rainfall forcing on simulated discharge . . . . .	89
3.6.3	Separate impact of floods and aquifers on the Niger basin . . . . .	90
3.6.4	Total terrestrial water storage . . . . .	107
3.6.5	Rainfall comparison . . . . .	110
3.6.6	Aquifer storage . . . . .	112
3.7	Sensitivity tests . . . . .	115
3.8	Chapter conclusions and perspectives . . . . .	120
<b>4</b>	<b>Contribution of the SWOT mission towards the improvement of the simulated water cycle</b>	<b>125</b>
4.1	Data Assimilation (DA) concepts . . . . .	126
4.1.1	Data assimilation variables . . . . .	127
4.1.2	The best linear unbiased estimator . . . . .	129
4.1.3	The extended Kalman Filter (EKF) . . . . .	130
4.1.4	Ensemble Kalman filter . . . . .	131
4.1.5	Variational data assimilation . . . . .	132
4.1.6	Data assimilation applications in global hydrology . . . . .	133
4.2	Assimilation of SWOT observations for the optimisation of TRIP parameters . . . . .	134
4.2.1	Choosing the SWOT data assimilation strategy . . . . .	134
4.2.2	Observing System Simulation Experiment . . . . .	135
4.2.3	SWOT Virtual mission . . . . .	136
4.2.4	Computation of variables used during the assimilation analysis . . . . .	137
4.2.5	Results . . . . .	156
4.3	Use of the optimal analysis for hydrologic forecasting . . . . .	178
4.4	Discussion . . . . .	181

---

4.5 Chapter conclusions and perspectives . . . . .	186
Conclusion et perspectives . . . . .	189
A A : Article published in HESS about ISBA-TRIP evaluation.	197
Bibliography	227



# Introduction

Les changements drastiques survenus ces dernières décennies, tant d'un point de vue politique, social, économique, ou environnemental, nous ont peu à peu conduit à réévaluer nos acquis. En effet, l'homme a cessé de considérer les ressources comme inépuisables, qu'elles soient naturelles, humaines ou financières. Les préoccupations liées au management des ressources, à l'environnement et au changement climatique ont pris une dimension internationale, et une part notable de l'action politique au sein des grandes puissances économiques. Pourtant, il est important de rappeler que les populations les plus sensibles aux fluctuations climatiques sont aussi généralement les plus dépourvues de moyens économiques et matériels, limitant ainsi leur capacité d'action et d'anticipation. Le système climatique est un mécanisme complexe qui, conditionné par le rayonnement solaire, fait interagir différentes composantes, parmi lesquelles l'atmosphère et les océans, et en moindre proportion la biosphère et les eaux continentales. Le cycle de l'eau décrit l'évolution temporelle et dynamique de l'eau liquide, solide ou de vapeur d'eau dans ces différents réservoirs. Bien que les eaux continentales ne représentent que 2.5% de l'eau totale présente sur terre, leur forte variabilité spatio-temporelle en fait un élément important du système climatique. De plus, étant donné leur volume relativement limité, la sensibilité des réservoirs continentaux aux aléas climatiques entraîne la réalisation rapide de conditions extrêmes telles que des inondations ou des sécheresses. En retour, les eaux continentales, via les différents échanges d'eau et d'énergie, influencent l'atmosphère, les océans mais aussi le climat, au moins à l'échelle régionale (Gedney et al. 2000, Douville et al. 2000a). Les dernières décennies ont vu une augmentation inquiétante des catastrophes naturelles dans le monde (Fig. I-1), dont plus de 60% sont liées à des causes hydrométéorologiques (inondations, sécheresses et tempêtes, International Disaster Database, [www.emdat.be](http://www.emdat.be)).

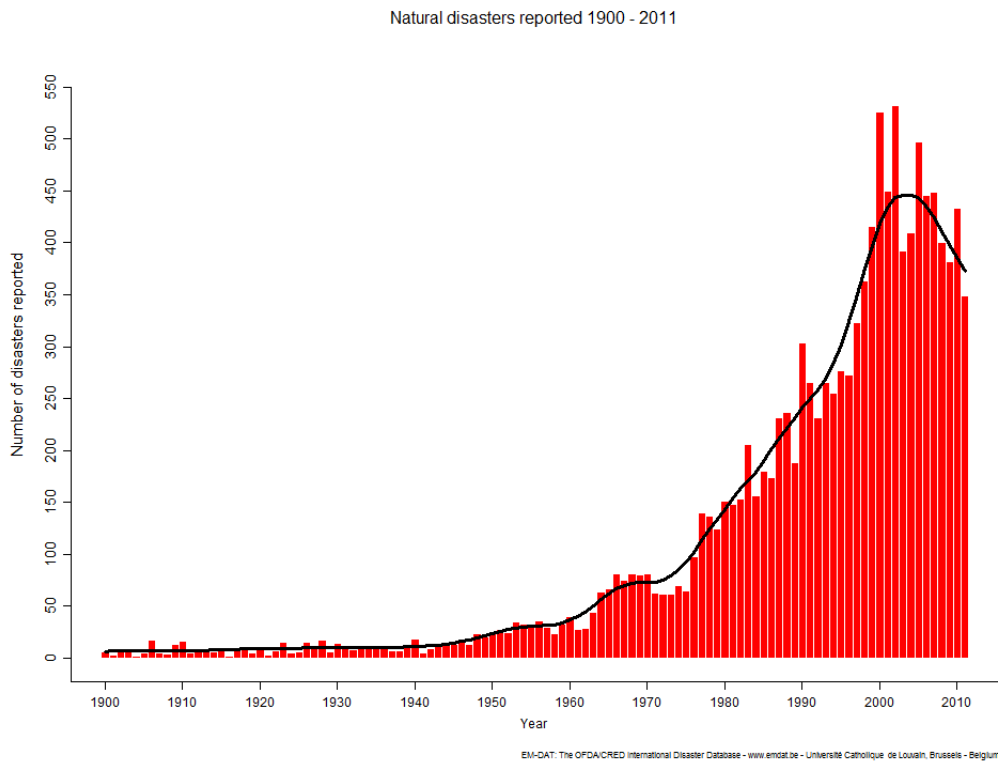


Figure I-1 : Nombre de désastres naturel recensés dans le monde entre 1900 et 2012. Source : EM-DAT, International Disaster Database, [www.emdat.be](http://www.emdat.be).

Comme le montre la Fig. I-2, toutes les régions du monde ne sont pas égales face à la fréquence de ces événements, dont le bilan économique et humain varie aussi fortement selon la zone touchée. Le suivi et la gestion des ressources d'eaux continentales est donc important afin de prévenir ces catastrophes climatiques.

Depuis les années 80, de nombreux schémas numériques de surface (LSMs) ont été développés afin de prendre en compte les interactions entre la surface, la biosphère et l'atmosphère dans les modèles atmosphériques à grande échelle (AGCMs et RCMs)<sup>1</sup>. Le but de ces modèles, appliqués à des résolutions généralement grossières (de 2° à 5°), est de représenter de façon synthétique les processus majeurs intervenant à l'interface sol-atmosphère, tout en utilisant un nombre de paramètres limité. Au départ relativement simples, ces modèles ont été améliorés afin de prendre en compte les processus liés à la végétation, à la neige et à l'hydrologie. L'essor grandissant des préoccupations concernant les ressources en eau a favorisé le développement des modèles de routage (RRMs) afin de représenter la dynamique des eaux continentales ainsi que l'évolution des principaux

<sup>1</sup>AGCM : Atmospheric Global Circulation Models, RCMs: Regional Circulation Models

réservoirs d'eau douce (Dümenil et Todini 1992, Habets et al. 1999b et c, Oki et al. 1999, Etchevers et al. 2001, Ducharne et al. 2003, Decharme et al., 2012).

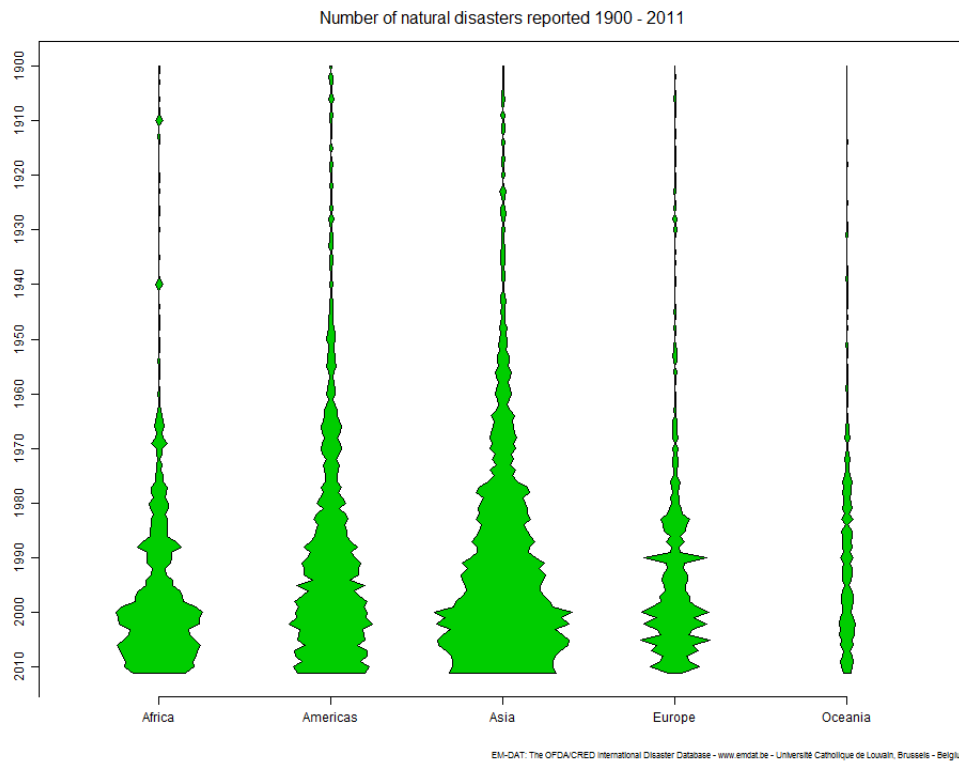


Figure I-2 : Nombre de désastres naturels recensés dans le monde entre 1900 et 2012 dans les différentes régions du monde. Source : EM-DAT, International Disaster Database, [www.emdat.be](http://www.emdat.be).

Cependant, la qualité des modélisations hydrologiques globales est soumise à différentes sources d'incertitudes. La première source d'incertitudes est due aux erreurs commises sur les prévisions météorologiques, notamment les précipitations, qui impactent directement l'hydrologie de surface. En effet, des événements pluvieux très localisés peuvent influencer l'hydrologie d'un bassin versant et, en cas de mauvaise localisation ou de mauvaise estimation de l'intensité de ces pluies, certains événements, telles que des crues rapides, ne pourront pas être prévus par les modèles. Des études sont actuellement menées afin d'améliorer la prévision des crues rapides (Vincendon et al., 2011), mais restent encore préliminaires. Aussi, généralement, pour ne pas prendre en compte ces incertitudes lors de la validation des simulations hydrologiques, les modèles sont évalués en mode 'offline', c'est-à-dire découplés d'un modèle atmosphérique, et auquel on prescrit un forçage atmosphérique issu de réanalyses, de données radar ou satellites, ou de données interpolées. Une seconde source importante d'erreur pour

l'hydrologie globale est due à la difficulté d'estimer correctement les paramètres hydrologiques des modèles. En effet, les propriétés hydrologiques des grands bassins, telles que les paramètres liés au sol, à la topographie, aux dimensions des rivières ou à la recharge des aquifères sont généralement peu connues, notamment dans les régions manquant de structures adéquates à la prise de mesures. Dans les modèles hydrologiques, ces paramètres sont souvent dérivés de relations géomorphologiques qui ne permettent pas un réalisme absolu. La dernière source importante d'erreur concerne le manque d'observations globales décrivant la dynamique spatiale et temporelle des eaux de surface, ainsi que l'évolution des stocks d'eau dans les différents réservoirs continentaux (Alsdorf et al., 2007). En effet, dans certaines régions, le contexte politico-économique limite la construction et/ou le maintien des stations de mesures in-situ ne permettant donc pas la validation ou la calibration des modèles d'hydrologie globale. C'est entre autres le cas du principal bassin de l'Afrique de l'Ouest, le Niger. Prenant sa source dans les Hautes terres de Guinée, il parcourt environ 4180km jusqu'au Nigeria où il rejoint l'océan Atlantique via un large delta (Fig. I-3). Traversant 9 pays, le fleuve Niger est une source d'eau importante pour les 100 millions de personnes qu'il approvisionne. Effectivement, dans ces populations principalement rurales, l'économie repose majoritairement sur des activités telles que l'élevage et l'agriculture qui sont directement dépendantes des ressources en eau. De plus, le climat en Afrique de l'Ouest est fortement conditionné par la mousson Africaine (OAM) dont les processus et les fluctuations sont encore la source de nombreuses incertitudes. La mousson africaine influence directement l'hydrologie du fleuve Niger et le stock d'eau des réservoirs profonds, notamment par le passage de lignes de grains qui apportent la majorité des pluies pendant la période de mousson (Lebel et al., 2002).

Au cours des dernières décennies notamment, elle a connu une forte variabilité, avec des années anormalement sèches succédant à des années anormalement humides (Nicholson, 2001; Lebel et al., 2009), mais aussi avec la succession de phases sèches et humides au sein d'une même saison. Le manque de connaissances concernant la mousson africaine a d'ailleurs été la principale motivation du projet AMMA (African Monsoon Multidisciplinary analysis, Redelsperger et al., 2006), auquel un large panel de scientifiques, de toutes nationalités confondues, a participé. Cette campagne de mesures visait entre autres à offrir les clés vers une meilleure compréhension des différents mécanismes entrant en jeu avant, pendant et après la mousson.

Le fleuve Niger est donc une source d'eau importante mais difficile à appréhender, principalement en raison des conditions météorologiques hétérogènes et donc complexes qu'il peut rencontrer. Traversant des régions très sèches au Sahel, il passe aussi par une zone d'inondations très large connue sous le nom de Delta intérieur du Niger. Ce delta, situé au Mali entre les latitudes [13°N – 16°N]

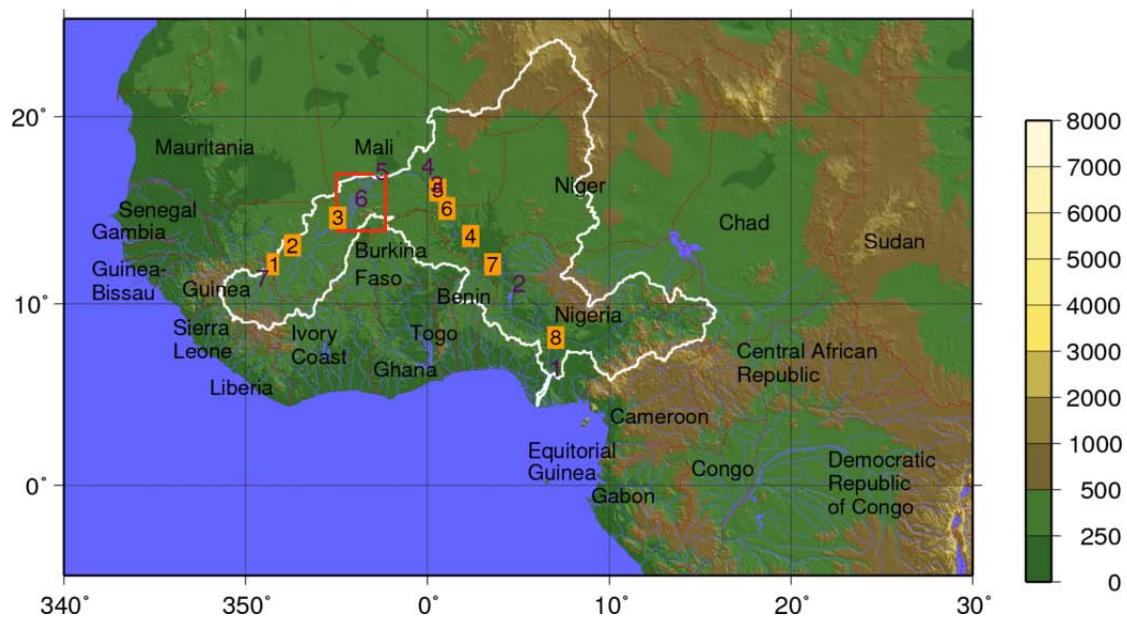


Figure 1: Figure I-3 : Carte du bassin du Niger (contour blanc). Le bassin prend sa source dans les hautes terres de Guinée et se déverse dans l'océan au Nigéria à travers un large delta. Le delta intérieur du Niger (carré rouge) est une zone importante d'inondations située au Mali. Les carrés jaunes représentent les stations de débits utilisées dans la thèse pour évaluer le modèle de surface. Les chiffres violets représentent les points où des données de hauteurs d'eau issues d'ENVISAT ont été utilisées.

et les longitudes [3°O-6°O], est annuellement inondé sur environ 25000km<sup>2</sup>. Ces zones inondées sont d'importantes sources d'évaporation (environ 44% de l'eau en entrée du Delta est évaporée, Andersen et al., 2005), susceptibles d'influencer l'atmosphère et le climat à l'échelle régionale (Shindell et al., 2004). De plus, elles contribuent à une forte diminution du débit en aval du delta (jusqu'à 60% de diminution entre le débit en amont et en aval du delta, Andersen et al., 2005). Or, les modèles de surface ne prennent généralement pas en compte ces zones inondées, ce qui conduit à des simulations biaisées en terme de débit et de flux d'évaporation dans ces régions.

La première partie de cette thèse consiste à évaluer le modèle couplé d'hydrologie globale ISBA-TRIP sur le bassin du Niger. Ce modèle, développé au Centre National de Recherches Météorologiques (CNRM) est utilisé actuellement dans les simulations climatiques, couplé au modèle ARPEGE (sigle). Le modèle de surface ISBA (Interactions Soil-Biosphere-Atmosphere; Noilhan and Planton, 1989) a pour rôle de simuler les bilans hydriques et énergétiques à l'interface entre la surface et l'atmosphère, tandis que le modèle de routage TRIP (Total Runoff Integrating Pathways; Oki, 1998) permet de convertir le ruissellement total produit par ISBA en débits. Dernièrement, un schéma d'inondations a été ajouté, afin d'évaluer l'impact des zones inondées sur les simulations hydrologiques (Decharme et al., 2011). Ce schéma considère une hauteur d'eau seuil au-delà de laquelle l'eau des rivières se répand dans des plaines d'inondations. Il prend en compte l'interception des précipitations par les plaines inondées, mais aussi l'évaporation et la réinfiltration de l'eau contenue dans ces zones. La première évaluation de ce schéma sur divers larges bassins du monde (Decharme et al., 2010), a permis de mettre en évidence l'impact des inondations sur le cycle hydrologique des rivières, qui se traduit généralement par une nette amélioration du débit simulé via une diminution non négligeable du débit en aval des plaines inondées. Cependant, malgré cette forte amélioration, l'existence d'un biais persistant sur le bassin du Niger avait été observé. Le travail de cette thèse a été d'évaluer le modèle sur le bassin du Niger et d'en déduire ses compétences et ses limitations. Les paramètres en entrée du modèle ont été corrigés régionalement afin d'améliorer les simulations. Le biais positif de débit simulé étant toujours observé à l'issue de cette première étude, différentes hypothèses ont été étudiées afin de l'expliquer. Parmi celles-ci, la présence dans cette zone d'un réservoir profond, approvisionné par l'eau issue du drainage, mais ne recommuniquant pas avec la rivière (on suppose que ce réservoir draine directement vers l'océan) nous a semblé pouvoir être une source importante d'erreur. En conséquence, un réservoir d'aquifère relativement simple a été ajouté au modèle durant cette étude. Ce réservoir profond est caractérisé par une constante qui spécifie le temps nécessaire à ce réservoir pour se vider presque totalement. Le 3ème chapitre de cette thèse propose donc de quantifier la contribution individuelle du schéma d'inondations et d'aquifère à la

modélisation des processus hydrologiques et hydrodynamiques du fleuve Niger. Tout d'abord, le modèle TRIP est utilisé en mode 'offline', c'est-à-dire découplé d'un LSM, afin de calculer les débits simulés par les 11 modèles impliqués dans le projet d'intercomparaison ALMIP (AMMA Land surface Model Intercomparison Project; Boone et al., 2009a). Cette première étude permet de montrer qu'aucun de ces modèles de surface n'est capable d'estimer correctement le débit en aval du delta intérieur du Niger. Le modèle ISBA-TRIP est alors utilisé en activant les zones inondées ainsi que les aquifères. Afin d'évaluer les simulations, de nombreux jeux de données ont été utilisés, provenant soit d'observations in-situ (débit), soit d'observations satellites (hauteurs d'eau, fractions inondées, stock d'eau total etc...). Dans une zone telle que celle-ci, où les observations sont peu nombreuses, ces différentes sources de données offrent des informations complémentaires sur l'état hydrologique du bassin. Dans d'autres études sur des bassins plus documentés, les observations de débits suffisent à valider les modèles hydrologiques. Par ailleurs, les inondations étant un phénomène important, puisqu'influençant la majeure partie du bassin ainsi que le climat régional, il est important d'évaluer la compétence du modèle à bien les localiser à l'aide des données de fractions inondées. Enfin, plusieurs jeux de pluies sont utilisés en forçage afin de prendre en compte les incertitudes liées aux précipitations (intensité, localisation ...). Cette étude montre que, malgré sa relative simplicité, le modèle ISBA-TRIP est capable de simuler correctement la dynamique des eaux de surface du Niger, ainsi que l'évolution du stock d'eau total dans le bassin versant. Tandis que le schéma d'inondations permet une meilleure simulation des débits en période humide, l'aquifère, quant à lui, permet une meilleure représentation des débits d'étiage.

Cependant, le manque d'observations ayant un bon recouvrement spatial et temporel empêche de valider totalement les simulations hydrologiques sur ce bassin. Par exemple, dans cette étude, seules huit observations de débit in-situ sont disponibles pour valider le débit simulé par ISBA-TRIP. En comparaison, lors d'un projet d'intercomparaison de modèles de surface sur le fleuve du Rhône (Boone et al., 2004), 145 mesures de débit ont été utilisées afin d'évaluer les modèles pour un bassin qui est plus de 25 fois plus petit que le bassin du Niger. Pour palier ce manque d'observations, de nombreux projets de télédétection ont vu le jour, offrant de nouvelles informations pour les modèles hydrologiques de grande échelle. Cependant, les limitations actuelles de résolution spatiale et du maillage de l'altimétrie nadir ne permettent pas la surveillance de la plupart des eaux des surfaces continentales (eg. TOPEX, JASON). Il est donc nécessaire de développer de nouveaux outils capables de surmonter ces limitations. C'est dans ce but que la NASA (National Aeronautics and Space Administration), en collaboration avec le CNES (Centre National d'Etudes Spatiales) et l'Agence Spatiale Canadienne (CSA-SC), a envisagé la mission satellite SWOT (Surface

Water Ocean Topography) dont le lancement est prévu en 2019. Le principal avantage de cette mission vient de l'utilisation d'un radar interférométrique appelé KaRIN (Ka-Band INterferometer pour radar interféromètre en bande Ka), donnant une trace au sol de 120km de large. Ainsi, avec sa large trace, le satellite SWOT couvrira tous les lacs, les rivières, réservoirs et océans de la terre au moins deux fois environ tous les 21 jours (jusqu'à 7 fois dans les hautes latitudes). L'altimétrie interférométrique permettra donc de fournir les hauteurs d'eau (et leurs dérivées spatio-temporelles) des fleuves, lacs, zones inondées et des océans avec une résolution horizontale de l'ordre de 50 à 100 mètres. D'un point de vue hydrologique, ces observations sont essentielles pour parfaire notre connaissance de la dynamique globale des eaux continentales, et leurs interactions avec les océans au niveau des estuaires. De plus, elles permettront aussi de surveiller l'évolution des stocks d'eau douce dans le contexte du changement climatique, notamment dans une région telle que le bassin du Niger, qui souffre du manque de données mesurées. En préparation de cette mission, diverses communautés scientifiques s'allient afin d'évaluer la contribution de SWOT à différents cas d'études, ainsi que de déterminer les différentes caractéristiques du satellite. Par exemple, à l'heure actuelle, si l'orbite du satellite est fixée à 22 jours, son sous-cycle est encore sujet à discussion dans la communauté scientifique. En effet, en fonction de la zone étudiée chaque sous-cycle présente des avantages et des inconvénients concernant sa répétitivité et son recouvrement. En hydrologie, il est nécessaire de savoir comment les données SWOT pourront être utilisées afin d'améliorer les prévisions des modèles hydrologiques, et de mieux prévoir les stocks d'eau continentale. Diverses études sont donc menées sur des bassins très différents de par leur taille et leur situation géographique afin de proposer des approches qui permettront de tirer le meilleur profit des données SWOT. L'assimilation de données semble offrir des perspectives prometteuses d'amélioration des prévisions hydrologiques (Andreadis et al., 2007; Biancamaria et al., 2011). Utilisée couramment en météorologie, elle permet de coller au plus près aux observations diverses tout en tenant compte des erreurs liées aux mesures des observations. Cependant, ces méthodes ne sont que peu utilisées dans le cadre de l'hydrologie à l'heure actuelle, et les études sont encore rares pour le moment, particulièrement à des échelles spatiales globales comme c'est le cas du modèle ISBA-TRIP. La deuxième partie cette thèse consiste donc à proposer une méthode d'assimilation des données SWOT qui permette d'améliorer les paramètres des modèles d'hydrologie globale. Durant cette thèse, qui consiste en une étude de pré-lancement de la mission, une méthode d'assimilation a donc été mise en place afin de réduire les incertitudes qui persistent sur certains paramètres d'entrée sensibles du modèle ISBA-TRIP. Cette méthode consiste à réaliser une expérience dite jumelle, très pratique lorsque l'on veut assimiler des observations qui n'existent pas encore comme c'est le

cas pour les données du satellite SWOT. Le principe est donc de générer des données virtuelles de hauteur d'eau SWOT à la résolution du modèle, à l'aide d'une simulation de référence (cette simulation est appelée 'vérité'). Puis, en prenant en compte des incertitudes sur les paramètres du modèle, une simulation perturbée est créée. L'assimilation consiste alors à utiliser les observations SWOT afin de corriger les paramètres incertains en entrée du modèle et d'obtenir ainsi une meilleure représentation de certaines variables dynamiques telles que les hauteurs d'eau et le débit du fleuve. Après une étude de sensibilité, il a été décidé d'utiliser l'assimilation pour corriger un paramètre hydrologique important, le coefficient de Manning. Le coefficient de Manning décrit la propriété du sol à 'freiner' l'écoulement, c'est donc un coefficient de frottement. Spatialement distribué, il est difficile à estimer et varie en fonction du type de sol, agissant directement sur la vitesse de l'écoulement, c'est-à-dire sur le débit. Il agit également sur la formation des zones inondées. L'algorithme fournissant l'analyse à l'issue d'un cycle d'assimilation est le BLUE (Best Linear Unbiased Estimator). Cette étude montre que l'assimilation de données permet une bien meilleure estimation des hauteurs d'eau, et, en moindre proportions, des débits sur la rivière. De plus, elle permet aussi une meilleure représentation de l'évolution des différents stocks d'eau continentale sur le bassin, ainsi qu'une meilleure simulation des inondations (occurrence, intensité) dans le Delta intérieur du Niger. Le biais du coefficient de Manning, en particulier, est nettement amélioré sur la rivière à l'issue de l'assimilation et semble converger vers une valeur optimale. Etant donnée la possible équifinalité du problème posé, ce résultat est satisfaisant. Enfin, le caractère prédictif de cette méthode est mis en évidence en utilisant le coefficient de Manning optimal obtenu lors de l'assimilation pour simuler l'hydrologie du bassin sur une période plus longue que celle de l'assimilation. Cette méthode offre donc des perspectives d'amélioration des processus hydrologiques représentés dans des simulations régionales ou globales, en couplage avec des modèles atmosphériques. De plus, elle offre la possibilité de meilleures prédictions des ressources en eau à échelle régionale, en temps réel ou sur des échelles de temps plus longues.

La mission SWOT va donc être un outil majeur vers une meilleure compréhension du cycle hydrologique global, paliant ainsi au manque d'observations qui limitait jusqu'ici les modèles numériques. Aussi, dans un climat où les tensions liées aux besoins en eau se font de plus en plus ressentir, une meilleure connaissance des ressources en eau et de leur évolution dans les réservoirs continentaux favoriserait la mise en place de plans de gestion efficaces, et limiterait l'impact sur les populations des aléas climatiques.

The significant social, economic and environmental changes that have occurred in the past several decades have changed our outlook on available resources. Indeed, it is now generally accepted that natural, human and financial resources are not infinite. Recently, the concerns about natural resource management under climate change have garnered international attention, even playing a role in political decision making. However, different regions of the world are not equal when faced with climate change: generally, the most exposed areas are also generally the least equipped to deal with it, limiting their abilities to anticipate (and possibly adapt) and make decisions (potential mitigation strategies). The climate is a complex system, involving the complex interactions between several components, such as the atmosphere, the oceans, and to a lesser degree, the biosphere and continental waters. The water cycle describes the temporal and dynamical evolution of water (in its liquid, solid or vapour form) within the different reservoirs of the climate system. Although continental water represents only 2.5% of total terrestrial water, its role in the climate system is far from negligible due to its high temporal and spatial variability. Indeed, considering their relatively limited volume, continental waters are highly sensitive to climate anomalies, which can result in extreme events such as droughts or floods. In return, continental waters can impact the atmosphere, the ocean and the regional climate via energy and water fluxes (Gedney et al., 2000; Douville et al., 2000a). During the last decades, the number of worldwide reported natural disasters has been significantly increased (Fig. I-1), with 60% of them being related to hydrometeorological causes (floods, droughts and storms: International Disaster Database, [www.emdat.be](http://www.emdat.be)). As shown in Fig.I-2, the frequency of natural disasters, as well as their social and economical impact are highly variable according to the affected area. Therefore, the monitoring and the management of continental water resources are required in order to minimize the impact of extreme conditions on the people of the affected regions. Since the 80's, numerous land surface schemes (LSMs) were developed in order to represent the interactions between the surface, the biosphere and the atmosphere in AGCMs and RGCMs. These models generally have a coarse resolution (from 2 to 5 °) and aim at describing, in a synthetic way, the major processes involved at the soil-atmosphere interface using a limited number of parameters and first order physics. Originally relatively simple, there were continuously improved in order to take into account diverse processes related to the vegetation (and Carbon), snow and hydrology. Rising concerns about water resource availability have lead to the development of river routing models (RRMs) to represent continental water dynamics and the evolution of fresh water reservoirs (Dümenil et Todini, 1992; Habets et al., 1999b and c, Oki et al., 1999; Etchevers et al., 2001; Ducharne et al., 2003; Decharme et al., 2012). However, global hydrological simulations are subject to many uncertainties limiting their performance, the most important of which

comes from errors in the input precipitation. Indeed, errors in precipitation can directly impact the hydrology of a watershed, and errors in spatial distribution or rain intensity may lead to a poor prediction of significant events such as flash floods. However, ongoing studies aim at better flash flood forecasting using numerical weather prediction models coupled to LSMs (Vincendon et al., 2011), even if such work is still fairly preliminary. To reduce these uncertainties within the framework of LSM validations, the models are generally run in offline mode, i.e. decoupled from an atmospheric model and forced by atmospheric data derived from re-analyses, radar and satellite observations or interpolated rain gauge measurements (or some combination of these). Another source of uncertainty is related to the difficulty to precisely estimate the hydrologic parameters used in the models. In fact, the hydrological characteristics of large basins, such parameters related to the soil, the topography, to the river dimensions or to aquifers, are generally not well known, especially in areas where measurement infrastructures are missing. Generally, these parameters are described in large scale hydrological model applications using geomorphological relationships which can be sometimes unrealistic (especially at smaller scales). One last major source of uncertainty arises due to the lack of global observations describing the surface water spatial and temporal dynamics, as well as the water storage evolution in the principal continental reservoirs (Alsdorf et al., 2007). Indeed, the political and economic context of some regions all but prevents the construction and maintenance of in-situ measurement stations which limits the calibration of hydrological models. This is currently the case for the Niger basin. With an approximate length of 4180 km (2600 miles), the Niger river is the largest river in West Africa. It's headwaters are in the Guinea Highlands in south-eastern Guinea, and the river ends in Nigeria, discharging through a massive delta into the Gulf of Guinea within the Atlantic Ocean (Fig. I-3). The Niger river crosses 9 countries and is the principal source of water for a population of approximately 100 million people. Indeed, the economy of such rural areas predominantly depends on activities such as agriculture or livestock farming which are highly conditioned by water resource availability. Moreover, the climate is mainly controlled by the West African monsoon (WAM), and many of the key processes modulating it's evolution and intensity, along with its variability are still not well understood (thereby limiting the predictability of the regional climate). The WAM directly impacts the hydrology of the Niger basin and the water storage in deep reservoirs via the precipitation which mainly occurs through squall lines during the monsoon season (Lebel et al., 2002). During the last several decades, West Africa has faced extreme climate variability with extended drought conditions following very wet periods (Nicholson, 2001; Lebel et al., 2009), but also with the succession of wet and dry phases inside the same monsoon season. In order to better understand processes responsible for the WAM formation and variability, the AMMA

project (African Monsoon Multidisciplinary Analysis, Redelsperger et al., 2006), was organized which gathered numerous scientists at an international level. The AMMA campaign sought a better understanding of the mechanisms involved before, during and after the monsoon. The Niger river is a major source of water in West Africa, but its hydrology is difficult to fully understand, especially because of the very heterogeneous climate encountered along the river. It crosses very dry areas in the Sahelian region while passing through a large flooding area known as the Niger inner delta. This delta, situated between the latitudes [13°N-16°N] and the longitudes [3°O-6°O], is annually flooded over about 25000km<sup>2</sup>. These flooded areas are significant sources of evaporation (about 44% of the incoming water to the delta is evaporated, Andersen et al., 2005) which can impact the atmosphere and the climate regionally. Moreover, they lead to a strong decrease of the discharge downstream of the inner delta (the difference of discharge downstream of the delta compared to upstream of the delta can be upwards of 60%, Andersen et al., 2005). Yet, the LSMs generally do not represent these flooded areas which can result in significant errors in the calculation of discharge and evapotranspiration in these regions.

The first part of this thesis presents the evaluation of the Continental Hydrological coupled system ISBA-TRIP over the Niger basin. This model was developed at the the Météo-France National Center for Meteorological Research (CNRM) and is currently used for climate prediction simulations coupled with the atmospheric model ARPEGE (Salas y Melia et al., 2005). The surface model ISBA (Soil-Biosphere-Atmosphere Interactions; Noilhan and Mahfouf, 1996) calculates water and energy budgets at the soil-atmosphere interface. The TRIP (Total Runoff Integrating Pathways; Oki, 1998) approach is used to convert the total runoff from ISBA into discharge. Recently, a flood scheme was added to the ISBA-TRIP model in order to estimate the impact of flooding on the hydrological processes (Decharme et al., 2011). This scheme considers a critical water height beyond which the water contained in the river overflows and fills the flooded areas. It accounts explicitly for the river routing, precipitation interception by the floodplains, the direct evaporation from the free water surface, and the possible water re-infiltration into the soil in flooded areas. A first evaluation of this scheme over several large world basins (Decharme et al., 2010) showed that the flooding scheme resulted in a significant improvement of the simulated discharge (via a decrease of the discharge downstream of the flooded areas). However, despite this improvement, the study showed that a positive discharge bias remained for certain rivers, in particular for the Niger river. The work presented in this thesis focuses on the Niger basin and highlights both the skill and limitations of the ISBA-TRIP model. The input hydrological parameters were regionally adjusted following a series of simple sensitivity tests in order for the model to better fit the discharge observations, however, a detailed model calibration was

not undertaken as such an approach would not be practical for application of such a model in a AGCM. Despite the adjusted parameters, the aforementioned positive discharge bias persisted. One possible hypothesis for this bias is that in this region, there is a deep aquifer which is essentially disconnected from the river and recharged by a portion of water from deep drainage. As a consequence, a relatively simple aquifer reservoir was added to the model during this study (formulated in a consistent manner with the other relatively simple prognostic equations of the model). This reservoir is characterized by a characteristic time scale which represents the time required for this reservoir to be almost completely empty.

In first part of this thesis, the individual impact of the floods and of the aquifer on the hydrologic and hydrodynamic processes of the Niger basin are quantified. First, the TRIP routing model was run in offline mode, i.e. uncoupled from a LSM, in order to calculate the discharge simulated by 11 model issued from the ALMIP (AMMA Land surface Model Intercomparison Project; Boone et al., 2009a) project. This first analysis highlights the fact that none of the ALMIP LSM models are able to correctly simulate the discharge downstream of the Niger inner delta (all models over-estimate the discharge). Then ISBA-TRIP is used in coupled mode (i.e. with the inclusion of the flooding scheme and of the aquifer reservoir). The model evaluation is done using diverse observational datasets from in-situ stations (discharge) or derived from satellite observations (water level, flooded fraction, water storage variations). In a region such as the Niger basin where observations are scarce, the use of diverse data sources provides complementary information for characterizing the water dynamics on a large scale. Moreover, as the flooding of the inner delta has a significant impact on the basin and potentially on the regional climate, it is of interest to evaluate the ability of the model to correctly model the expanse of the flooded areas using observed flooded fractions. Finally, several rainfall fields are used as forcing to take into account the uncertainties due to errors in the estimation of precipitation (location, intensity etc...). The evaluation shows that, considering its relative simplicity, the ISBA-TRIP model is able to reasonably simulate the surface water dynamics and the total water storage variations over the basin. The flooding scheme leads to increased discharge during the rainy season while the aquifer allows a better simulation of low flows during the dry season. However, a complete validation of the hydrological model is limited by the lack of observations with a good spatial and temporal coverage. During this study for example, only 8 in-situ discharge stations were available for comparison with the model, while 145 discharge in-situ stations were used during a LSM inter-comparison project over the Rhône river (Boone et al., 2004) which is more than 25 times smaller than the Niger basin. In order to compensate for this lack of observations, remote sensing technologies are under development and offer a

new perspective for global hydrology. However, the current limitations due to the low spatial resolution of the nadir altimetry do not allow a good monitoring of most of continental waters (eg. TOPEX, JASON). New tools are then required in order to provide better observations of surface water dynamics. The future Surface Water Ocean Topography (SWOT) satellite mission is a joint CNES-NASA project which will deliver maps of water surface elevation (WSE) with an unprecedented resolution of 100m. It will provide observations of rivers wider than 100 m and water surface areas above 250 x 250 m over continental surfaces between 78S and 78 N. The launch of this satellite is tentatively planned for 2019. The main advantage of SWOT is the use of an interferometric radar Karin (Ka-band Radar Interferometer: frequency of 35,6 GHz), which was developed at JPL. The swath width is 120km in width, which will enable the coverage of many lakes, rivers oceans and water reservoirs at least twice every 21 days (up to 7 times at high latitudes). The interferometric altimeter will provide surface water levels (and other observations spatially and temporally derived from water levels) with a horizontal spatial resolution ranging from 50 to 100m. For hydrology, these observations will be useful to better understand the global dynamics of continental waters and their interactions with the atmosphere and the oceans. Moreover, they will be used for water storage monitoring within the framework of climate impact studies. In order to prepare the SWOT mission, several scientific communities (namely oceanography, hydrology, and cryosphere) are evaluating the contribution of the SWOT mission to different case studies and there is also ongoing work to determine some of the satellite characteristics. For example, the satellite orbit is fixed at 22 days but the sub-cycle is not yet determined. Indeed, each sub-cycle presents its own advantages or drawbacks related to its repetition and coverage. For hydrology, it is necessary to determine how the SWOT data can be used to improve hydrological simulations and to better predict continental water storage. Several studies are thus currently ongoing over diverse world basins in order to propose efficient approaches for using SWOT observations. Data assimilation seems to be a promising perspective for the improvement of hydrological modelling (Andreadis et al., 2007; Biancamaria et al., 2011). Commonly used in operational meteorology and oceanography, data assimilation enables the use of diverse observations while taking into account the errors related to the measurements. However, these methods are not yet as extensively used in hydrology and related works are rare, especially for large scale applications (such as the ISBA-TRIP model). As a pre-launch study, the second part of this thesis presents a preliminary method to assimilate SWOT virtual water level in order to improve the ISBA-TRIP global hydrological model parameters. For this, an Observing System Simulation Experiment (OSSE) was done using so-called virtual SWOT observations of water levels. This type of experiment is useful within the framework of a pre-launch study because no ob-

---

servations exist yet. SWOT virtual water levels are first generated on the model grid using a reference simulation (this simulation is considered as the 'truth'). Then, taking into account the errors due to parameter uncertainties, a perturbed simulation is created. Data assimilation consists in using SWOT virtual observations to correct certain key model input parameters and get a better estimation of hydrodynamical variables such as the water levels and the river discharge. As a preliminary work for data assimilation, sensitivity tests were performed and it was decided to use the assimilation to correct a key hydrological parameter, the Manning coefficient. The Manning coefficient describes the ability of the river bed roughness (soil, vegetation, etc...) to slow down the river flow and can be considered as a drag coefficient. This spatially distributed parameter is not easy to estimate since it varies considerably. Moreover, it directly impacts the flow speed and thus the discharge. It is also a critical factor for the formation of floods in the model. The algorithm used to provide the analysis after one assimilation cycle is the BLUE (Best Linear Unbiased Estimator). This study shows that data assimilation can be used in order to obtain a better estimation of water levels, and, to a lesser extent, of the river discharge. Moreover, the continental water storage variations and the floods occurring in the inner delta (occurrence, intensity) are better represented. The Manning coefficient bias (relative to the «truth» simulation) is improved over the river and converges towards an optimal value which is a good result considering the equifinality hypothesis characterizing such a study (where an optimal set of parameters is sought). Finally, the predictive property of this method is highlighted using the optimal Manning coefficient obtained during the assimilation application for hydrological simulations over a longer time period than that of the assimilation. Therefore, the data assimilation method presented here offers a good perspective for the improvement of hydrological processes currently represented in regional and global atmospheric models using SWOT data. Moreover, it offers a possibility to get better predictions of water resources variations at real time or for longer time scales. The SWOT mission will compensate for the lack of observation data at the global scale, and therefore it has the potential to drastically improve our understanding of the global hydrologic cycle. With the potential for increased conflicts related to water availability, a better knowledge of continental water dynamics and variations could improve the use of these resources in a way to reduce the social and economic impact of climate change.



# Land surface processes and continental hydrology : role in climate

---

## Contents

---

<b>1.1</b>	<b>The water cycle . . . . .</b>	<b>18</b>
<b>1.2</b>	<b>Land surface hydrology . . . . .</b>	<b>19</b>
<b>1.3</b>	<b>Energy balance of continental surfaces . . . . .</b>	<b>22</b>
<b>1.4</b>	<b>Land-Climate interactions. . . . .</b>	<b>25</b>
<b>1.5</b>	<b>Modeling of hydrologic processes at regional and global scales . . . . .</b>	<b>27</b>
1.5.1	Land surface models . . . . .	27
1.5.2	River routing models . . . . .	34
<b>1.6</b>	<b>Evaluation of CHSs : from local to global scale . . . . .</b>	<b>36</b>
1.6.1	Local evaluation . . . . .	36
1.6.2	Regional and global evaluation : Classic methods. . . . .	37
1.6.3	The future SWOT satellite mission . . . . .	38
<b>1.7</b>	<b>Modeling of the Niger river basin : A scientific, social and economic challenge. . . . .</b>	<b>43</b>
1.7.1	Geo-demographical environment of the Niger river Basin .	43
1.7.2	Climatic conditions, rainfall variability and water resources availability . . . . .	45
1.7.3	The inland delta, a complex region for hydrologic model- ing. . . . .	49
1.7.4	The African Monsoon Multidisciplinary Analysis (AMMA) program . . . . .	50

---

## 1.1 The water cycle

The term 'water cycle' describes the complex processes contributing to the continuous movement of water on, above and below the earth's surface. This cycle is considered as closed and water is constantly recycled through its various states : liquid, solid and vapor. The transfers are done between three principal reservoirs which constitute the hydrosphere : oceans, atmosphere and the continents. The sun is the principal driver of the water cycle : under specific conditions of temperature and pressure, the water will go from one of its state to an other. Solar radiation heats the oceans and continental waters, leading to evaporation. Plants uptake soil moisture from the root zone and this water is lost to the air as transpiration, while intercepted air (snow) is lost as transpiration (sublimation). Direct evaporation from open water or soil surfaces and transpiration from plants are not easy to separate from mixed surfaces at the spatial scale of a single plant, so that the combined process is usually referred to as evapotranspiration. Evaporated water rises in the atmosphere, where cooler temperatures cause it to condense into clouds, which are then transported around the globe by air currents. Under microphysical processes and gravity, this water falls over earth's surface as rain or snow. Precipitation over land either flows over the surface in the form of surface runoff, infiltrates into the land surface, or it is intercepted by the vegetation canopy and part of it is directly evaporated without reaching the ground. The surface runoff can collect locally in puddles or ponds, as depression storage, or in gullies or larger channels where it continues as streamflow, which finally ends up in a larger water body such as lakes, rivers or oceans. The infiltrated water may flow rapidly through the near-surface soil layers to exit into springs or adjacent streams, or it may percolate more slowly to be stored in aquifers as groundwater. This groundwater, after a variable time, will seep out into the natural river system, lakes and other open water bodies. Soil layers and other geologic formations, whose pores and interstices can transmit water are called aquifers. When an aquifer is in direct contact with the land surface, it is referred to as unconfined. The interface in an unconfined aquifer, where the water pressure equals the atmospheric pressure, is called the water table. Although the water table is not literally a free surface separating a saturated zone from a dry zone, it is generally assumed to be the upper boundary of the groundwater. Thus, the groundwater refers to the water located below the water table, while soil moisture or soil water generally refers to the water above the water table. The partly saturated zone situated between the water table and the land surface is called the vadoze zone. Soil layers containing water which is separated from the surface by an impermeable layer are referred to as confined aquifers. Streamflow can be supplied both by surface runoff and subsurface flow. The schematic representation of the water cycle is shown in Fig.1.1., as well as

the volume of water flowing annually through the different phases of the hydrologic cycle in units relative to the annual precipitation on the land surface (1119,000km/year; Maidment, 1993) which is set equal to 100 units on Fig.1.1. The evaporation from ocean (424 units) is seven times larger than the evaporation from land surface (61), making the ocean the principal source of precipitation over the earth's surface. The surface water flow provides almost all the discharge going to the ocean (38 units out of 39 in total going to the ocean) and is counter-balanced by an equivalent net inflow of atmospheric water vapor from the oceans to the land regions.

As a closed system, the interactions between the different reservoirs are of major importance to better understand the climate variability. The residence time of water in a reservoir differs greatly according to the reservoir considered. For example, the mean residence time of a water molecule in the atmosphere is very short, usually from days to a week or two. It can take weeks to months for water to move through surface drainage networks depending upon the complexity of the geomorphologic network. Water may be stored for months to years in soil water and individual water molecules may remain in deep groundwater, glaciers and ocean basins for decades to 10,000 or more years.

Although land surface water represents only 3.5 % of the earth's total water, its role and impact on climate variability has been subject of numerous investigations (Houwelling et al.,1999; Matthews, 2000, Bousquet et al., 2006, Taylor, 2010; Taylor et al., 2011). Moreover, due to the relatively small volumetric capacity of continental reservoirs, the variability of land waters in space and time is highly dependant on the climate and more precisely on precipitation, resulting in extreme events such as droughts or floods. Thus, continental hydrological processes must be considered in climate and water management impact studies, at least at regional scale (Gedney et al., 2000; Douville et al., 2000; Douville, 2003; Douville, 2004; Molod et al., 2004; Lawrence and Slater, 2007; Alkama et al., 2008).

## 1.2 Land surface hydrology

For modeling applications, a quantitative representation of the hydrologic cycle is given by a mass conservation equation, or water balance, which depends on the considered scale. This water balance can be written in its basic form as :

$$\frac{\partial W}{\partial t} = F_{in} - F_{out} \quad (1.1)$$

where  $W(kg/m)$  (including lakes, rivers, flooded zones, aquifers, intercepted precipitation and soil moisture) represents the total water storage,  $t(s)$  is the time,

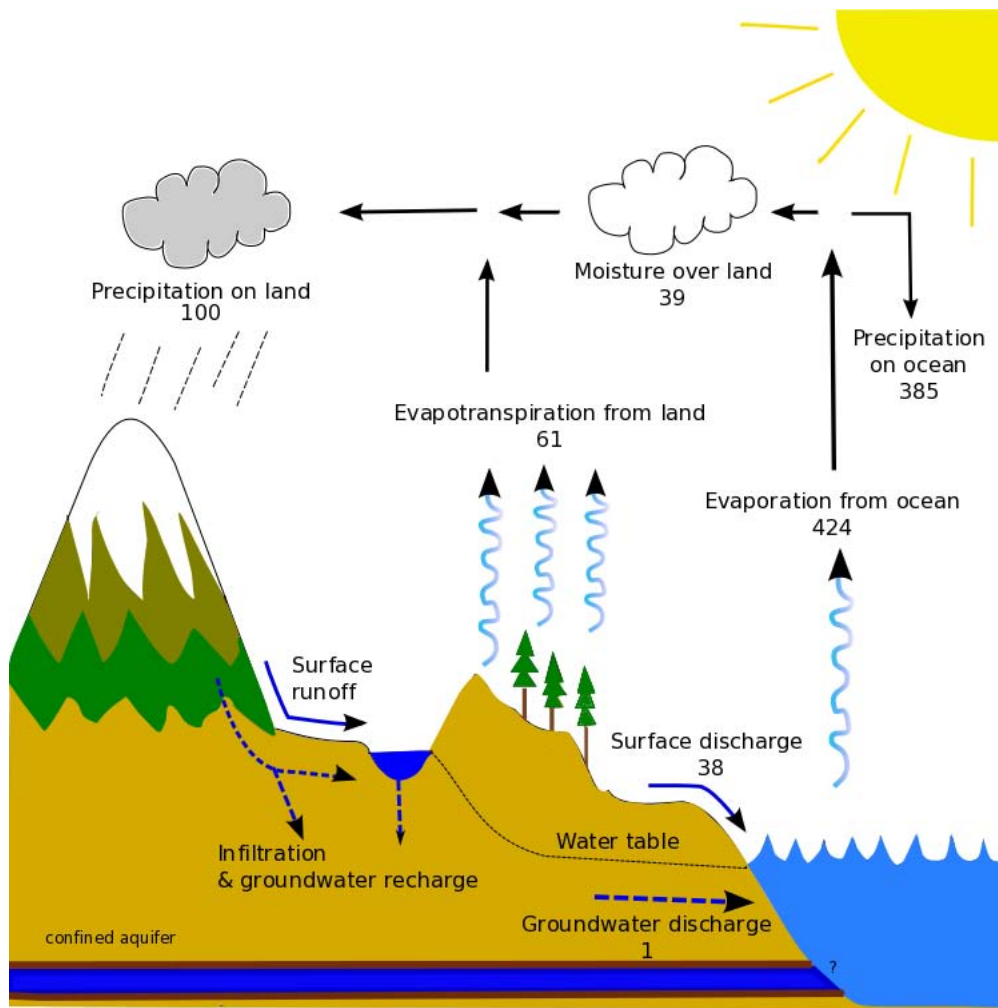


Figure 1.1: The hydrologic cycle with annual volumes of flow given in units relative to the annual volume of precipitation on the earth's land surface, figures are from Maidment, 1992

$F_{in}$  and  $F_{out}$  are respectively the net water mass inflow and outflow.

Generally, hydrologic studies are done at the watershed (or drainage basin) scale which is defined as an area over which all the water issued from precipitation, melting snow or ice converges to a single point, usually the outlet of the basin (see Fig. 1.2). In a drainage basin, no water other than precipitations (solid or liquid) enters the system, and water which is not stored evacuates either by evaporation or through the exit of the basin, joining another waterbody such as a lake, a river, a reservoir or an ocean. A drainage basin is generally separated from adjacent basins by a drainage divide defined according to the topography.

Considering the basin as a single hydrologic unit, and according to the previous equation, the water balance can be expressed as :

$$\frac{\partial W}{\partial t} = P - (Q_s + Q_{sb} + E) \quad (1.2)$$

The precipitation  $P(kg.m.s^{-1})$  is the water mass inflow of the basin, while  $Q_s(kg.m.s^{-1})$ ,  $Q_{sb}(kg.m.s^{-1})$ ,  $E(kg.m.s^{-1})$ , respectively correspond to the surface runoff, the sub-surface runoff and the evapotranspiration which together represent the water mass outflow of the basin. Even with reliable data on precipitation and runoff,  $E$  and  $W$  remain as unknown variables of the equation. Thus, to close the water balance expressed in equation 1.2, it must be applied over sufficiently long periods, so that  $\frac{dW}{dt}$  becomes less significant.

The water balance is highly dependant on several environmental factors, either natural or anthropogenic. It depends on the topography but also on soil and vegetation properties which can be largely heterogeneous over the basin. For example, soil infiltration capacity is closely related to the type of soil and vegetation. Steep topography will encourage runoff production while gentle landscapes will favour water infiltration storage. A dense vegetation cover, such as forests, will inhibit runoff and drainage formation, decrease streamflow speed and prevent flood occurrence. On the contrary, dry soil will encourage runoff and flood occurrence. Anthropogenic activities, such as crops or urban areas, also impact soil humidity and total runoff formation. Land use changes, from natural vegetation to agriculture, can also impact runoff by changing evaporation. Land use changes, from surface natural vegetation to agriculture, can also impact runoff by changing evapotranspiration.

Due to the strong interactions between the soil and the atmosphere (see section 1.3), the water balance of the basin is also greatly dependant on atmospheric conditions. Evapotranspiration will depend on the heat, humidity and wind speed of the lower atmospheric layers. But the first atmospheric factor impacting the water budget of the basin remain the precipitations, due to their strong variability in time (intra/inter annual variability), space (local, regional or global scale), amount and intensity. The study of the water cycle will then

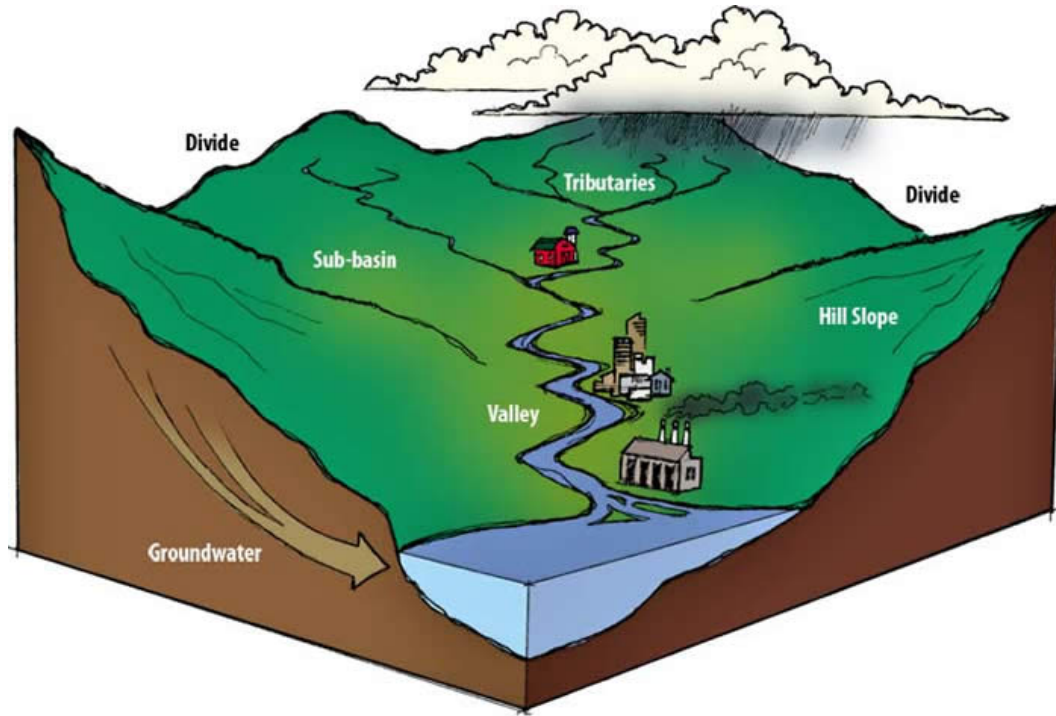


Figure 1.2: Schematic representation of a watershed.

require the consideration of this multi-scale aspect, especially for larger basins.

### 1.3 Energy balance of continental surfaces

The solar radiation  $R_g(W.m^2)$  is the principal catalyst of land-atmosphere energy exchanges. The solar radiation reaching continental surfaces can be altered by different factors such as slope and aspect of the surface, but also its reflection or absorption by aerosols, clouds or various gases. In addition, the atmosphere also emits long wave radiation to the surface which contributes to its warming,  $R_a(W.m^2)$ . The ability of the surface to reflect shortwave radiation is called albedo and is a key component of the energy budget. The surface albedo,  $\alpha$ , is globally heterogeneous and highly dependant on the surface properties. The total all-wavelength albedo is defined by the ratio of the solar energy reflected by the surface over the total solar energy reaching the surface. The part of the radiation which is not reflected is absorbed by the surface and contributes to its warming. The continental surface emits longwave radiation to the atmosphere,  $R_t$ , defined by the Stefan-Boltzman law as :

$$R_t = \varepsilon\sigma T_s^4 \quad (1.3)$$

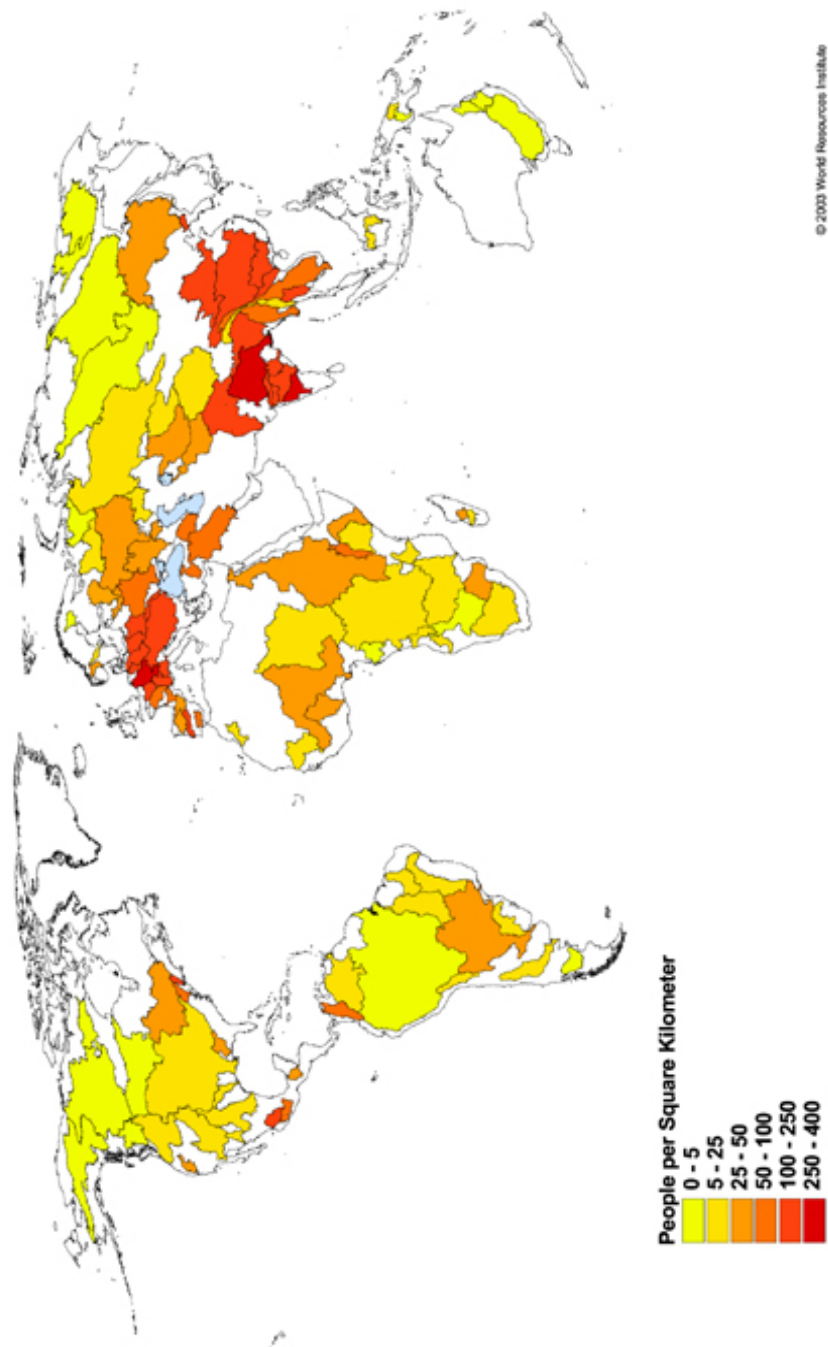


Figure 1.3: World watersheds map. For hydrologic studies, the watershed is considered as a hydrologic unit. However, this 'unit' vary widely in shape and size as shown on this figure. This map also shows the population density by basin expressed as people per square kilometer. The most densely populated basins are found in India, China, Central America, and parts of Europe. In Africa the most populated basins are Lake Turkana, Niger, Nile, Mangoky, Limpopo, Shaballe, and Volta, from World Resources Institute, 2003.

where  $\sigma(W.m^2.K^4)$  is the Stefan-Boltzman constant, and  $\varepsilon$  is the effective surface emissivity.  $T_s(K)$  represents the effective radiative temperature of the surface, which contains contributions from the different surfaces (bare soil, snow, vegetation etc ...). Thus, the net radiation flux of the continental surface can be written as follows :

$$R_n = R_g(1 - \alpha) + \varepsilon(R_a - \sigma T_s^4) \quad (1.4)$$

where  $R_g(1 - \alpha)$  is the net shortwave radiation flux of the surface and  $\varepsilon(R_a - \sigma T_s^4)$  is the net longwave radiation flux of the surface.

The net radiation flux is the preponderant component of the energy budget. It gives an information about the amount of energy available at the surface for transformation into heat fluxes via physical or biological processes. Thus, the energy budget of a composite surface-vegetation-atmosphere system can be written as :

$$R_n = L.E + H + G \quad (1.5)$$

where  $L.E(W.m^2)$  is the latent heat flux,  $H(W.m^2)$  is the sensible heat flux and  $G(W.m^2)$  is the conductive heat flux of the soil. The effects of photosynthesis are included in  $E$ .  $G$  is a conductive flux, which means that the energy is transferred relatively slowly, without matter or particule modification. It is directly proportionnal to the temperature gradient between a reference depth and the land surface, and to the thermal conductivity of the underlying surface (soil, organic, material, water, ice) :

$$G = \lambda_s(T_s - T_r) \quad (1.6)$$

where  $\lambda_s(W.m^2.K^1)$  is the soil thermal conductivity between reference depth and the land surface. The latent and sensible heat fluxes are defined as turbulent exchanges which means that the energy transfers are done through air displacement between the surface and the lower atmosphere layers (Jacob, 1999). The vertical movement of the air is driven by bouyancy effects in the surface layer (interface between land and atmosphere) characterized by large vertical gradients. The sensible heat flux is directly proportionnal to the temperature gradient between the surface and the atmosphere :

$$H = \rho_a c_p C_H V_a (T_s - T_a) \quad (1.7)$$

where  $c_p(J.kg^{-1}K^{-1})$  and  $\rho_a(kg.m^{-3})$  are respectively the air specific heat and density,  $V_a(m.s^{-1})$  is the air velocity,  $T_s(K)$  and  $T_a(K)$  are the surface and atmosphere temperatures ( $T_a$  corresponds to the value at a reference height).  $C_H$  is an exchange coefficient which depends on stability, which is a function of gradients and surface roughness characteristics. In contrast to the latent heat flux,

the sensible heat flux results in a temperature modification of the lower layers of the atmosphere. If water is present at the surface, and if the amount of energy enables the phase change of water into vapor, then evaporation can occur. The latent heat flux corresponds to the heat transfer, from the surface to the atmosphere, associated with the evaporation process (transfer of water mass). It is proportionnal to the specific humidity gradient between the surface and the atmosphere :

$$LE = L_v \rho_a C_H V_a (q_s - q_a) \quad (1.8)$$

where  $L_v (J.kg^{-1})$  is the latent heat of vaporization,  $q_a (kg.kg^{-1})$  and  $q_s (kg.kg^{-1})$  are respectively the specific humidity of air and the surface. This energy flux is said to be latent because the heat transferred during the evaporation process is liberated later on, through the condensation process, for the formation of clouds. The water and energy budget equations are directly coupled through the evaporation process. Thus, both budgets must be considered when investigating surface-atmosphere interactions.

## 1.4 Land-Climate interactions.

Land surface processes directly impact the dynamics of the atmosphere's lower layers on relatively short time scales (eg. convection) and these effects are transmitted to larger time scales into higher levels of the atmosphere. Early on in climate change investigations, the impact of the surface on the global climate was questioned. Richardson (1922) was the first to refer to the atmosphere and the upper layers of the soil as a combined system, and stressed on the fact that the forecast for the land and sea must be done along with that for air. So did one of the pioneers of global climate modeling in 1969, Manabe, when he explicitly represented the evaporation of earth's surface in his General Circulation Model (GCM). His model accounted for time evolution of soil humidity and snow cover, and for the computation of surface evaporation. He found that the explicit representation of earth's surface processes led to a more realistic distribution of precipitation, but also heat and radiation fluxes. Since then, the representation of surface processes in GCMs has been constantly improved, highlighting their significant role, especially for climate modeling. Many processes have been found to have impacts on the climate, at least regionnaly, and need to be represented in GCMs :

- Charney et al. (1975) showed the strong interactions between surface albedo and precipitation
- soil humidity controls the partitioning of the net radiation and ground fluxes into sensible and latent fluxes at the surface (Deardorff, 1977).

- Land waters have been shown to play an important role in atmosphere and ocean dynamics (Alkama et al., 2008; Dirmeyer, 2000, 2001; Douville, 2000, 2003, 2004; Gedney et al., 2000; Koster et al., 2000b, 2002; Lawrence and Slater, 2007; Molod et al., 2004). The energy and water fluxes at the surface modulate the lower atmosphere layers. The continental fresh water flux to the ocean is an important information for ocean dynamics. Its impact on thermohaline circulation and gulf stream is questioned in many studies (refs).
- large-scale snow cover anomalies produce short term local cooling at mid-latitudes (Namias, 1985; Dewey, 1977; Barnett et al., 1989; Cohen and Rind, 1991) by modifying surface properties and hydrology. Douville and Royer (1996b) and Orsolini et al. (2009), showed the impact of snow cover on Northern Hemisphere circulations.
- Natural wetlands are assumed to be important sources and sinks of Methane, thus playing a significant role in radiative and chemical balances in the atmosphere (Houwelling et al., 1999; Matthews, 2000; Bousquet et al., 2006; Taylor, 2010).
- soil moisture has significant feedbacks with the atmosphere : evaporation of soil moisture impacts precipitation patterns at global and seasonal scales (Koster et al., 2004) and influences convection in Sahel (Taylor et al., 2006, 2011, Taylor and Lebel, 1998).
- vegetation canopies also impact surface properties by increasing the roughness, reducing albedo (canopies are less reflective than bare soil) and modulating soil humidity (canopies prevent the near-surface soil region from drying out and can access the deep soil moisture), (Douville and Royer, 1996a; Dickinson and Henderson-Sellers, 1988; Garratt, 1993; Polcher, 1995).
- depending on environmental properties, vegetation acts as a sink or a source of carbon dioxide and other gases (Jarvis, 1976; Niyogi and Raman, 1997). The vegetation seasonal and interannual growth is also a factor impacting the surface feedbacks to the atmosphere. Indeed, warm and wet climatic conditions can stimulate the increase of vegetation cover and thus, enhance plants evapotranspiration and carbon emissions. In contrast, droughts can result in a rapid decrease in the vegetation cover (Betts et al., 1997; Calvet et al., 1998).

Due to these feedbacks from land surface and hydrologic processes with the atmosphere, there is a need to better represent land surface processes in weather prediction and earth system models. The rapidly growing concerns about climate

## **1.5. Modeling of hydrologic processes at regional and global scales**<sup>27</sup>

---

change issues, and the need to simulate regional climate more precisely on the time scales of several decades and to better quantify the impact of changes in terms of weather and precipitation, is leading to a better appreciation of the land surface in the climate system. More recently, the interest in land-use activities and water availability has encouraged the inclusion of more realistic soil and vegetation schemes in RCMs and GCMs. The next section gives a review of the methods used for the modeling of land surface processes in GCMs.

### **1.5 Modeling of hydrologic processes at regional and global scales**

Since the 80's, various CHSs schemes have been developed, the method mostly depending on the scale of the studied issue. For water management applications on the watershed scale, highly parameterized, geographically specific models can be used to provide accurate estimates of streamflow and reservoir status (Zagona et al., 2001; Dai and Labadie, 2001; Habets et al., 2008). For global scale applications however, the challenge is to get a realistic representation of major surface hydrologic and hydrodynamic processes using computationally efficient, easily parameterized, comparatively simple and physically based routing methodologies. Because of the long timescales involved with soil moisture, and because of the diurnal cycle of the forcing (the net radiation at the surface), the land-surface parameterization schemes need to deal accurately with timescales ranging from minutes to several months. Moreover, the land surface hydrologic processes are highly heterogeneous and difficult to parameterize with the dimensions of AGCM grid areas. Thus compromises in the representation of surface processes, have to be made. Currently, the representation of the surface component of the hydrological cycle in AGCMs is done using continental hydrological systems (CHSs) composed of land surface models (LSMs), which provide the lower boundary conditions for heat, momentum and mass. Some AGCMs go further and include river routing models (RRMs) which are used to convert the runoff simulated by the LSMs into river discharge. RRM transfer the continental freshwater into the oceans at specific locations (as source terms for the ocean model component).

#### **1.5.1 Land surface models**

In this section, the methods used in LSMs and their chronology are detailed. This section is divided in several parts, each one focusing on one main process represented by LSMs. The section ends with a brief presentation of various LSMs intercomparison projects aiming at better understanding land surface processes and their interactions with climate.

### 1.5.1.1 Water and Energy balance at the soil-atmosphere interface

In climate applications, the main role of LSMs is to provide the lower flux boundary conditions of heat, moisture and momentum (and more recently, particulate matter, such as dust, and chemical species such as carbon) to the turbulence parameterization within atmosphere models. If the modeling of surface processes has greatly improved through years, the first LSMs were designed in a relatively simple way. In these early models, the surface effect on the atmosphere was generally implicitly represented (such as prescribing a soil moisture climatology) or, mainly for time computation issues, based on simple approximate equations. As said in section 1.2.1, Manabe (1969), was the first to represent land surface processes in an AGCM. To represent continental surfaces, he used the so called 'bucket' approach (Budyko, 1956), which consists of representing the soil water by a single 1m depth reservoir, assumed to contain most of the soil moisture variations (Romanova, 1954), as well as the entire root system. This reservoir is defined by its porosity,  $W_{sat}$ , that is the maximum volume of water that can be stored in the soil. The evaporation is calculated as a fraction of the potential evaporability,  $E_p$  :

$$E = E_p \frac{W}{W_k} \quad (1.9)$$

where  $W$  is the actual soil humidity and  $W_k$  is a critical value fixed to 75% of  $W_{sat}$ . If the soil humidity exceeds  $W_{sat}$ , then surface runoff is generated. No subgrid sub-surface runoff or drainage processes are represented. This method allowed the representation of evaporation from the soil without resolving the diffusion equation (Alpatev, 1954) . However, the 'bucket' method is limited by the use of only one soil layer, which generally leads to an overestimation of evaporation after rain events (Viterbo, 2001). In fact, for bare soil, it is an observational fact that, after a very brief period at the potential rate, evaporation is greatly reduced after the loss of water in the first few cm of the soil.

Moreover, the soil heat flux is completely neglected resulting in a phase delay in the diurnal cycle of the soil temperature, but also in an overestimation of the ground temperature (Deardorff, 1978). To model the soil heat flux, different methods were proposed. Some studies included it in a parameterized form (Gadd and Keers, 1970; Kasahara and Washington, 1971; Nickerson and Smiley, 1975). However, in these methods, the soil heat capacity is assumed to be zero, resulting in ground temperature biases (Deardorff, 1978). Deardorff (1978) used the force restore method proposed by Bhumralkar (1975) and Blackadar (1976) to implicitly resolve the heat diffusion equation and take into account the soil heat capacity. The force-restore model, developed by Deardorff, has a thin near-surface layer that changes temperature based on atmospheric forcings within diurnal cycle and an underlying thick layer whose temperature remains

## **1.5. Modeling of hydrologic processes at regional and global scales**<sup>29</sup>

---

relatively constant, following the diurnal cycle mean variations. The result is that the flux from a deep soil layer tends to 'restore' the top layer. The force-restore method was also adopted to describe the temporal evolution of surface humidity which allowed a more realistic soil behaviour during a rain event in terms of evaporation and water storage in deep layers, and a better resolution of the diurnal cycle of soil evaporation. This method is an alternative to a more complicated multilayer soil model which requires more computation. However, still no deep drainage was represented, limiting the realism of the models. To solve this problem, several parameterizations have been developed. Among them, Famiglietti and Wood (1994a-b), proposed a gravitationnal drainage directly proportionnal to the soil hydraulic conductivity while Mahfouf and Noilhan, (1996) developed a gravitationnal drainage based on the force restore method. Currently, owing to increased computing power and increasing applications requiring detailed soil profile information, the tendency is towards multi-layer explicit representation of vertical heat and soil moisture transfers (Boone et al., 1996; Stieglitz et al., 1997; Boone et al., 2000; Habets et al., 2003; Yang et Niu, 2003; Gedney et Cox, 2003).

### **1.5.1.2 Vegetation**

Vegetation affects the climate by modifying the energy, momentum, and hydrologic balance of the land surface. A vegetated area generally has a lower albedo than a bare soil, thus impacting the radiation balance by increasing the absorbed radiation at the surface. The canopies interact with the atmosphere through evaporation and the interception of precipitation. A soil with vegetation is generally rougher than a bare soil, thereby facilitating the turbulent exchanges with the atmosphere. Finally, the water content of the soil is also impacted by the presence of vegetation through the transpiration process. Deardorff included an explicit vegetation layer in a LSM in 1978 in order to better simulate the processes related to the vegetation and its interactions with land and atmosphere. The vegetation is characterized mainly by its density, roughness and albedo. It interacts with both the atmosphere and the ground through heat and moisture exchanges. The inclusion of the vegetation resulted in a more realistic calculation of ground temperature (Deardorff, 1978). However, the vegetation heat capacity is neglected in this study. In 1989, Noilhan and Planton, developed the Soil-Biosphere-Atmosphere Interactions scheme (ISBA), in which the soil and vegetation are part of a single system, sharing a single energy equation. This model is based on the bucket approach, and the force-restore method is applied for the calculation of soil temperature and humidity. In one grid cell, the soil is defined by its texture and its vegetation type which implicitly accounts for the vegetation processes, without any added equation. This approach has been used

for many years with success for GCM applications. But recently, more models are going towards implementation of explicit vegetation in order to be more consistent with more sophisticated carbon and vegetation dynamics, snow processes and heat transfers.

The gross resolution of GCMs in comparison with the spatial variability of vegetation cover and properties, has lead to the developpment of an explicit representation of the different surfaces to better approximate the potentially non-linear interactions using the so called tile parameterization. It consists of dividing the grid cell into a number of smaller scale patches, characterized by differing soil and vegetation parameters. The equations describing the evolution of the surface energy and water balances are then applied in each of these sub-domains, resulting in a separate energy and water budget for each patch (Avisar and Pielke, 1989; Koster and Suarez, 1992; Liang et al., 1994; Essery et al., 2003). The surface-area weighted grid box average fluxes then interact with a single grid box mean atmosphere. This method is now used in some operationnal NWP applications, and in an increasing number of RCM/GCMs.

#### **1.5.1.3 Snow cover and ice**

The snow cover is an important component of the cimate system. Indeed, the high snow reflectivity increases the surface albedo, thus decreasing the amount of radiation absorbed by the surface. Moreover, its high thermal emissivity and low surface roughness also contribute to decrease the surface temperature. Snow cover therefore induces a greater stability of the atmospheric boundary layer. Also, it acts as a thermal isolator of the sub-surface due to its low heat conductivity. The optical properties of snow cover are highly heterogeneous in space and vary considerably according to the season. From the hydrologic point of view, the snow melting water is distributed between surface runoff and infiltration that, in turn, affects shallow and deep soil layer water content and surface fluxes of heat and moisture into the following summer season. Some parameterization schemes represent the snow cover as part of the soil-vegetation-ice system, with a common energy balance for all these three components (Douville et al., 1995). In some cases, the snow cover can be explicitly represented with its own temperature and its own energy balance. The diurnal cycle of ice freezing/melting can also be represented (Cox et al., 1999; Boone and Etchevers, 2001). The inclusion of ice freezing/melting generally leads to improved atmospheric simulations for high-latitude regions (Cox et al., 1999; Giard and Bazile; 2000).

#### **1.5.1.4 Carbon cycle**

The recent interest about the enhanced greenhouse effect has lead to a growing number of studies related to the impact of an increasing  $CO_2$  concentration in

## 1.5. Modeling of hydrologic processes at regional and global scales 31

---

the atmosphere. The net assimilation of  $CO_2$  by the vegetation was found to be contributing process to the carbon cycle (Douville et al., 2000b). The amount of  $CO_2$  present in the atmosphere impacts on the stomatal conductance of the vegetation, ie its ability to transpire (Meidner and Mansfield, 1966; Jacobs et al., 1996). In response, changes in the transpiration alters the latent heat flux, which, according to the energy balance equation, modifies the sensible heat flux (Niyogi and Raman, 1997, Pielke, 2001; Shaw and Doran, 2001; Buermann et al., 2001). Precipitation along with temperature and soil moisture are also important factors which impact the stomatal conductance of plants, and thus the transpiration and their uptake of carbon dioxide via photosynthesis. Vegetation can be both a sink or source of carbon, depending on its age and the carbon demand. All these elements modulate the vegetation growth and maintenance. The basic functioning of terrestrial biosphere and its interactions with climate are well detailed by Arora (2002). Thus, the biospheric processes (photosynthesis, respiration and phenology of plants) make vegetation a dynamic component of climate simulations. Obviously, LSMs used in climate change simulations with increasing  $CO_2$ , but without dynamic vegetation neglect the interactions between biosphere and climate (Pritchard et al., 1999). To represent the stomatal response of the vegetation to the atmosphere in LSMs, different approaches are used. The meteorological approach, based on a simple parameterization of stomatal resistance developed by Jarvis (1976) is commonly used in operational meteorological models (Noilhan and Planton, 1989; Pleim and Xiu, 1995; Viterbo and Beljaars, 1995; Bosilovich and Sun, 1995; Alapaty et al., 1996, Calvet et al., 1998). In these models, the stomatal response is modeled as a function of meteorological parameters such as air temperature, ambient vapor pressure, radiation and soil moisture availability. In the ISBA-A-gs model, Calvet and Soussana (2001) also simulate the green Leaf Area Index (LAI) by using a simple growth model. However, for climate analysis, the more recent tendency is to use a physiological approach, which employs a more rigorous plant gas response, such as carbon assimilation rates or night respiration (Sellers et al., 1996; Foley et al., 1996). Note that the ISBA-A-gs model has since been modified and also uses these methods (Calvet et al., 2008).

### 1.5.1.5 Subgrid hydrology

At spatial scales considered by climate models (approximately  $10^4 km^2$ ), it is known that surface fluxes can vary nonlinearly primarily due to subgrid variations in soil and vegetation properties, soil moisture and precipitation (Dirmeyer et al., 1999, Boone et al., 2004, Decharme and Douville, 2006). In recent years, an increasing number of LSMs have adopted the so-called tile approach for which the gridbox surface is divided into a series of subgrid patches (e.g., Avissar and Pielke

1989; Koster and Suarez 1992; Seth et al. 1994). This method has the advantage of explicitly representing very distinct surface types, and that specific properties (such as elevation, soil type, and land cover) can be assigned to each tile. The main disadvantage is that a potentially large number of variables and parameters must be stored in memory and computational expense can be greatly increased compared to the effective surface treatment. This is an especially important consideration for numerical weather prediction (NWP) or GCM applications, so the tile method must be used depending of the intended application.

Subgrid processes have direct impact on hydrologic processes, especially runoff generation. Indeed, the subgrid variability of soil humidity is a key component for Dunne runoff generation. Dunne runoff occurs over saturated soil during a precipitation event. Subgrid precipitation variability generates Horton runoff over areas where precipitation intensity is larger than soil infiltration capacity. In contrast to Dunne runoff, the soil is a priori not saturated when Horton runoff happens. This kind of runoff is appropriate for dry areas while Dunne runoff usually occurs in wet areas. There are numerous methods that parameterize subgrid hydrology as a function of the variability in soil properties (Liang et al. 1994; Liang and Xie 2001). Probability distribution functions can be applied to certain key LSMs variables (such as soil moisture) using statistical moments calculated from observations (Wetzel and Chang 1988; Entekhabi and Eagleson 1989). Other studies use a 'variable infiltration capacity' scheme, VIC, to compute surface runoff (Zhao 1992, Dümenil et Todini 1992, Wood et al. 1992). The most common approach to take account of Dunne runoff generation is to explicitly represent the subgrid soil moisture using subgrid topographic information (Sivapalan et al., 1987; Famiglietti and Wood, 1994a-b; Stieglitz et al., 1997; Koster et al., 2000a; Ducharne et al., 2000; Chen et Kumar, 2001; Habets and Saulnier, 2001; Pellenq, 2002; Seuffert et al., 2002; Warrach et al., 2002; Gedney and Cox, 2003; Niu and Yang, 2003). Such methods are based on the TOPMODEL concept (Beven and Kirkby 1979, Sivapalan et al. 1987). The subgrid parameterization of atmospheric forcing variables, such as precipitation coverage, or air temperature heterogeneities, can also be modeled (Dolman and Gregory 1992; Liang et al. 1996). The most common approach to represent precipitation variability is to use probability functions of event occurrence to distribute precipitation intensity over the region.

#### **1.5.1.6 LSM Intercomparison projects**

In recent years, the skill of existing LSMs have been investigated through various intercomparison projects on an international level. The Project for Intercomparison of Land Surface Parameterization Schemes (PILPS) has examined the state of different Soil-Vegetation-Atmosphere Transfer (SVAT) schemes over several

## **1.5. Modeling of hydrologic processes at regional and global scales**

---

annual cycles (Henderson-Sellers et al. 1993, 1996). The atmospheric forcing and soil parameters were identical for all the LSMs making simulations. This project contributed to an increase in the understanding of LSMs and led to many model improvements in terms of both physics and numerics. In all of the PILPS phases (Henderson-Sellers et al. 1995), the LSMs were used in so-called offline mode (i.e., the LSM is uncoupled from an atmospheric model and is therefore driven using prescribed atmospheric forcing either from observations, satellite products, atmospheric model data, or some combination of those three sources), and the resulting simulations were compared to observational data. The first attempt by PILPS to address LSM behavior at a regional scale was undertaken in PILPS-2c (Wood et al. 1998). The Global Soil Wetness Project, Phase 2 (GSWP-2; Dirmeyer et al. 2006a) was an offline global-scale LSM intercomparison study that produced the equivalent of a land surface reanalysis consisting in 10-yr global datasets of soil moisture, surface fluxes, and related hydrological quantities. Results from this experiment were used extensively by the GCM community, most notably to examine soil moisture-atmosphere interactions (Dirmeyer et al., 1999; Douville et al., 1999). The Rhône aggregation LSM intercomparison project (Boone et al. 2004) differed from the above-mentioned studies because the impact of changing the spatial scale on the LSM simulations was investigated. More recently, the AMMA LandSurface Model Intercomparison Project I (ALMIP I) was undertaken. ALMIP I, which is a part of the African Monsoon Multidisciplinary Analysis project (AMMA), was motivated by an interest in fundamental scientific issues and by the societal need for improved prediction of the West African Monsoon (WAM) and its impacts on West African nations (Redelsperger et al., 2006). As part of this project, ALMIP I focused on the better understanding of land-atmosphere and hydrological processes over Western Africa (Boone et al., 2009a). LSMs were run offline with prescribed atmospheric forcing consisting in a combination of observations, satellite products and atmospheric model output data. All of the LSMs used the same computational grid at a  $0.50^\circ$  spatial resolution. The resulting LSM simulations were used extensively for hydrological modelling, regional scale water budget estimates, mesoscale atmospheric case studies, numerical weather prediction models studies and regional atmospheric chemistry modelling (Dominguez et al., 2010; Boone et al., 2010; Grippa et al., 2011; Pedinotti et al., 2012). The results are also used for the evaluation of regional and global scale atmospheric models within the AMMA Atmospheric Model Intercomparison Project (AMMA-MIP, Hourdin et al., 2010) and the GEWEX-sponsored West African Monsoon Modelling Evaluation Project (WAMME, Xue et al., 2010, Boone et al., 2010). A second phase of ALMIP is currently carried out (Boone et al., 2009b). In ALMIP Phase 2, LSMs will be evaluated using observational data from three heavily instrumented supersites from the AMMA-Couplage de l'Atmosphère Tropicale et

du Cycle Hydrologique (CATCH) observing system (Mali, Niger, and Benin). In addition to evaluation using field data, LSM simulations will also be compared to results from detailed vegetation process and hydrological models that have already been extensively validated over this region. The results will be used in conjunction with those from ALMIP-1 in an effort to evaluate the effect of scale change on the representation of the most important processes from the local to the regional scale. In the present work, the diagnostics of ALMIP LSMs are used to investigate the impact of a flooding scheme on the simulated discharge. The advantage of using ALMIP models data is that each LSM can simulate a different runoff response, therefore the use of an ensemble of inputs allows to quantify the impact of the flooding scheme in regards of the modeling uncertainties.

The growing interest in climate impact studies, and especially the impact of climate change on water availability, has lead to an increase in river routing, floodplain and aquifer parameterizations for GCMs and increased number of regional scale hydrological studies. Indeed, water resource issues increased the role of Continental Hydrologic Systems (CHSs) in providing seasonal and interannual predictions of major river basins dynamics. These new issues required the improvement of RRM, with the addition of several hydrologic processes, such as flooding or deep drainage in groundwater reservoirs. The next section gives a summary of the past and current development of RRM.

### **1.5.2 River routing models**

Generally speaking, LSMs do not explicitly model water exchanges laterally from one grid cell to another. River routing models (RRMs) were developed to account for the lateral dynamics of continental water and convert runoff calculated by LSMs into discharge. The growing interest in climate impact studies required the improvement of RRM, with the addition of several hydrologic processes, such as flooding or deep drainage in groundwater reservoirs. This section gives a summary of the past and current development of RRM.

As said previously, in AGCM applications, it is most important to close the water budget and get a good representation of the water storage and freshwater fluxes leaving a particular basin. The first role of routing models is to convert runoff calculated by LSMs into river discharge which allows the comparison of surface runoff from LSMs to discharge estimates. Over long time scales, water storage can be neglected, so that given precipitation and discharge from observations, one can quantify basin-scale evaporation estimates. Some routing models, however, also account for the horizontal dynamics of sub-surface runoff and its vertical diffusion to deeper soil layers. In 1989, an early influential effort at large scale routing was done by Vorosmarty et al., who prepared a river routing network for the Amazon basin at a  $0.5^\circ$  resolution. Runoff produced

## 1.5. Modeling of hydrologic processes at regional and global scales 35

---

by a water balance approach was routed through the network using a linear transfer model, with flow time calculated as a function of flow length, estimated subgrid scale sinuosity, and grid scale velocities estimated on the basis of mean downstream discharge (Leopold et al., 1964). A similar linear transfer model was adopted by Miller et al. (1994) for application within the Goddard Institute for Space Studies (GISS) General Circulation Model (GCM) at the global scale. In their formulation, runoff produced by a GCM at  $4^\circ \times 5^\circ$  was routed to the ocean through a  $2^\circ \times 2.5^\circ$  network in which flow direction was determined by topography and velocity was a function of the slope. Because the scale of the implementation was quite coarse, slope based estimates of velocity were intentionally calculated to yield low values, providing an implicit correction for subgrid scale sinuosity and the time it would realistically take runoff to work its way through the river system. Sausen et al. (1994) implemented a linear routing scheme for the European Center Hamburg (ECHAM) GCM, with transport parameters semi-objectively calibrated to match observed flow in major gauged rivers. In a study of the Amazon River system, Costa and Foley (1997) adopted the velocity estimation procedure of Miller et al. (1994). As a refinement, they estimated the sinuosity coefficient independently for each tributary within the Amazon basin, and they adjusted velocities as a function of stream order. Costa and Foley (1997) further divided runoff into surface and subsurface components and applied differential source retention times to each. Further variants on the Miller et al. (1994) approach include the global hydrological routing algorithm (HYDRA, Coe, 2000), which was implemented at a  $5^\circ$  resolution and included variability in surface waters, and made some adjustments to the Miller et al. (1994) method for calculating distributed velocities. Oki and Sud (1998) and Oki et al. (1999) continued this line of application through the development of the topographically corrected integrating pathways for routing models, TRIP (Total Runoff Integrating Pathways). Arora and Boer (1999) implemented a time evolving velocity that depends on the amount of runoff generated in the GCM land grid, using Mannings equation to estimate flow velocities for a river channel with a rectangular section. At Meteo France, Decharme et al. (2008, 2011) used the TRIP approach to implement a flood routing scheme into the ISBA (Interaction Soil Biosphere Atmosphere)-TRIP CHS. The scheme accounts explicitly for the river routing, precipitation interception by the floodplains, the direct evaporation from the free water surface, and the possible re-infiltration into the soil in flooded areas. The regional and global evaluations of this scheme at a  $1^\circ$  spatial resolution emphasized the importance of floodplains in the continental part of the hydrologic cycle, through generally improved river discharges and a non-negligible increase of evapotranspiration (Decharme et al., 2011). A groundwater reservoir was also added to the routing scheme in order to take into account the temporary storage capacity of deeper soil layers and their potential

feedbacks on surface waters.

## 1.6 Evaluation of CHSs : from local to global scale

Observation data describing the water dynamics and storage variations are useful to evaluate CHSs simulated diagnostics. In this aim, in-situ data have been extensively used, but are limited by their time and spatial coverage. To compensate for this lack, remote sensing technologies have been developed and continually improved. This part aims at describing the general methods used for evaluation of LSMs, and the available datasets for this evaluation. In the framework of the present work, which focuses on the hydrologic processes of the Niger basin, the datasets used for the evaluation of the continental hydrology simulated by CHSs will be more detailed.

### 1.6.1 Local evaluation

The general evaluation of LSM processes is done over small areas using local in situ datasets. To this end, many local datasets have been collected, consisting in turbulent, conductive and radiative fluxes, soil humidity, snow cover, vegetation density (André et al. 1986, Mahfouf et Noilhan 1991, Braud et al. 1993, Giordani et al. 1996, Goutorbe et al. 1997, Delire et al. 1997, Calvet et al. 1998, Pellenq 2002, etc., Lebel et al., 2009). The need for insitu datasets has given rise to international measurement campaigns. Recently, the AMMA-CATCH project focused on measuring and understanding land surface properties and processes in West Africa (Lebel et al., 2009). The observing system was based on three intensively instrumented mesoscale sites in Mali, Niger and Benin that sample across the 100-1300 mm/annum rainfall gradient of the Sahel, Sudan and North- Guinean bioclimatic zones. These measurements allowed a better understanding of the role of surface processes in relation to surface-boundary layer interactions, vegetation dynamics at seasonal to decadal time-scales, diurnal cycles of land surface fluxes (Gounou et al., 2012), the role of soil moisture in initiating convection (Taylor et al., 2011), and meso to regional scale water balance (Peugeot et al., 2011; Bock et al., 2011). For hydrology, discharge datasets are used to evaluate the runoff simulated by LSMs. Due to the recent concerns about pressure on water resources related to climate change, the need to represent deeper soil layers (groundwaters and aquifers) in LSMs has grown in modelers community (Decharme et al., 2008, 2010; Vergnes et al., 2012). In the field, several methods have been set up to collect datasets about groundwater recharge (Scanlon et al., 2006; Vouillamoz et al., 2007; Seguis et al., 2011). However, if

these datasets are useful for calibrating the models at local scale, because of the high temporal and spatial variability of land surface properties and processes, their use for global applications is limited.

### 1.6.2 Regional and global evaluation : Classic methods.

In the recent years, remote sensing technologies have been developed to compensate for the lack of spatially distributed datasets. These technologies generally provide a large coverage which is more appropriate for global applications, especially in areas where in-situ data are scarce. Such areas are generally non-industrialized regions with poor infrastructure and geopolitical issues, such as most of the African continent or part of the Arctic (Alsdorf et al., 2007). Applications of satellite remote sensing give a promising perspective for improvement, from a point scale parametrisation to a much more spatially oriented perspective on land surface and hydrological variables and processes.

There is a variety of remote sensing technologies, each of them providing useful tools for LS modeling, depending on the variable one wants to observe and of the temporal and spatial scale of the problem (Stisen, 2007). Geostationary satellites can capture detailed diurnal variations in rainfall, temperature and radiation, hereby providing valuable information on the energy and water fluxes at the surface. These data are appreciable for short time scale analysis. Other surface variables, such as leaf area index (LAI) and albedo are generally better described using polar orbiting sensors, which have higher spatial resolution and are subject to less angular effects (Stisen, 2007), but have a lower temporal sampling. Combining the benefits of both geostationary and polar orbiting data in LSMs is a useful way of getting most information out of remote sensing data. This is due to the fact that surface fluxes depend on both highly dynamic climate variables (temperature, radiation and rainfall) and less dynamic surface parameters (vegetation and LAI). Thermal infrared remote sensing can be used to estimate land surface temperature, which is a direct indicator of moisture status and evaporative state (Kustas et al., 1989). The disadvantage of using thermal infrared data is that it requires completely clear sky conditions due to the high sensitivity to clouds. Due to the highly dynamic nature of surface temperature, the methods based on remote sensing of surface temperature are always instantaneous. Other remote sensing techniques, such as the optical remote sensing of vegetation, require cloud free conditions. However, due to the low temporal variability of surface parameters, these can be estimated using temporal compositing methods. Rainfall and radiation can be estimated from remote sensing of the cloud properties and consequently do not require clear sky conditions (Adler et al., 2000; Milford et al., 1996).

For hydrologic applications, it is valuable for modelers to get information

about the continental water dynamics. Indeed, in situ discharge data, for example, give 1-dimensional information which quantifies water movement in a confined river channel, but does not give any information about the lateral dynamics of water. In more hydrologically complicated areas, the presence of wetlands and floodplains, which are three-spatial-dimension processes, cannot be adequately resolved using one-spatial-dimension observations (Alsdorf et al., 2007). In 2009, the Soil Moisture and Ocean Salinity Mission (SMOS) satellite was launched, as part of a joint CNES-ESA project aiming at estimating global soil moisture and ocean salinity from space (Kerr et al., 2000, 2010). Soil moisture is a key variable for hydrological modeling since it controls surface energy fluxes, but also informs about land water storage in the surface first few centimeters. The earth's time-variable gravity field from the Gravity Recovery and Climate Experiment (GRACE; Tapley et al. 2004) mission launched in 2002 provides water storage evolution estimates and allows direct evaluation of Total Water Storage (TWS) simulated by LSMs (Decharme et al., 2010; Grippa et al., 2011), although at a relatively coarse spatial resolution. If valuable improvements have been made in satellite remote sensing, the spatial extent and variability of wetlands, lakes, reservoirs and other water bodies are poorly documented globally. Yet, they strongly affect biogeochemical and trace gas fluxes between the land and the atmosphere but also the hydrological cycle of many large river basins and the freshwater transport to the ocean (Richey et al., 2002; Frey and Smith, 2007; Decharme et al., 2008). The French spatial Institute, CNES (Centre National d'Etudes Spatiales), in collaboration with the NASA (National Aeronautic and Space Administration), recently proposed a satellite mission which will provide maps of surface water levels and extent, giving a tool for modelers to better understand and model three-dimensional spatial hydrological processes.

### **1.6.3 The future SWOT satellite mission**

The future Surface Water Ocean Topography (SWOT) satellite mission is a joint CNES-NASA project which will deliver maps of water surface elevation (WSE) with an unprecedented resolution of 100m. It will provide observations of rivers wider than 100 m and water surface areas above 250 x 250 m over continental surfaces between  $78^{\circ}S$  and  $78^{\circ}N$ . The launch of this satellite is tentatively planned for 2019. This satellite will be a usefull tool to observe and better understand the global freshwater dynamics, in particular for regions such as the Niger basin where water resources are limited and geopolitical issues restrict the exchange of hydrological data. The SWOT mission will benefit from the technical experience of two main previous missions, the SRTM (Shuttle Radar Topography Mission; Farr et al., 2007) and the WSOA instrument (Wide Swath Ocean Altimeter; Fu and Rodriguez, 2004). During the SRTM mission,

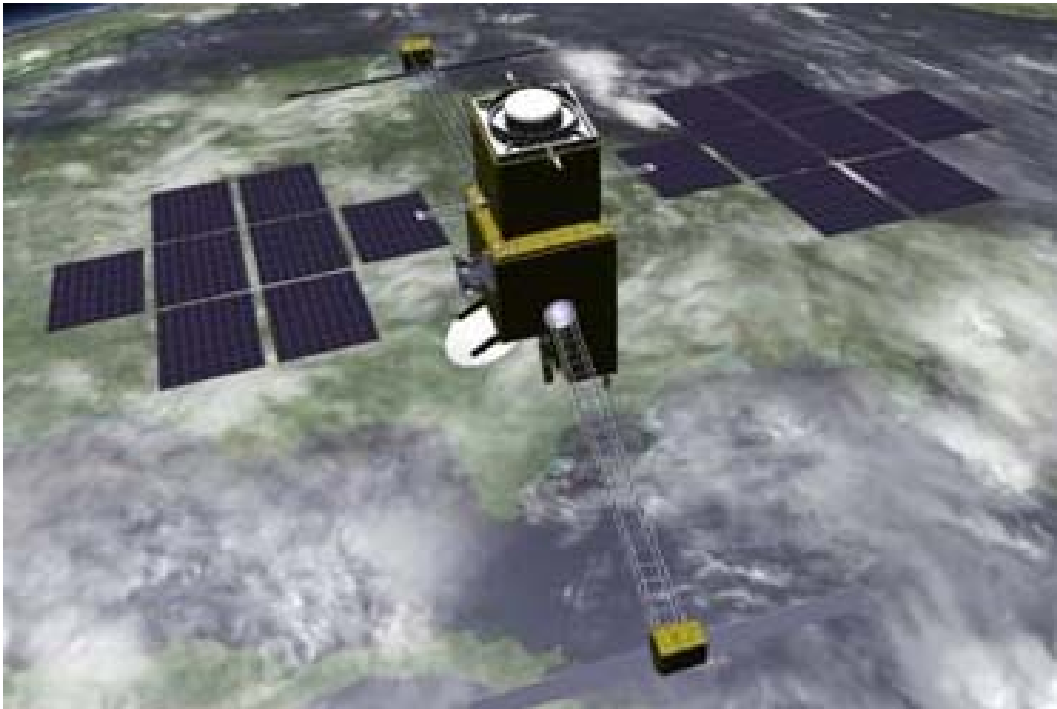


Figure 1.4: Artists rendition of the SWOT satellite in orbit.

in 2000, two interferometric radars were placed on the Endeavour spatial platform, at the extremities of two 10 m baselines. They allowed the measurement of surface topography with an appreciable precision (16m), coverage (80% of continental surfaces), and resolution (90m). Interest needed in large swath altimetry was, at first, an initiative from the hydrologic science community, with the Water Elevation Recovery mission (Water Elevation Recovery; Mognard et al., 2005) which aimed at measuring continental water elevations. The Water Elevation Recovery mission was renamed WATER-HM (Water And Terrestrial Elevation Recovery - Hydrosphere Mapper ; Alsdorf et al., 2007), after oceanographers also joined the project. In 2007, the mission was selected by NASA, as one of the 15 Earth Observation satellites which will be developed within 10 years. On this occasion, the satellite was renamed SWOT (Surface Water Ocean Topography).

The main advantage of SWOT is the use of an interferometric radar Karin (Ka-band Radar Interferometer) in a Ka band (i.e. frequency of 35,6 GHz), which was developed at JPL. Conventional altimeters use ranging measurements, which require additional a priori assumptions (e.g., the first return is from the nadir direction) in order to obtain heights and location measurements. In addition, because altimeters are nadir looking instruments, they can only provide along-track one-dimensional measurements. These limitations of radar

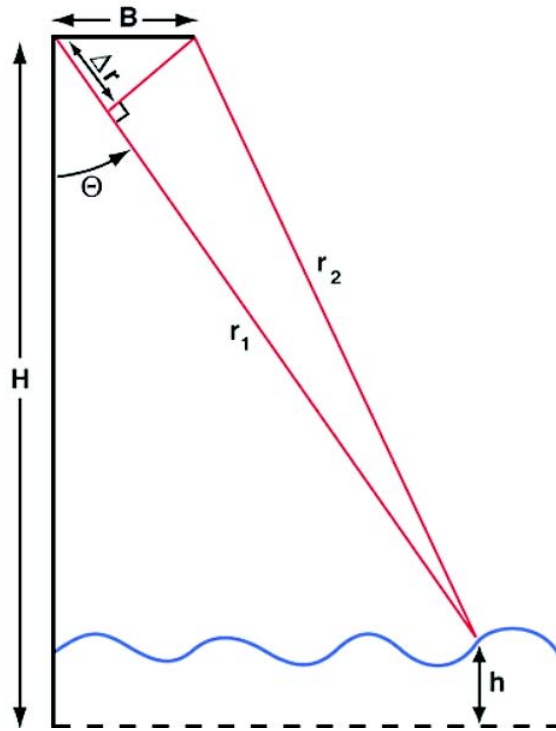


Figure 1.5: Interferometric method concept.

altimetry can be overcome by using a technique called synthetic aperture radar interferometry (IFSAR). Radar interferometry determines the location of the target by measuring the relative delay (or phase shift) between the signals from two antennas that are separated by a baseline distance (see Fig.1.5). Using geometry, the location of the range measurements in the plane of the observation can be determined. The measurement triangle is made up of the baseline  $B$ , and the range to the two antennas,  $r_1$  and  $r_2$ . The baseline is known by construction and knowledge of the spacecraft attitude. The range  $r_1$  is determined by the system timing measurements. The range difference between  $r_1$  and  $r_2$  is determined by measuring the relative phase shift  $\gamma$  between the two signals. The phase shift is related to the range difference  $\delta_r$  by the equation  $\gamma = 2\pi\delta_r/\lambda$ , where  $\lambda$  is the radar wavelength. The additional information required for determining the measurement location, the incidence angle, can be obtained from the range difference by means of the relationship  $\gamma = 2\pi B \sin(\theta)/\lambda$ . Given these measurements, the height  $h$  above a reference plane can be obtained using the equation  $h = H - r_1 \cos(\theta)$  (Lu et al., 2007).

The formulas given here are appropriate for mapping heights relative a reference plane (more details about mapping heights relative to a curve surface are given by Rosen et al., 2000). The spatial resolution is dependent on the bandwidth (the range resolution in the cross-track direction) and antenna size (the azimuth resolution in the alongtrack direction). According to the SWOT scientific requirements (Rodriguez, 2009), the vertical precision of height measurements will be about  $10\text{cm}$  for a  $1\text{km}^2$  pixel. The error of surface water extent estimation will be less than 20% of the considered surface. The SWOT satellite will provide 2 dimensional maps of land waters, with global coverage, which will provide valuable information about hydrological three-spatial-dimension phenomenon, such as wetlands and floodplains. This was not possible with previous altimeters (TOPEX/POSEIDON, JASON 1 and 2). The nominal SWOT lifetime is 3 years (aiming 5 years). The first months period will be a calibration/validation period, followed by the nominal phase. The nominal phase consists of 22-day repetitivity orbits, which represent a complete global coverage for a  $140\text{km}$  swath. It will have a  $970\text{km}$  altitude and a  $78^\circ$  angular position.

Land water storage and the associated fresh water fluxes or discharge play a fundamental role in the global water cycle. However, measurements of the land water storage and fluxes are scarcely available at regional to global scales, particularly in closed basins. This situation is generally worse in regions where anthropogenic pressures on the already limited water resources is high, such as the Sahelian zone of West Africa (Redelsperger et al., 2006). A better understanding and monitoring of hydrological processes are needed to improve food security and socio-economic stability in such regions, especially because of the uncertainty in the future evolution of water resources in response to anticipated global climate change. But instead of increasing observational networks in response to such needs, the coverage in such regions (and in general, globally) is currently decreasing. River routing parameterizations use very simple assumptions, largely owing to parameter uncertainty and a lack of high quality spatially distributed evaluation data (such as discharge) over large parts of the globe. Moreover, it has been shown by inter-comparing a large ensemble of independent LSMs driven by realistic atmospheric forcing that on a global scale, the land surface flux with the highest uncertainty (least agreement defined as the largest inter-model variability) is the runoff (Dirmeyer et al., 2006). Indeed, once such a parameterization has been transferred to the AGCM or NWP model, it is applied over the entire globe (even for basins where offline precipitation estimates might have been poor or where discharge for evaluation was not available). The seemingly logical choice to address this issue is to use remotely sensed data in offline mode. Indeed, spaceborne platforms can be used to estimate certain hydrological variables to within a reasonable accuracy (Alsdorf et al., 2007). However, current monitoring strategies do not give complete global coverage of these variables. SWOT would

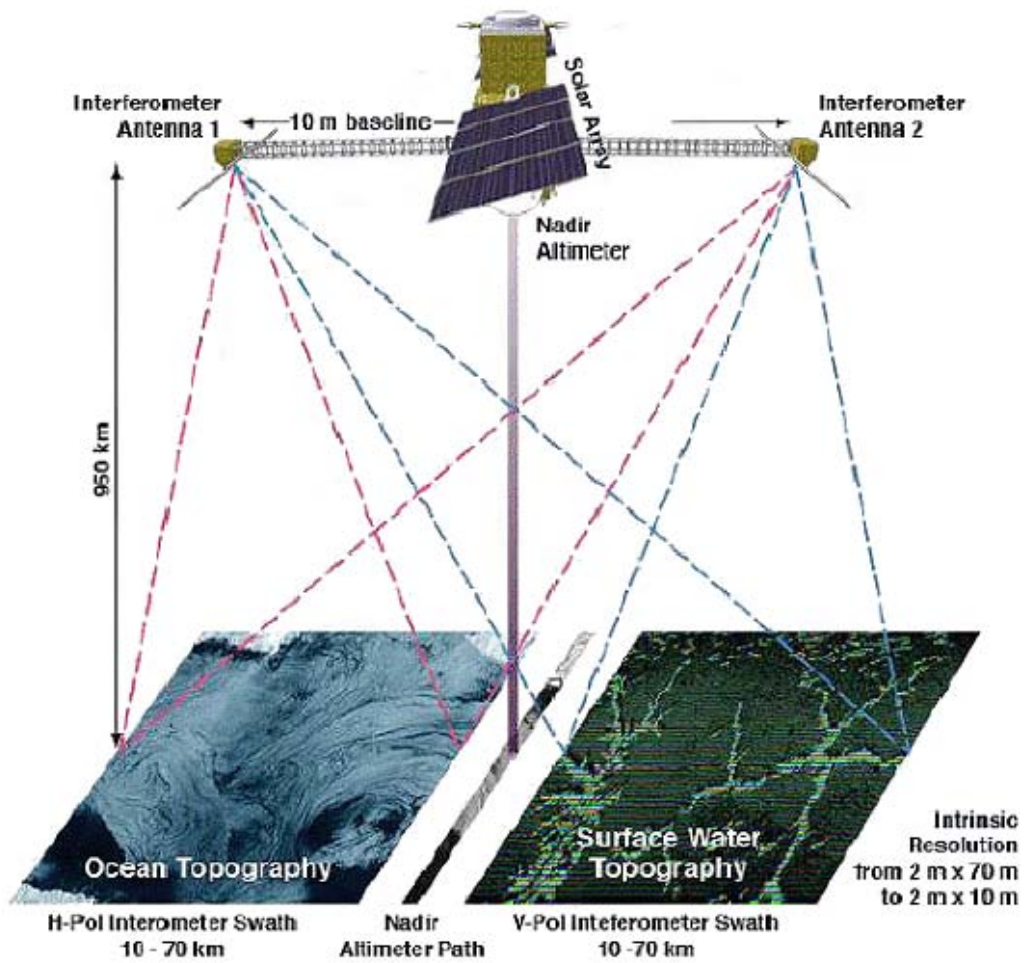


Figure 1.6: SWOT satellite concept. It is made of two interferometric radars placed at the extremities of two 10 m baselines. The interferometers swaths are 60km large each. A nadir altimeter is situated in the middle of the system.

provide the first possibility to improve the river routing, the representation of lakes and hydrological model parameterizations within LSMs at a relatively high spatial resolution over all of the globe using a data assimilation strategy. Tendencies in water height change and spatial coverage could be directly assimilated into river routing and floodplain parameterizations, which would then result in improved estimates of discharge on a global scale. The more realistic estimates of river routing could then be used to improve LSM runoff parameterizations and, by extension, estimates of evaporation.

A realistic simulation of the hydrological impacts of seasonal climate anomalies and global warming by AGCMs will be critical for ecology and human activities. While the continental land component of such models continue to improve through incorporation of better soils, topography, land use and land cover maps, not to mention advances in soil physics, cold-season processes and the representation of the Carbon cycle, their representations of the surface water balance are still greatly in error in large part because of the absence of a coherent observational basis for quantifying river discharge and surface water storage globally (Alsdorf et al., 2007). The improved representation of global scale hydrology will not only have an impact on the estimates of freshwater discharge into the oceans, but it also has the potential to improve the estimate of continental evaporation and therefore have an influence on the atmospheric circulation and precipitation simulated by such models. Such improvements would be useful not only for climate scenarios, but also for seasonal weather prediction and water resource management.

## **1.7 Modeling of the Niger river basin : A scientific, social and economic challenge.**

During the 1970s and 1980s, West Africa has faced extreme climate variations with extended drought conditions. Of particular importance is the Niger basin, since it traverses a large part of the Sahel and is thus a critical source of water for an ever-increasing local population in this semi arid region. However, the understanding of the hydrological processes over this basin is currently limited by the lack of spatially distributed surface water and discharge measurements. This chapter gives a review of the main characteristics of the Niger basin.

### **1.7.1 Geo-demographical environment of the Niger river Basin**

The Niger River Basin is located between the meridians of  $11^{\circ}30'$  west and  $15^{\circ}$  east, from Guinea to Chad; and between the parallels of  $22^{\circ}$  north and  $5^{\circ}$  north,

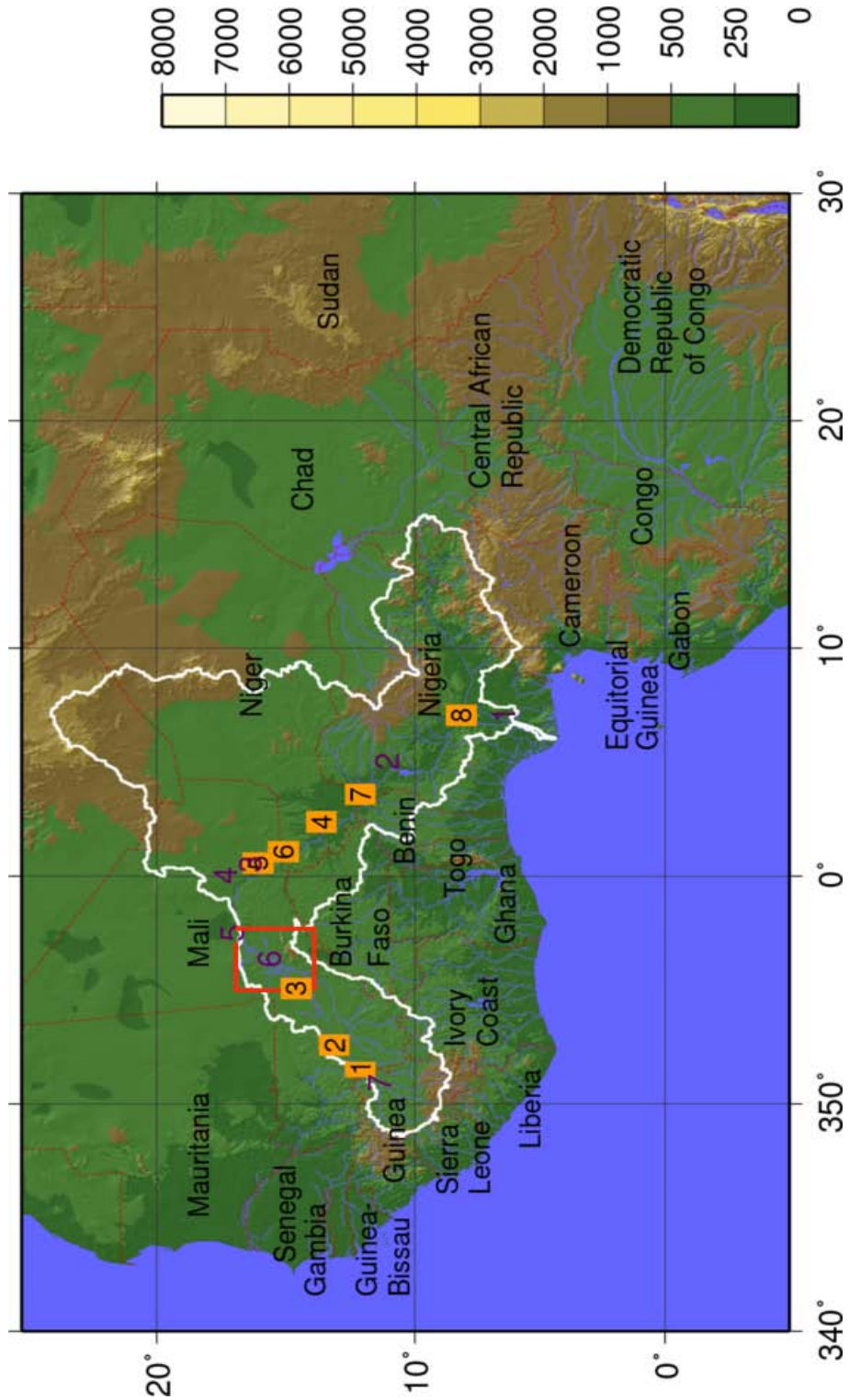


Figure 1.7: The Niger river basin. The spatial resolution is  $0.5^\circ \times 0.5^\circ$ . The white contour is the delimitation of the Niger basin. The yellow squares are the stations where discharge observations are available: (1) Banankoro, (2) Koulikoro, (3) Ke Macina, (4) Niamey, (5) Ansongo, (6) Kandadji, (7) Malanville (8) Lokoja. The purple boxes represent the sites where satellite-based height change observations are used for evaluation. The legend indicates the terrain elevations from GTOPO30 (m). The red square indicates the inner delta region.

extending from the Hoggar Mountains to the Gulf of Guinea. The Basin extends 3,000 kilometers from east to west and 2,000 kilometers from north to south. Originating in the Guinean highlands within the regions of Haute Guinée and Guinée Forestière in the Fouta Djallon Massif, the Niger River is the third-longest river in Africa (4,200 kilometers), after the Nile and the Congo. It ends in Nigeria, discharging through a massive delta into the Gulf of Guinea within the Atlantic Ocean. On its way through Mali, it traverses a vast, spreading floodplain called the Inland Delta. The Inland Delta, averaging 73,000 square kilometers, dissipates a significant proportion of the flow of the river through absorption and evaporation (Andersen et al., 2005). From the headwaters to the Niger Delta and taking into account the hydrologically active area, the Basin has an average area of about 1.5 million square kilometers. The Niger river is shared by nine countries in West and Central Africa according to the following approximate percentage (Andersen et. al, 2005) : Benin (2.5 percent), Burkina Faso (3.9 percent), Cameroon (4.4 percent), Chad (1.0 percent), Cote d'Ivoire (1.2 percent), Guinea (4.6 percent), Mali (30.3 percent), Niger (23.8 percent), and Nigeria (28.3 percent). The population living in the Basin is estimated at 100 million, with an average growth rate of 3 percent per year. Table 1. summarizes the socio-economic statistical characteristics of the Niger basin countries. As shown in this table, the socio-economic situation of the Basin countries relies on many river-related activities (agricultural productions, freshwater fishing and livestock farming). Also, the availability of water resources is a capital issue for the economic and social development of the basin population. The next section gives a brief review of the climatic conditions of the West African region, focusing on the rainfall anomalies observed during the last decades, and their impact on the Niger river flow and water availability.

### **1.7.2 Climatic conditions, rainfall variability and water resources availability**

The complexity of the Niger basin is related to the fact that it traverses very different climatic zones, from the tropical humid Guinean coast where it generally rains every month of the year, to the desertic Saharian region with very little precipitation. In between, the river flows through the Soudanian and the Sahelian zones. The Soudanian zone is located between 7° – 10°N, and is predominantly covered by savanna or plains, with a mixture of tropical or subtropical grasses and woodlands. The Sahel is a semi-arid region with sparse vegetation. The basin is characterized by two distinct annual seasons : a wet season and a dry season. The region is generally warm, although the high mountains and Sahara desert can experience relatively extreme temperature ranges. The climatic conditions of the Niger basin are closely related to the movement of air masses of the

<i>Parameter</i>	<i>Benin</i>	<i>Burkina Faso</i>	<i>Cameroon</i>	<i>Chad</i>	<i>Côte d'Ivoire</i>	<i>Guinea</i>	<i>Mali</i>	<i>Niger</i>	<i>Nigeria</i>
Total area (millions km <sup>2</sup> )	0.114	0.274	0.475	1.284	0.322	0.246	1.24	1.27	0.924
Population (millions)	6.75	10.7	14.9	8.3	15.4	7.1	10.6	10.7	114
Population increase (%/year)	3.1	2.3	2.3	3.2	2.1	3.1	2.2	3.5	2.7
Urban population (%)	39.9	18	48.1	23.5	45.8	32.1	29.4	20.1	43.1
GDP/person (US\$)	933	965	1,573	850	1,653	1,934	753	753	853
Estimated population 2025 (millions)	11.5	21.7	27.8	13.4	29.9	14	22.7	19.2	235
Agricultural production (1,000 tons)									
Rice	36	89	65	100	1,162	750	590	54	3,400
Peanuts	—	205	160	372	144	182	140	—	2,783
Corn	662	378	600–850	173	573	89	341	5	5,127
Millet	29	979	71	366	65	10	641	2,391	5,956
Sugar cane	—	—	—	280	—	220	303	174	675
Cotton	150	136	75–79	103	130	16	218	—	55
Livestock (head, millions)									
Beef	1.35	4.55	5.90	5.58	1.35	2.37	6.06	2.17	19.8
Sheep	0.63	6.35	3.80	2.43	1.39	0.69	6.0	4.31	20.5
Freshwater fishing (1,000 tons)	44	—	89	6	68	103	108	6	383
Within Niger Basin									
Hydrologically active									
Area (10 <sup>3</sup> km <sup>2</sup> ) <sup>a</sup>	37.50	58.5	66.0	15.0	18.0	69.0	454.50	357.0	424.50
(%)	2.50	3.90	4.40	1.0	1.20	4.60	30.30	23.80	28.30
Population (millions)	1.95	2.12	4.46	0.08	0.80	1.60	7.80	8.30	67.60
(%)	2.10	2.20	4.70	0.10	0.80	1.70	8.20	8.80	71.40

*Source:* Data are primarily based on recent (2004) national multisector studies on the assessment of opportunities and constraints to development of each country's portion of the Niger River Basin, prepared with support from the World Bank (Cameroon, Chad, Guinea, and Nigeria) and the Canadian International Development Agency (CIDA) (Benin, Burkina Faso, Côte d'Ivoire, Mali, and Niger).

*Note:* — = not available. Values in italics relate to data involving the entire country; data in plain text relate to the part of the country located in the Niger River Basin.

a. [http://www.riob-info.org/gwp/PP\\_Niger.pdf](http://www.riob-info.org/gwp/PP_Niger.pdf). The hydrologically active area of the Niger River Basin is 1.5 million square kilometers.

Table 1.1: Socioeconomic statistical characteristics of the Niger river basin countries (from Andersen et al., 2005).

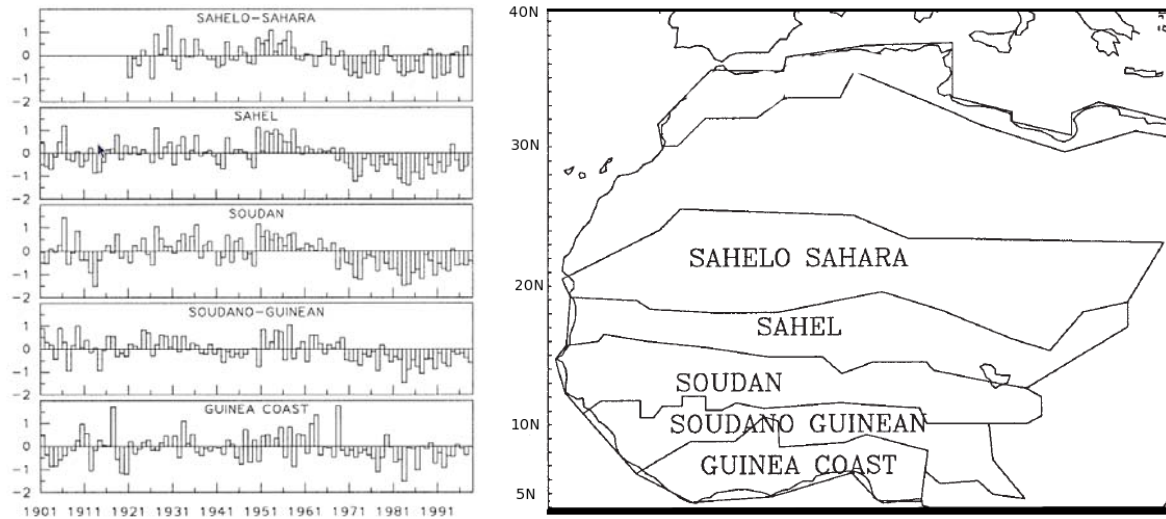


Figure 1.8: Rainfall fluctuations 1901 to 1998, expressed as a regionally averaged standard deviation (departure from the long-term mean divided by the standard deviation). Locations of the regions are indicated in map at the right (From Nicholson, 2001).

Intertropical Convergence Zone (ITCZ), north and south of the equator. During summer, (from June to September), the solar radiation intensifies and heats the surface. Following the excursion of the sun, the monsoon develops over WA, bringing the ITCZ northward, with humid and unstable maritime equatorial air and relatively cool temperatures. The monsoon is generally longer and stronger in the Southern part of the basin, along the Guinean coast. During the dry season (covering winter and spring from December to May), the North-easterly Harmattan wind brings hot, dry air and high temperatures. Annual rainfall has a strong spatial variability ranging from less than 100 mm in the Sahel to more than 1200mm on the Guinean coast (Andersen et al., 2005). The basin is characterized by relatively low orography except few mountains ranges upstream of the river, in the Guinean highlands.

In the last few decades, West Africa endured extreme rainfall anomalies, with severe droughts during the 1970's and the 1990's (Nicholson, 1980, 2001; Lebel et al., 2009, Kasei et al., 2010). Nicholson calculated the regional rainfall fluctuations (as the departure from long term mean rainfall divided by the standard deviation) over the period 1901-1991 and showed a general decline in rainfall in Western Africa from 1968 to 1991 (Fig.1.8). A reduction of about 25% of the annual rainfall was found in the 1968-1989 period compared to the 1950-1967 mean at Niamey (Le Barbe and Lebel, 1997).

Rainfall anomalies generally result in runoff and river discharge anomalies. Indeed, Lebel et al. (2005) observed that, over the Niamey catchment, a relative precipitation anomaly would lead to a relative discharge anomaly at least twice as large at the Niamey gauging station. This close relationship between annual rainfall and annual runoff was generalized over the West African basin by d'Orgeval and Polcher (2007). Olivry (1998) observed a long-term relationship between rainfall and river flow, which is greatly influenced by the groundwater baseflow. Indeed, after several dry years, the groundwater base flow is reduced, leading to a lower river flow. The return to a 'standard' river flow requires the replenishment of groundwaters, which is possible only after several wet years. This return is referred by Olivry as the 'memory of the river'. This observation has led to an increasing number of studies and measurements of aquifer recharge in West Africa by hydrodynamics or geochemical methods (Leblanc et al., 2007; Leduc et al., 2000; Lutz et al., 2009; Huneau et al., 2011; Vouillamoz et al., 2007; Le Gal La Salle et al., 2001; Seguis et al., 2011). Most of the time, these measurements are local and not easy for use in regional hydrologic simulations due to the assumed spatial variability of groundwater recharge. More recent studies have shown the impact of land use changes, (deforestation and increase of cultivable areas), on the annual discharge of the Niger river (Descroix et al., 2008; D'Orgeval and Polcher, 2007; Fritsch, 1990; Snelder and Bryan, 1995; Bergkamp, 1998; Casenave and Valentin, 1992). Indeed, in the past decades, land use changes have increased the surface runoff resulting in two main phenomenon. In exoreic areas, the rise of surface runoff contributes to more water in the river, resulting in an enhanced river flow. In endoreic areas, the runoff contributes to the formation of new ponds and lakes which infiltrate and supply the groundwater. The cycle of the Niger river is then influenced by many natural or anthropogenic factors which makes it difficult to get a good prediction of water availability in the future.

According to the Intergovernmental Panel on Climate Change (IPCC), extreme events, such as droughts, heat waves and heavy precipitation will become more frequent with climate change (Kasei et al., 2010), which can have devastating consequences for the population (loss of livestock and crop production provoking food shortage and hunger, disease epidemics, population movement, etc...). In July 2012, half a year's worth of rain fell in the Dosso Region (140km from Niamey) in just 24 hours destroying thousands of homes and leaving at least 75.000 people homeless. All of these people were affected by the Sahel Food Crisis and many of their farms (along with the 2012 crops) were destroyed. Two weeks later, Niamey was also hit by flash flooding. The Non-Governmental Organisation, 'Plan Ireland', reported the consternation and impotence of the population faced with such an event : 'In 30 years, the river has never come so far and we have never had such flooding' (from <http://reliefweb.int/>).

Also, the pressure on water resources due to climate variability and its impact on food production, can act as a source of international conflicts in WA. In 1998, low water levels in the Akosombo dam in Ghana caused an energy crisis, which many blamed on Burkina Faso's enhanced use of water resources upstream of the Volta basin (Kasei et al., 2010). Yet, such extreme situations could be avoided, or at least, their impact could be reduced, with a better prediction of the rainy season and more detailed water impact studies at seasonal and regional time scales. Of particular interest for such studies, is the inland delta, situated in Mali, which has an average spatial extent of 75.000 square kilometers, which dissipates a significant proportion of the flow of the river through evaporation and to a lesser extent, infiltration. Indeed, the inland delta is annually flooded, enhancing evaporation over the wetlands. This evaporation impacts the atmospheric dynamics, but also, the water cycle of the basin through the reduction of the river flow. Thus, the inland delta is a complex zone of the Niger basin, for which all of the main processes must be correctly represented in LSMs. The next section focuses on the inland delta and its dynamics.

### **1.7.3 The inland delta, a complex region for hydrologic modeling.**

The inland delta region, with its system of lakes on both banks of the Niger river, is located between the latitudes  $13^{\circ}N - 16^{\circ}N$  and the longitudes  $3^{\circ}W - 4^{\circ}W$ . It extends downstream from the hydrological stations at KeMacina on the Niger river to the station at Dire in the North. It is both supplied in runoff by the Niger and the Bani rivers. The hydrological characteristics of the inland delta area are largely dependant on two aspects (Andersen et al., 2005) :

- exogenous runoff conditions, with most of the water resources coming from upstream areas, with higher rainfall;
- Morphological and climatological conditions specific to the inland delta, affecting runoff (water loss, flooding) and water balance (evaporation, infiltration).

The inland delta is subject to significant annual variability, with large flooding during summer (see Fig.1.9). The average flooded area over the period 1955-1996, estimated by Mahé et al.(2009), using a method based on the hydrological balance, is assumed to be about  $24.000 km^2$ . The Inland Delta storage capacity varies from 7 cubic kms to 70 cubic kms. Through this delta, a significant amount of water is lost ( approximately 40% ) via evaporation, and in a lesser proportion, infiltration. This relative loss represents an annual volume loss ranging from 7 cubic kms for a dry period to 25 cubic kms for wet years (Andersen et al.,

2005). The average input and output discharges are approximately 1490 and 900  $m^3.s^{-1}$  respectively, over the period 1955-1996 (Mahé et al., 2009). The analysis of three typical years (wet, average and dry respectively in 1954, 1968 and 1985) by Andersen et al., showed that the water loss through the delta is positively correlated with the amount of rainfall over the basin.

Fig.1.10 shows the difference between the annual volume of water in the inland delta from Ké Macina to the outlet at Diré. In an average year, 60 cubic kilometers arrive from upstream and 30 cubic kilometers are lost by evapotranspiration, corresponding to the extent of the flooded area in this reach, which can vary from 5,000 square kilometers to more than 30,000 square kilometers from the driest to the wettest years.

Another characteristic of the inland delta, is that the flooding occurring in this zone impacts the discharge downstream from the delta. Fig.1.11 shows the observed in situ discharge in Koulikoro, situated upstream from the inland delta, and in Niamey situated downstream from the delta (see Fig.1.7 for localizations). These observed data have been provided by the Authorithé du Bassin du Niger (ABN) as part of their Niger-HYCOS Project. While the discharge in Koulikoro presents a one-peak pattern, caused by the local seasonal rainfall, at Niamey, the maximum flows are usually twofold: a first wet seasonal peak flow and an upstream dry seasonal peak flow. The first high-water discharge, occurs soon after the local rainy season in September while a second peak is observed in December with the arrival of the delayed flood from upstream (Andersen et al., 2005). May and June are the low-water months. It should also be noted that the difference of discharge amplitude between Niamey and Koulikoro (in Koulikoro, the discharge is more than twice higher than in Niamey) is due to the loss of water in the inland delta. These characteristics of the delta will be investigated further in Chapter 3.

The diverse processes occurring in the inland delta have an impact on the water and energy budget of the basin, but also influence the water storage and discharge, locally and upstream from the delta. For these reasons, those processes, such as flooding and evaporation from floodplains, must be considered in LSMs if one wants a consistent representation of the hydrology and hydrodynamics of the Niger basin and to properly account for potential atmospheric interactions.

#### **1.7.4 The African Monsoon Multidisciplinary Analysis (AMMA) program**

The dramatic changes in precipitation observed in West Africa during the latter decades of the 20<sup>th</sup> century, as well as the large climate change projection uncertainties, were major motivations for the AMMA program (<http://www.amma->

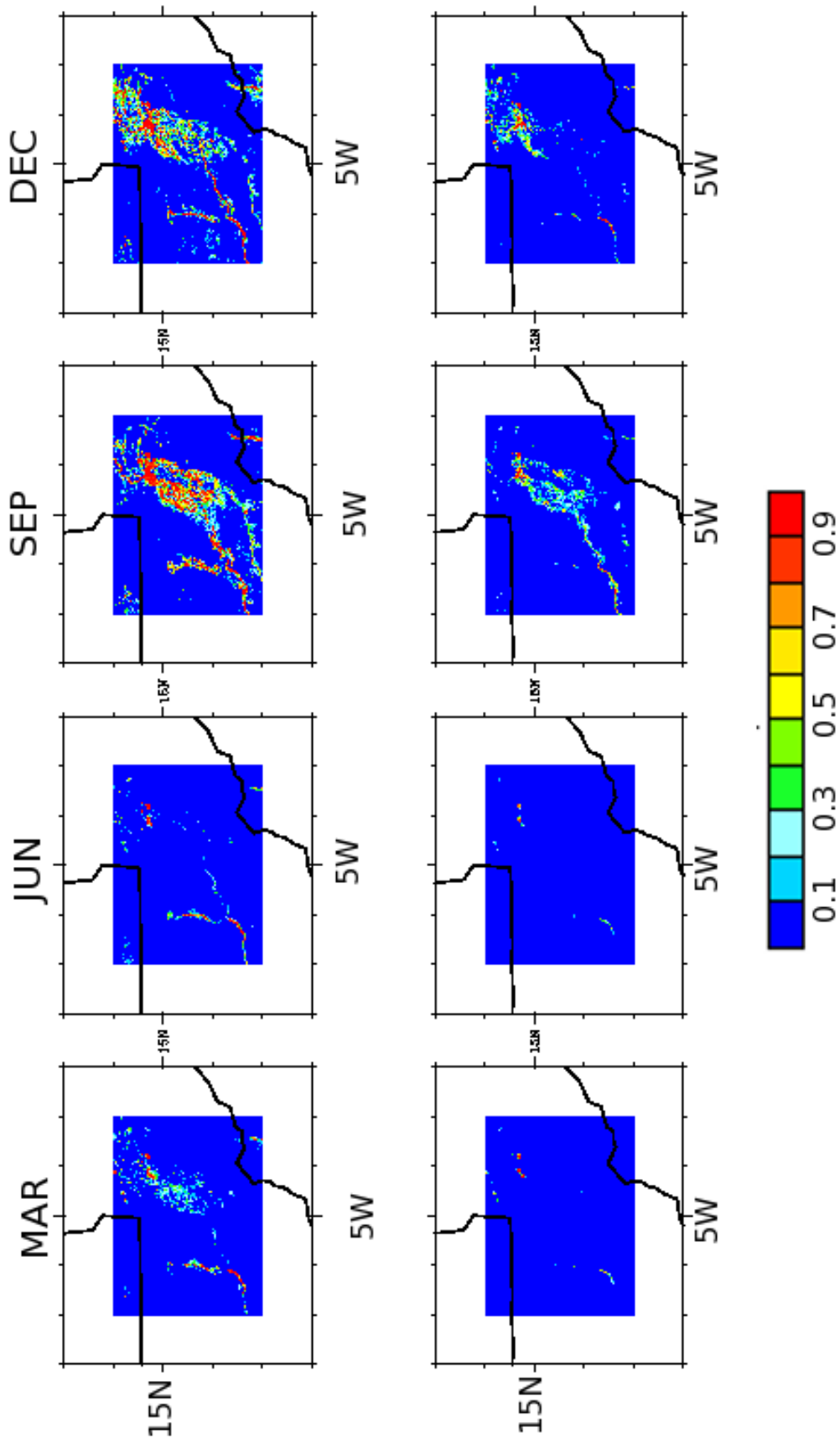


Figure 1.9: Flooded zones derived from the MODIS satellite mission ( the datasets are issued from J.F. Crétaux, LEGOS, see Part 3.5 for more details).

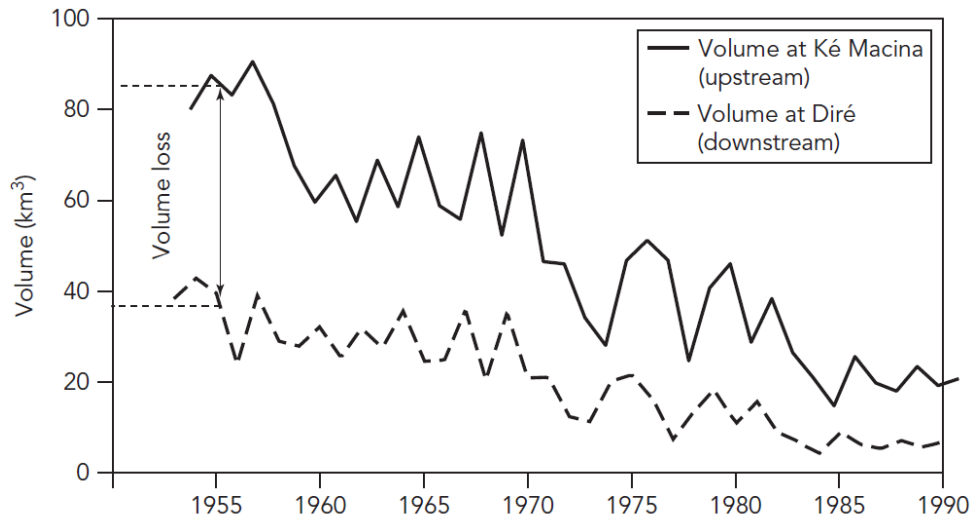


Figure 1.10: Evolution of the yearly volume loss in the Inland delta from 1955 to 1990 (from Andersen et al., 2005).

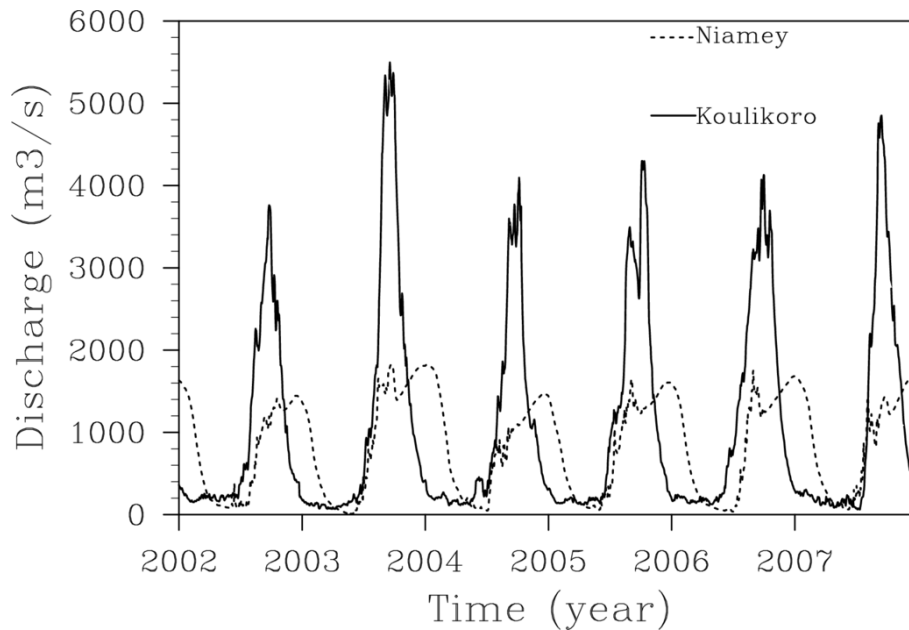


Figure 1.11: Time evolution of the observed discharge in Koulikoro (full line) and in Niamey (dashed line) from 2002 to 2007. The datasets have been provided by the Autorité du Bassin du Niger (ABN) as part of their Niger-HYCOS project ([www.whycos.org](http://www.whycos.org)).

international.org). This project, launched in 2002, was motivated by the need to determinate the mechanisms responsible for the decline in rainfall over the West African region. To attain this goal, all of the processes involved in the WAM formation, variability and persistence have been investigated in AMMA. This international program gathered scientists from more than 40 organisations from Europe and Africa. As a major outcome of the project, it is hoped that the improvement of climate and weather forecasts will enable a better management of water resources, food security and public health.

The monsoon system involves diverse interactions between the ocean, the land surface and the atmosphere. Studying these processes over a wide range of scales from micro to global scales will lead to a better understanding of the monsoon system. A number of issues are still not well understood, notably the mechanisms involved in the onset of the monsoon, and the timing of retreat. Factors involved in the triggering, maintenance and decay of convective systems have also been studied, and continue to be the subject of ongoing research. A better understanding of the water cycle in WA will help to improve our understanding of the variability of the monsoon from diurnal to seasonal time periods. It is known that aerosol optical thickness can be particularly high over the region, but its precise role in the monsoon system is only now being explored (Kocha et al., 2012). Finally, the program aims at understanding the interactions between the monsoon and the global climate from a physical and chemical perspective in order to increase our confidence in the predicted climate over the Sahelian region.

The field campaign aimed at observing the atmosphere, the ocean, the land surface, and their interactions at different space and time scales ( Lebel et al., 2010 ). The Long term Observing Period (LOP) is concerned with observations of interannual to decadal variability of the WAM. It was operated from 2002 to 2010 over the three main mesosites with enhanced measures of rainfall amounts and surface properties. The Enhanced Observing Period (EOP) was operated over the period 2005-2007, and aimed at documenting the annual cycle of the surface and atmospheric conditions. Extra radiosoundings were launched along the meridional transect, enhanced surface measurements were carried out, ground-based instruments (radars, profilers) were operated at different sites. In addition, oceanic measurements were done on research vessels in the Gulf of Guinea. The Special Observing Periods (SOP) were devoted to detailed observations of processes taking place at key stages of the WAM with high temporal and spatial resolutions. They were dedicated to the intensive observation of the meridional transect and a large range of instruments was deployed (for further details, see Redelsperger et al., 2006).



# The ISBA-TRIP Continental Hydrologic System

---

## Contents

---

<b>2.1</b>	<b>The ISBA force restore land surface model . . . . .</b>	<b>55</b>
2.1.1	Pronostic variables and atmospheric forcing . . . . .	56
2.1.2	ISBA input parameters . . . . .	59
2.1.3	Energy budget . . . . .	62
2.1.4	Water budget . . . . .	62
2.1.5	Evapotranspiration . . . . .	63
2.1.6	Hydrology . . . . .	63
<b>2.2</b>	<b>The TRIP routing model . . . . .</b>	<b>66</b>
2.2.1	Governing equations . . . . .	66
2.2.2	River discharge and groundwater outflow . . . . .	67
2.2.3	The flooding scheme . . . . .	69

---

## 2.1 The ISBA force restore land surface model

As ISBA was designed for meteorological models, it represents a compromise between being a relatively simple scheme, and describing the most important components of land surface processes. The physics are simple and based on the bucket approach. The simplicity of the scheme is achieved by the calibration of several important coefficients with more sophisticated models and experimental data (Noilhan and Mahfouf, 1996). The scheme includes the treatment of soil heat and water flow, water interception by vegetation, aerodynamic transfer processes in the atmospheric surface layer, and a simplified treatment of radiation. The scheme uses the force restore model for soil heat and water content (Blackadar, 1976; Deardorff, 1977) and computes evaporation from soil, intercepted water and transpiration (Mahfouf and Noilhan, 1991). Other important

features of the scheme include a representation of gravitational drainage (Mahfouf and Noilhan, 1996), the introduction of soil/vegetation heat capacity, the inclusion of a snow scheme based on the force restore method (Douville et al., 1995), representation of the Dunne runoff using the VIC approach (Habets et al., 1999a), addition of a third soil layer (Boone et al., 1999), inclusion of subgrid hydrology (Habets et al., 1999b; Etchevers et al., 2001; Decharme and Douville, 2007), explicit representation of snow with a three-layer scheme (Boone and Etchevers, 2001). A multiple-soil-layer version, ISBA-DIF, has also been developed (Boone et al., 2000; Decharme et al., 2012), but the current study uses the 3-hydrological soil layer option. Finally, the ISBA-TRIP CHS has been developed to form a link between continental water and oceans or seas. Note that ISBA-TRIP is currently used in climate simulations, coupled to the GCM from Meteo-France, ARPEGE.

The ISBA model is run as part of the SURFEX (SURface EXternalisée for externalized surface) platform developed by Météo-France in cooperation with the scientific community ([www.cnrm.meteo.fr/surfex/](http://www.cnrm.meteo.fr/surfex/)). This platform is composed of various physical models for natural land surface, urbanized areas, lakes and oceans (see Fig.2.1). It also simulates chemistry and aerosols surface processes and can be used for assimilation of surface and near surface variables. SURFEX has its own initialisation procedures and can be used in a stand alone mode (used in this work) or coupled to an atmospheric model. In this study, only the natural land surface processes (ISBA) were activated as the Niger river basin is a mostly natural region with very little urbanization.

### 2.1.1 Pronostic variables and atmospheric forcing

In the ISBA-3L version (Fig.2.2), the soil is divided in 2 reservoirs : a root reservoir,  $w_2$ , of depth  $d_2$ , and a deep reservoir,  $w_3$  of thickness  $d_3 - d_2$ , where  $d_3$  is the total soil depth. A superficial layer,  $w_1$ , of depth  $d_1$ , is included in the root reservoir. The ISBA-3L model (without the snow scheme) calculates the temporal evolution of 6 pronostic variables representing the surface temperature  $T_S$ , the water content in the three soil layers,  $W_i$  and the water interception by the canopy,  $W_r$ . The ISBA model is run in offline mode and forced by atmospheric variables, listed in table 2.2. These atmospheric variables are generally available at time steps ranging from 30 minutes to 6 hours in offline mode. Note that the scheme includes a representation of the snow which will not be fully described here, as the simulations will focus on West Africa. However, details about the snow scheme can be found in several studies (Douville et al., 1995; Boone and Etchevers, 2001).

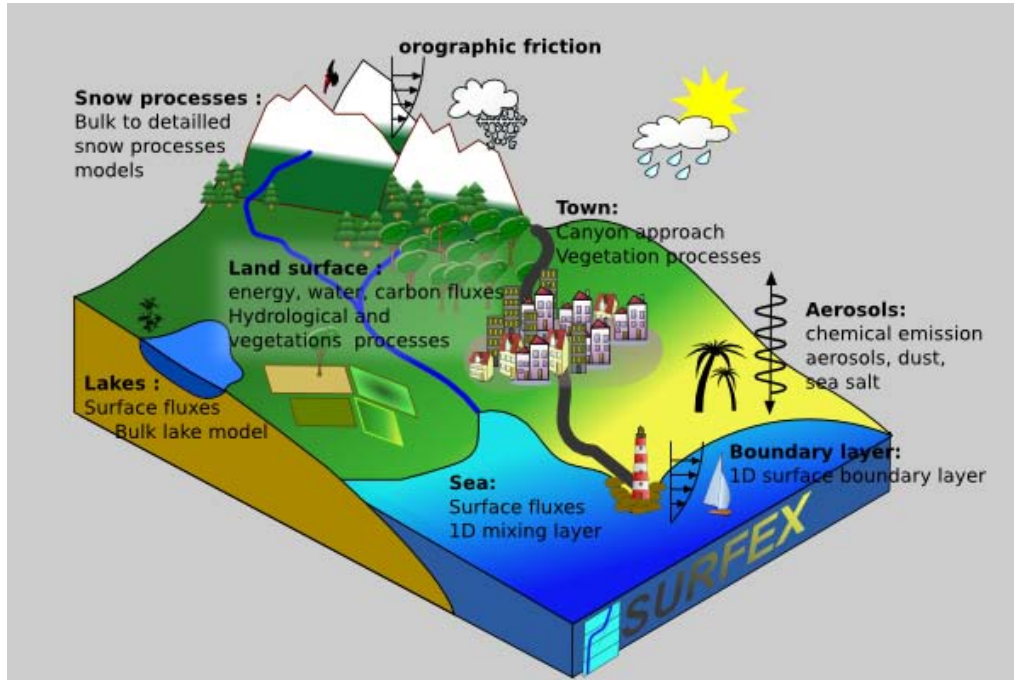


Figure 2.1: Surfex platform concept

Pronostic variables	Symbols
<b>Energy budget</b>	
Surface Temperature	$T_s$
Deep soil temperature	$T_2$
<b>Water budget</b>	
Water content for each soil layer	$w_i (i = 1, 3)$
Interception water storage by canopy	$w_r$

Table 2.1: Pronostic variables of ISBA

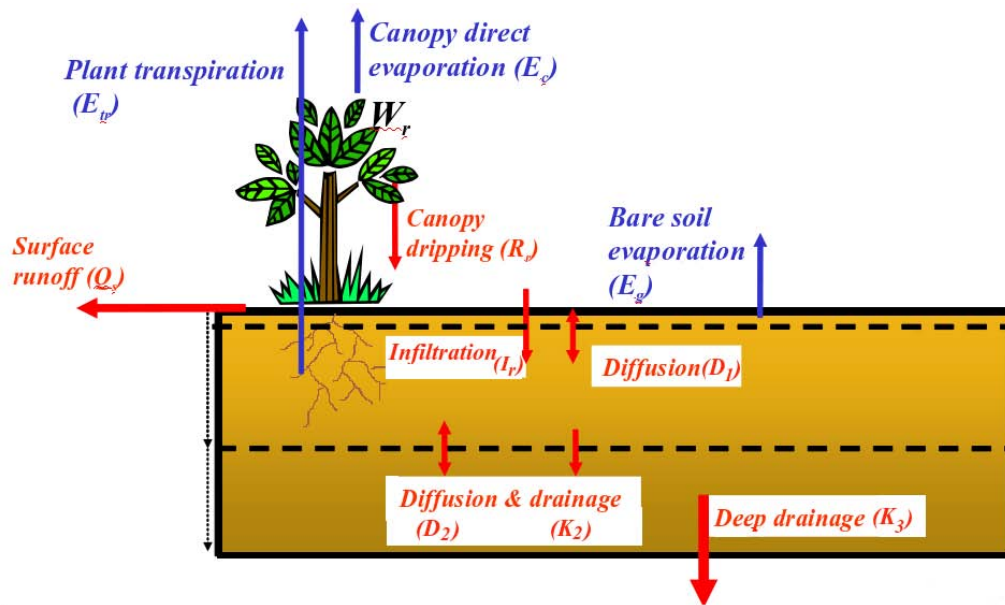


Figure 2.2: ISBA 3-L configuration (without the snow scheme). This model version includes 3 hydrologic layers divided in two main reservoirs: the root zone layer,  $w_2$ , of depth  $d_2$ , and the deep drainage zone,  $w_3$  of depth  $d_3$ . The surface superficial layer,  $w_1$ , of depth  $d_1$ , is included in the root zone layer. In this superficial layer, the heat transfers between the soil and the atmosphere are calculated and it is sufficiently thin to resolve the diurnal cycle.  $K$  and  $D$  are the drainage and diffusion in the soil.  $I_r$  is the surface water infiltration which includes the water dripping from the canopy,  $d_r$ , the water precipitated on the soil minus the total surface runoff,  $Q_s$ . The total evaporation is represented by the sum of the transpiration from the vegetation,  $E_{trans}$ , and the evaporation from the canopy,  $E_{canop}$ , and from the bare soil,  $E_{soil}$ . The canopy water storage is represented by  $W_r$ . Snow and soil ice are not shown.

Atmospheric variables	Symbols	Unities
Solar radiation	$R_G$	$W.m^{-2}$
Atmospheric radiation	$R_A$	$W.m^{-2}$
Liquid precipitation	$R_r$	$kg.m^{-2}.s^{-1}$
Solid precipitation	$S_r$	$kg.m^{-2}.s^{-1}$
Air temperature at $z_{ref}$	$T_a$	$K$
Horizontal wind speed at $z_{refv}$	$V_a$	$m.s^{-1}$
Air specific humidity at $z_{ref}$	$q_a$	$kg.kg^{-1}$
Surface atmospheric pressure	$P_s$	$Pa$

Table 2.2: Atmospheric variables needed to force the ISBA-TRIP model.  $z_{ref}$  is a reference level for  $T_a$  and  $q_a$ , generally considered as 2m (although it can be higher, for example when applied to a GCM).  $z_{refv}$  is the reference height for wind speed which is not necessarily the same as  $z_{ref}$  in offline mode (generally it is 10m, although it is identical to  $z_{ref}$  in coupled mode).

### 2.1.2 ISBA input parameters

ISBA input parameters are related to soil and vegetation and can be constant or time evolving in order to represent the seasonal evolution of soil and vegetation. They have been chosen, so that the model is able to characterize the main physical parameters while attempting to reduce the number of independent variables. They can be divided in two categories : primary parameters that need to be specified at each model grid point, and secondary parameters which values can be derived from the primary parameters (see table 2.3). The primary parameters describe the nature of the land surface and its vegetation coverage : the percentage of sand and clay in the soil, the different vegetation types, the depth of the deep soil layers, the albedo and emissivity of the surface. The secondary parameters, associated with the soil type, are evaluated from the sand and clay composition of the soil (Giordani et al., 1996; Noilhan and Lacarrère, 1995) whereas those related to the vegetation can either be derived from the vegetation types, or from existing classification or observations.

#### 2.1.2.1 Soil related input parameters

First of all, the soil is defined by its texture (sand/clay fractions), on which depend the general characteristics of the soil. The water flux in the soil is calculated using Darcy's law and the vertical fluxes are proportionnal to the product of the hydraulic conductivity ( $k$ ) times the gradient potential matrix ( $\phi$ ). These two variables are related to the soil water content by the relationships (Brooks and Corey, 1966) :

Primary parameters	Secondary parameters	Symbols
<b>SOIL</b> Clay fraction Sand fraction	Saturation or porosity Field capacity Wilting point Saturated soil water potential Saturated soil hydric conductivity Slope of the retention curve Soil thermal coefficient at saturation	$X_{clay}$ $X_{sand}$ $w_{sat}$ $w_{fc}$ $w_{wilt}$ $\phi_{sat}$ $k_{sat}$ $b$ $C_{Gsat}$
<b>VEGETATION</b> Vegetation type	Fraction of vegetation Minimal surface resistance Leaf area index Roughness length for momentum and heat	$veg$ $R_{smin}$ $LAI$ $z_0$
<b>BOTH</b> Soil depth Albedo Emissivity Soil/vegetation heat capacity	$C_T$	$d_{i,i=2,3}$ $\alpha$ $\varepsilon$

Table 2.3: ISBA input parameters

$$k = k_{sat} S_w^{2b+3} \quad (2.1)$$

$$\phi = \phi_{sat} S_w^{-b} \quad (2.2)$$

where  $b$  is the slope of the retention curve,  $k_{sat}(m.s^{-1})$  is the saturated hydraulic conductivity, and  $\phi_{sat}(m)$  is the saturated soil water potential.  $S_w$  is the soil relative saturation and is defined as :

$$S_w = w/w_{sat} \quad (0 < S_w < 1) \quad (2.3)$$

where  $w_{sat}$  is the soil porosity.

The values of  $\phi_{sat}$ ,  $w_{sat}$ ,  $k_{sat}$  and  $b$  are determined by Clapp and Hornberger (1978) for 11 soil textures.

Two other parameters are used to describe the soil hydrologic characteristics. The wilting point volumetric moisture content,  $w_{wilt}$ , is defined by inverting equation 2.2. and considering a low soil water potential equal to -150m (Jacquemin and Noilhan, 1990). Below this value, the soil water potential is generally too small for the plants to extract water from the soil. The field capacity volumetric moisture content,  $w_{fc}$ , is obtained through the inversion of equation 2.1., considering that the soil hydraulic conductivity is equal to  $10^{-4}m.day^{-1}$  (Wetzel et Chang 1987). Below this value of the soil hydraulic conductivity, no gravitational drainage occurs (it is assumed to be negligible).

The heat diffusion in the soil is calculated using Fourier's law. The heat flux is proportionnal to the product of the vertical temperature gradient and the soil thermal conductivity. The soil thermal conductivity and heat capacity are related to the soil water content and texture via the relationships ( McCumber and Pielke, 1981; Al Nakshabandi and Kohnke, 1965) :

$$c_g = (1 - w_{sat})c_{soil} + wc_w, \quad (2.4)$$

$$\lambda = 418exp[-log_{10}(-\phi) - 4.7] \quad (\lambda \geq 0.171), \quad (2.5)$$

where  $\lambda$  is the heat conductivity ( $W.m^{-1}.K^{-1}$ ),  $c_w$  and  $c_{soil}$  are respectively the heat capacities of water and bare soil and  $c_g(J.K^{-1}.m^{-3})$  is the total heat capacity of the soil.

### 2.1.2.2 Vegetation related input parameters

These parameters are used to describe the vegetation mean characteristics over each grid cell. They give information about the fraction of vegetated area, the density of the vegetation and its biophysical properties, which are needed for the calculation of the water and energy budgets relative to the vegetation. The fractional vegetation cover,  $veg$ , is used to treat separately, the evapotranspiration

from the vegetation and the evaporation from bare soil, which is defined over the relative area of the cell as  $(1 - veg)$ . The Leaf Area Index (LAI), expressed in  $m^2.m^{-2}$ , is related to the density of the vegetation. It controls the amount of transpiration and interception by the canopy and can vary seasonally. The minimum stomatal resistance,  $R_{smin}$ , represents the stomatal resistance when the leaf is at full water capacity, at full sunlight and when the vapor pressure effect is negligible. It impacts plant transpiration and depends on the type of plant considered. The vegetation roughness length,  $z_0$ , depends on its structure and affects the intensity of turbulent fluxes. The effective soil-vegetation albedo and emissivity are averaged over the grid.

### 2.1.3 Energy budget

The energy budget of the soil-vegetation system at the surface can be written as follows :

$$\begin{cases} G = R_n - H - LE, \\ LE = L_v(E_{soil} + E_{veg}) \end{cases} \quad (2.6)$$

where  $L_v(J.kg^{-1})$  is the latent heat of vaporisation,  $E_{soil}$  is the evaporation of bare soil and  $E_{veg}$  is the evapotranspiration from the vegetation. It is split into the portion coming from the interception reservoir,  $E_r$ , and from the root zone via transpiration,  $E_{transp}$  (plant water storage is assumed to be negligible). The model calculates the temporal evolution of the surface temperature  $T_s$ , representing the temperature of the system soil-vegetation at the surface, and of the deep soil temperature,  $T_2$  :

$$\frac{\partial T_s}{\partial t} = C_T(R_n - H - LE) - \frac{2\pi}{\tau}(T_s - T_2), \quad (2.7)$$

$$\frac{\partial T_2}{\partial t} = \frac{1}{\tau}(T_s - T_2), \quad (2.8)$$

where  $C_T(m^2.K.J^{-1})$  is the thermal inertia coefficient related to the soil-vegetation composite.  $\tau(s)$  is a time constant fixed to 1 day. The terms  $R_n$ ,  $H$  and  $LE$  are detailed in section 1.2 (equations 1.4 to 1.7).

### 2.1.4 Water budget

ISBA-3L calculates the temporal evolution of the water content in the 3 hydrological layers,  $w_1$ ,  $w_2$  and  $w_3$  (see Fig.2.2), as well as in the interception reservoir,  $w_r$  :

$$\frac{\partial w_1}{\partial t} = \frac{C_1}{\rho_w d_1}(I_r - E_{soil}) - D_1 \quad w_{min} \leq w_1 \leq w_{sat}, \quad (2.9)$$

$$\frac{\partial w_2}{\partial t} = \frac{1}{\rho_w d_2} (I_r - E_{soil} - E_{transp}) - K_2 - D_2 \quad w_{min} \leq w_2 \leq w_{sat}, \quad (2.10)$$

$$\frac{\partial w_3}{\partial t} = \frac{d_2}{(d_3 - d_2)} (K_2 + D_2) - K_3 \quad w_{min} \leq w_3 \leq w_{sat}. \quad (2.11)$$

$$\frac{\partial w_r}{\partial t} = veg \times P - E_r - R_r \quad 0 \leq w_r \leq w_{r_{max}}. \quad (2.12)$$

$I_r(kg.m^2.s^{-1})$  represents the surface infiltration (see Fig.2.2) and is expressed as :

$$I_r = (1 - veg)P + R_r - Q_s, \quad (2.13)$$

where  $P(kg.m^2.s^{-1})$  is the liquid precipitation, and  $Q_s(kg.m^2.s^{-1})$  is the surface runoff.  $R_r(kg.m^2.s^{-1})$ , is the canopy drip, which occurs only if  $w_r > w_{r_{max}}$ .  $E_r$  is the evaporation flux from the intercepted water by the canopy.  $K$  and  $D$  represent the drainage and diffusion fluxes in the soil and will be detailed in section 2.1.6.

## 2.1.5 Evapotranspiration

The simulated evapotranspiration is the sum of evaporation from bare soil and evapotranspiration from the vegetation. The evaporation from bare soil,  $E_{soil}$ , is related to the gradients of humidity, pressure and temperature between the surface and the atmosphere :

$$E_{soil} = (1 - veg)\rho_a C_H V_a [h_u q_{sat}(T_s, P_s) - q_a] \quad (2.14)$$

where  $(1 - veg)$  is the fraction of soil which is not covered by the vegetation,  $q_a$  is the air humidity,  $h_u$  is the soil relative humidity and  $q_{sat}(T_s, P_s)$  is the saturated specific humidity at temperature  $T_s$  and pressure  $P_s$ .

The evapotranspiration from the vegetation is expressed as :

$$E_{veg} = veg\rho_a C_H V_a h_\nu [q_{sat}(T_s, P_s) - q_a] \quad (2.15)$$

The Halstead coefficient,  $h_\nu$ , takes account of the direct evaporation from the canopy. Is it defined as :

## 2.1.6 Hydrology

### 2.1.6.1 Soil diffusion

The vertical soil diffusion terms  $D_1$  and  $D_2$ , from equations (2.9), (2.10) and (2.10) are expressed as :

$$\begin{cases} D_1 = \frac{C_2}{\tau}(w_1 - w_{geq}), \\ D_2 = \frac{C_4}{\tau}(w_2 - w_3) \end{cases} \quad (2.16)$$

$D_1$  represents the vertical water transfers between the surface and the root zone layers.  $D_2$  represents the vertical water transfers between the root zone and the deep soil layers. The sense of the flux depends on the sign of the humidity gradient  $w_2 - w_3$ . The surface volumetric water content at the balance of gravity and capillary forces,  $w_{geq}$ , is described using the soil hydraulic parameters from Clapp and Hornberger (1978) :

$$\frac{w_{1geq}}{w_{sat}} = \frac{w_2}{w_{sat}} - a \left( \frac{w_2}{w_{sat}} \right)^p \left[ 1 - \left( \frac{w_2}{w_{sat}} \right)^{8p} \right], \quad (2.17)$$

where  $a$  and  $p$  are empirical parameters depending on soil texture. When  $w_1 > w_{1geq}$ , then the water transfer is done from the surface layer to the root layer. When  $w_1 < w_{1geq}$ , then the superficial layer is recharged in water by the sublayer.

### 2.1.6.2 Drainage

The drainage terms,  $K_2$  and  $K_3$ , are expressed as :

$$\begin{cases} K_2 = \frac{C_3 d_3}{\tau d_2} \max[0, (w_2 - w_{fc})], \\ K_3 = \frac{C_3}{\tau} \frac{d_3}{(d_3 - d_2)} \max[0, (w_3 - w_{fc})] \end{cases} \quad (2.18)$$

where  $\tau(s)$  represents the restore constant of one day and  $w_{fc}(m^3.m^{-3})$  is the field capacity volumetric water content.  $K_2$  represents the gravity flux from root zone to drainage layer and  $K_3$  represents water leaving the upper soil column which can then be routed or transferred depending on another model.

### 2.1.6.3 Force-restore coefficients

The force-restore coefficients  $C_1$ ,  $C_2$  (Noilhan and Planton 1989), and  $C_4$  are calibrated against multilayer soil hydrological models, and  $C_3$  is computed analytically (Mahfouf and Noilhan, 1996). The  $C_1$ ,  $C_2$ , and  $C_3$  force-restore coefficients are expressed as :

$$\begin{cases} C_1 = C_{1sat} \left( \frac{w_{sat}}{w_g} \right)^{(b/2)+1}, \\ C_2 = C_{2ref} \left( \frac{w_2}{w_{sat} - w_2 + w_l} \right), \\ C_3 = \frac{\tau(2b+2)k_{sat}}{d_3[(w_3^*/w_{sat})^{-2b-2} - 1]} \end{cases} \quad (2.19)$$

where  $C_{1sat}$  and  $C_{2ref}$  are parameters,  $w_l$  is a small numerical value, and  $w_3^*$  is a function of  $w_{fc}$  and  $w_{sat}$ .

### 2.1.6.4 Surface runoff

The right partitioning of total runoff into surface runoff (fast runoff component) and drainage (slow runoff component) is a crucial process for the simulation of river discharge (Lohmann et al. 1998; Boone et al. 2004; Decharme, 2007) at the hourly to the daily time scale. The surface runoff over saturated areas, named Dunne runoff, is dependant on the subgrid variability of soil moisture. In ISBA, it is computed using a simple TOPMODEL approach (Beven and Kirkby, 1979). Beven and Kirkby (1979) and Silvapalan et al. (1987) proposed a simple hydrological forecasting model, named TOPMODEL. This approach attempts to combine the important distributed effects of channel network topology and dynamic contributing areas for runoff generation. The coupling between ISBA and TOPMODEL was first introduced by Habets and Saulnier (2001) using the two-layer soil hydrology. Then, it was generalized to the three-layer version of ISBA (Decharme et al. 2005). A saturated fraction,  $f_{sat}$ , is then simulated where precipitation is entirely converted into surface runoff (Decharme et al., 2006). The TOPMODEL approach takes into account topographic heterogeneities explicitly (Decharme and Douville, 2006). In addition, this approach is coupled with a sub-grid exponential distribution of the soil maximum infiltration capacity in order to enable the infiltration excess runoff mechanism, named Horton runoff (Decharme and Douville, 2006). As seen before, the Horton runoff occurs for a rainfall intensity that exceeds the effective maximum infiltration capacity. It is then dependant on the subgrid variability of rainfall and soil hydraulic properties. To account for the sub-grid variability in liquid precipitation,  $P_i$ , an exponential probability density distribution,  $f(P_i)$  is used (Entekhabi and Eagleson 1989). The main assumption is generally, that the rainfall intensity is not distributed homogeneously over the entire grid cell. At a low-resolution, a fraction,  $\mu$ , of a grid cell affected by rainfall is determined, using the results of Fan et al. (1996), who showed an exponential relationship between the fractional coverage of precipitation and rainfall rate, based on their analyses of over 2 years radar observations and rain gauge measurements over the Arkansas-Red river basin in the southern plains of the USA. The expression of  $f(P_i)$  is then :

$$f(P_i) = \frac{\mu}{P_{mean}} e^{\frac{-\mu P_i}{P_{mean}}}. \quad (2.20)$$

where  $P_{mean}$  is the mean rainfall rate over the grid cell. The Horton runoff is calculated by integrating the difference between the local rainfall and the local maximum infiltration capacity,  $I_i$  (Entekhabi and Eagleson 1989) :

$$Q_S^H = \mu \int_{I_i}^{\infty} (P_i - I_i) f(P_i) dP_i. \quad (2.21)$$

Finally, the total surface runoff can be expressed as follows:

$$Q_S = Q_S^D + (1 - f_{sat})Q_S^H. \quad (2.22)$$

where  $f_{sat}$  the fraction of each grid cell that is saturated, and  $Q_S^D$  is the Dunne runoff expressed as :

$$Q_S^D = P_{g_{sat}} \quad (2.23)$$

where  $p_g$  is the through-fall rate. More details can be found in Decharme and Douville, 2006.

## 2.2 The TRIP routing model

### 2.2.1 Governing equations

The TRIP RRM was developed by Oki and Sud (1998) at the University of Tokyo. It was first used at Météo-France to convert the model simulated runoff into river discharge using a global river channel network at a  $1^\circ$  resolution. The original TRIP model is only based on a single surface prognostic reservoir,  $S$  (kg), whose discharge is linearly related to the river mass using a uniform and constant flow velocity.

In the ISBA-TRIP CHS (Decharme et al., 2011), TRIP takes into account a simple groundwater reservoir,  $G$  (kg), and a variable stream flow velocity computed via Manning equation (Decharme et al., 2010; Appendix A). In addition, ISBA-TRIP includes a two-way flood scheme in which a flooded fraction,  $f_{\text{flood}}$ , of the grid cell can be determined (Decharme et al., 2008, 2011). The flood dynamics are described through the daily coupling between the ISBA land surface model and the TRIP river routing model, including a prognostic flood reservoir,  $F$  (kg). This reservoir fills when the river height exceeds the critical river bankfull height,  $h_c$  (m). The flood interacts with the soil hydrology through infiltration,  $I_f$  ( $\text{kg s}^{-1}$ ), with the overlying atmosphere through precipitation interception  $P_f$  ( $\text{kg s}^{-1}$ ), and through free water surface evaporation  $E_f$  ( $\text{kg s}^{-1}$ ). These three terms are calculated by multiplying, respectively, the total infiltration, precipitation interception and water surface evaporation over the grid cell by the ratio of flooded area to the grid area. This results in a system of three prognostic equations:

$$\begin{cases} \frac{\partial G}{\partial t} = Q_{\text{sb}} - Q_{\text{out}}^G \\ \frac{\partial S}{\partial t} = Q_{\text{in}}^S + Q_{\text{out}}^G + (Q_{\text{out}}^F - Q_{\text{in}}^F) - Q_{\text{out}}^S \\ \frac{\partial F}{\partial t} = Q_{\text{in}}^F + (P_f - I_f - E_f) - Q_{\text{out}}^F \end{cases} \quad (2.24)$$

where  $Q_{\text{sb}}$  ( $\text{kg s}^{-1}$ ) is the deep drainage from ISBA,  $Q_{\text{out}}^G$  ( $\text{kg s}^{-1}$ ) the groundwater outflow,  $Q_{\text{in}}^S$  ( $\text{kg s}^{-1}$ ) the sum of the surface runoff from ISBA within the grid cell

with the water inflow from the upstream neighboring grid cells, and  $Q_{\text{out}}^S$  ( $\text{kg s}^{-1}$ ) is the simulated discharge, while  $Q_{\text{in}}^F$  and  $Q_{\text{out}}^F$  ( $\text{kg s}^{-1}$ ) represent the flood inflow and outflow, respectively. See Appendix A and B for more details.

The global evaluation of the ISBA-TRIP CHS model at a  $1^\circ$  by  $1^\circ$  resolution suggested that the model may not take into account some important process such as the presence of large aquifers in certain regions (Decharme et al., 2011). Also, by comparing the chemical composition of river water and groundwater, Fontes et al. (1991) demonstrated that significant aquifer recharge occurs in the Niger Inland Delta region, especially during summer flooding. For these reasons, a simple linear aquifer reservoir was added to the model. This reservoir was made to be consistent with the groundwater reservoir,  $G$ , but with a significantly longer time delay factor,  $\tau_{\text{aq}}$  (s). This results in a new system of four prognostic equations:

$$\begin{cases} \frac{\partial G}{\partial t} = \alpha Q_{\text{sb}} - Q_{\text{out}}^G \\ \frac{\partial S}{\partial t} = Q_{\text{in}}^S + Q_{\text{out}}^G + (Q_{\text{out}}^F - Q_{\text{in}}^F) - Q_{\text{out}}^S \\ \frac{\partial F}{\partial t} = Q_{\text{in}}^F + (P_f - I_f - E_f) - Q_{\text{out}}^F \\ \frac{\partial A_{\text{q}}}{\partial t} = (1 - \alpha) Q_{\text{sb}} - Q_{\text{out}}^{\text{Aq}}, \end{cases} \quad (2.25)$$

where  $\alpha$  represents the fraction of deep drainage going into the groundwater reservoir while the rest of the drainage  $(1 - \alpha)$  goes into the aquifer. Unlike the groundwater reservoir, we assume that the aquifer reservoir local feedbacks are negligible, but contribute to the flow at the mouth of the river. The aquifer outflow  $Q_{\text{out}}^{\text{Aq}}$  ( $\text{kg s}^{-1}$ ) can be written as follows:

$$Q_{\text{out}}^{\text{Aq}} = \frac{A_{\text{q}}}{\tau_{\text{Aq}}} \quad , \quad (2.26)$$

where  $\tau_{\text{Aq}}$  (s) is a constant and uniform time delay factor, which represents the characteristic timescale for the aquifer reservoir to drain laterally to the ocean (out of the basin). This simple approach is currently motivated mainly by the lack of data describing the water table, which would be required for a more detailed approach. Fig.2.3 illustrates the configuration of the ISBA-TRIP CHS model used in this study.

### 2.2.2 River discharge and groundwater outflow

The river discharge simulated by TRIP (Eq. 1) is computed using a streamflow variable velocity,  $v$  ( $\text{m s}^{-1}$ ), and via the Manning's formula:

$$Q_{\text{out}}^S = \frac{v}{L} S \quad \text{with} \quad v = \frac{\kappa}{n_{\text{riv}}} R^{2/3} s^{1/2}, \quad (2.27)$$

where  $L$  (m) is the river length that takes into account a meandering ratio of 1.4 as proposed by Oki and Sud (1998),  $s$  ( $\text{m m}^{-1}$ ) is the downstream river height

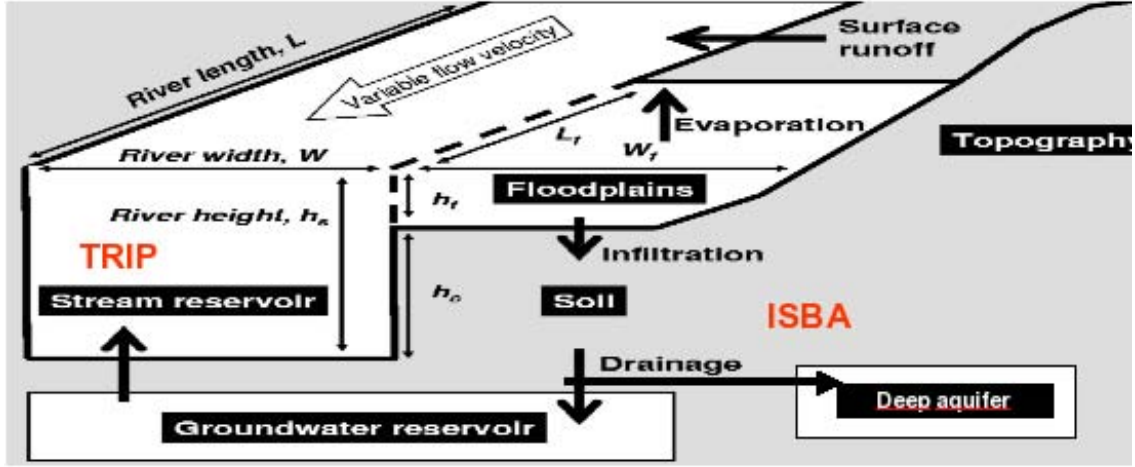


Figure 2.3: Total Runoff Integrating Pathways (TRIP) model configuration.

loss per unit length approximated as the river bed slope,  $R$  (m) the hydraulic radius,  $\kappa$  ( $\text{m}^{-3} \text{s}^{-1}$ ) a constant equal to 1, and  $n_{\text{riv}}$  the dimensionless Manning friction factor which varies from the upstream part to the mouth of each basin. The river bed slope is indeed a critical parameter to compute velocity via the Manning formula. The STN-30p Digital Elevation Model (DEM) provided at  $0.5^\circ \text{C}$  by  $0.5^\circ \text{C}$  resolution by the ISLSCP2 database (<http://www.gewex.org/islscpdata.htm>) has been used. The STN-30p DEM was heavily edited to represent the actual elevation along the river network on a global scale, based on the aggregated HYDRO1 K DEM at 1 km resolution. Further adjustments were made to eliminate some of the unrealistic rapid slope changes in the STN-30p DEM along the global river network. Yamazaki et al. (2009) included a realistic sub-grid-scale topography for a more reasonable representation of the river height loss. This inclusion could be considered as a possible improvement of the representation of the river bed slope in the TRIP model. The hydraulic radius is related to the stream water depth,  $h_s$  (m), calculated from the stream water mass,  $S$  (kg), assuming a rectangular river cross-section (Arora and Boer, 1999):

$$R = \frac{W h_s}{W + 2 h_s} \quad \text{where} \quad h_s = \frac{S}{L W \rho_W}, \quad (2.28)$$

where  $\rho_W$  ( $\text{kg m}^{-3}$ ) is the water density, and  $W$  (m) the bankfull river width. See section 3.3 for detailed expressions of  $W$ ,  $h_s$  and  $L$ .

The TRIP groundwater outflow (Eq. 1) is computed using the following simple linear relationship proposed by Arora and Boer (1999):

$$Q_{\text{out}}^G = \frac{G}{\tau} \quad (2.29)$$

where  $\tau$  (s) is an uniform and constant time delay factor of the groundwater reservoir which is fixed to 30 days. This groundwater reservoir does not represent the groundwater dynamics but only delays the groundwater flow contribution to the surface river reservoir within a particular grid cell: the deep drainage is fed into the surface reservoir with a time delay factor of  $\tau$ . More details can be found in Decharme et al. (2010).

### 2.2.3 The flooding scheme

A simplified rectangular geometry is assumed in TRIP to represent the cross section between the floodplain and the river reservoirs in each grid cell. River flooding arises when the water height of the stream reservoir is higher than the critical bankfull height,  $h_c$  (m), and the flood outflow and inflow from this reservoir (Eq. 1) are given by:

$$\begin{cases} Q_{\text{in}}^F = \frac{v_{\text{in}}}{W + W_f} M_f \\ Q_{\text{out}}^F = \frac{v_{\text{out}}}{W + W_f} \min(M_f, F), \end{cases} \quad (2.30)$$

where  $W_f$  (m) is the floodplain width, and  $M_f$  (kg) the potential inflow (positive  $M_f$ ) or outflow (negative  $M_f$ ). This outflow assumes an equilibrium state between the stream and the floodplain water depth:

$$M_f = \rho_W L_f W (h_s - h_c - h_f) , \quad (2.31)$$

where  $L_f$  (m) and  $h_f$  (m) are the length along the river and the depth of the floodplains,  $h_s$  (m) the water height of the stream reservoir, and  $h_c$  (m) the critical bankfull river height.  $W + W_f$  represents the distance covered by  $M_f$  from the stream to the floodplains or conversely.  $v_{\text{in}}$  and  $v_{\text{out}}$  ( $\text{m s}^{-1}$ ) are the flood inflow and outflow velocities, respectively, computed using the Manning's formula:

$$v_{\text{in,out}} = \frac{s_{\text{in,out}}^{1/2}}{n_f} R_{\text{in,out}}^{2/3} , \quad (2.32)$$

where  $n_f$  is the Manning roughness coefficient for the floodplains that varies according to the vegetation type (Decharme et al., 2011), while  $s_{\text{in,out}}$  ( $\text{m m}^{-1}$ ) and  $R_{\text{in,out}}$  (m) are the inflow (or outflow) slope and hydraulic radius, respectively, at the interface between the floodplain and the river stream.

The flood inflow and outflow velocities computed using the Manning's formula require the hydrological slope between the floodplain and the river stream:

$$\begin{cases} s_{\text{in}} = \frac{\max(0, h_s - h_c - h_f)}{(W + W_f)/2} \\ s_{\text{out}} = \frac{\max(0, h_f + h_c - h_s)}{(W + W_f)/2}. \end{cases} \quad (2.33)$$

They also require the hydraulic radius assumed rectangular and calculated as follows:

$$\left| \begin{array}{l} R_{\text{in}} = \frac{L_f \times \max(0, h_s - h_c)}{L_f + 2 \times \max(0, h_s - h_c)} \\ R_{\text{out}} = \frac{L_f h_f}{L_f + 2h_f}, \end{array} \right. \quad (2.34)$$

where  $W_f$  (m),  $L_f$  (m) and  $h_f$  (m) are the width, the length and the depth (respectively) of the floodplains,  $h_s$  (m) the water height of the stream reservoir,  $h_c$  (m) the critical height of the river bed, and  $W$  (m) the stream river width. The  $h_f$  is calculated in each grid-cell with the help of the actual distribution of the local height,  $h_i$  (m), determined at a 1 km by 1 km resolution. The assumption is that each pixel,  $i$ , represents a sub-basin into a given grid-cell that can be potentially flooded. Each subbasin has a triangular form and is associated with a fraction,  $f_i$ , of the grid cell area,  $A$ . The  $h_i$  is computed using the local slope,  $\tau_i$  ( $^\circ$ ) and flow direction data given by the HYDRO1 K dataset (Verdin and Greenlee, 1996):

$$h_i = l \sqrt{\alpha_i} \tan\left(\frac{\sigma_i \pi}{180}\right), \quad (2.35)$$

where  $l$  (m) is the characteristic length of one pixel equal to 1000 m, and  $\alpha_i$  is equal to 1 if the local flow direction is north, south, east, or west, and to 2 elsewhere. Therefore, for each  $h_i$  a potential mass of flood,  $V(h_i)$  (kg), can be simply calculated using a discrete equation:

$$V(h_i) = \rho_w \sum_0^i V_i \text{ where } V_i = \frac{A f_i h_i}{2}. \quad (2.36)$$

The sub-grid distributions of the flooded fraction and the flood depth allow the determination of  $f_{\text{flood}}$ , and  $h_f$  at each time step and in each grid-cell via the comparison between the water mass in the floodplain reservoir,  $F$ , computed by TRIP (Eq. 4) and the sub-grid distribution of this potential mass  $V(h_i)$ :

$$F = V(h_i) \Rightarrow \left| \begin{array}{l} f_{\text{flood}} = \sum_0^i f_i \\ h_f = h_i. \end{array} \right. \quad (2.37)$$

When  $f_{\text{flood}}$  is known within the grid cell,  $W_f$  and  $L_f$  are simply calculated as follows:

$$\left| \begin{array}{l} L_f = \max(0.001, r \sqrt{f_{\text{flood}} A}) \\ W_f = \frac{A f_{\text{flood}}}{L_f}, \end{array} \right. \quad (2.38)$$

where, again,  $r$  is the meandering ratio fixed to 1.4 as recommended by Oki and Sud (1998).

Finally, the precipitation interception by the floodplains,  $P_f$ , the re-infiltration,  $I_f$ , and the direct free water surface evaporation,  $E_f$ , (Eq. 1) are estimated by

---

ISBA.  $I_f$  occurs if the flooded fraction,  $f_{\text{flood}}$ , calculated according to the subgrid topography (Decharme et al., 2011), is superior to the soil saturated fraction,  $f_{\text{sat}}$ , and depends on the soil maximum infiltration capacity. In other words, the floodplains cannot infiltrate the fraction of the grid-cell for which the soil is saturated. To a first approximation, this represents the fact that actual floodplains evolve according to the presence of shallow aquifers and water table depth variations.



# Evaluation of the ISBA-TRIP CHS over the Niger basin using in-situ and satellite derived data

---

## Contents

---

<b>3.1</b>	<b>Domain</b>	<b>74</b>
<b>3.2</b>	<b>Methodology</b>	<b>76</b>
<b>3.3</b>	<b>TRIP specific parameters for the Niger river basin</b>	<b>77</b>
<b>3.4</b>	<b>Atmospheric forcing dataset input for ISBA-TRIP</b>	<b>78</b>
<b>3.5</b>	<b>Evaluation datasets</b>	<b>81</b>
3.5.1	Observed discharge	83
3.5.2	Satellite-based flooded area	83
3.5.3	Satellite-based Water Height	85
3.5.4	Satellite-based total terrestrial water storage	85
<b>3.6</b>	<b>Results</b>	<b>85</b>
3.6.1	Improvement of LSMs simulated discharges due to river flooding	85
3.6.2	The impact of rainfall forcing on simulated discharge	89
3.6.3	Separate impact of floods and aquifers on the Niger basin	90
3.6.4	Total terrestrial water storage	107
3.6.5	Rainfall comparison	110
3.6.6	Aquifer storage	112
<b>3.7</b>	<b>Sensitivity tests</b>	<b>115</b>
<b>3.8</b>	<b>Chapter conclusions and perspectives</b>	<b>120</b>

---

In order to better model the global water cycle, Decharme et al. (2008, 2011) used the TRIP approach to implement a flood routing scheme into the ISBA-TRIP CHS. The scheme accounts explicitly for the river routing, precipitation

interception by the floodplains, the direct evaporation from the free water surface, and the possible re-infiltration into the soil in flooded areas. The regional and global evaluations of this scheme at a  $1^\circ$  by  $1^\circ$  spatial resolution emphasized the importance of floodplains in the continental part of the hydrological cycle, through generally improved river discharges and a non-negligible increase of evapotranspiration (Decharme et al., 2011). However, it was noticed that over some basins, including the Niger, the discharge was still overestimated (Decharme et al., 2011). A possible identified cause was that these regions might overlie large aquifers that can be relatively uncoupled to the river. The purpose of this study (Pedinotti et al., 2012) is to evaluate the performance of the ISBA-TRIP CHS model over the Niger basin using comparisons with in situ measurements as well as recently available satellite derived data from 2002 to 2007. In accordance with the recommendations of Decharme et al. (2011), a new simple aquifer reservoir was implemented to simulate the water storage at longer temporal scales, in 'confined' aquifers. This section gives the detailed methodology adopted for the evaluation of the model, as well as for the study of the model sensitivity to the parameterization and forcing uncertainties.

### **3.1 Domain**

With an approximate length of 4180 km (2600 miles), the Niger river is the largest river in West Africa. It begins in the Guinea Highlands in southeastern Guinea and ends in Nigeria, discharging through a massive delta into the Gulf of Guinea within the Atlantic Ocean. The domain used for the simulations presented in the next chapter is delineated by the white contour in Fig.3.1. It delineates the Niger watershed, i.e. such that all of the water issued from precipitation, melting snow or ice, converges to a single point, usually referred to as the outlet of the basin. In reality, part of the water do not reach the large rivers draining to the ocean (Descroix et al., 2009). These areas where surface runoff does not attain the main rivers network are called 'endorheic' and cover almost half of the area of the Niger river basin. These areas do not contribute to the discharge of the river itself, thus reducing its hydrologically effective area. This covers mostly the Northern basin, which is a very dry area, characterized by relatively few precipitation.

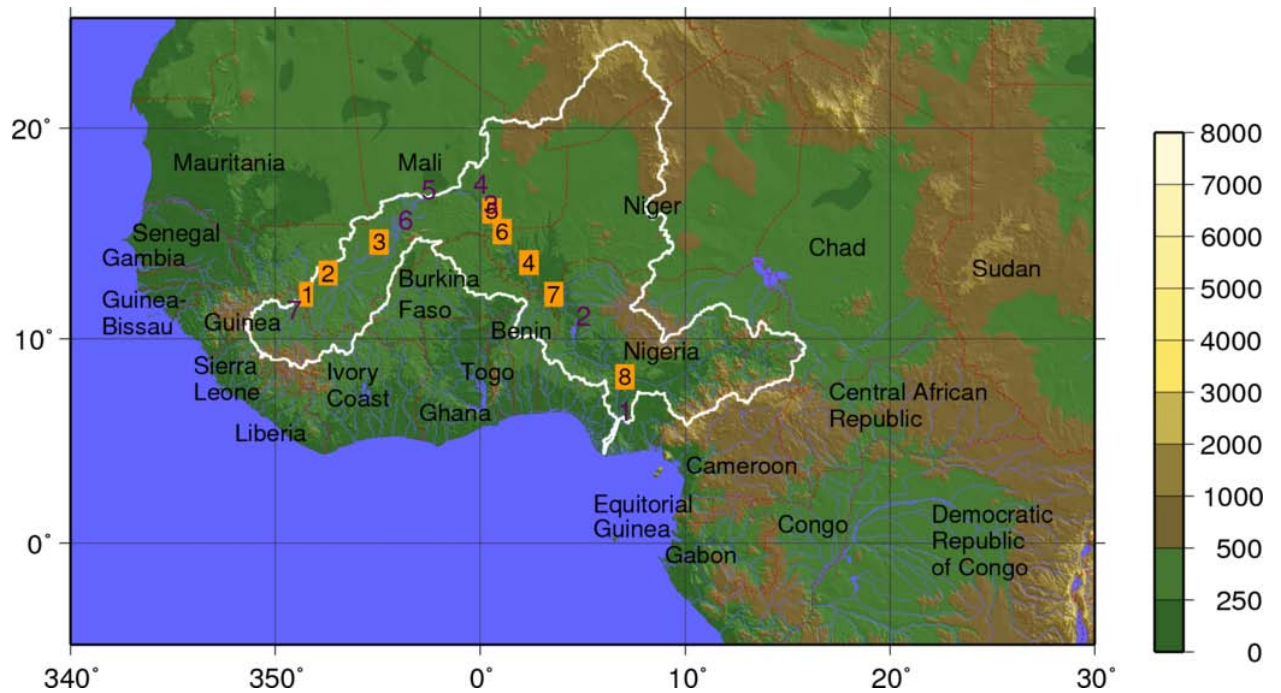


Figure 3.1: The Niger river basin. The spatial resolution is  $0.5^\circ \times 0.5^\circ$ . The white contour is the delimitation of the Niger basin. The yellow squares are the stations where discharge observations are available: (1) Banankoro, (2) Koulikoro, (3) Ke Macina, (4) Niamey, (5) Ansongo, (6) Kandadji, (7) Malanville (8) Lokoja. The purple boxes represent the sites where satellite-based height change observations are used for evaluation. The legend indicates the terrain elevations from GTOPO30 (m).

## 3.2 Methodology

- Impact of floodplains

In order to determine the impact of the flooding scheme on river discharge, we first simulated the river routing using TRIP but without activation of floods (i.e. in offline mode). For this simulation, simulated runoff from multiple LSMs were used within TRIP in order to see the spread in discharge from an ensemble of LSMs (and to see if ISBAs behavior was consistent with other similar models). ALMIP I, which is a part of the AMMA project, was motivated by an interest in fundamental scientific issues and by the societal need for improved prediction of the West African Monsoon (WAM) and its impacts on West African nations (Redelsperger et al., 2006). As part of this project, ALMIP I focused on better understanding land-atmosphere and hydrological processes over Western Africa (Boone et al., 2009a). LSMs were run offline with prescribed atmospheric forcing consisting in a combination of observations, satellite products and atmospheric model output data. All of the LSMs used the same computational grid at a  $0.5^\circ$  spatial resolution. The advantage of using ALMIP data is that each LSM can simulate a different runoff response, therefore we use an ensemble of inputs. In the current study, 11 simulations are used over the 2002-2007 period. TRIP is used to compute daily outputs of discharges along the river and water mass storage for each activated reservoir. Next, the ISBA-TRIP CHS coupled model is used with and without the flooding scheme to quantify the impact of the scheme on the discharge and the surface energy budget. As the TRMM-3B42 rainfall (see the Section 3.4 for details) was used as forcing for the ALMIP experiment, the same forcing is used for the ISBA-TRIP CHS simulation with and without the flooding scheme. The goal is to determine the impact of activating the flooding scheme, taking account the runoff uncertainties by using runoff diagnostics from diverse LSMs.

- Impact of aquifers

In a study by Decharme et al. (2011), it was suggested that, once the flooding scheme activated, the remaining bias in simulated discharge, observed in the Niger river, could result from the fact that the basin, in some regions, might overlie a deep aquifer which is uncoupled from the river. Also, by comparing the chemical composition of river water and groundwater, Fontes et al. (1991) demonstrated that significant aquifer recharge occurs in the Niger Inland Delta region, especially during summer flooding. Regarding this assessment, it was decided to implement a single linear aquifer reservoir in the TRIP model using a formulation which is consistent with

the other reservoirs while introducing a minimum number of parameters (see Chap. 2 for details). In the second part of this study, the deep aquifer reservoir is activated and deep drainage water is then distributed between deep soil layers and this aquifer reservoir. The model is run using four rainfall data sets (see section about forcing for details) to take rain uncertainty into account in a simple manner, leading to 16 different simulations. Comparison with both in situ and remote sensing data will allow us to evaluate the simulated surface processes, the impact of the inclusion of floodplains and aquifers, and the ability of the model to estimate the river discharge.

### 3.3 TRIP specific parameters for the Niger river basin

The baseline parameter values are presented in this section. Note that the sensitivity of the model to these parameters will be investigated in Sect.3.7. For the model evaluation, the time delay parameters for the groundwater and deep aquifer reservoirs are fixed to 30 days and 4 years, respectively (Eq.s 2.25). The aquifer parameter  $\alpha$  is initially fixed at  $3/4$  (which implies that  $1/4$  of the drainage flows into the deep aquifer). The aquifer reservoir is defined equally in each pixel. The river width is an important parameter because it modulates both the river flow speed and the floodplain dynamics. It is computed over the entire TRIP network via an empirical mathematical formulation that describes a simple geomorphological relationship between  $W$  and the mean annual discharge at each river cross section (Knighton, 1998; Arora and Boer, 1999; Moody and Troutman, 2002; Decharme et al., 2011):

$$W = \max(30, \beta \times Q_{yr}^{0,5}) \quad (3.1)$$

where  $Q_{yr}^{0,5}(m_{s_1}^3)$  is the annual mean discharge in each grid cell estimated using the global runoff database from Cogley (1979). As discussed in Decharme et al. (2011), the  $\beta$  coefficient can vary drastically from one basin to another (Knighton, 1998; Arora and Boer, 1999; Moody and Troutman, 2002). Decharme et al. (2011) proposed that  $\beta$  varies according to climatic zone and fixed  $\beta$  to 20 for monsoon-dominated basins and to 13 for semi-arid and arid basins. As the Niger river flows through both such climate zones, two different values are used within the Niger basin:  $\beta$  is 20 for the branch of the river going from the river mouth ( $5^\circ N$ ) to  $12^\circ N$  and  $\beta$  is fixed to 10 for the remaining branch of the river. The spatial distribution of the river width is shown in Fig.3.2. The key parameter for the floodplain parameterization is  $h_c$ , the critical river bank-full height (Decharme et al., 2008, 2011). In this study, as proposed by Decharme

et al. (2011), it is computed according to the river width via a simple power function:

$$h_c = W^{1/3} \quad (3.2)$$

The spatial distribution of  $h_c$  is shown in Fig.3.2. However, owing to both the uncertainties in this parameter and its impact on model results, sensitivity tests will be carried out using arbitrary  $h_c \pm 20\%$  (Decharme et al., 2008), leading to an increase or decrease in bank-full height up to  $2m$ .

Finally, as in Decharme et al. (2010), the Manning friction coefficient,  $n_{riv}$ , varies linearly and proportionally to  $W$  from 0.04 near the river mouth to 0.1 in the upstream grid cells (Fig.3.2):

$$n_{riv} = n_{min} + (n_{max} - n_{min}) \times \left( \frac{W_{mouth} - W}{W_{mouth} - W_{min}} \right) \quad (3.3)$$

where  $n_{riv}$  represents the Manning  $n$  factor of the grid cell,  $n_{max}$  and  $n_{min}$  the maximum and the minimum values of the Manning friction factor (0.1 and 0.04, respectively),  $W_{min}(m)$  represents the minimum river width value and  $W_{mouth}(m)$  corresponds to the width of the mouth of each basin within the TRIP network.

### **3.4 Atmospheric forcing dataset input for ISBA-TRIP**

The atmospheric state variables are based on the European Centre for Medium Range Forecasts (ECMWF) ECMWF numerical weather prediction (NWP) model forecasts for the years 2002-2007. The forcing variables consist in the air temperature, specific humidity, wind components at 10 m, and the surface pressure, all at a 3 h time step. Because of the importance of having accurate incoming radiation fluxes and precipitation which are spatially and temporally coherent, and because of the potentially significant errors in these variables derived from NWP models over this region (e.g. see Boone et al., 2009a), merged satellite products are used. The downwelling longwave and shortwave radiative fluxes are provided by the LAND-SAF project (Geiger et al., 2008).

Concerning precipitation, the TRMM 3B42 product (Huffman et al., 2007) is used by default for the first study, as it was used for the ALMIP simulations. However, to investigate the dependence of the model diagnostics to rainfall uncertainties, it was decided to run the model using three other frequently used large-scale precipitation data sets: CMORPH, PERSIANN and RFE2. The NASA Tropical Rainfall Measuring Mission (TRMM) started in 1997 and is a partnership between NASA (National Aeronautics and Space Administration) and JAXA (Japan Aerospace Exploration Agency). First, each microwave satellite observation (SSM/I, TMI, AMSR, and AMSU) is converted to a rainfall

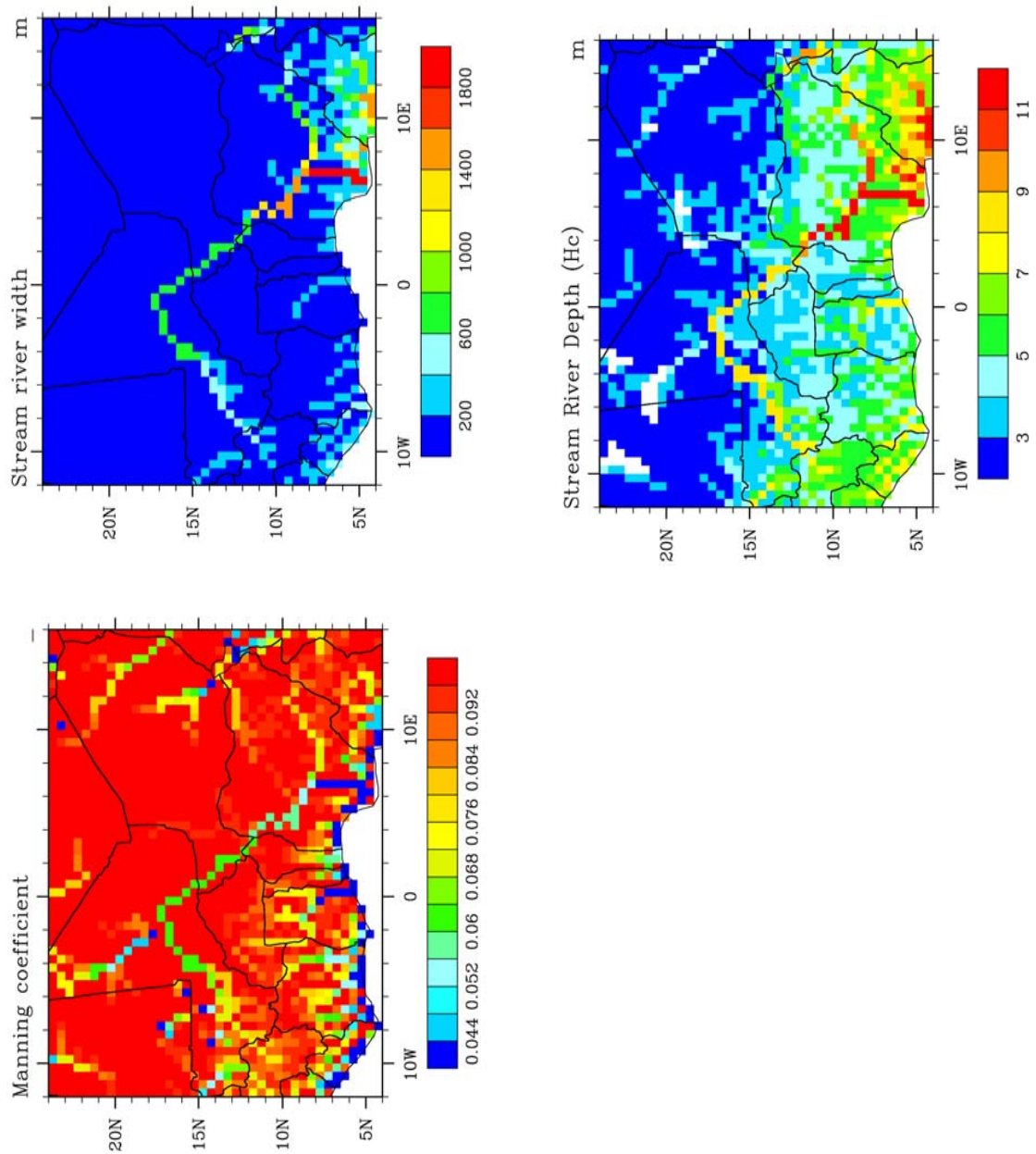


Figure 3.2: Spatial distribution of the river width (up left), of the river depth (up right) of the Manning coefficient (down left).

estimate using its proper algorithm. Then the microwave precipitation estimates are calibrated and combined (using probability matching of precipitation rate histograms). After this, infrared precipitation estimates (GMS, GOES, Meteosat and NOAA-12) are created using the calibrated microwave precipitation, and the MW and IR estimates are combined. As a last step, monthly accumulated rain gauge data from CAMS (Climate Assessment and Monitoring System) produced by NOAA CPC and rain gauge product from the GPCC, are incorporated [Huffman et al., 2007]. TRMM data sets are available at a 3-hour temporal scale and at  $0.25^\circ \times 0.25^\circ$  spatial resolution from  $60^\circ$  N to  $60^\circ$  S latitude. For this study, the precipitation data were interpolated to a  $0.5^\circ$  grid cell to be coherent with the resolution used herein.

The CMORPH (CPC MORPHing technique, <http://www.cpc.ncep.noaa.gov/products/janowiak/cmorph.shtml>) product [Joyce et al., 2004] has been developed by the Climate Prediction Centre (CPC) at the National Oceanic and Atmospheric Administration (NOAA). It was introduced in 2002 and is constructed from similar inputs as those used in TRMM-3B42. However, the algorithm takes a different approach by taking advantage of the superior precipitation estimates of the microwave data and the higher temporal resolution of the IR data, while compensating for the sparse time-sampling of the microwave and weak instantaneous connection between infrared data and precipitation rate [Laws et al., 2004]. The data used for this study are available at a 30-minute time step (here we use the 3-hour time step product for consistency) and  $0.25^\circ$  spatial resolution in a global belt extending from  $60^\circ$  N to  $60^\circ$  S. As for the TRMM datasets, CMORPH was interpolated at a  $0.5^\circ$  spatial resolution.

The PERSIANN (Precipitation Estimation from Remotely Sensed Information using Artificial Neural Networks, <http://chrs.web.uci.edu/persiann/>) algorithm was developed at the CHRS (Center for Hydrometeorology and Remote Sensing) at the University of California, Irvine, in 2000. It provides global precipitation estimation using combined geostationary and low orbital satellite imagery [Hsu et al., 1997]. The PERSIANN products are available at a  $0.25^\circ \times 0.25^\circ$  spatial resolution and interpolated on a  $0.5^\circ$  resolution grid. This dataset is also available at a 30 minute timestep, but we use the 3h time step product in the current study. The spatial coverage is the global band from  $50^\circ$  N to  $50^\circ$  S latitude.

The RFE2.0 product was developed at NOAA by the CPC [Xie and Arkin, 1996]. The algorithm merges infrared (GOES Precipitation Index), passive microwave (AMSU, SSM/I) and gauges measurements. This product is available at  $0.1^\circ \times 0.1^\circ$  spatial resolution and at daily time step. Note LSMs intended to be coupled with atmospheric models resolve the diurnal cycle (which is the type of scheme we are using in this study), so that a daily time step precipitation product can not be used as-is. However, several studies have shown that RFE2 [Laws

et al., 2004) produces rainfall over the Sahel agrees better with observed values than the other available rainfall products (e.g. Pierre et al., 2011; Jobard et al., 2011). Therefore, a second set of rainfall forcing data was created by disaggregating the daily RFE2 to a three hour timestep using the TRMM rainfall data. The monthly total RFE2 rainfall is well preserved using this simple downscaling method. This rain forcing is referred to as RFE-Hybrid (RFEH) herein.

A basic intercomparison of rainfall datasets was done using TRMM-3B42 as a reference, as it is the forcing used for the ALMIP experiment. For every set of precipitation,  $P$ , the monthly precipitation difference,  $P - TRMM$ , has been calculated over the period 2003-2006. This difference is calculated from July to September, which covers the main wet season (Fig. 3.3). For every month, the mean precipitation rates over the basin are also presented. This intercomparison shows significant positive biases from CMORPH and PERSIANN, compared to TRMM. These biases are observed in the major part of the basin with a maximum in July at the source of the Niger river in the Guinean highlands. Important positive biases are also observed in the Eastern Niger basin, especially for CMORPH datasets. These high differences between precipitation products correspond to mountainous regions where the estimation of rainfall is generally more difficult. The monthly precipitation rates over the basin, from CMORPH and PERSIANN, are much larger than the mean precipitation from TRMM. In July especially, CMORPH and PERSIANN observe respectively 50% and 70% more precipitation than TRMM. The comparison of RFEH with TRMM rainfall shows a general amplitude coherence between both datasets. A previous study from Pierre et al. (2011), has made the intercomparison of TRMM-3B42, CMORPH and RFE2.0 over the period 2004-2007 in the Sahelian region. The 3 satellite derived rainfall products were also tested against interpolated rain gauges measurements. The time scale used for the satellite products intercomparisons is from 1 to 10 days, and the spatial resolution is of  $0.25^\circ \times 0.25^\circ$  to  $0.5^\circ \times 0.5^\circ$  which is suitable for our study. Pierre et al. showed that, while TRMM-3B42 and RFE2.0 were in good agreement concerning rainfall amounts, there was a clear overestimation of the CMORPH product which is coherent with our observation. Given the strong differences between precipitation satellite-derived datasets, it is reasonable to hypothesize that they will impact the simulation of surface processes and hydrology.

## 3.5 Evaluation datasets

The general evaluation of CHSs at the regional or the global scale is not easy due to the lack of large observational datasets, especially over the West Africa. The implementation of routing models enables the direct comparison of simulated

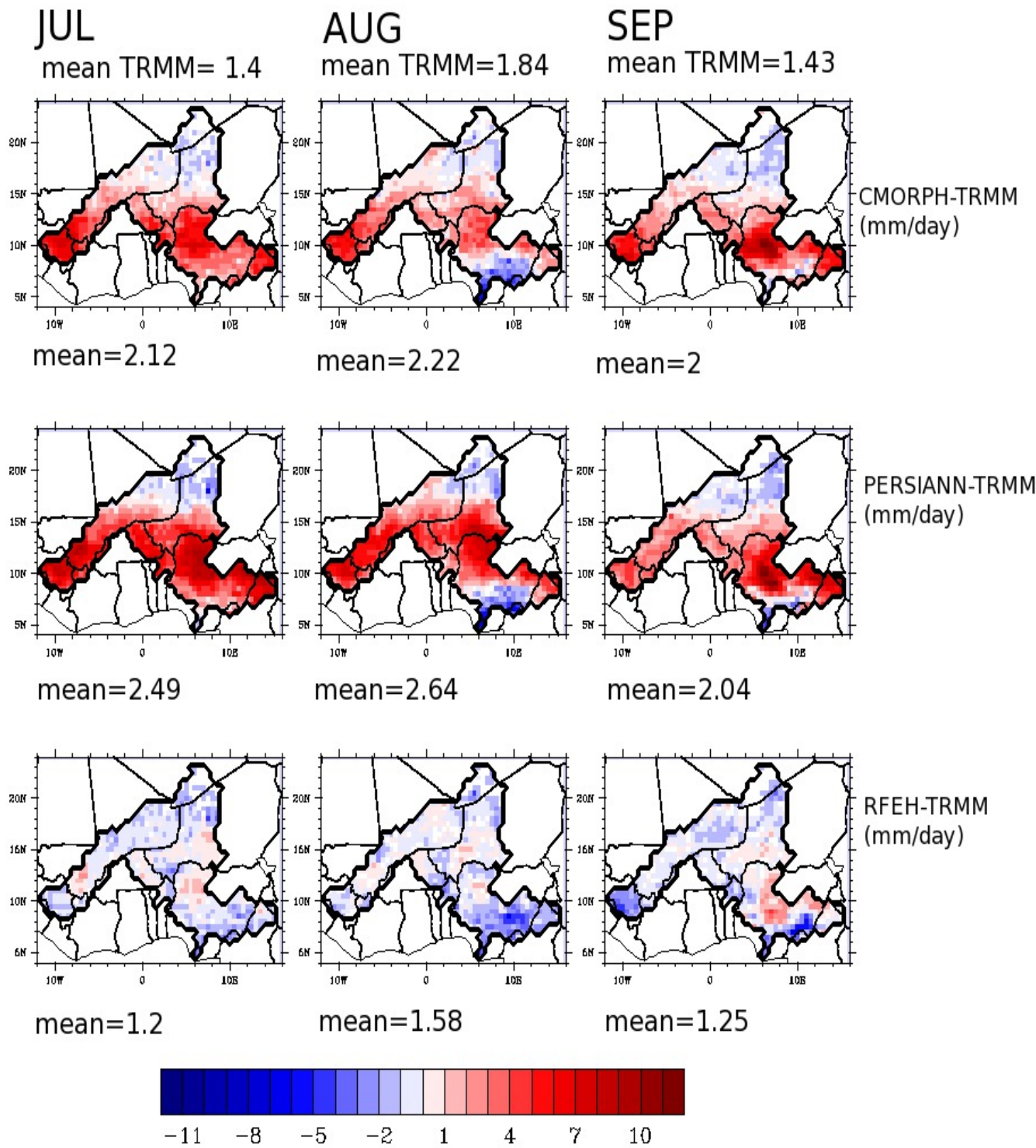


Figure 3.3: Monthly average of rain differences from July to September.

runoff from LSMSs with in situ discharge data. However, discharge observations are sparse over the Niger basin. Moreover, the constant improvement of hydrodynamical models, with the addition of explicit and more detailed mechanisms necessitates a better knowledge of land water dynamics and reservoir storage. In this study, an effort was made to use of a maximum of in situ and satellite derived datasets in order to evaluate the ISBA-TRIP CHS. The satellite derived datasets take profit of the merging remote sensing technologies and enable a first estimation of surface water dynamics and water storage variations, which is particularly usefull for evaluating the simulated floodplains and water distributed in the different model reservoirs.

### 3.5.1 Observed discharge

Over the evaluation period of the current study (2002-2007), the simulated discharges are compared with daily gauge measurements along the Niger river from the Niger Basin Authority (ABN) as a part of the Niger-HYCOS (HYdrological Cycle system Observing System: WMO/TD-No. 1282, 2005) project. These data are available in Koulikoro, Banankoro, Ke-Macina, Kandadji, Niamey, Ansongo, Malanville and Lokoja (represented by the yellow squares in Fig.3.1).

### 3.5.2 Satellite-based flooded area

Satellite-derived inundation estimates are used to evaluate the spatial distribution and the time evolution of the flooded areas. Two different products are used. The first product is based on data from the MODIS (Moderate Resolution Imaging Spectroradiometer) multispectral imaging system installed onboard the Terra and Aqua satellites. In this study, the surface reflectance product (MOD09GHK) is used, which is defined as the reflectance that would be measured at the land surface if there were no atmosphere. The spatial resolution is 500m for the corresponding MODIS images and the coverage is global (Vermote et al., 2002). In order to detect open water and aquatic vegetation in arid and semi arid regions, a classification is performed using the fact that water surfaces do not reflect in the visible and near infra-red part of the spectrum. A threshold value has been estimated for reflectance in the MODIS frequency band-5 1230 1250 nm and for the NDVI index (Tab. 3.1) in order to delineate the shallow, sediment laden, and open water over the Inner Niger Delta, and also in order to distinguish between aquatic vegetation and vegetation on dry land. It has been assumed that small values of surface reflectance in band-5 characterize open water, independent of the NDVI index. When the surface reflectance in band-5 increases to the median value, depending on the NDVI index, it is assumed that there is a partial coverage of dry land by water, aquatic vegetation or vegetation on dry land. Finally,

**Chapter 3. Evaluation of the ISBA-TRIP CHS over the Niger basin**  
**84 using in-situ and satellite derived data**

	Open water	Mix water/Dry land	Aquatic vegetation	Vegetation	Dry land
Band 5	<1200	>1200 & <2700	>1200 & <2700	>2700	>2700
NDVI	No test	<0.4	>0.4	>0.4	<0.4

Table 3.1: Threshold values used for the classification surface type used to monitor flood events. Band unit of reflectance is internal HDF-EOS data format specific to the Modis data and do not correspond to usual reflectance unit.

dry land is assumed when the NDVI is small and surface reflectance in band-5 is large. NDVI has been shown to be a robust index for monitoring temporal changes of the vegetation photosynthetic activity (Lyon et al., 1998; Lunetta et al., 2006). In the arid environment, a high level of vegetation photosynthetic activity can only be sustained by the presence of surface water or groundwater discharge. If dense enough, the aquatic vegetation and hydrophilic plants can mask underlying water and should be included in the estimate of the total area of the floodwaters. The NDVI ranges from negative values (open water) to >0.5 for dense vegetation.

The second product consists in global estimates of the monthly distribution of surface water extent at about 25 km sampling intervals. These data were generated from complementary multiple satellite observations, including passive (Special Sensor Microwave Imager) and active (ERS scatterometer) microwaves along with visible and near infrared imagery (advanced very high resolution radiometer; AVHRR). These estimates were first developed over 1993 2000 (Prigent et al., 2007), adjusted and extended over 1993 2004 (Papa et al., 2010b) and recently recomputed for the entire period 1993 2007. This dataset has been extensively evaluated at the global scale (Papa et al., 2010b) and at river basin scale, including the Niger river (Papa et al., 2008). In the present study, this dataset is aggregated to a 0.5° resolution and referred to as PP. Because PP does not distinguish between the diverse anthropogenic and/or natural water bodies, while the ISBA-TRIP output must be compared only with flooded areas, two additional datasets are used to hybridize PP in order to conserve information on flood inter-annual variability only: the Global Lakes and Wetland Database (GLWD; Lehner and Doll, 2004) and the Monthly Irrigated and Rainfed Crop Areas (MIRCA2000; Portmann et al., 2010) database. The corresponding final product is named CPP in this study. The methodology is described in detail by Decharme et al. (2011), and so it is not detailed here.

### 3.5.3 Satellite-based Water Height

Water height changes over the basin are evaluated using the HYDROWEB hydrological database ([http://www.legos.obs-mip.fr/en/equipes/gohs/resultats/i\\_hydroweb](http://www.legos.obs-mip.fr/en/equipes/gohs/resultats/i_hydroweb)). The water level time series are based on altimetry measurements from ENVISAT satellite. Seven sites were chosen for the evaluation, one upstream of the Niger inner delta, four downstream of the delta and two in the delta. The data are available at a regular 35 days time step (with occasional missing data) from November 2002 to the end of 2007 (Calmant et al., 2008).

### 3.5.4 Satellite-based total terrestrial water storage

Total Water Storage (TWS) variations over the entire basin are evaluated using data from the Gravity Recovery and Climate Experiment (GRACE; Tapley et al., 2004). GRACE provides monthly TWS variation estimates based on highly accurate maps of the Earth's gravity field at monthly intervals at a resolution of approximately 300 400-km (Wahr et al., 2004; Swenson et al., 2003). The instrumentation and onboard instrument processing units are described in detail in Haines et al. (2003). Here, we used 60 months (from January 2003 to December 2007, excluding June 2003 and January 2004 because products are not available) of the Release 04 data produced by the Center for Space Research (CSR at The University of Texas in Austin), the Release 4.1 data produced by the Jet Propulsion Laboratory (JPL), and the GeoForschungsZentrum (GFZ) Release 04 (more details concerning GRACE data are available online at <http://grace.jpl.nasa.gov/data/>). The combination of these data with those datasets, described in the previous paragraphs within this section, permit the evaluation of the distribution of water in the different TRIP reservoirs and to have a first estimation/validation of the aquifer water storage variations. The next chapter presents the results of the ISBA-TRIP simulations and evaluation with the datasets cited above.

## 3.6 Results

### 3.6.1 Improvement of LSMs simulated discharges due to river flooding

The evaluation of the simulated river discharge is important for hydrological applications as well as for climate studies. Previous studies (Bonan, 1995; Coe et al., 2008; Decharme et al., 2008, 2011; Alkama et al., 2010; Dadson et al., 2010) have shown that the inclusion of a flooding scheme can impact the hydrological cycle by increasing the average evaporation and reducing the simulated discharge,

which leads to a better estimation of the latter. Indeed, while an increasing number of LSMs used for large scale hydrological or GCM applications use river routing, most of these models do not represent floodplains. Flooded zones can be significant sources of evaporation and have a significant impact on the surface water storage, and their exclusion can result in an overestimation of the discharge for basins with significant annual flooding.

In order to examine the importance of modeling flood plains in the Niger basin, the TRIP RRM model was used in offline mode (i.e. without the flooding scheme) to convert simulated runoff and drainage from 11 LSMs into discharge. The LSMs considered for this study were part of the ALMIP I project (Boone et al., 2009a). Fig. 3.4 shows the mean daily discharges simulated by the ALMIP models (black line) for several locations along the river. The blue range is the difference between the minimum and the maximum value of discharges simulated by the models and the red line is the observed discharge. The corresponding statistics are given in Table 3.2. Due to the bias in precipitation for years 2005 to 2007 (discussed in part 3.6.5), the statistics are calculated from 2002 to 2004 in order to better reflect the model performance. In terms of observed discharge, there is a clear change of behaviour after the delta (Niamey, Ansongo, Kandadji, Malanville, Lokoja) compared to upstream of the delta (Banankoro, Koulikoro, Ke Macina). Indeed, the discharge before the delta is almost twice as large as that downstream of the delta. This reflects the significant impact of the inner delta on the discharge amplitude due to the floodplains. The first three discharge time series shown in Fig. 3.4 are located before the inner delta area (Banankoro, Koulikoro and Ke Macina). For these three locations, the discharge is reasonably represented by the ALMIP models. A bias in discharge is observed in 2005, 2006 and 2007 where the models simulate a smaller discharge compared to the previous years. This is most likely due to a bias in the rain forcing and will be discussed in Part 3.6.5. However, for the sites located downstream of the inner delta area (Niamey, Kandadji, Ansongo, Malanville and Lokoja) all of the ALMIP land surface models clearly overestimate the discharge leading to poor results compared to the three locations before the inner delta. In Malanville, the mean simulated discharge is around 5 times higher than that observed over this period. At the other sites (Niamey, Kandadji, Ansongo, and Lokoja), the mean simulated discharge is 2 to 2.8 times higher than observed.

The temporal variability of the discharge is generally well captured by the models as seen by the relatively good correlation scores (see Table 3.2). The green line represents the discharge simulated by the ISBATRIP CHS model with the flooding scheme activated. The results can be separated into three classes. First, in Banankoro and Koulikoro (before the inner delta), the discharge and thus the scores are not significantly changed, essentially because no floods occur in these places. Second, after the inner delta (Niamey, Ansongo, Kandadji, Malanville

Corr.	Ban	Kou	KeM	Nia	Ans	Kan	Mal	Lok
ALMIP	0.97	0.83	0.5	0.8	0.73	0.73	0.82	0.78
ISBA–TRIP NF	0.98	0.9	0.7	0.76	0.73	0.74	0.75	0.81
ISBA–TRIP F	0.86	0.86	0.23	0.59	0.56	0.58	0.69	0.82
NS								
ALMIP	0.9	0.63	−0.2	−23.32	−23	−19.31	−62.42	−2.95
ISBA–TRIP NF	0.81	0.57	−0.95	−24.6	−22.9	−23.07	−57.08	−2.27
ISBA–TRIP F	0.69	0.7	−0.34	−0.52	−0.91	−0.37	−4.42	0.02
RMS								
ALMIP	0.58	0.76	0.6	3.54	4.04	3.61	5.25	1.66
ISBA–TRIP NF	0.81	0.81	0.76	3.63	4.36	3.93	5.03	1.51
ISBA–TRIP F	1.04	0.68	0.63	0.89	1.14	0.94	1.54	0.83

Table 3.2: Daily statistic scores of the discharge for the ALMIP LSMs and ISBA/TRIP with and without flooding from 2002 to 2004. TRMM-3B42 is used as forcing.

and Lokoja), discharge decreased considerably (50 %) in Niamey, Kandadji, Ansongo and Malanville and 26 % in Lokoja. The root mean square error (rms) has decreased considerably compared to the simulation without flooding scheme (see Tab. 3.2). Indeed, part of the water in the floodplains evaporates, while part infiltrates into the flooded soil thereby reducing the stream reservoir water storage and discharge. The Nash-Sutcliffe coefficient or efficiency (eff), which evaluates the capacity of the model to reproduce daily dynamics of the discharge, is also improved. Finally, in Ke Macina, the discharge is deteriorated by the addition of the flooding scheme. Among the sites before the inner delta, Ke Macina is the closest to the delta. It is likely that the model floods occur too soon upstream of the delta. This can be directly linked to a poor parametrisation or model parameter value (such as the river width) in this particular area. In the 3 locations upstream of the delta, there is a significant decrease of the simulated discharge in 2005, 2006 and 2007 which is not observed. This reduction of the discharge is observed for all the LSMs as well as for both configurations of ISBA-TRIP (with and without floods) and is more likely to be due to rainfall errors.

In conclusion, in this section it was shown that general known LSMs overestimate the discharge in the Niger basin, especially downstream from the inner delta which is known as a significant flooded area, which is not represented by the models. Indeed, floodplains act as a water reservoir and evaporation source which contribute to the decrease of the water amount in the river stream, resulting in a decrease of discharge. The inclusion of the flooding scheme in the ISBA-TRIP simulation results in a significant decrease of discharge and thus better statis-

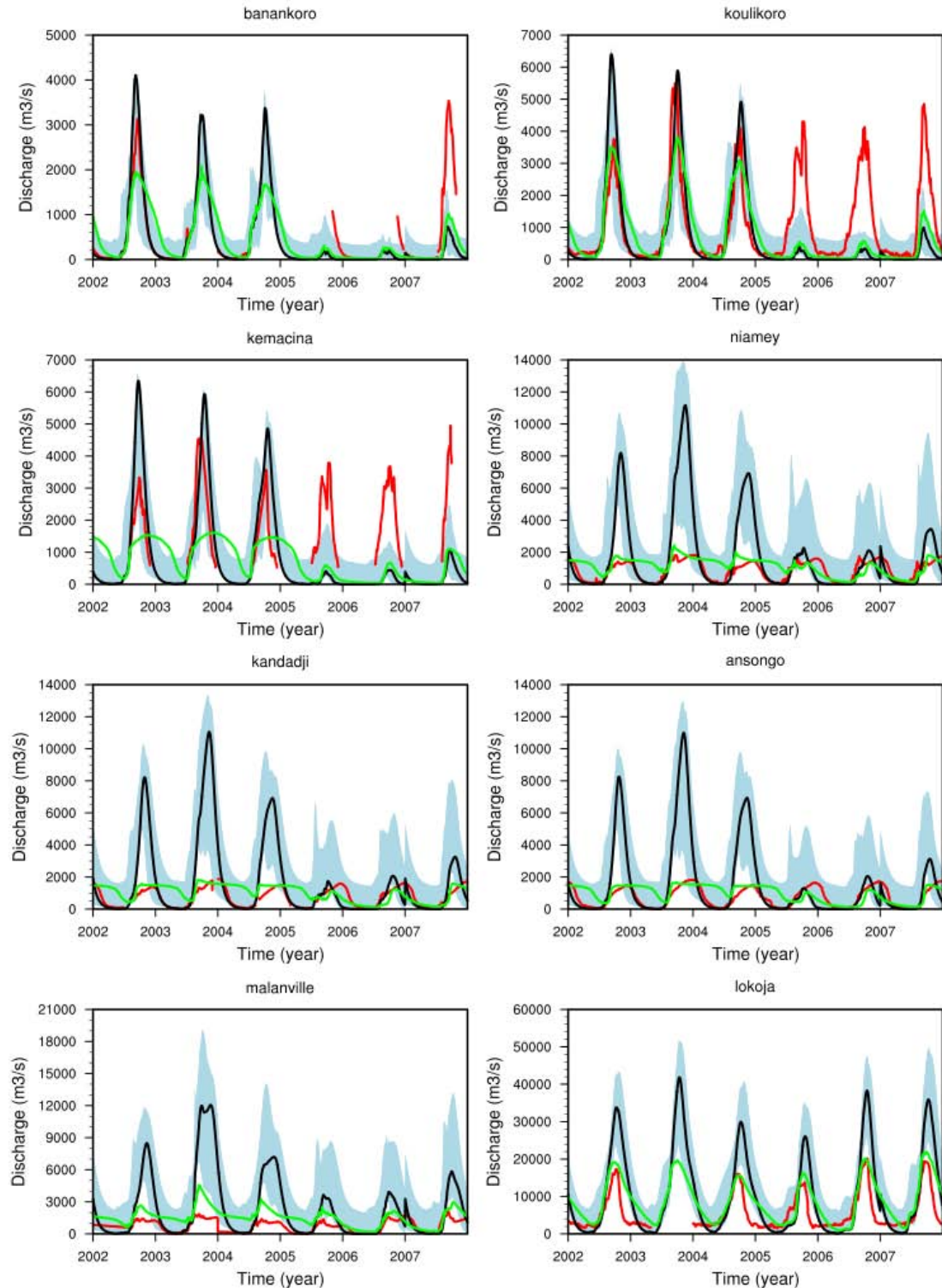


Figure 3.4: Daily discharges (2002–2007) simulated by the ALMIP LSMs without floods (average, black line) and by ISBA-TRIP using the flooding scheme (green). Observations are in red and the blue range is limited by the minimum and maximum discharge simulated by LSMs. The TRMM-3B42 rain product is used as forcing input.

tical scores. However, previous studies (Decharme et al., 2010, Fontes et al., 1991) have shown that the presence of a deep and more or less confined aquifer may also impact the Niger basin water cycle, and explain the bias of discharge, remaining in the simulations. For this reason, a simple linear aquifer reservoir was developed and implemented into the ISBA-TRIP CHS model in order to estimate the impact of a deep aquifer storage reservoir on the TRIP hydrological processes. The separate impacts of floods and aquifer on the water and energy budget is discussed in Part 3.6.3. However, before going deeper in this study, it was necessary to evaluate the impact of the rainfall forcing on the simulations. Indeed, previously, the TRMM-3B42 precipitation product was used as default to run ISBA-TRIP, as it was the forcing used to run all the ALMIP LSMs. However, other products are available at suitable time and spatial resolutions during the studied period.

### 3.6.2 The impact of rainfall forcing on simulated discharge

The rainfall forcing is probably one of the main sources of uncertainty in regional and global scale hydrological model applications. In order to take this factor into account, several standard precipitation datasets were used as input for the ISBA-TRIP coupled model. The precipitation datasets were chosen according to their coverage, time and spatial resolution. Four datasets were kept for the evaluation of the flood scheme : TRMM, CMORPH, PERSIANN and RFEH (see the description of atmospheric forcing in Sect. 3.4 for details). The discharge simulated by ISBA-TRIP with and without floods and forced by each precipitation forcing are shown in Figs 3.5-3.6. The corresponding statistical scores are listed in Table 3.3. In both cases (with and without floods), CMORPH and PERSIANN generally lead to similar results. In the previous section (Sect. 3.6.1), it was shown that there was an overestimation of the discharge at the locations situated downstream of the Niger basin without the flood scheme. This problem was largely resolved by the addition of floodplains (see Sect. 3.6.1). In addition, the use of CMORPH and PERSIANN as rainfall forcings leads to an overestimation of the discharge at all of the locations with observations. Moreover, the bias of the amplitude is more significant than when using TRMM precipitation (12 to 25 times higher than observations), even if the correlation is well captured by the model. With no flooding scheme, as was the case with TRMM, the discharge amplitude is improved, even if the discharge is still overestimated compared to the two other precipitation products. Moreover, the correlation is greatly deteriorated. Indeed, the annual patterns of the discharge, due to the monsoon cycle, and especially the low flow discharge, are hardly observable in the CMORPH and PERSIANN discharges. A study from Pierre et al. (2011), was carried over the Sahelian belt and showed that the CMORPH product clearly overestimates

rainfall amounts, while both TRMM3B42 and RFE2.0 were in good agreement with krigged rain gauge data over this region. This overestimation is the likely cause of the discharge overestimation. Moreover, the intercomparison of rainfall forcing made in Sect. 3.4, also showed a significant bias between CMORPH and TRMM, especially in the Guinea Highlands, which an important source of water for the rest of the Niger river.

ISBA-TRIP underestimates the discharge both with and without the flooding scheme upstream of the inland delta and when forced by RFEH. However, the discharge is generally well simulated downstream of the delta, especially when the flooding scheme is activated. The low flows are better simulated with RFEH. As a result of this intercomparison of rainfall forcings (through their impact on ISBA-TRIP discharge), it was decided to continue the evaluation of the model using only TRMM and RFEH.

### **3.6.3 Separate impact of floods and aquifers on the Niger basin**

The importance of representing floodplains in LSMs was presented and emphasized in Sect. 3.6.1. However, some model deficiencies remain, such as a bias of discharge in Ke Macina (possibly due to an oversimplification of or missing processes in the model, or the need for more or improved model parameters), in addition to an over-estimated of the recession flow during the dry season. In fact, the discharge remains relatively high during the dry season compared to the observations, which implies that there is too much water in the river. Several reasons for this can be identified, such as underestimated evaporation, an underestimation of the water in flooded areas or the neglect of aquifers. Anthropogenic activities (dams, agriculture and water use for domestic consumption) are not explicitly accounted for and can also explain part of the bias between observed and simulated discharge, especially during the dry season when the population might need to extract more water from the river due to the lack of rain. In order to investigate the impact of aquifers on the discharge, a relatively simple and linear aquifer reservoir was added to the model. It was formulated in a manner which is consistent with the other TRIP reservoir governing equations. This reservoir is supplied by a fraction of the soil drainage and it does not supply water back the river.

In order to better understand the separated impacts of aquifers and floods, four different configurations of the model are tested in this study:

- no flooding scheme and no aquifer reservoir (NOAQNF);
- flooding scheme activated, no aquifer reservoir (NOAQF);

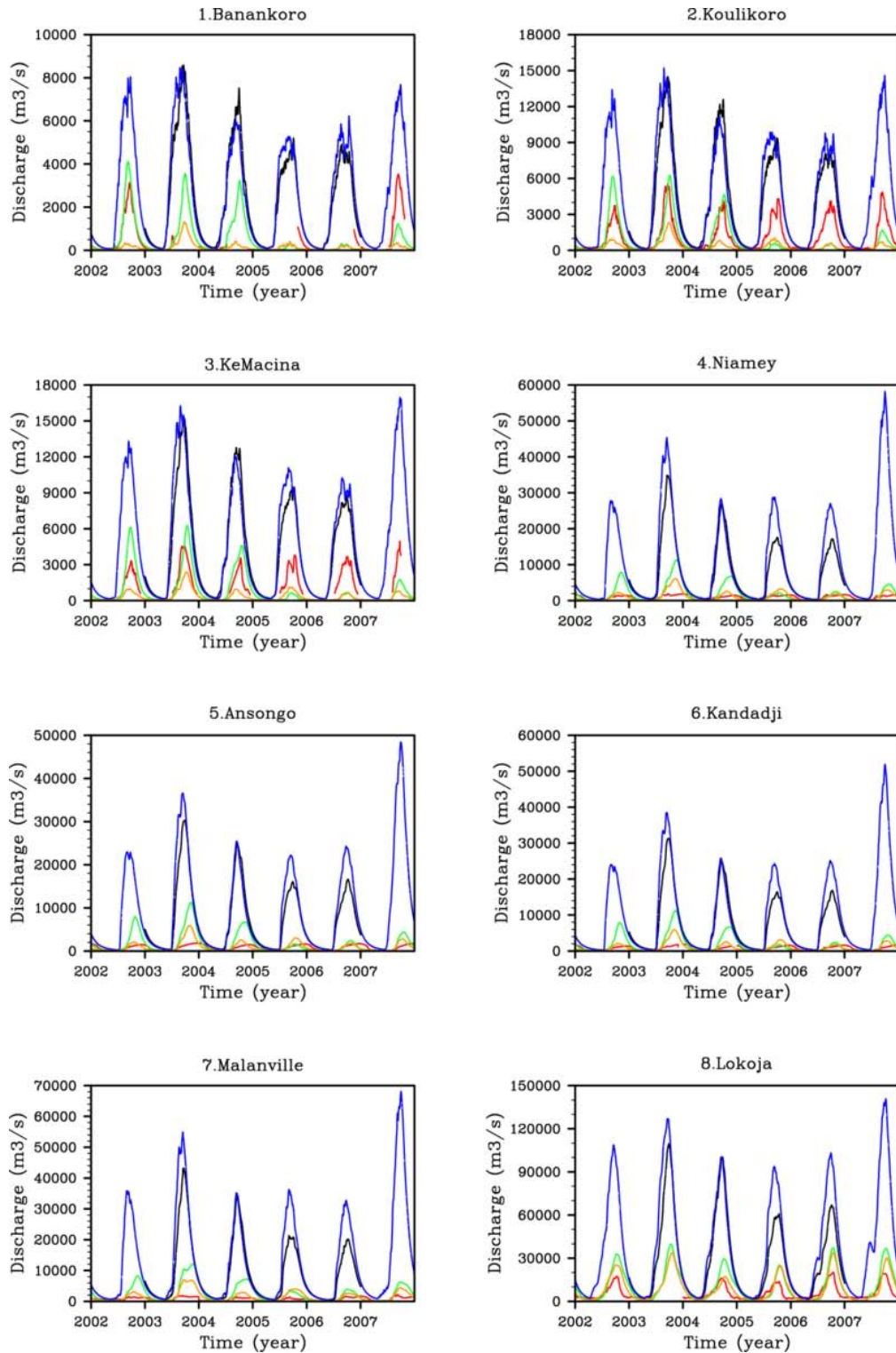


Figure 3.5: Simulated discharge using different rainfall products as input forcing : TRMM (red), CMORPH (black), PERSIANN (blue) and RFEH (orange). Observations are in red. The flooding scheme is not activated.

Chapter 3. Evaluation of the ISBA-TRIP CHS over the Niger basin  
92  
using in-situ and satellite derived data

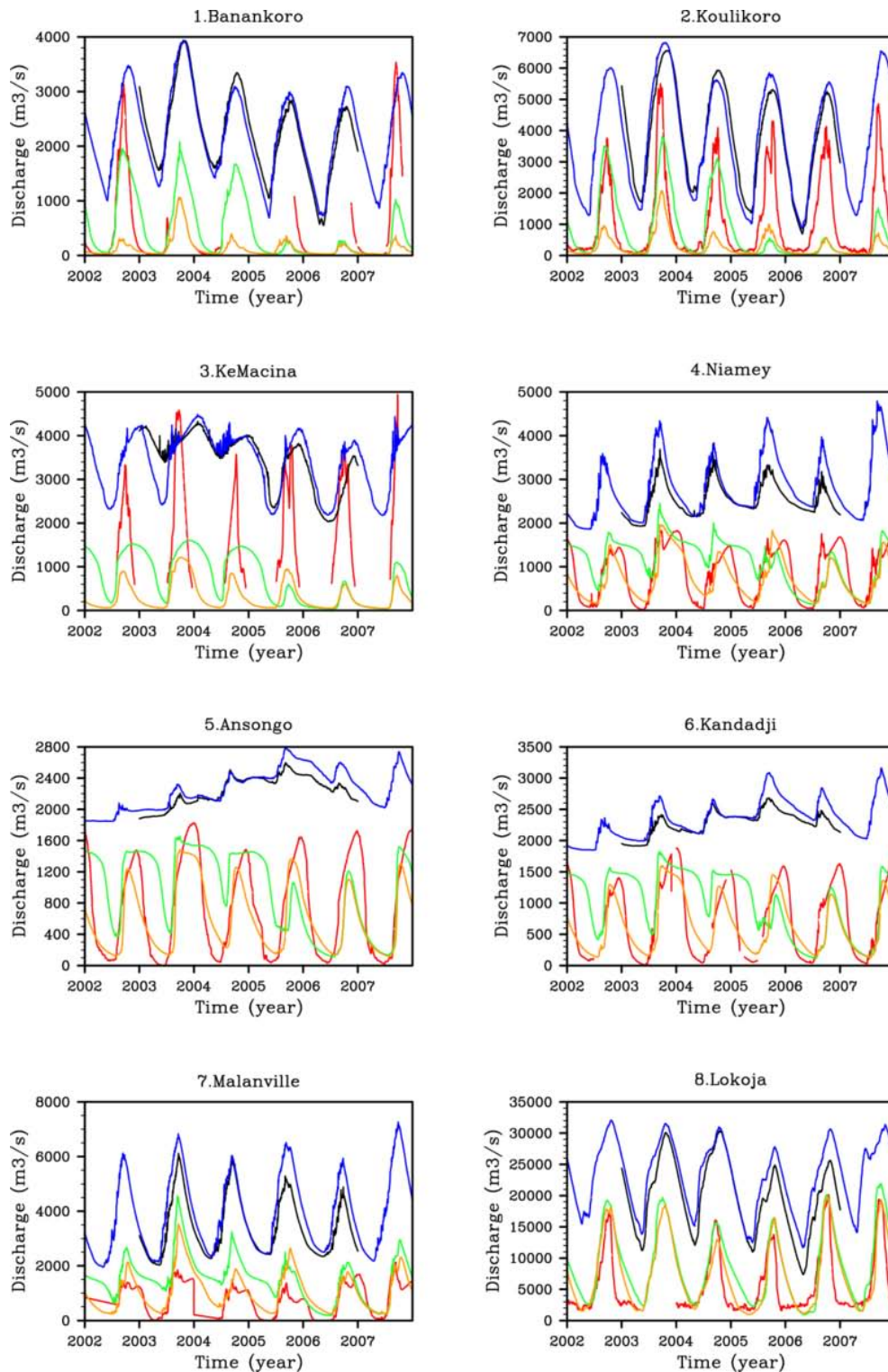


Figure 3.6: As in Fig. 3.5, except the flooding scheme is activated.

Corr	Ban	Kou	KeM	Nia	Ans	Kan	Mal	Lok
TRMM NF	0.79	0.67	0.31	0.63	0.6	0.58	0.68	0.83
TRMM F	0.71	0.6	0.17	0.43	0.46	0.4	0.65	0.81
CMORPH NF	0.61	0.88	0.7	0.62	0.48	0.53	0.79	0.91
CMORPH F	0.24	0.36	0.02	0.23	0.19	0.2	0.33	0.8
PERSIANN NF	0.89	0.85	0.64	0.53	0.36	0.41	0.71	0.95
PERSIANN F	0.68	0.75	0.19	0.56	0.26	0.39	0.68	0.66
RFEH NF	0.89	0.81	0.65	0.68	0.63	0.62	0.69	0.8
REFH F	0.92	0.82	0.61	0.79	0.84	0.81	0.7	0.79
NS								
TRMM NF	0.58	0.23	-1.53	-13.22	-13.58	-11.88	-27.82	-1.59
TRMM F	0.49	0.27	-1.33	-0.21	-0.31	-0.07	-2.19	0.19
CMORPH NF	-26.24	-8.02	-31.72	-291.91	-249.68	-290.57	-513.19	-34.46
CMORPH F	-3.35	-2.98	-2.23	-5.4	-4.1	-4.57	-16.36	-5.5
PERSIANN NF	-5.6	-11.13	-45.95	-669.51	-474.01	-594.52	-1131.05	-72.71
PERSIANN F	-3.43	-4.22	-1.83	-10.64	-6.15	-7.75	-35.27	-12.32
RFEH NF	-0.05	0.03	-1.3	-1.48	-1.11	-1.58	-6.02	-0.34
RFEH F	-0.05	0.01	-1.66	0.59	0.62	0.63	-0.14	0.45
RMS								
TRMM NF	1.18	1.05	0.82	2.65	3.04	2.92	4.07	1.4
TRMM F	1.3	1.03	0.79	0.77	0.91	0.84	1.36	0.79
CMORPH NF	7.84	3.57	3.07	12.19	12.66	13.9	19.91	5.17
CMORPH F	3.8	2.4	0.93	1.78	1.84	1.88	3.16	2.22
PERSIANN NF	4.68	4.19	3.53	18.21	17.75	19.41	25.54	7.47
PERSIANN F	3.83	2.75	0.87	2.4	2.18	2.35	4.57	3.18
RFEH NF	1.87	1.19	0.78	1.11	1.18	1.28	2.01	1.01
RFEH F	1.87	1.2	0.84	0.45	0.5	0.49	0.81	0.64

Table 3.3: Scores of the simulations using different rainfall products as forcing. The precipitation dataset and indication of whether the flooding scheme is activated (F) or not (NF) is shown in the leftmost column. The symbols Corr, NS, and RMS represent the correlation coefficient, Nash-Sutcliff value, and the root mean square error, respectively.

- no flooding scheme, insertion of aquifer reservoir (AQNf);
- flooding scheme activated, insertion of aquifer reservoir (AQF).

Two different rainfall datasets are also used as forcing : TRMM-3B42 and RFEH.

### **3.6.3.1 Discharge**

The simulated discharge for the four configurations when the model is forced by TRMM-3B42 and RFEH, respectively, is shown in Figs 3.7 and 3.8, and the corresponding statistical scores for each configuration are shown in Tab. 3.4 with the best scores indicated by bold type. The statistics are generally better when both floods and aquifers are represented in the model, especially downstream of the inner delta when the model is forced by TRMM-3B42 (see Table 3.4). Upstream of the delta, the Nash-Sutcliffe coefficient and the RMS are generally better without aquifers with both forcing. With RFEH, the aquifers do not lead to a systematic improvement of the scores; however, they do not lead to a significant degradation either.

Before the inner delta, the introduction of aquifers impacts the discharge mostly by reducing the monsoon peak, resulting in a deterioration of the rms score. This deterioration might be due to the 'simplicity' of the aquifer reservoir parametrisation. Indeed, the aquifer is homogeneously defined over all the domain and can generate biases in regions where this aquifer either does not exist or has a minor role.

Downstream of the inner delta, the aquifer impacts mostly the recession flow in two ways: it lengthens the period of maximum discharge and it reduces the discharge during the low flow period. This results in a deterioration in model performance during the period, except in Lokoja where the period and the recession law are improved (Fig. 3.7). When the model is forced by TRMM, the presence of aquifers considerably improves the recession during the dry season. The reduction of low flows is explained by the fact that the river empties faster after the rainy season which results in a more realistic discharge during the dry season. In terms of statistics, the scores (ratio, rmse, eff) are similar or slightly deteriorated, except in Malanville and Lokoja where they are improved. The correlation score, however, is improved at all of the sites. The sensitivity of the model to the choice of the time delay factor  $\tau_{Aq}$  and the fraction  $\alpha$  will be presented in Sect.3.8.

The scores are greatly improved by the addition of the flooding scheme for the locations situated downstream from the inner delta. The configuration with floods and aquifers generally leads to a good improvement of the scores in the sites located after the inner delta when the model is forced by the TRMM rainfall datasets. It is less obvious when the model is forced by RFEH rainfall. However,

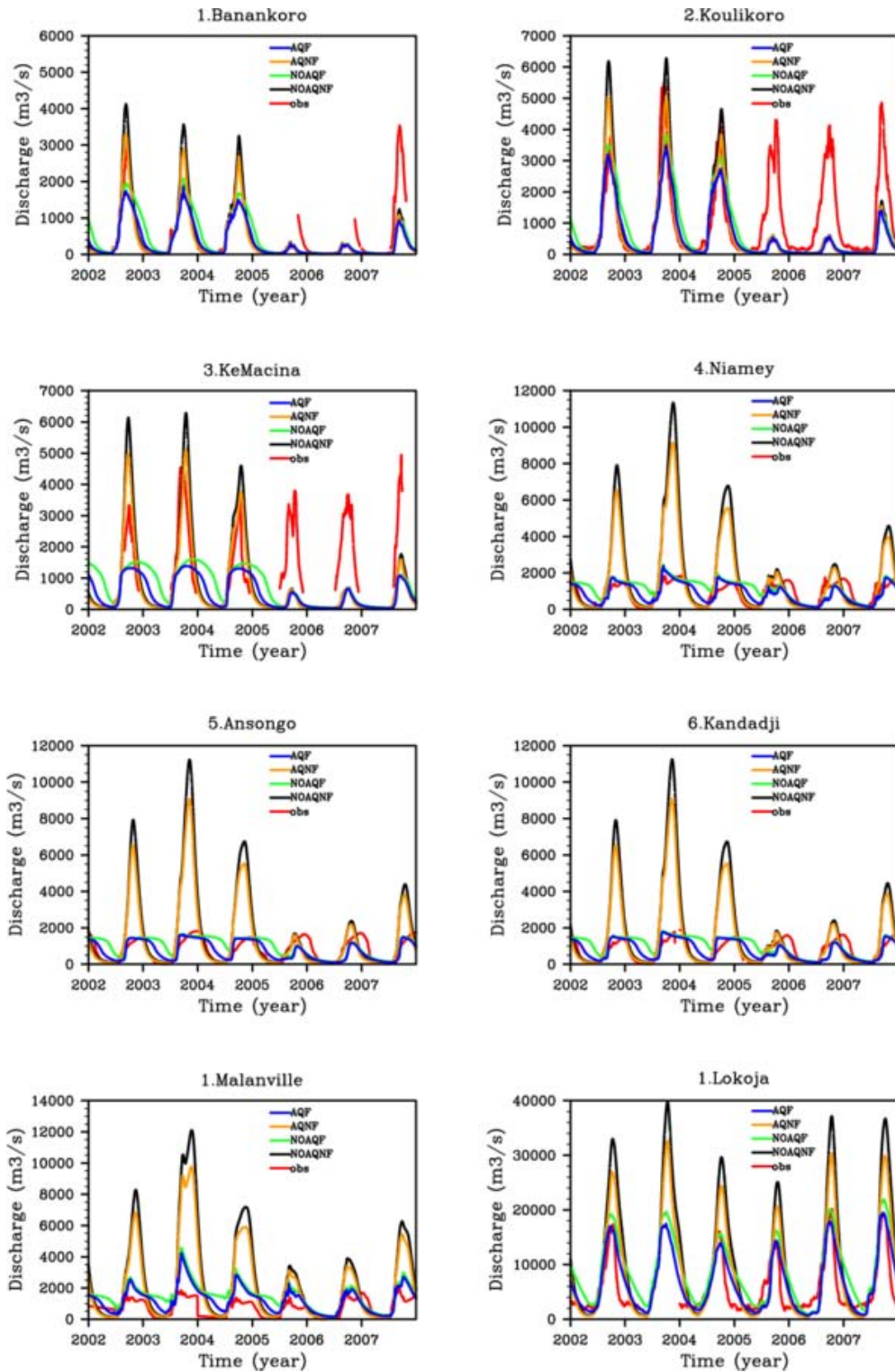


Figure 3.7: Daily discharges (2002–2007) simulated by ISBA-TRIP in the 4 different configurations of the model. Observations are in red. The TRMM-3B42 rain product is used as forcing input.

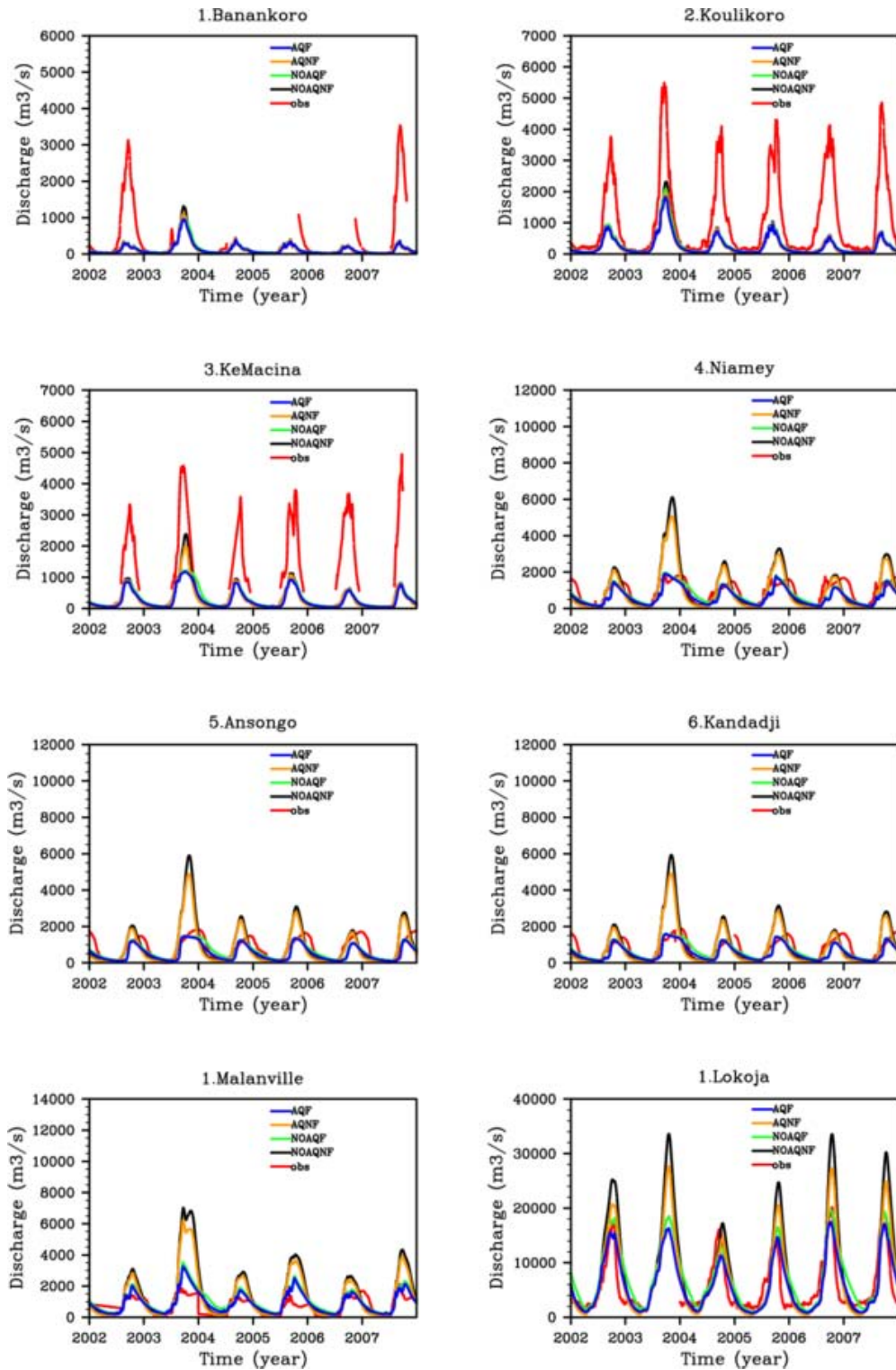


Figure 3.8: Daily discharges (2002–2007) simulated by ISBA-TRIP in the 4 different configurations of the model. Observations are in red. The RFEH rain product is used as forcing input.

Corr. TRMM	Ban	Kou	KeM	Nia	Ans	Kan	Mal	Lok
NOAQNF	<b>0.98</b>	0.9	0.7	0.76	0.74	0.73	0.75	0.81
NOAQF	0.86	0.86	0.23	0.59	0.58	0.56	0.7	0.82
AQNF	0.97	<b>0.91</b>	<b>0.74</b>	0.76	0.73	0.72	<b>0.77</b>	0.83
AQF	0.94	0.9	0.43	<b>0.81</b>	<b>0.86</b>	<b>0.83</b>	0.73	<b>0.87</b>
Corr. RFEH								
NOAQNF	0.9	0.88	0.79	0.71	0.65	0.66	0.74	0.82
NOAQF	0.91	0.89	0.7	0.84	0.86	0.85	0.7	0.8
AQNF	0.89	0.9	<b>0.82</b>	0.7	0.63	0.65	<b>0.75</b>	0.83
AQF	<b>0.92</b>	<b>0.91</b>	0.78	<b>0.84</b>	<b>0.86</b>	<b>0.85</b>	0.74	<b>0.87</b>
NS TRMM								
NOAQNF	0.81	0.57	-0.94	-24.62	-23.07	-26.86	-57.08	-2.27
NOAQF	0.69	0.7	-0.34	-0.53	-0.36	-0.91	-4.42	0.02
AQNF	<b>0.94</b>	<b>0.8</b>	<b>0.17</b>	-14.83	-13.88	-16.76	-35.98	-0.59
AQF	0.82	0.31	-0.43	<b>0.49</b>	<b>0.64</b>	<b>0.41</b>	<b>-1.97</b>	<b>0.66</b>
NS RFEH								
NOAQ-NF	<b>-0.005</b>	<b>0.25</b>	<b>-0.58</b>	-2.58	-2.1	-2.85	-10.17	-0.06
NOAQ-F	-0.01	0.23	-1.09	<b>0.69</b>	<b>0.7</b>	<b>0.71</b>	-0.51	0.4
AQ-NF	-0.02	-0.17	-0.81	-1.41	-1.18	-1.71	-6.31	0.48
AQ-F	-0.03	0.15	-1.19	0.64	0.63	0.69	<b>0.008</b>	<b>0.7</b>
RMS TRMM								
NOAQNF	0.81	0.81	0.76	3.63	3.93	4.36	5.03	1.51
NOAQF	1.04	0.68	0.63	0.89	0.94	1.14	1.54	0.83
AQNF	<b>0.46</b>	0.56	<b>0.49</b>	2.85	3.48	2.45	4.01	1.05
AQF	0.79	<b>0.56</b>	0.65	<b>0.51</b>	<b>0.63</b>	<b>0.61</b>	<b>1.14</b>	<b>0.49</b>
RMS RFEH								
NOAQNF	<b>1.88</b>	<b>1.08</b>	<b>0.69</b>	1.36	1.41	1.62	2.2	0.86
NOAQF	1.88	1.1	0.79	<b>0.4</b>	<b>0.44</b>	<b>0.44</b>	0.81	0.65
AQNF	1.89	1.14	0.73	1.12	1.18	1.36	1.78	0.6
AQF	1.9	1.15	0.81	0.43	0.49	0.46	<b>0.66</b>	<b>0.45</b>

Table 3.4: Daily statistical discharge scores for the four configurations (NOAQNF, NOAQF, AQNF, and AQF) forced by TRMM-3B42 and RFEH from 2002 to 2004. Whether the flooding scheme is activated (F) or not (NF) is adjacent to the model configuration (leftmost column). The symbols Corr, NS, and RMS represent the correlation coefficient, Nash-Sutcliff value, and the root mean square error, respectively.

when the aquifers deteriorate the scores, the deterioration is small compared to the improvements (see Lokoja for example) and likely due to an erroneous or overly-simplistic parametrisation of aquifers in these regions. However, recall that global applications do not aim at calibrating input parameters but at detecting the key processes which impact the evolution of the water cycle. Finally, all of the configurations have difficulty reproducing the discharge in 2005, 2006 and, to a lesser extent, in 2007.

### **3.6.3.2 Flooded fraction**

The quantification of wetland extent is an important step towards a better representation of surface water dynamics. In this study, the time and spatial distribution of wetlands were evaluated over the inner delta region, which is a large inundated area, and over the whole basin. Figs 3.9a-b show the time evolution of the mean monthly flooded fraction (in %) averaged over the inner delta region and over the Niger basin, respectively, with and without aquifers, when the model is forced by TRMM. Figs 3.9c-d present the same results when the model is forced by RFEH. Only the two configurations with and without aquifers are shown as there is no simulated flooded fraction without the flooding scheme. The blue range in Fig. 3.9a and c represents the interval between the minimum and the maximum MODIS derived (JFC) flooded fraction. Over the delta, the simulated flooded fraction is generally included in this range, although it tends to be on the low end when the model is forced by RFEH. These results are reasonable since the MODIS classification (JFC) fraction includes wetted vegetation and near-surface saturated soils. With both rainfall datasets, the presence of aquifers results in a reduction of flooded areas. But the impact of aquifers on the flooded fraction is more obvious for the simulation forced by TRMM rainfall. Indeed, the aquifers greatly improve the period of the floods. However, as shown in Figs 3.9.a-c, the CPP product fractions are approximately 3 times higher than the modelled values over the basin and 10 times higher over the delta. This can be explained by the fact that the multi-satellite method can encounter some difficulties in accurately discriminating between very moist soils and standing open water, likely overestimating the actual fraction of inundations (Papa et al., 2010a, b). Model deficiencies may also explain this bias. They can be related to routing deficiencies due to a bad parametrization, or to LSMs deficiencies in the calculation of floodplains evaporation and/or infiltration.

Fig. 3.10 (panels a and b) shows the time series of de-seasonalized anomalies (obtained by subtracting the 12-year mean monthly value from individual months and then dividing by the standard deviation) over the delta and over the basin, with and without aquifers, when the model is forced by TRMM. Panels c and d present the same results when the model is forced by RFEH. Over the delta, the

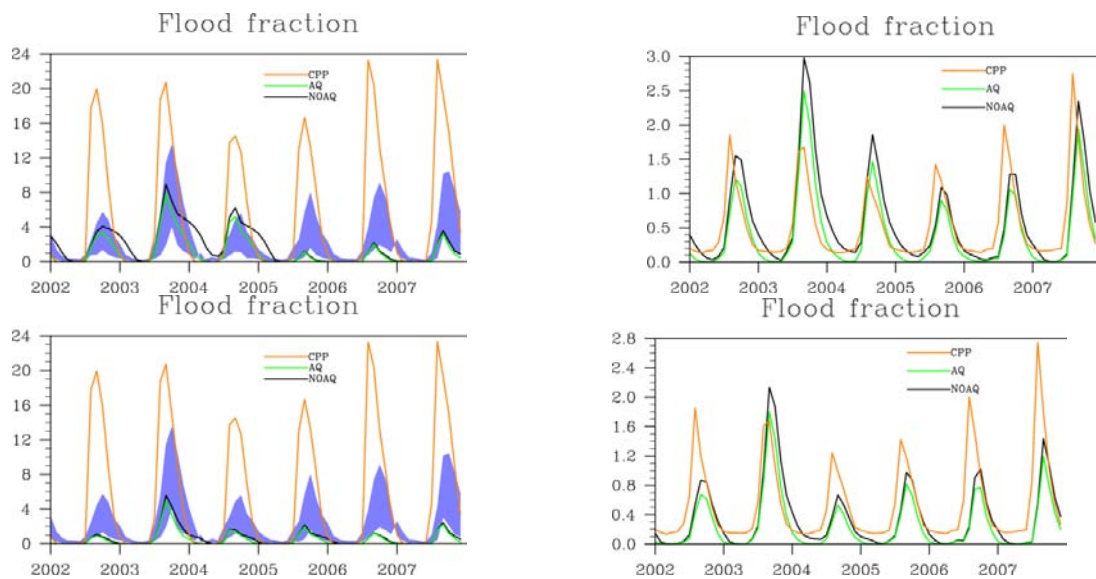


Figure 3.9: **(a)** Time evolution of the mean monthly flooded fraction (in %) averaged over the inner delta region. The model is forced by TRMM-3B42. The blue range is the interval between the minimum and the maximum MODIS classification (JFC) flooded fraction. **(b)** Time evolution of the mean monthly flooded fraction (in %) averaged over the basin. The model is forced by TRMM-3B42. **(c)** Time evolution of the mean monthly flooded fraction (in %) averaged over the inner delta region. The model is forced by RFEH. The blue range is the interval between the minimum and the maximum MODIS classification (JFC) flooded fraction. **(d)** Time evolution of the mean monthly flooded fraction (in %) averaged over the basin. The model is forced by RFEH.

results shown in panels a and c suggest that the model and the data are in good agreement with respect to their time variations, with a better phasing between CPP and ISBA/TRIP. Over the basin, the CPP and model anomalies globally corroborate in phase and amplitude.

The monthly relative CPP flooded fraction averaged over the period 2002–2007 is shown in Fig. 3.11. The monthly values have been divided by the maximum monthly value over 2002–2007 to determinate the main observed flooded areas. According to these observations, the main inundations occur between July and December in three principal regions: the inner delta in Mali, the Northern Nigeria and the Southern basin. The relative flooded fraction simulated by ISBA-TRIP when the model is forced by TRMM is shown in Fig. 3.12. Globally, the floods occur in the same main regions than observed in the CPP dataset. Fig. 3.13 shows the monthly spatial correlation between CPP and ISBA-TRIP when the model is forced by TRMM with floods and aquifers. Over the 3 principal inundated regions, the correlation is larger than 0.4. This correlation does not change significantly according to the configuration of the model.

The impact of flooded areas on total evaporation was investigated. For this, only the grid cells with a flooded fraction higher than 15 % for the configuration NOAQF were considered. These cells represent 11 % of the basin if the model is forced by TRMM and 7 % of the basin if the model is forced by RFEH rainfall. Fig. 3.14 presents the averaged relative difference of total monthly evaporation simulated on these cells with (red) and without (blue) floodplains when the model is forced by TRMM. The evaporation from flooded areas is generally higher with the flooding scheme than without floods, especially during the monsoon and post-monsoon periods (from 20 to more than 50 % larger). The same general conclusions were found for the simulations forced by RFEH (not shown).

### **3.6.3.3 Evaporation**

The impact of the flooding scheme on the surface energy budget was also investigated. The total evaporation includes evaporation from the soil, flooded areas, evaporation from the canopy and evapotranspiration from the vegetation. As shown in Fig. 3.15, the flooding scheme contributes to an increase in the evaporation mainly over the inland delta and in the southern part of the basin during the summer season, which are areas which generally experience significant floods.

The impact of the inland delta region over the discharge has been shown previously. Here, we want to investigate its impact on the evaporation flux. For this, we looked at the relative difference of total evaporation over the delta [13° N–16° N; 3° W–6° W] between the simulations NOAQNF and NOAQF when the model is forced by TRMM (the results are similar with RFEH). This is shown in Fig. 3.16 (blue solid line). Moreover, we added the relative difference of dis-

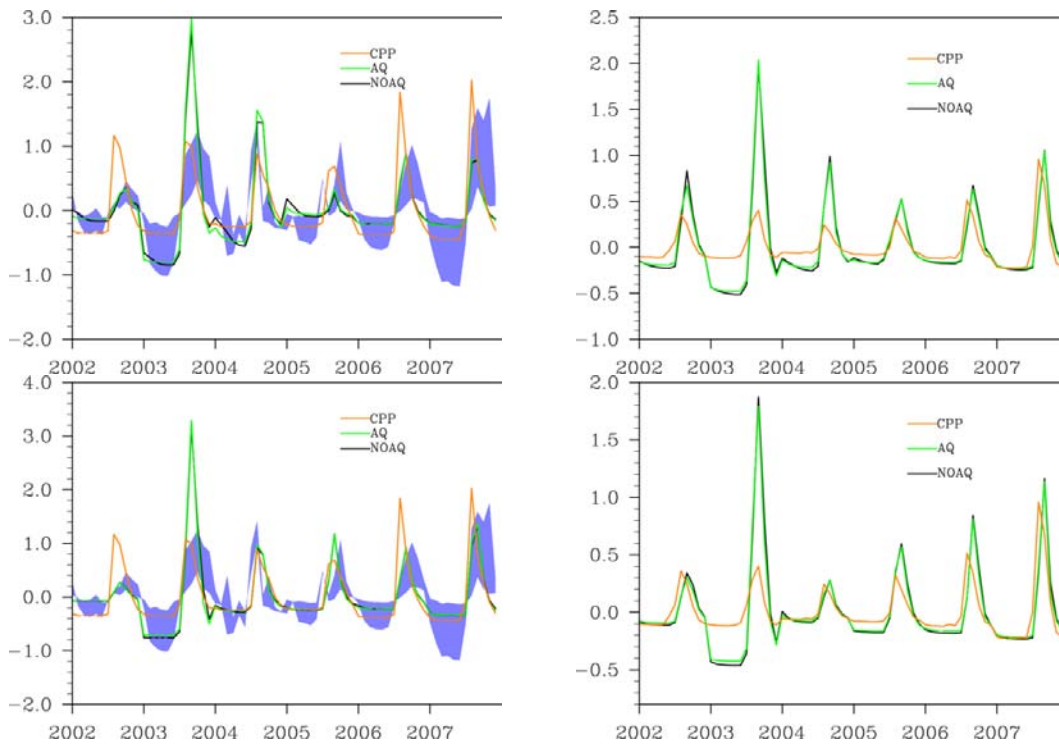


Figure 3.10: **(a)** and **(c)** Time series of deseasonalized flood fraction anomalies (obtained by subtracting the 6-year mean monthly value from individual months and then dividing by the standard deviation) over the delta. The blue range on the left figure delineates the maximum and minimum possible anomalies from MODIS (JFC) products. The CPP product is orange. ISBA-TRIP without aquifers is in black and ISBA-TRIP with aquifers is in green. The TRMM-3B42 is used as forcing for **(a)** and RFEH is used for **(c)**. **(b)** and **(d)** Time series of deseasonalized flood fraction anomalies (obtained by subtracting the 6-year mean monthly value from individual months and then dividing by the standard deviation) over the basin. The CPP product is orange. ISBA-TRIP without aquifers is in black and ISBA-TRIP with aquifers is in green. The TRMM-3B42 is used as forcing for **(b)** and RFEH is used for **(d)**.

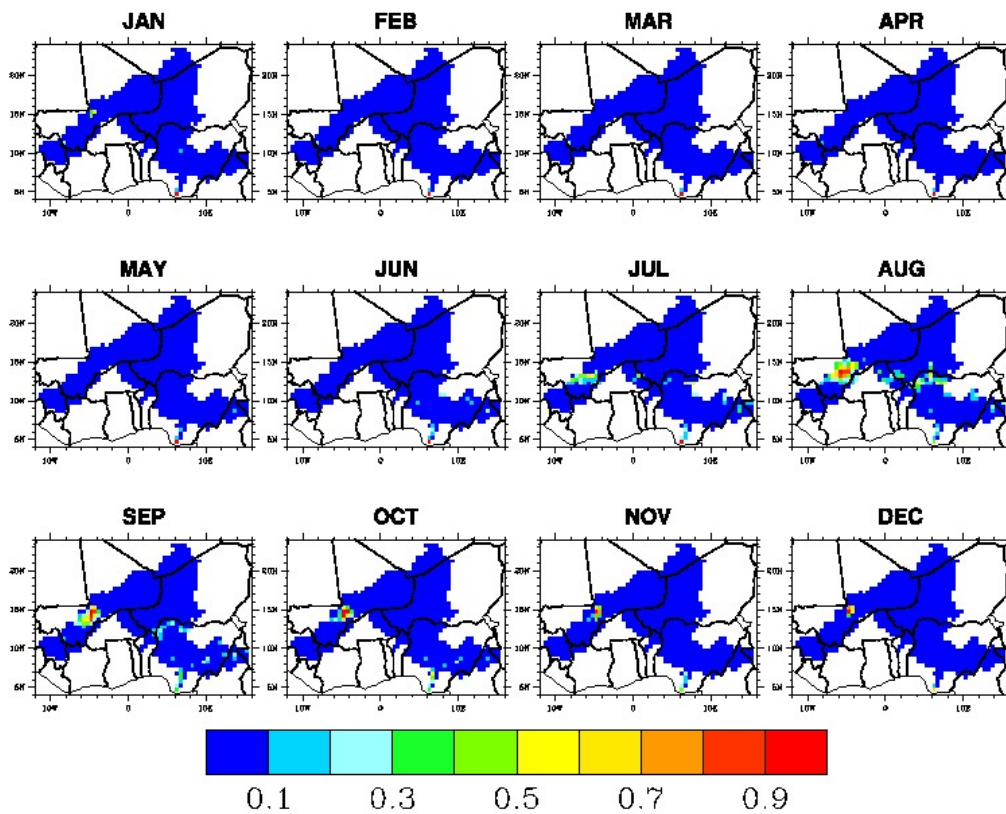


Figure 3.11: Spatial distribution of the normalized CPP flooded fraction averaged over 2002–2007 (the monthly value is divided by the maximum monthly value between 2002 and 2007).

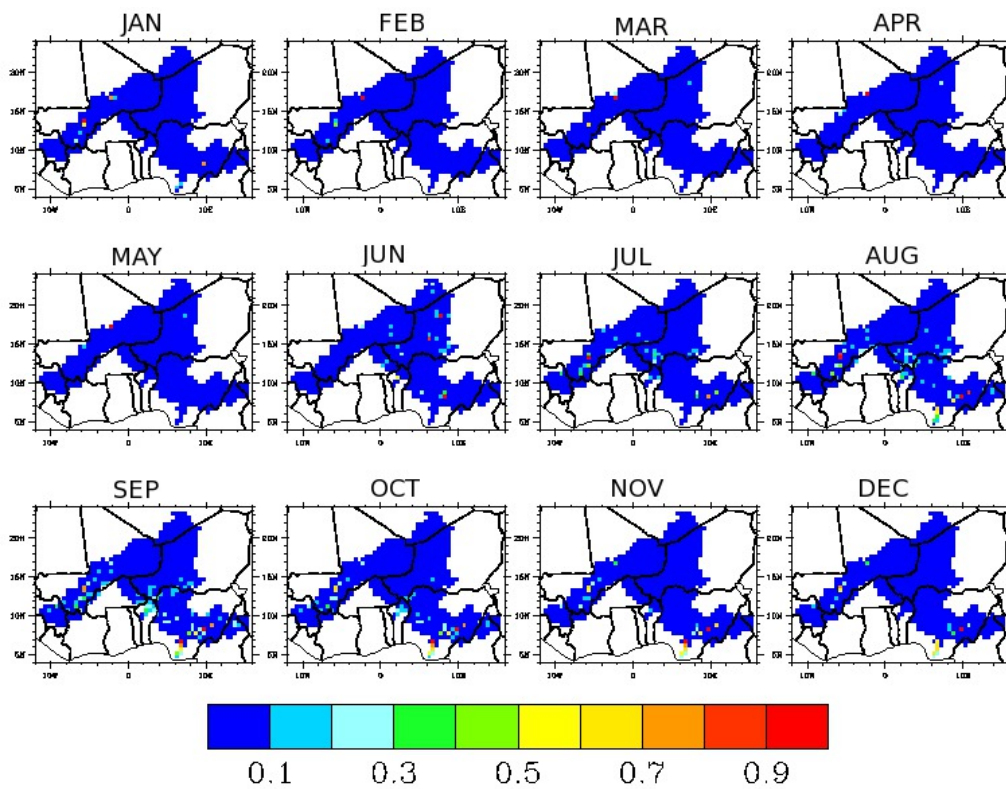


Figure 3.12: As in Fig. 3.11, except for ISBA-TRIP simulation forced by TRMM (the monthly value is divided by the maximum monthly value between 2002 and 2007).

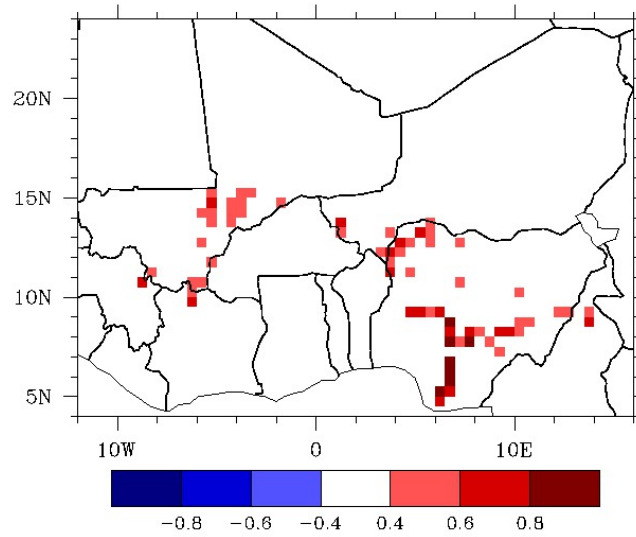


Figure 3.13: Spatial monthly correlation between ISBA-TRIP and CPP over 2002–2007.

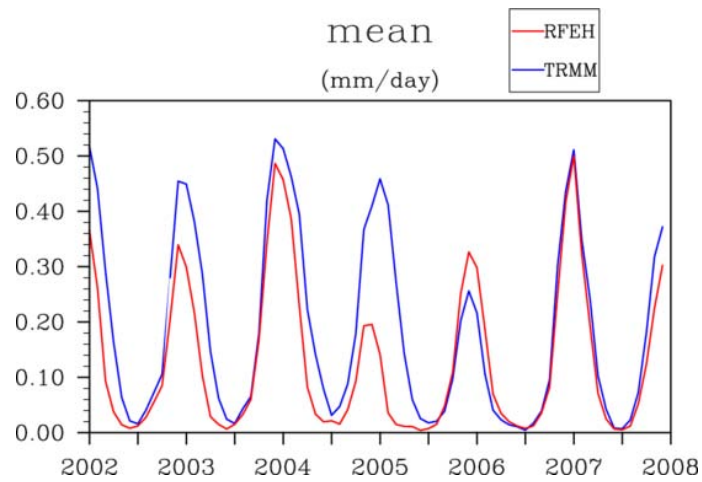


Figure 3.14: Time evolution of the relative difference of evaporation between the two configurations NOAQ-NF and NOAQ-F. Only the cells with a monthly flooded fraction above 15 % from 2002-2007 are considered for the calculation.

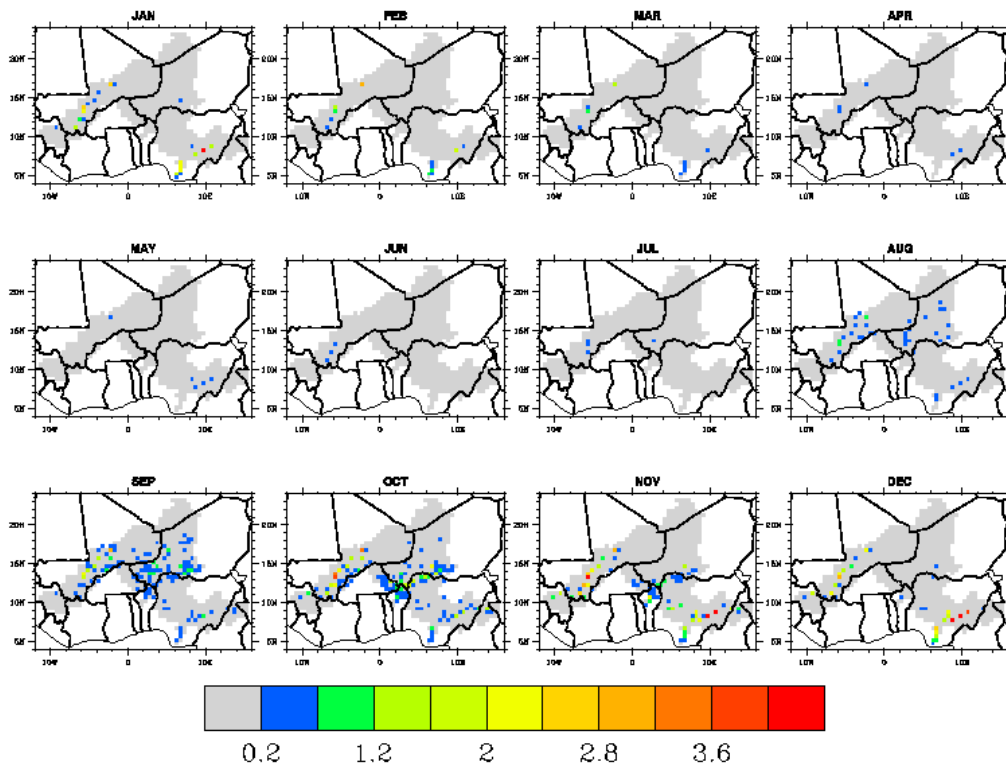


Figure 3.15: Difference of evaporation between the simulations NOAQF and NOAQNF averaged over the period 2002-2007. TRMM rainfall are used as forcing. The difference is calculated only when the mean monthly evaporation without the flooding scheme is bigger than  $1\text{mm}\cdot\text{day}^{-1}$ .

charge between Niamey and Koulikoro (black solid line). Ke Macina is closer to the delta, but as many data are missing on this station, we looked at Koulikoro for the comparison. The dashed lines represent the absolute discharge in Niamey (green) and Koulikoro (red). During the monsoon, the observed discharge in Niamey is 40 to 80 % less than in Koulikoro, as noticed before. However, while the discharge in Koulikoro decreases rapidly at the end of the rainy season, the discharge in Niamey remains at its maximum value and even increases a little, resulting in a second peak of discharge. While the second peak corresponds to the flood signal of the upper Niger basin delayed by the inner delta and has been observed for decades, the first peak is likely related to increased contribution of the tributaries located downstream from the delta that appeared in the past 10 to 15 years (Amogu et al., 2010). The transition between the monsoon and the post-monsoon regime is also visible if we look at the total evaporation simulated with and without the flooding scheme over the delta. Indeed, during the monsoon, there is hardly any difference of evaporation between the two simulations. But, during the post-monsoon, the model including floodplains simulates 30 % more evaporation than without the flooding scheme. The floodplains intensify the creation of evaporation over the delta and the time correlation with the second peak of discharge in Niamey suggest that they also have an impact on the recession flow by lengthening the period of maximum discharge. From 2005 to 2007, we notice a weaker evaporation over the delta than during previous years. This is coherent with the simulated discharge which is also very weak during these three years.

#### **3.6.3.4 River height change**

To complete the evaluation of surface water dynamics, the river height time changes are compared to estimates from the HYDROWEB hydrological database developed by the LEGOS/GOHS (Calmant et al., 2008) which gives estimations of height changes at several points along the Niger river (Fig. 3.1). The seven locations used for comparison are noted in purple in Fig. 3.1. The bias error on the HYDROWEB water levels measures is estimated to be around 20 cm and the peaks of water height changes are within a range between 2 and 4 m. Since our interest is to be able to peaks, this error is considered as relatively small for evaluating water height changes. The water level changes are represented in Fig. 3.17 for the four configurations when the model is forced by TRMM-3B42 rainfall. The statistical scores are represented in Table 3.5 for the two rainfall datasets. The scores are generally improved by the presence of the flooding scheme. The addition of aquifers is more relevant when the model is forced by TRMM rainfall than RFEH. However, the scores are not greatly deteriorated by the presence of aquifers and considerably improved at the other sites. Without

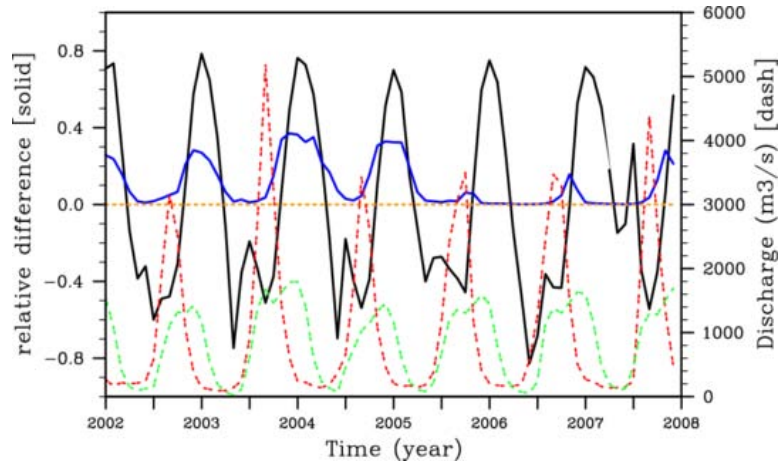


Figure 3.16: Time evolution of the relative difference of simulated total evaporation between the simulation NOAQ-NF(1) and NOAQ-F(2), over the inner delta, when the model is forced by TRMM-3B42 (solid blue line). The relative difference is the ratio  $((2)(1))/((2) + (1))$ . Time evolution of the relative difference of observed discharge between Niamey and Koulikoro (solid black line). Time evolution of the discharge in Niamey (dashed green line) and Koulikoro (dashed red line).

floodplains, the peaks of water height changes are overestimated. The model also overestimates the peaks of positive height changes which might be due to forcing anomalies (rain) or to model deficiencies. Indeed, the surface runoff might be false in some areas and, if overestimated, results in an overestimation of water height variation during rain events. Also, uncertainties in the river bed slope can also result in an overestimation of the water height changes in the valleys. Moreover, Yamazaki et al. (2011) showed the limitation of the kinematic wave approach. Indeed, when kinematic wave equation is used for the discharge calculation, for which the predictability of water surface elevation becomes more error prone in flat river basins with floodplains. However, no attempt is made to calibrate these parameters here, which would be a long and difficult process and which is not necessarily relevant for use in a GCM.

### 3.6.4 Total terrestrial water storage

For water resources management, it is of interest to evaluate the time evolution of total water storage (TWS) in LSMs and the contribution of each continental reservoir to the total water storage variations. As no available observations inform about the water storage variations of each continental reservoir, we used

Chapter 3. Evaluation of the ISBA-TRIP CHS over the Niger basin  
108  
using in-situ and satellite derived data

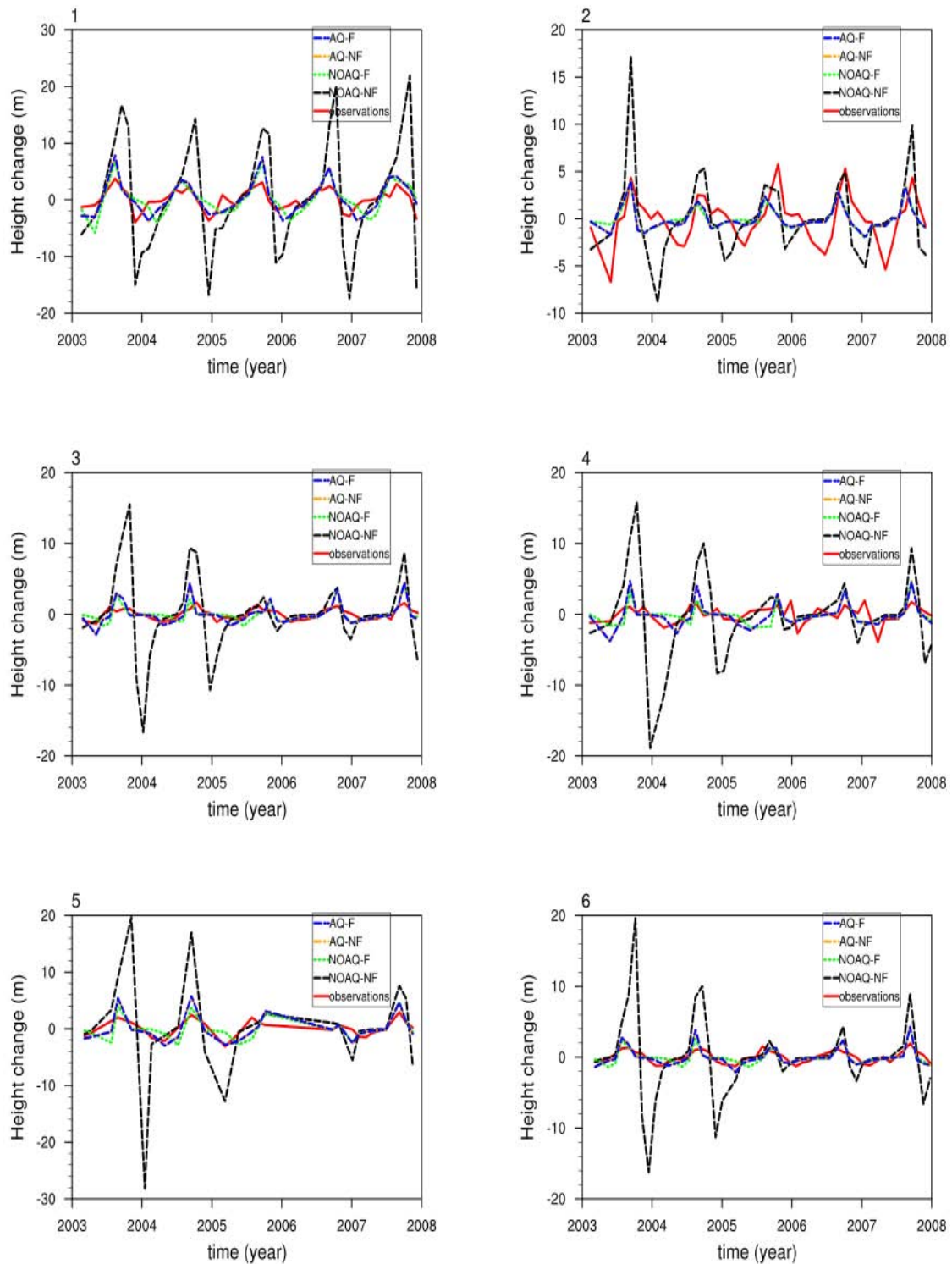


Figure 3.17: Water level changes when the model is forced by TRMM.

Corr. TRMM	1	2	3	4	5	6	7
NOAQNF	0.77	0.43	0.42	0.3	0.53	0.54	0.6
NOAQF	0.56	0.38	0.48	0.36	0.5	0.6	0.69
AQNF	<b>0.79</b>	0.38	0.41	0.3	0.54	0.53	0.61
AQF	0.7	<b>0.44</b>	<b>0.62</b>	<b>0.48</b>	<b>0.75</b>	<b>0.69</b>	<b>0.7</b>
Corr. RFEH							
NOAQNF	0.7	0.41	0.42	0.25	0.48	0.48	0.76
NOAQF	0.59	<b>0.43</b>	<b>0.65</b>	0.45	<b>0.69</b>	<b>0.76</b>	0.81
AQNF	<b>0.73</b>	0.39	0.41	0.24	0.49	0.48	0.79
AQF	0.68	0.4	0.63	<b>0.45</b>	0.67	0.74	<b>0.84</b>

Table 3.5: Correlations of the river height changes (from 2002 to 2007). The best scores are highlighted in bold. The symbols have the same meaning as in Tab. 3.3.

total continental water storage variations issued from the GRACE satellite mission. Fig. 3.18 to 3.21 show the comparison between 3 GRACE satellite products that estimate the total water storage (TWS) change globally at  $1^\circ$  resolution (the blue range in the lower panels represents the difference between the maximum and minimum monthly observation values) and the water storage change in all of the reservoirs of the ISBA-TRIP model, averaged over the basin for the 4 studied configurations. The left panels represent the inter-annual variations (monthly means) and the right panels are the intra-annual variations (2003–2007 average for each month). The blue curve on the lower panels represents the mean water storage change of the Niger basin in all of the ISBA-TRIP reservoirs. The upper panels contain the water storage change in each reservoir (averaged over the basin) and the middle panels present the time evolution of the rain, drainage, runoff and evaporation over the basin. In this figure, only the results for the configuration AQ-F forced by TRMM are shown but Table 3.6 presents the correlations for each configuration. The comparison of ISBA-TRIP water storage change with the GRACE products over the Niger basin shows a very good correlation between the simulation and observations (more than 0.78) independent of the configuration considered.

The contributions of each reservoir to the total water storage change appear in the Table 3.7 for the configuration AQ-F. Although the uppermost soil layers (approximately 1 to a few meters) comprise most of the total water storage change over the basin (49%), the contribution of the other reservoirs, such as the groundwater and the aquifer, are not negligible (17% each). The contribution of flooded zones is less (4%), but since their impact on evaporation is not negligible, they must be considered also. These results emphasize the need for

Corr. TRMM	CSR	JPL	GFZ
NOAQ-NF	0.82	0.82	0.77
NOAQ-F	0.87	0.87	0.83
AQ-NF	0.84	0.83	0.79
AQ-F	0.87	0.86	0.82
Corr. RFEH			
NOAQ-NF	0.82	0.83	0.79
NOAQ-F	0.86	0.87	0.83
AQ-NF	0.83	0.84	0.8
AQ-F	0.86	0.86	0.83

Table 3.6: Correlations of the model TWS with GRACE TWS (from 2002 to 2007).

	River	Soil	Floods	Aquifer	Groundwater
Storage ( $\text{mm day}^{-1}$ )	13	49	4	17	17

Table 3.7: Contribution of the reservoirs for the configuration AQ-F forced by TRMM (%). The storage terms are averaged from 2002-2007.

considering all such reservoirs in LSMs in order to close the water budget. Generally, studies compare the GRACE water storage change to the water storage change in the hydrologic soil layers only, i.e. the first soil meters (green curve in the last panel). However, this approximation is likely less valid for regions with significant storage in flooded zones and deeper soil layers since the contribution of these two reservoirs to the total water storage are not necessarily negligible.

### 3.6.5 Rainfall comparison

In order to better understand the discharge bias observed in the results between 2005 and 2007, a comparison of the rain datasets was done for every year. The averaged monthly ratio for every year  $(\text{TRMM} - \text{RFEH})/(\text{TRMM} + \text{RFEH})$ , which represents the relative bias of one dataset to the other, has been calculated when the monthly sum  $(\text{TRMM} + \text{RFEH})$  is bigger than  $1\text{mm/day}$ . The most significant differences are observed during the monsoon period and are visible in Fig. 3.19 which presents the previous ratio for the months of July, August and September 2002–2007. The basin is delimited by the black contour. Of note, significant differences are seen in the upper basin over the Guinea Highlands. From 2002 to 2004, the TRMM rainfall gives 20 to 80% more rainfall than RFEH. This area is the main source region for the river and this difference prob-

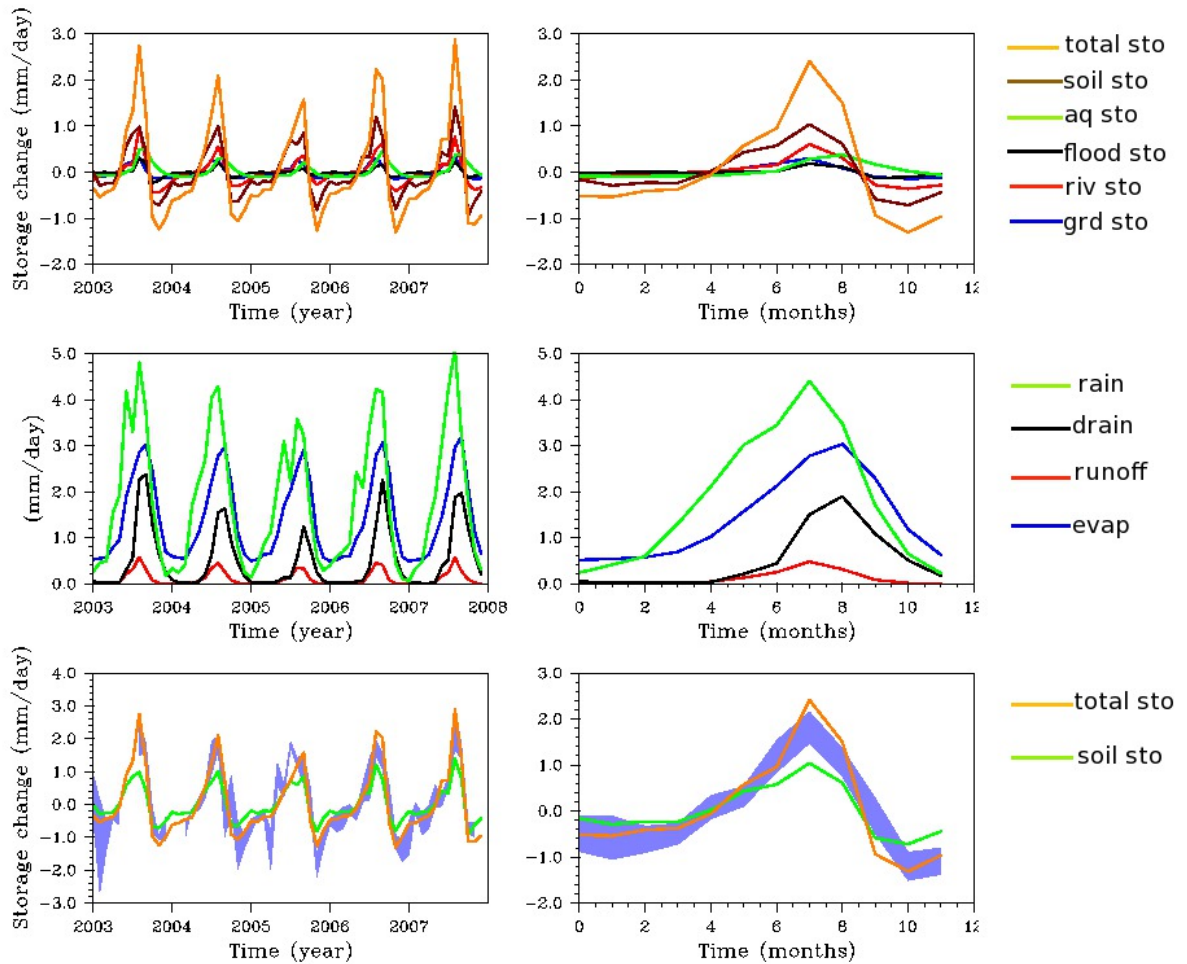


Figure 3.18: Basin water storage change ( $\text{mm day}^{-1}$ ) of each reservoir (top). Time evolution of rain, runoff, drainage and evaporation over the basin (middle). Basin water storage change ( $\text{mm day}^{-1}$ ) in all reservoirs compared to GRACE datasets (down). The blue range is the difference between the maximum and the minimum GRACE products values. Left panels represent interannual variations (monthly averages) and right panels are the annual variations (each month is averaged over the whole 5 year period).

ably explains the fact that the discharge simulated when the model is forced by TRMM is generally bigger than the discharge when the model is forced by RFEH, in particular, when there is no flooding scheme (twice as large as than RFEH). Moreover, the discharge simulated using TRMM rainfall has a longer recession period, probably due to the fact that there is more water going from the floodplains to the river after the flooding season. Fig. 3.19 also shows that in 2005, 2006 and 2007, the relative bias between the two datasets is no longer obvious. Upon further examination of the discharge during these 2 years, it is seen that the two rainfall products produce a very similar discharge amplitude, which results in a significant reduction of the discharge amplitude simulated by TRMM in comparison with previous years. One possible cause for the reduction in input rainfall is that the gauge analysis source was changed from the GPCC Monitoring analysis to the Climate Prediction Center (CPC) Climate Analysis and Monitoring System (CAMS) in May, 2005. This change was made to take advantage of the timeliness in CAMS, but in retrospect it introduced a discontinuity in the error characteristics of the gauge analysis owing to fewer gauges being used (G. J. Huffman, personal communication, 2012). The effect was spatially variable, but seems to be relatively large over the headwater region of the Niger.

### **3.6.6 Aquifer storage**

Despite a generally good performance of the ISBA-TRIP model on the global scale, it was noted that the discharge was still overestimated over certain basins, which was found to be the case for the Niger (Decharme et al., 2011). A possible identified cause was that these regions might overlie large aquifers that can be

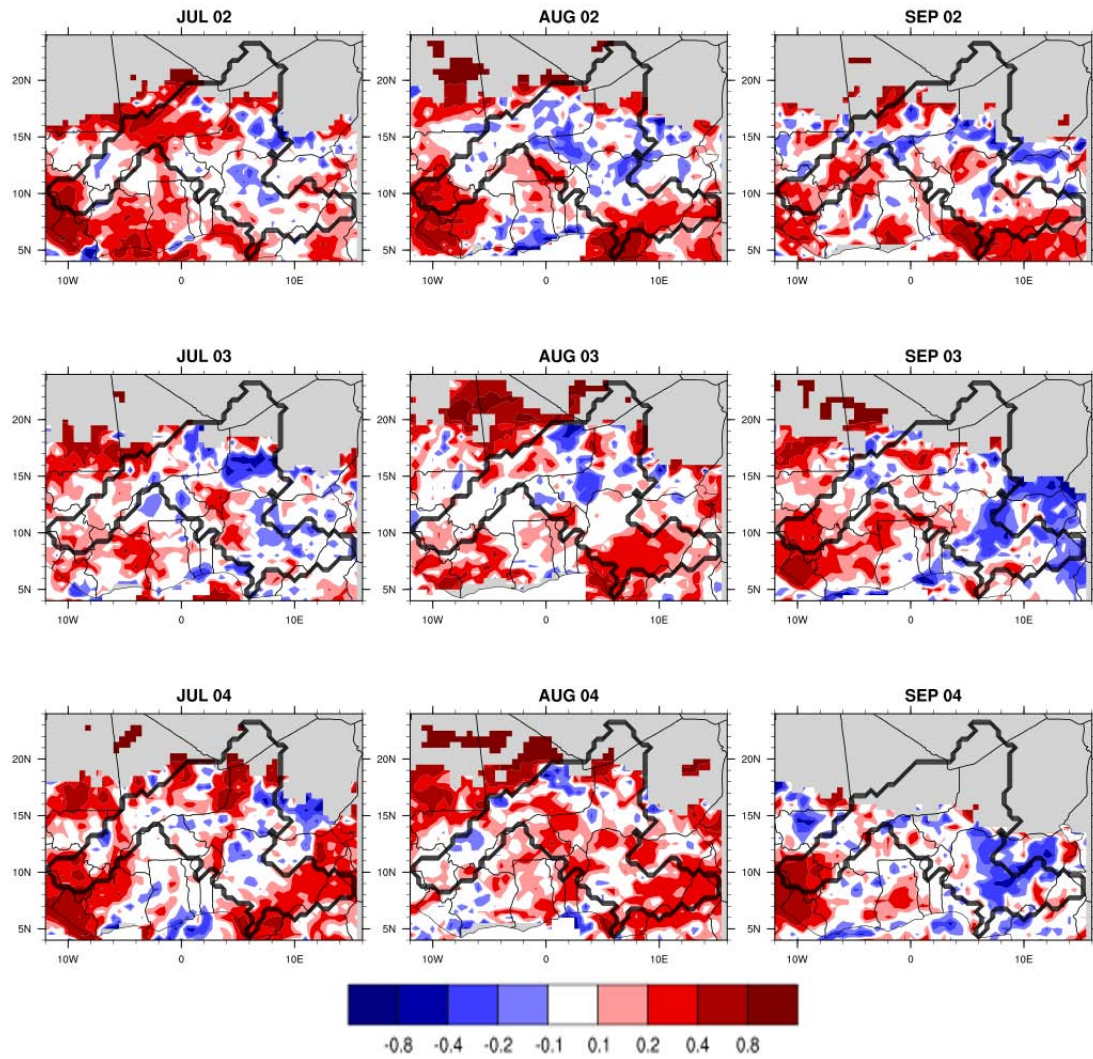


Figure 3.19: Rainfall monthly averaged ratio  $(\text{TRMM} - \text{RFEH}) / (\text{TRMM} + \text{RFEH})$ . The ratio is calculated only when the sum  $\text{TRMM} + \text{RFEH}$  exceeds  $1 \text{ mm.day}^{-1}$

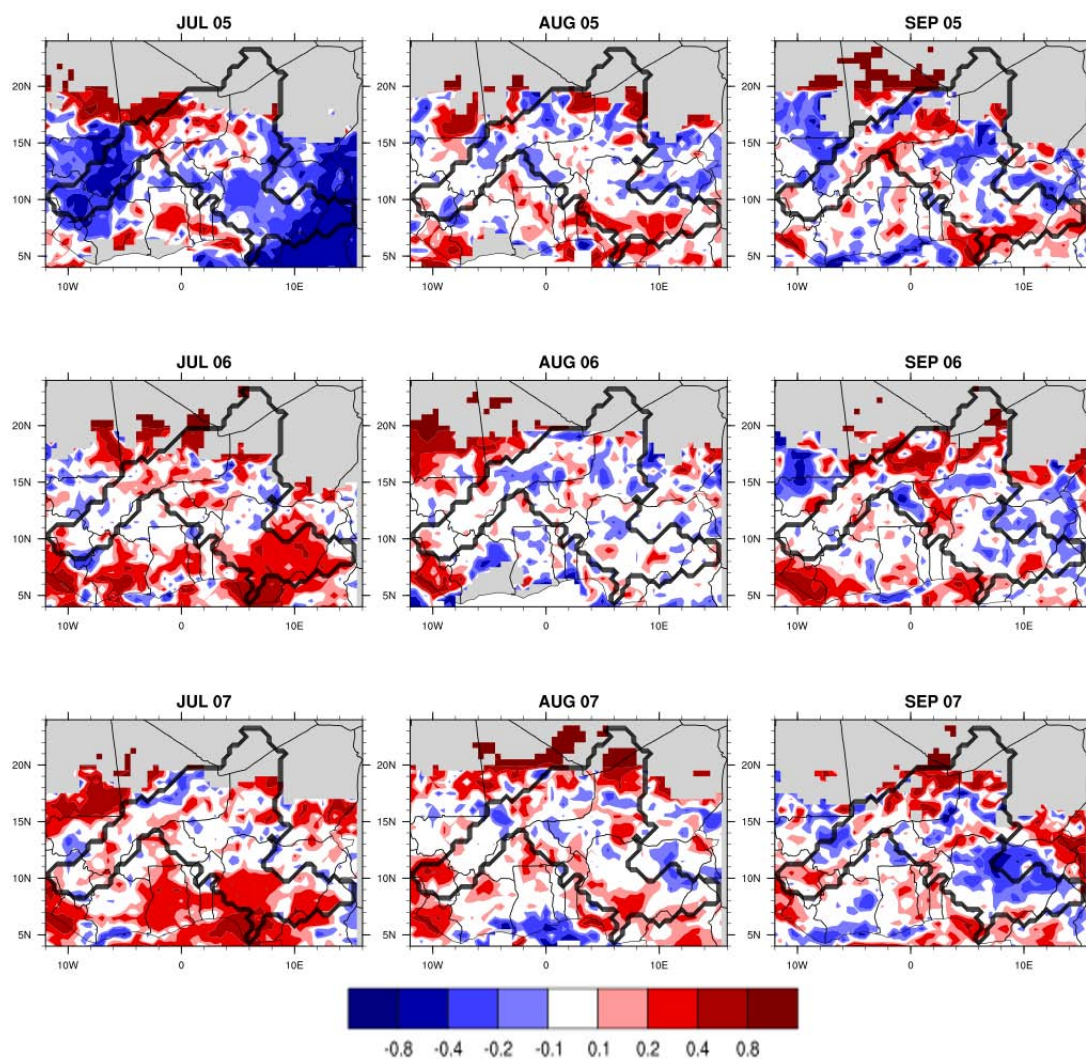


Figure 3.20: voila

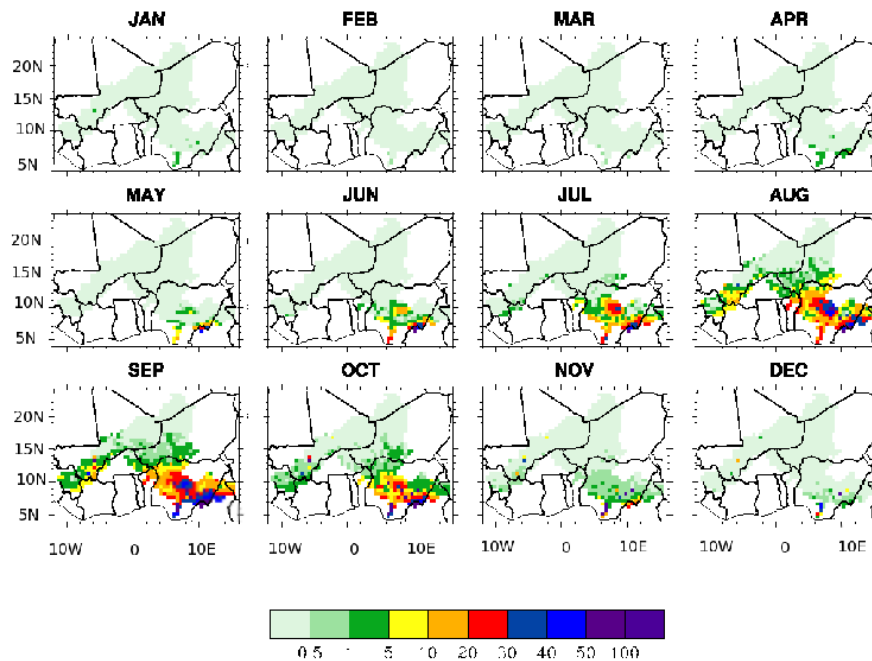


Figure 3.21: Aquifer recharge distribution ( $\text{mm yr}^{-1}$ )

relatively uncoupled to the river. The available data concerning the aquifer storage are generally very localized, making the comparison with such a large scale model difficult or even not relevant. Fig. 3.20 shows the repartition of the aquifer recharge over the basin when the model is forced by RFEH. As expected, the aquifer recharge is very heterogeneous over the basin and follows the rainfall patterns. There is also more aquifer recharge when the model is forced by TRMM than by RFEH. The aquifer reservoir is a relatively simple single-parameter linear reservoir and thus cannot represent high frequency fluctuations and distribution of the aquifer recharge. However, the analysis of total water storage has shown that its contribution to this total storage is not negligible and must be taken into account to reproduce the evolution of the water budget.

### 3.7 Sensitivity tests

Sensitivity tests were performed to determine the input parameters which have the most significant impact on the simulations. For global simulations, it is preferable that the model is not sensitive to too many parameters since tuning is a long and fastidious process at the global scale and spatially distributed global scale observational data is currently rather limited. Generally, physiographic

relationships or the derivation of secondary parameters are preferred. The sensitivity of the ISBA-TRIP model to several key input parameters was investigated in this study in order to test their importance for a single regional scale basin. The Tab 3.8 presents the key input parameters and the variations applied. The RFEH rainfall datasets were used for this study but the sensitivity tests using TRMM-3B42 rainfall datasets lead to the same tendencies with lesser extent when forced by RFEH. Both rainfall datasets were used for this study. However, as sensitivity tests generally lead to the same tendencies according to the rainfall dataset used as forcing, the different figures show the results for only one rain forcing.

The impact of the river critical height,  $h_c$ , on the simulated discharge was examined first. The river width  $W$  is kept at the default value. Increasing the critical height by 20% leads to 5% less flooded fraction over the inner delta and in the southern part of the basin. The evaporation also decreases over the flooded zones by 4 to 12% (relative bias). Conversely, when decreasing the river height by 20%, the flooded fraction is 5% more over the same areas and the evaporation is increased by 14 to 24%. The water height changes are also influenced by the critical height modification. Over the 7 virtual sites, an increase of  $h_c$  globally increases the water height changes (+30%), while a decrease of  $h_c$  decreases the water height changes (-16%). This can be explained by the fact that a river with a small  $h_c$  will be flooded earlier and the water will spread more rapidly over the surrounding area, making the river water level less sensitive to rain events. In terms of inter-annual discharge, increasing or decreasing  $h_c$ , respectively, increases or decreases the amplitude of the discharge by 5 to 15% (Fig. 3.21 a and b). However, the annual variability of the discharge is not changed by a modification of the critical height. In Niamey, Ansongo and Kandadji, the increase of  $h_c$  leads to better statistical scores, which might suggest that the model overestimates the flood extent in these areas. In contrast, in Malanville, the scores are better when reducing the critical height, which suggests an underestimation of flooding at this site. In Lokoja however, the scores are better for the standard simulation.

The impact of the river width,  $W$ , was also investigated. The critical height is held constant. Increasing  $W$  increases the amplitude of the discharge by around 6%, while decreasing arbitrary  $W$  by 20% decreases the discharge by 9% (Fig. 3.21c and d). The water height changes vary differently according to the site. For example, for location 1 (see Fig. 3.1 for locations), a 20% reduction of the river width reduces the mean water height changes by 35% over the studied period. However, for locations 2, 4, 5, 6 and 7, the mean water height changes increase by 15% to 28% and there is no change for location 3. Indeed, water height changes depend on the topography which is modified with river width variations. The evaporation over the flooded areas is reduced by 3 to 9%

Case 1	$h_c$	Spatially distributed constant in time	a. +20 % b. -20 %
Case 2	$W$	Spatially distributed constant in time	a. +20 % b. -20 %
Case 2	$n_{riv}$	Spatially distributed constant in time	a. +20 % b. -40 %
Case 4	$\tau$	Constant in space and time	$\tau = 60; 90$
Case 5	$\tau_{aq}$	Constant in space and time	$\tau_{aq} = 1; 16$
Case 7	$\alpha$	Constant in space and time	$\alpha = \frac{1}{4}, \frac{1}{2}, \frac{3}{4}$

Table 3.8: ISBA/TRIP key input parameters and the variations applied for sensitivity tests.

when  $W$  increases by 20 %, and it is increased by 4 to 16 % when  $W$  decreases by 20 %. This occurs since as  $W$  decreases for the same  $h_c$ , the river capacity is less potentially leading to more floods thereby increasing floodplain and land surface (as the flood retreats) evaporation. There are no significant impacts of  $W$  and  $h_c$  on the total water storage change. Indeed, the storage of the different reservoirs and the amount of drainage are only slightly changed by the modification of these parameters.

The mean value of the Manning coefficient,  $n_{riv}$ , is around 0.075 and most of the pixels have values above 0.06 (see Fig. 3.21). Since the Niger basin covers a large area, the soil properties are very heterogeneous all over the basin, making it necessary to use spatial distributions of soil parameters. Two new distributions of  $n_{riv}$  were created and used to run the model: one distribution in which  $n_{riv}$  is arbitrarily reduced by 20 % and the other one in which it is increased by 20 %.

In order to keep a value included in a reasonable range (between 0.03 and 0.1), all the values out of this range after modification are set equal to the closest value in this range. Fig. 3.22 shows the behaviour of the discharge for each distribution of  $n_{riv}$ . Increasing the Manning coefficient delays the response of the river to rain events. Indeed, small values of the coefficient speed the rise in water level and increase discharge amplitude. Also, the decrease of the discharge after the rainy season is faster when  $n_{riv}$  is smaller. We can also notice that when  $n_{riv}$  is bigger, the model is better able to dissociate the different rain events and two peaks of discharge appear. Flooded areas and evaporation are higher for large values of  $n_{riv}$  as the water flows more slowly in the river bed, generating smaller river height changes, and flooded areas empty to the river more slowly. The evaporation increases by 14 % over main evaporation areas when  $n_{riv}$  is 20 % higher and decreases when it is 20 % smaller. Flooded areas are 15 % higher over the inner delta area when the Manning coefficient increases and

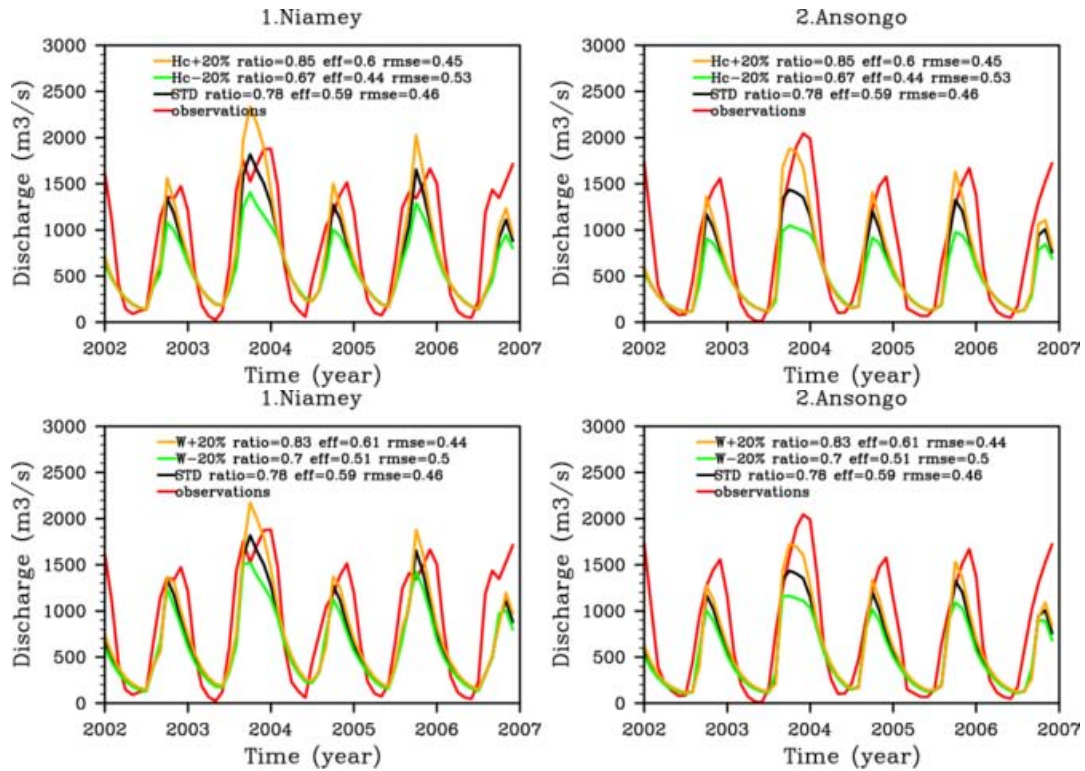


Figure 3.22: Impact of modifications of the critical height  $h_c$  (a and b, up) and of the river width  $W$  (c and d, down) on the discharge (RFEH is used as forcing). The standard run stands for the simulation AQ-F with standard parameters (used for the simulations in previous sections).

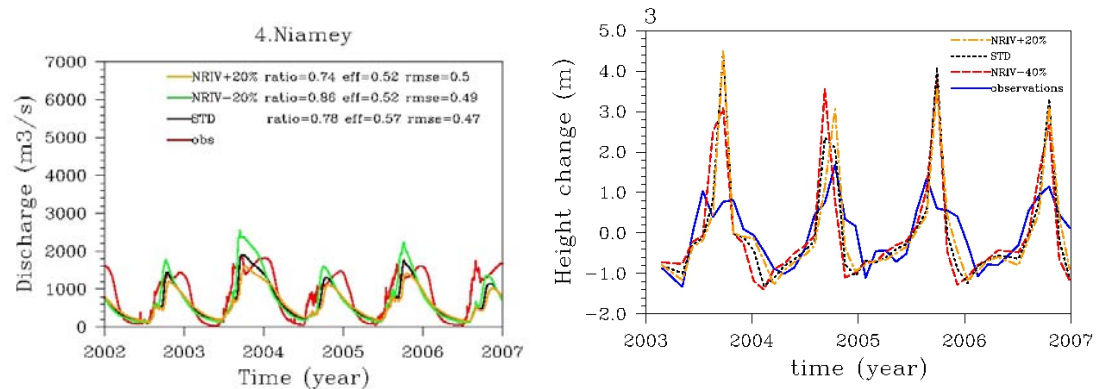


Figure 3.23: Impact of the Manning coefficient on the river discharges and on the river height changes (RFEH is used as forcing). The standard run stands for the simulation AQ-F with standard parameters (used for the simulations in previous sections).

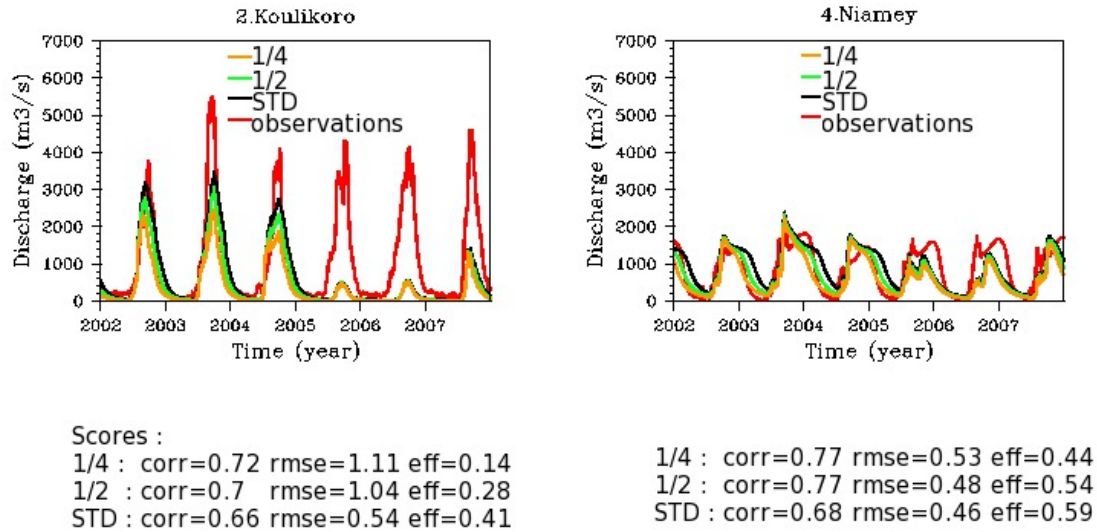


Figure 3.24: Impact of aquifer distribution factor  $\alpha$  on the discharge (TRMM is used as forcing). The standard run stands for the simulation AQ-F with standard parameters (used for the simulations in previous sections).

15% smaller when it decreases. The increase of  $n_{\text{riv}}$  also delays the water height changes, while small values of  $n_{\text{riv}}$  decrease the peaks of river height changes. However, the impact of this coefficient on the water height change is more or less significant according to the observation sites, and for most of them this impact is not obvious. Finally, these modifications of  $n_{\text{riv}}$  have no significant impact on the total water storage change. Thus, the current distribution used in the model is the most reasonable according to the scores. The model is quite sensitive to Manning coefficient, which seems coherent. Since this coefficient is used for the calculation of the flow speed, it will impact the discharge, but also the creation of floods. We also investigated the impact of increasing the groundwater reservoir's time delay factor on discharge, which extends the time of exchange between the groundwater reservoir and the river. Decharme et al. (2010) estimated that a time delay factor of the order of 30–60 days is generally

for global simulations. The increase of  $\tau$  impacts the discharge on the descending phase by deteriorating the recession law. The scores are not significantly changed by the increase of  $\tau$ . The total water storage is not highly dependant on  $\tau$  either (the mean variation represents about 5% of the mean water storage change). However, previous results emphasized that this parameter is important since it increases the residence time of water storage in the basin and allows a more realistic simulation of the discharge.

Finally, we investigated the impact of the aquifer parameters. The reduction

of the distribution factor  $\alpha$  (which means an increase of the water going to the aquifer) decreases the discharge amplitude before the inner delta and accelerates the recession of the discharge after the inner delta (see Fig. 3.23). The scores are not significantly changed by the value of  $\alpha$  when the model is forced by RFEH and they are only modified slightly only few changes when forced by TRMM-3B42. The aquifer reservoir time delay factor also has virtually no impact on the discharge as aquifers are assumed to be too deep and too slow to impact directly the river discharge. Modifications of  $\tau_{Aq}$  have a negligible impact on the total water storage of the basin (the mean variation represents less than 10% of the mean water storage change). However, the simulation is done over a relatively short period (5 years) over which the aquifer time delay factor might be less significant. Over longer periods of time, as for example for climatic studies, it is possible that water storage by aquifers and water discharge to the ocean has a significant impact on the water budget, and thus  $\tau_{Aq}$  could be one key parameter contributing to the water balance.

### 3.8 Chapter conclusions and perspectives

This study investigated the impact of a linear flooding scheme and a simple aquifer storage on the hydrological simulation of the Niger basin, using the ISBA-TRIP Continental Hydrologic System. The simulations are done at a  $0.5^\circ \times 0.5^\circ$  resolution over the 2002-2007 period. The flood scheme accounts explicitly for the precipitation interception by the floodplains, the direct evaporation from the free water surface and the possible re-infiltration into the soil. The deep aquifer reservoir has no feedback with the river locally and drains water to the river mouth over a comparatively long timescale. The model has been developed for use in climate model applications (coupled to the ARPEGE GCM at Météo-France) where the representation of processes such as evaporation from the continental surface and freshwater fluxes to the ocean are fundamental to the global water budget. These applications especially aim at detecting strong anomalies in the future climate, and for this reason we focused on evaluating the ability of the model to reproduce inland water anomalies. Four rainfall datasets were used for the simulation with the flooding scheme activated. However, it was found out that CMORPH and PERSIANN lead to significant overestimations of the discharge (which was consistent with cited studies which showed that these two rainfall products have large positive biases over this region) so that these two datasets were then not used for the rest of the model evaluation.

Considering the relative simplicity of the routing channel, the model provides a good estimation of the surface water dynamics: the spatio-temporal variability of the flooded areas, the river discharge and the river water height changes. The

flooding scheme decreases streamflow and increases evaporation over flooded areas. The impacts of floods on the water fluxes and storage terms are found to be coherent with other studies (Coe et al., 2008; Decharme et al., 2008, 2011; Dadson et al., 2010), thus we further emphasize the need for representing these processes in GCMs. Moreover, the observed data from the ABN have shown a clear change of behaviour of the discharge after the inner delta compared to the discharge before the delta (the discharge is reduced by nearly a factor of two), highlighting the role of the delta in the discharge reduction. This is coherent with the impact of the flooding scheme on the simulated discharge (divided by two after inclusion of floodplains in the model). However, it seems that in ISBA-TRIP, floods occur too early upstream of the delta, as suggested by the results in Ke Macina where the simulated discharge starts to be reduced while it is not the case in the observations. This might be due to poor values of the river parameters, such as river width in this particular region. The aquifer reservoir reduces the low flows and impacts the recession law, especially when the model is forced by TRMM. Moreover, its contribution to the total water budget is not negligible, and thus the consideration of aquifer processes is necessary to better simulate the evolution of the water cycle components. And indeed, several studies qualitatively suggest the presence of a deep water storage reservoir. Note that recently an option to include a detailed representation of aquifers has been introduced into the ISBA-TRIP CHS (Vergnes et al., 2012). However, the quality of the input and observational data required to evaluate the scheme is currently lacking over the Niger basin. For this reason we have opted for a more simple linear reservoir approach in this study (consistent with the other TRIP reservoirs). But future work will include evaluations using this more detailed aquifer scheme as needed data (to define the required geomorphological parameters) becomes available.

The results also suggest that the coupled land surface and river routing model provides a reasonable estimation of inland hydrological processes of the Niger basin when the flood scheme is activated and a deep aquifer is considered. Several diverse datasets have been used for model evaluation such as river discharge, spatial and temporal evolution of flooded areas and water height changes measured by satellite. These data provide basic constraints for estimating the subsurface water storage and dynamics, but also the shallow soil water content and the groundwater storage, which are linearly related to the surface water. The comparison with GRACE total water storage dataset also show a good ability of the model to reproduce the evolution of total inland water.

Evapotranspiration is the remaining water budget component, but large scale observations are not available. The evaluation of this variable has been done within the context of several other studies. The ISBA surface temperature was evaluated using brightness temperatures from AMSR (de Rosnay et al., 2009),

which is related to the surface energy budget and near surface soil moisture; and the monthly sensible heat fluxes aggregated from local scale observations to the ALMIP grid square were evaluated for a semi-arid region within the Niger basin. Finally, regional scale water budget studies were performed over West Africa using ISBA evaporation estimates (Meynadier et al., 2010). All of the aforementioned studies imply that monthly scale evaporation estimates are reasonable. Moreover, Mahe et al. (2009), estimated the water losses of the inner delta of the Niger river and their evolution from 1924 to 1996. They estimated the total evapotranspiration from the delta to be about  $800 \text{ mm yr}^{-1}$  over the period 1924–1996, varying between  $400 \text{ mm yr}^{-1}$  (1984) and  $1300 \text{ mm yr}^{-1}$  (1924). The total evapotranspiration calculated by ISBA over the period 2002–2006 is  $662 \text{ mm yr}^{-1}$ , which is contained in the range estimated by the previous study. They also related the water losses in the delta to the expansion of the floodplains, highlighting the importance of considering floods in a LSM.

However, some model deficiencies remain and can be due to different factors:

- A bias in the runoff and drainage calculated by the LSM. Further improvements could be obtained by calibrating the relevant parameters, but such a procedure would need to be extended to the global scale which is currently quite difficult since needed observational data is sparse at this scale, for certain basins in particular. Some new calibration methods using virtual stations/satellite data are promising in this regard.
- An over-simplified routing model. Indeed, global scale routing models are generally parametrized by geomorphologic relationships, which is not always realistic. Spatially distributed basin-specific parameters would undoubtedly improve the simulations.
- Rain biases can also be the origine of model biases. In this study, we have seen that the generally accepted two best rainfall datasets over this region give significantly different results.

Input rainfall uncertainties can also be the cause of biases in the simulations, as shown in Sect. 4.1 where the model, forced by two different rain datasets, gives significantly different results. In this paper, only the TRMM-3B42 and TRMM-RFE2-hybrid rain dataset, RFEH, were used for the bulk of the validation. However, other rain datasets were used as input rainfall to run the ISBA-TRIP model, such as PERSIANN from the Center for hydrometeorology and remote sensing (CHRS) and CMORPH from the United States National Oceanic and Atmospheric Administration (NOAA). The results of the simulations using both of these rainfall datasets showed a significant overestimation of the discharge (about 5 times higher than with the RFEH forcing for both

CMORPH and PERSIANN forcing, and twice higher for the TRMM forcing) at all discharge observation sites, even with the representation of floods and aquifers. This is consistent with the work of Pierre et al. (2011) who showed that CMORPH dataset clearly overestimates precipitation over the Sahel. Improved spatially distributed remotely sensed datasets which are more precise for hydrological applications are thus needed. For example, the Megha-Tropique satellite project <http://meghatropiques.ipsl.polytechnique.fr/> will potentially provide improved precipitation products over regions such as the Niger, and thus will be used in future studies using models such as ISBA-TRIP (and will hopefully permit an improved modeled hydrological cycle and understanding).

Sensitivity tests have shown that a good routing model is required to optimize the simulation errors. For example, Fig. 3.21 shows that while increasing  $h_c$  in Niamey, Kandadji and Ansongo would improve the simulation score, it would have the opposite effect in Malanville. Thus, improvements in remote sensing technologies should help to create time series maps of the spatially distributed evolution of inland waters (river width, flooded areas expansion, river height) and thus compensate the lack of in situ measurements. These data could then either be used as input data and replace geomorphologic relations used currently to describe these parameters, or they will be assimilated into the model to correct simulation errors.

In GCMs, the input parameters, such as the Manning coefficient, critical height, river width and depth, are defined by empirical relationships which might not give the best results for all modelled basins, since the main objective of such parameterizations is to give the best overall global results. However, for regional or basin scale studies, these relationships lead to non-negligible known errors which could be reduced using satellite data. Indeed, satellite data could be used to spatially distribute parameters by basin and then could contribute to the development of a global database describing the major river characteristics, at least the stream width and the river bankfull height. This is an important step if GCM climate scenario output is to be used for water resource management at the regional scale. The joint CNES-NASA satellite project SWOT will provide water heights and extent at land surface with an unprecedented 50-100 m resolution and precision (centimetric accuracy when averaged over areas of 1 km; Durand et al., 2010). These data will then either be used as input data and replace geomorphologic relations used currently to describe surface parameters, or they will be assimilated into the model to correct model errors. Indeed, a small number of recent studies have begun to quantify the benefits of such a mission for land surface hydrology. For this purpose, synthetic water elevation data were created using the JPL Instrument Simulator (Rodriguez and Moller, 2004) and assimilated into CHS systems (Durand et al., 2008; Biancamaria et al., 2010). In all of these studies, the assimilation of synthetically generated SWOT measure-

### **Chapter 3. Evaluation of the ISBA-TRIP CHS over the Niger basin 124 using in-situ and satellite derived data**

---

ments helped to reduce model errors and improved river discharge simulation. Other studies have used SWOT simulated data as inputs in algorithms to obtain estimates of river depth and discharge (Andreadis et al., 2007; Durand et al., 2010; Biancamaria et al., 2010, 2011). These preliminary results are promising and show the current need for such a mission, and the potential for improving the representation of hydrological processes in current models. Consequently, the work presented in the next chapter will consist of integrating synthetic SWOT data into a suitable assimilation system to determine their impact on the simulated discharge using the ISBA-TRIP CHS described herein.

# Contribution of the SWOT mission towards the improvement of the simulated water cycle

---

## Contents

---

<b>4.1</b>	<b>Data Assimilation (DA) concepts . . . . .</b>	<b>126</b>
4.1.1	Data assimilation variables . . . . .	127
4.1.2	The best linear unbiased estimator . . . . .	129
4.1.3	The extended Kalman Filter (EKF) . . . . .	130
4.1.4	Ensemble Kalman filter . . . . .	131
4.1.5	Variational data assimilation . . . . .	132
4.1.6	Data assimilation applications in global hydrology . . . . .	133
<b>4.2</b>	<b>Assimilation of SWOT observations for the optimisation of TRIP parameters . . . . .</b>	<b>134</b>
4.2.1	Choosing the SWOT data assimilation strategy . . . . .	134
4.2.2	Observing System Simulation Experiment . . . . .	135
4.2.3	SWOT Virtual mission . . . . .	136
4.2.4	Computation of variables used during the assimilation analysis . . . . .	137
4.2.5	Results . . . . .	156
<b>4.3</b>	<b>Use of the optimal analysis for hydrologic forecasting . .</b>	<b>178</b>
<b>4.4</b>	<b>Discussion . . . . .</b>	<b>181</b>
<b>4.5</b>	<b>Chapter conclusions and perspectives . . . . .</b>	<b>186</b>
	<b>Conclusion et perspectives . . . . .</b>	<b>189</b>

---

The previous chapter showed the skill and the limitations of the ISBA-TRIP CHS at simulating the hydrologic and hydrodynamic processes of the Niger river. Considering the relative simplicity of the routing channel, the model provides a

good estimation of the surface water dynamics: the spatio-temporal variability of the flooded areas, the river discharge and the river water height changes. However, some model deficiencies remain, among them is the relatively simple model parameter definitions. Indeed, in large scale models, the parameters used to describe the hydrodynamics are generally few and derived from geomorphologic relationships, leading to model errors. Moreover, in some regions, such as the Niger basin, the lack of spatially distributed datasets is a limitation to having a good description of the soil characteristics. The future Surface Water and Ocean Topography (SWOT) satellite mission will deliver maps of water surface elevation (WSE) with an unprecedented resolution and provide height and slope observations of rivers wider than 100 m and water surface areas above 250 x 250 m over continental surfaces between  $78^{\circ}S$  and  $78^{\circ}N$ . This mission was planned in order to compensate for the lack of relatively high resolution global datasets characterizing continental surface water storage. In the previous study, sensitivity tests were performed to determine the main sources of uncertainty among the TRIP parameters. The Manning coefficient is a roughness coefficient which conditions the surface water dynamics and thus impacts the water levels and discharge. However, this parameter is difficult measure directly. The aim of this chapter is to investigate how the SWOT water levels products could be used to reduce Manning coefficient related uncertainties. Since the SWOT observations are not available yet and also to assess the skill of the assimilation method, the following study is carried out within the framework of an Observing System Simulation Experiment. SWOT virtual measurements are produced using a reference ISBA-TRIP simulation. Here, it is assumed that modeling errors are only due to Manning uncertainties (neglecting the other sources of modeling errors cited in the previous chapter) and the impact of the assimilation system on the Niger River modeling is then quantified. First, a brief review of data assimilation concepts and their applications in hydrology is made. Then, the methodology used to build the assimilation scheme is explained, and the main variables of the assimilation problem are described. Finally, the impact of the assimilation on the main hydrological variables of the Niger basin are presented.

## 4.1 Data Assimilation (DA) concepts

Data assimilation methods were developed in order to estimate the state of a dynamical system by combining various information from diverse sources. In the past 2 decades, they have been used extensively for operational weather forecasting and oceanography but, in recent years, have been applied to an increasing range of earth science disciplines, such as hydrology, glaciology etc... Information used to describe the system generally comes from numerical models or observa-

Symbol	Variable
$\mathbf{y}^0$	Observation vector
$\mathbf{x}^b$	Background vector
$\mathbf{x}^a$	Analysis vector
$M$	Model (non linear)
$H$	Observation operator
$H(x^b)$	Model equivalent in the observation space
$\mathbf{R}$	Observation error covariances matrix
$\mathbf{B}$	Background error covariances matrix
$\mathbf{A}$	Analysis error covariances matrix
$\mathbf{H}$	Jacobian matrix of $H$
$\mathbf{K}$	Gain matrix
$\mathbf{d} = \mathbf{y}^0 - \mathbf{H}(\mathbf{x}_b)$	innovation vector

Table 4.1: Principal variables used in data assimilation methods

tions which are more or less directly associated with the studied system. While most of the time measurements are imperfect and sparse in space and time, the model provides an extensive description of the approximate solution of the physical problem. However, its parameters are not precisely known and time and spatial discretizations induce consistency errors compared to the true state. So both observations and the model are subject to uncertainties. One main advantage of data assimilation is that it can handle incomplete and/or indirect datasets from different sources, and combine them in order to get an optimal value of the 'real' state of the model. The resulting so-called 'analysis', considers the accuracy of the observations (measurements) and the model estimation (background). Before giving a brief description of existing data assimilation concepts, the main variables involved in data assimilation methods are presented in Tab.4.1.

#### 4.1.1 Data assimilation variables

Although the dynamical processes that need to be estimated are continuous, data assimilation, as a correction of a model state, is presented as a discretized (in time and space) problem. Therefore, the different variables used to describe the model state and the observations are represented by vectors and matrices. The period on which the analysis problem is applied is called the assimilation period or window or cycle. The analysis is usually applied sequentially over several cycles as observations become available. The information (observations and model prediction) available over this period are used to estimate an optimal

analysis vector  $\mathbf{x}^a$ , which enables the reduction of model error over this same period as well as over a forecast period.

#### 4.1.1.1 State and control vectors

The state vector describes the discrete state of the model, i.e. the simulated field(s) defined at the grid points of the computational domain. The analysis problem is generally not solved for all of the variables simulated by the model, as the dimension of the system can be beyond computer capacities. It not only takes into account the state variables but also model parameters if they are subject to critical uncertainties. The choice of the variables on which the analysis problem will be applied is thus a critical step of the data assimilation. The most relevant is to focus on those which have the highest uncertainty and to which the system is highly sensitive. These variables are then gathered to form the control vector. It is this vector that will be corrected through the assimilation method. In the context of parameter optimization, the control vector is reduced to a set of  $n$  parameters, defining the control space. It is an approximation of the true control vector,  $\mathbf{x}^t$ , which represents the true values of these  $n$  parameters which are, in reality, unknown. Data assimilation aims at determining an optimal value of the control vector, called the analysis and denoted by  $\mathbf{x}^a$ , which is closer to  $\mathbf{x}^t$  than the background  $\mathbf{x}^b$ , the *a priori* value of the control vector. However, the independent correction of certain variables can lead to physical inconsistencies due to the model equations. In this case, multivariate covariances must be used in order to keep physical consistency between the model variables, and the assimilation increment is applied to all of these variables.

#### 4.1.1.2 Observation vector

The observation vector,  $\mathbf{y}^0$ , consists in all of the available observation data describing the system over the assimilation period. This information is generally sparse in time and space and possibly not directly related to the control variables. While assimilation aims at correcting the model state or a set of distributed parameters, the number of observations over one assimilation period is generally fewer than the dimension of the control space; the analysis problem is said to be underdetermined. This is usually not the case when assimilation is used to correct a spatially uniform parameter. In this case, the system is said to be overdetermined.

#### 4.1.1.3 Observation operator

In order to combine the observational and background information, which are not always described in the same space, an observation operator,  $H$ , going from

the control space to the observation space, is required. For a given state,  $x$ ,  $H(\mathbf{x}) = \mathbf{y}$  is in the observation space. In the context of a model state correction,  $H(\mathbf{x})$  is obtained either by selecting the required fields on the model grid cell (if model and observation spaces are the same), or by an interpolation process (from grid points to observationnal points). However, for parameter optimizations, the matrix  $H$  is a combination of the model integration  $M$  and of either a selection or an interpolation process. In this case, the observation operator is generally non-linear. Some assimilation methods require the linearization of  $H$ , denoted by  $\mathbf{H}$ , which is identified as the Jacobian matrix which consists in a Taylor expansion of  $H$  in the vicinity of a reference value of the control vector  $\mathbf{x}^g$  (usually the background,  $\mathbf{x}^b$ ).

#### 4.1.2 The best linear unbiased estimator

The BLUE algorithm relies on two major assumptions:

- The background and the observation errors are unbiased.
- the variations of the observation operator in the vicinity of the background state are linear: for any  $\mathbf{x}$  close enough to  $\mathbf{x}_b$ ,  $H(\mathbf{x}) - H(\mathbf{x}_b) = \mathbf{H}(\mathbf{x} - \mathbf{x}_b)$ , where  $\mathbf{H}$  is a linear operator.

The vector  $\mathbf{x}$ , of dimension  $n$ , represents the pronostic variables of a model  $M$ . The vector  $\mathbf{y}^0$ , of dimension  $p$ , represents the observations. The observation error,  $\varepsilon^0$ , is known via an observation covariances matrix, noted  $\mathbf{R}$  ( $\mathbf{R} = E[\varepsilon^0 \varepsilon^{0T}]$ ). Then, if  $\mathbf{y}^t$  is the true trajectory projected onto the observation space,  $\mathbf{y}^0$  and  $\mathbf{y}^t$  are related by the relationship :

$$\mathbf{y}^0 = \mathbf{y}^t + \varepsilon^0 \quad (4.1)$$

$H$  is the observation operator, from which obtain the equivalent of the state vector in the observation space is obtained :

$$\mathbf{y}^t = H(\mathbf{x}^t) \quad (4.2)$$

The Jacobian matrix  $\mathbf{H}$  is thus a linear approximation of  $H$  :

$$\mathbf{H} = \frac{\partial H}{\partial \mathbf{x}} \quad (4.3)$$

The a priori estimate (or background) of the true state (before the analysis is carried out),  $\mathbf{x}^b$ , is given by the model, with an error  $\varepsilon^b$  which is described by the background error covariance matrix,  $B = E[\varepsilon^b \varepsilon^{bT}]$  :

$$\mathbf{x}^b = \mathbf{x}^t + \varepsilon^b \quad (4.4)$$

The assumption that the observation and background errors are unbiased can be stated as :

$$\begin{aligned} E[\varepsilon^0] &= 0 \\ E[\varepsilon^b] &= 0 \end{aligned} \quad (4.5)$$

The BLUE algorithm attempts to find an analysis which is a linear combination of the background and the observations :

$$\mathbf{x}^a = L\mathbf{x}^b + K\mathbf{y}^0 \quad (4.6)$$

where L is a linear operator and K is called the gain matrix.

The analysis is an estimation of the true state  $\mathbf{x}^t$  with an error  $\varepsilon^a$ , which is also supposed to be unbiased ( $E[\varepsilon^a] = 0$ ). This error is characterized by an analysis error covariance matrix,  $\mathbf{A}$  ( $\mathbf{A} = E[\varepsilon^a \varepsilon^{aT}]$ ), which can be described as (Bouttier and Courtier, 1999):

$$\mathbf{A} = (\mathbf{I} - \mathbf{K}\mathbf{H})\mathbf{B}(\mathbf{I} - \mathbf{K}\mathbf{H})^T + \mathbf{K}\mathbf{R}\mathbf{K}^T \quad (4.7)$$

The analysis is a linear combination of the background state and of the innovation vector  $\mathbf{d} = \mathbf{y}^0 - H(\mathbf{x}^b)$  :

$$\mathbf{x}^a = \mathbf{x}^b + \mathbf{K}(\mathbf{y}^0 - H(\mathbf{x}^b)) \quad (4.8)$$

The trace of the matrix  $\mathbf{A}$  is the variance of the analysis error. The analysis problem is then reduced to the minimisation of  $\mathbf{A}$ . This is ensured when K is equal to (Bouttier and Courtier, 1999) :

$$\mathbf{K} = (\mathbf{B}^{-1} + \mathbf{H}^T \mathbf{R}^{-1} \mathbf{H})^{-1} \mathbf{H}^T \mathbf{R}^{-1} \quad (4.9)$$

The analysis,  $\mathbf{x}^a$ , can then be expressed as :

$$\mathbf{x}^a = \mathbf{x}^b + (\mathbf{B}^{-1} + \mathbf{H}^T \mathbf{R}^{-1} \mathbf{H})^{-1} \mathbf{H}^T \mathbf{R}^{-1} (\mathbf{y}^0 - H(\mathbf{x}^b)) \quad (4.10)$$

Finally, for the matrix  $\mathbf{A}$  to be minimal, the gain matrix,  $\mathbf{K}$  is expressed using equation (4.7):

$$\mathbf{K}\mathbf{B}\mathbf{H}^T(\mathbf{H}\mathbf{B}\mathbf{H} + \mathbf{R})^{-1} \quad (4.11)$$

### 4.1.3 The extended Kalman Filter (EKF)

This sequential method is an extension of the BLUE algorithm (Gelb ,1974) within the framework of a sequential data assimilation, in which each background is provided by a forecast that starts from the previous analysis. It is adapted

to the real-time assimilation of observations distributed in time into a forecast model  $M$ . In this method, the analysed state, as well as the analysis error, are propagated from one assimilation cycle to the other. The assumptions made here are the same than for the BLUE algorithm. Over one assimilation window, the method is similar to the BLUE. The difference arises from the fact that the analysed state,  $\mathbf{x}^a(t)$ , is integrated by the non linear model until the next assimilation step. Then,  $M(x^a(t))$  is used as the background vector at time  $t + 1$ . The deviation of the forecast prediction from the true evolution is called the model error, it is assumed that it is not biased and that the model error covariance matrix,  $\mathbf{Q}(t)$  is known. This leads to a system of 4 equations, 2 equations for the analysis and 2 others which are used to propagate the errors.

$$\mathbf{x}_b(t + 1) = \mathbf{M}(\mathbf{x}_a(t)) \quad (4.12)$$

Assuming that the model  $M$  is linear, the matrix  $\mathbf{B}$  at time  $t + 1$  is then identified to the propagated matrix  $\mathbf{A}$  (Gelb, 1974; Ricci, 2004)

$$\mathbf{B}(t + 1) = \mathbf{M}\mathbf{A}(t)\mathbf{M}^T \quad (4.13)$$

where  $\mathbf{M} = \frac{\partial M}{\partial x}$ , and

$$\mathbf{x}_a(t) = \mathbf{x}_b + \mathbf{K}(t)[\mathbf{y}(t) - H(t)\mathbf{x}_b(t)] \quad (4.14)$$

$$\mathbf{A}(t) = [\mathbf{I} - \mathbf{K}(t)\mathbf{H}(t)]\mathbf{A}(t) \quad (4.15)$$

where the gain matrix  $\mathbf{K}$  is calculated as :

$$\mathbf{K}(t) = \mathbf{B}(t)\mathbf{H}^T(t)[\mathbf{H}(t)\mathbf{B}(t)\mathbf{H}^T(t) + R(t)] \quad (4.16)$$

This method necessitates storage capacity to propagate the matrix  $\mathbf{A}$ . Moreover, the estimation of  $\mathbf{M}$  is usually difficult. In addition, the operation of making the matrix product is generally fastidious.

#### 4.1.4 Ensemble Kalman filter

The EnKF is an ensemble method in which the estimation of the matrices used to calculate the analysis are estimated using an ensemble of simulations (Evensen, 2004). This way, the matrix products are made easier. The analysis vector  $\mathbf{x}_a$  is written as :

$$\mathbf{x}_a = \mathbf{x}_b + \mathbf{B}\mathbf{H}^T(\mathbf{H}\mathbf{B}\mathbf{H}^T + \mathbf{R})^{-1}(\mathbf{y}^0 - H(\mathbf{x}_b)) \quad (4.17)$$

To estimate the terms of this equation, an ensemble of background simulations with different initial conditions is launched. Then the matrix products are described as (Evensen, 2004):

$$\mathbf{B}\mathbf{H}^T \approx E[(\mathbf{x}_b - \bar{\mathbf{x}}_b)(H(\mathbf{x}_b) - \overline{H(\mathbf{x}_b)})^T] \quad (4.18)$$

$$\mathbf{HBH}^T \approx E[(H(\mathbf{x}_b) - \overline{H(\mathbf{x}_b)})(H(\mathbf{x}_b) - \overline{H(\mathbf{x}_b)})^T] \quad (4.19)$$

$$\mathbf{B} \approx E[(\mathbf{x}_b - \overline{\mathbf{x}_b})(\mathbf{x}_b - \overline{\mathbf{x}_b})^T] \quad (4.20)$$

where  $\overline{\mathbf{x}} = E[\mathbf{x}]$ .

The background matrix at time  $t + 1$  is obtained by propagating the analysed state :

$$\mathbf{B}(t + 1) \approx \mathbf{A}(t + 1) \approx E[(\mathbf{x}_a - \overline{\mathbf{x}_a})(\mathbf{x}_a - \overline{\mathbf{x}_a})^T]. \quad (4.21)$$

This method is useful since it allows the calculation of the analysed state without explicitly calculating the matrices of Eq. 4.16. However, it necessitates a large number of runs.

#### 4.1.5 Variational data assimilation

The variational assimilation technique aims at finding the optimal analysis,  $\mathbf{x}_a$ , field that minimizes a cost function,  $J$ . The cost function is then defined as the weighted distance between  $\mathbf{x}$  and the background  $\mathbf{x}_b$ , plus the weighted distance to the observations  $\mathbf{y}^0$  :

$$J(\mathbf{x}) = \frac{1}{2} (\mathbf{x} - \mathbf{x}_b)^T \mathbf{B}^{-1} (\mathbf{x} - \mathbf{x}_b) + [\mathbf{y}^0 - H(\mathbf{x})]^T \mathbf{R}^{-1} [\mathbf{y}^0 - H(\mathbf{x})] \quad (4.22)$$

The minimum of  $J(\mathbf{x})$  is obtained for  $\mathbf{x} = \mathbf{x}_a$  such that

$$\frac{\partial J}{\partial \mathbf{x}} = \nabla_{\mathbf{x}} J(\mathbf{x}_a). \quad (4.23)$$

Assuming that the analysis is close to the truth,  $\mathbf{x}$  can be written  $\mathbf{x} = [\mathbf{x}_b + (\mathbf{x} - \mathbf{x}_b)]$ . Then, assuming that  $\mathbf{x} - \mathbf{x}_b$  is small, the observation operator can be linearized :

$$\mathbf{y}^0 - H(\mathbf{x}) = \mathbf{y}^0 - H[\mathbf{x}_b + (\mathbf{x} - \mathbf{x}_b)] = \mathbf{y}^0 - H(\mathbf{x}_b) - \mathbf{H}(\mathbf{x} - \mathbf{x}_b). \quad (4.24)$$

where  $\mathbf{H}$  is the adjoint of the linear operator.

The gradient of  $J$  with respect to  $\mathbf{x}$  is written (when  $H$  is linear) :

$$J(\mathbf{x}) = \mathbf{B}^{-1} (\mathbf{x} - \mathbf{x}_b) + \mathbf{H}^T \mathbf{R}^{-1} (\mathbf{y}^0 - H(\mathbf{x}_b)). \quad (4.25)$$

$J$  is a minimum when  $\nabla J(\mathbf{x}_a) = 0$ , which leads to an equation for  $\mathbf{x}_a - \mathbf{x}_b$  :

$$J(\mathbf{x}) = \mathbf{B}^{-1} (\mathbf{x}_a - \mathbf{x}_b) + \mathbf{H}^T \mathbf{R}^{-1} (\mathbf{y}^0 - H(\mathbf{x}_b)) \quad (4.26)$$

and the analysis  $\mathbf{x}_a$  is :

$$\mathbf{x}_a = \mathbf{x}_b + \mathbf{B}^{-1} \mathbf{H}^T \mathbf{R}^{-1} \mathbf{y}^0 - H(\mathbf{x}). \quad (4.27)$$

This method does not explicitly consider the time variable. Thus, it can be used over a temporal cycle or assimilation window, to find an optimal initial state which allows an optimal evolution of the model (closer to the observations over this period). The variational technique is useful because it does not require the propagation of the error matrices.

#### 4.1.6 Data assimilation applications in global hydrology

Remote sensing data are usually used for hydrological applications as input parameters (or forcing data), or for model calibration (e.g. Andersen et al., 2002; Stisen, 2008, Campo et al., 2006). Recently, automatic calibration methods using remote sensing water levels have been developed for hydrological models calibration (Getirana, 2010; Milzow et al., 2011). These methods are based on optimization algorithms that attempt to find the best parameters that fit with the observed data. However, unlike DA methods, they do not consider observation and modeling errors. The interest in DA for global scale hydrology applications is relatively new, and few applications have been reported.

Drusch et al. (2009) used observations of 2m air temperature and soil moisture to evaluate a Kalman filter based soil moisture analysis system and its impact on the operational ECMWF integrated forecast system. They showed that the impact of EKF on the forecast skill of the operational weather forecast model was neutral but gave the promising possibility to better constrain the soil water content with more accurate soil moisture estimates. Neal et al. (2009) assimilated water level estimates derived from multi-temporal SAR imagery into a coupled hydrological and hydrodynamic model of an ungauged basin. In a similar approach, Montanari et al. (2009) used SAR-derived water levels to update the model states of a simple rainfall-runoff model, which was coupled to a one-dimensional flood inundation model. Pereira-Cardenal et al. (2011), investigated the potential of using ENVISAT water levels observations in a real time or near real time context to update a semi distributed hydrological model state variables, applying an Ensemble Kalman Filter. The method was applied to the Syr Darya River Basin, a  $7000\text{km}^2$  complex mountainous region. They showed that the assimilation allowed a better real time estimation of reservoir levels over the region. However, because of the state updating procedure used in this study, consisting in adding or abstracting water from reservoirs, the method is limited to medium-term forecasting, and is not suitable for long-term water resources scenario calculations, where mass balance has to be maintained. Salamon and Feyen (2009) used the residual resampling particle filter to assess parameter,

precipitation and predictive uncertainty in the distributed rainfall-runoff hydrological model LISFLOOD for a the Meuse catchment using discharge measurements. They showed that the equifinality hypothesis (several different solutions can lead to a good estimation of the discharge) was a limitation to the correction of a distributed hydrological parameter even in a physically based hydrologic model. Moreover, he emphasized the strong effect of rainfall uncertainties on the analysis. Finally, the results showed that accounting for parameter uncertainty only during a calibration phase was not sufficient to properly predict uncertainty, limiting the application of the method for hydrologic forecasting over longer time periods.

These application of DA in hydrological modeling have shown the skill possibility to use remote sensing data in order to improve the model states or the parameters. However, they also showed the limitations due to the generally low spatial and temporal resolution of these datasets. For the correction of distributed input parameters for example, they showed the limitations related to the equifinality issue which might lead to non-physical solutions of the DA system. With its high spatial and temporal resolution, the SWOT satellite offers a possibility to better constrain DA applications in large scale hydrology.

## 4.2 Assimilation of SWOT observations for the optimisation of TRIP parameters

### 4.2.1 Choosing the SWOT data assimilation strategy

SWOT will provide global 2D maps of water levels at an unprecedented resolution, allowing a better estimation of surface water spatial and temporal evolution. Before its launch, which is currently planned for 2019, scientific studies must be carried out in order to report on the possibilities of using SWOT products in fields such as oceanography or hydrology. This will help in making critical decisions, such as the choice of the satellite orbit for the validation/calibration phase. In hydrology, the SWOT satellite data will be a crucial tool for complicated issues, such as water resource management and global hydrological modeling. Indeed, our knowledge of global continental water variations is currently limited by the lack of observations. Such observations could help to improve the validation of large scale hydrologic models. Data assimilation applications in hydrology have been gaining interest recently, due to the increase of remote sensing observations. They generally consist in using observed data of discharge or soil humidity to improve model states, and are usually applied to basin catchments (Reichle et al., 2002; Pauwels and De Lannoy, 2006; Zaitchik et al., 2007; Crow and Ryu, 2009). These methods have been shown to be useful for real time water resource

management applications.

For climate change or scenario applications, in which simulations can be launched over several decades or even hundreds of years, it is not possible to correct the land surface model state since no future observations are available. Thus, assimilation can be used over a calibration period either to correct model parameters or potentially improve physics. As a pre-launch study, the first part of this work consisted in choosing an assimilation strategy which would be appropriate for GCM applications. As shown by the sensitivity tests of Chapter 3, the uncertainties of some of the TRIP hydrologic parameters induce significant errors in the simulation of the discharge and water levels. If some of these parameters will be better estimated with the improvement of remote sensing technologies (river width, topography etc...), other parameters such as the Manning coefficient, although important, remain difficult to evaluate precisely. Therefore, it was decided to develop an assimilation method of SWOT observed water elevations to reduce the uncertainties on this parameter. The methodology used to develop the assimilation method of SWOT virtual observations is presented in the next section.

### **4.2.2 Observing System Simulation Experiment**

The Observing System Simulation Experiment (OSSE) aims at simulating the data that would be observed by the measurement platform, and using them as observations for the data assimilation (DA) problem. This method is particularly useful within the framework of the preparation step of the SWOT satellite mission, since it allows a quantification of the contribution of the satellite data to the modeling of the Niger basin before launch. The concept of OSSE is presented in Fig 4.1. First, the method necessitates a realistic modeling of the studied basin (Chapter 3). Indeed, the model must be able to simulate the major hydrodynamic processes of the basin so that the simulated observations will better fit the reality. The ISBA-TRIP set-up evaluated in the Chapter 3, with the inclusion of a flooding scheme and an aquifer reservoir, will be considered as the 'truth'. Then, a simulator is used to generate the SWOT observations at the grid points of the model. These data actually represent what the SWOT instrument would measure if the model was exactly representing the real conditions. To account for the modeling uncertainties, the 'truth' is then perturbed. Finally, an assimilation scheme is built and applied to the perturbed run in order to obtain a corrected simulation, which is closer to the 'truth'. In this study, the assimilation aims at correcting input parameters of the TRIP routing model, which are associated with uncertainties, using SWOT virtual water levels. The contribution of such a correction to the ISBA-TRIP modeling, will be estimated by comparing the model distributed and mean diagnostics (water level, discharge, water storage

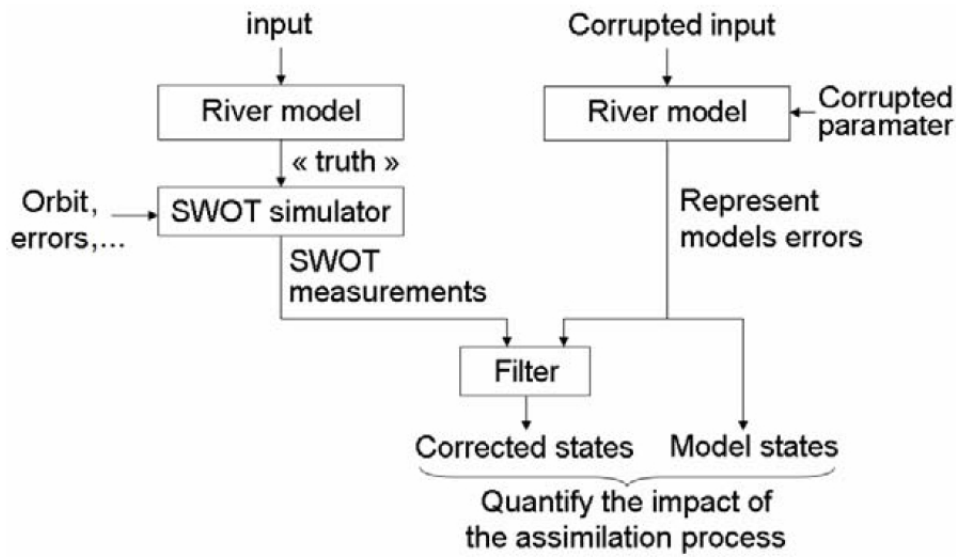


Figure 4.1: Observing System Simulation Experiment (OSSE) concept (from Biancamaria, 2009).

...) with and without assimilation.

### 4.2.3 SWOT Virtual mission

For this study, the model configuration AQF from Chapter 3 is considered as the 'truth'. This run is then used to generate the SWOT observations, with the help of a relatively simple simulator. According to the prescribed orbit and swath, the simulator provides an ensemble of SWOT tracks and related dates, which are adjusted on the ISBA-TRIP grid. These tracks are provided for the orbital period and then repeated over the entire year 2002 (assuming that the satellite starts its first orbit on January, 1st 2002). The year 2002 is chosen as the beginning of the simulation period used for the model evaluation. Only the water levels observed over the river mask are kept for the assimilation (see Biancamria, 2011 for more details about the simulator). To take into account the observation uncertainties, an error is then added to the observations (see section 4.2.3.2).

The SWOT simulator was used for a 22-day repeat nominal orbit, which represents a complete global coverage for a 140km swath. For the calibration/validation phase, multiple orbits can be considered in the [800-1000km] altitudes range (Rodriguez, 2012). Among the available orbits, two orbits have been selected for this study (see table 4.2). The repeat period corresponds to

Orbit	Altitude	Inclination	Repeat cycle	Sub-cycle
1dsbc	870km	78°	22 days	1 day
3dsbc	970km	78°	22 days	3 days

Table 4.2: SWOT calibration orbits characteristics, Rodriguez, 2012.

the minimum time in which the satellite flies over exactly the same ground location. Given, the orbit parameters and the earth rotation speed, it requires a fixed number of satellite revolutions. For all of these revolutions, the part of the orbit that goes from North to South corresponds to the descending track and the one that goes from South to North corresponds to the ascending track. These ascending and descending tracks cross the equator at different times during one repeat period. The difference between these crossing times for two adjacent ascending (or descending) tracks during a repeat period is the orbit subcycle. The 970 *km* altitude orbit has a 3 days subcycle, whereas the 870 *km* altitude orbit has a 1 day subcycle. The 870 *km* altitude orbit is filling the earth eastward. These two orbits both have global coverage, but they do not 'fill' this coverage similarly. The 1-day subcycle orbit has two adjacent swaths every day, meaning that each river basin will be well sampled in few days, but then there will be no observation for multiple days (Fig 4.2). The 3-day subcycle orbit has two adjacent swaths every 3 days meaning that the ground tracks will be more regularly distributed in space and time. Yet, there will be no close observation every day (Fig 4.3). Thus, these two orbits present specific advantages and disadvantages related to their spatial and temporal coverage over the domain. The assimilation method efficiency related to each sub-cycle will be investigated.

## 4.2.4 Computation of variables used during the assimilation analysis

### 4.2.4.1 Choice of the control variable

The sensitivity tests performed in the previous chapter were done to determine the most sensitive TRIP parameters which impact the major hydrological processes of the Niger basin. The Manning roughness coefficient,  $n_{riv}$ , is used for flow calculations in the river stream, via the Manning formula (Eq.2.27). Due to its close relationship with water levels and discharge, it is one of the most important empirical parameters in the field of hydrology, hydraulics and other surface water flow related science and engineering. It was shown in Section 3.7, that a modification of this parameter has a significant impact on the hydrological variables over the Niger basin. Thus, a good estimation of this coefficient in

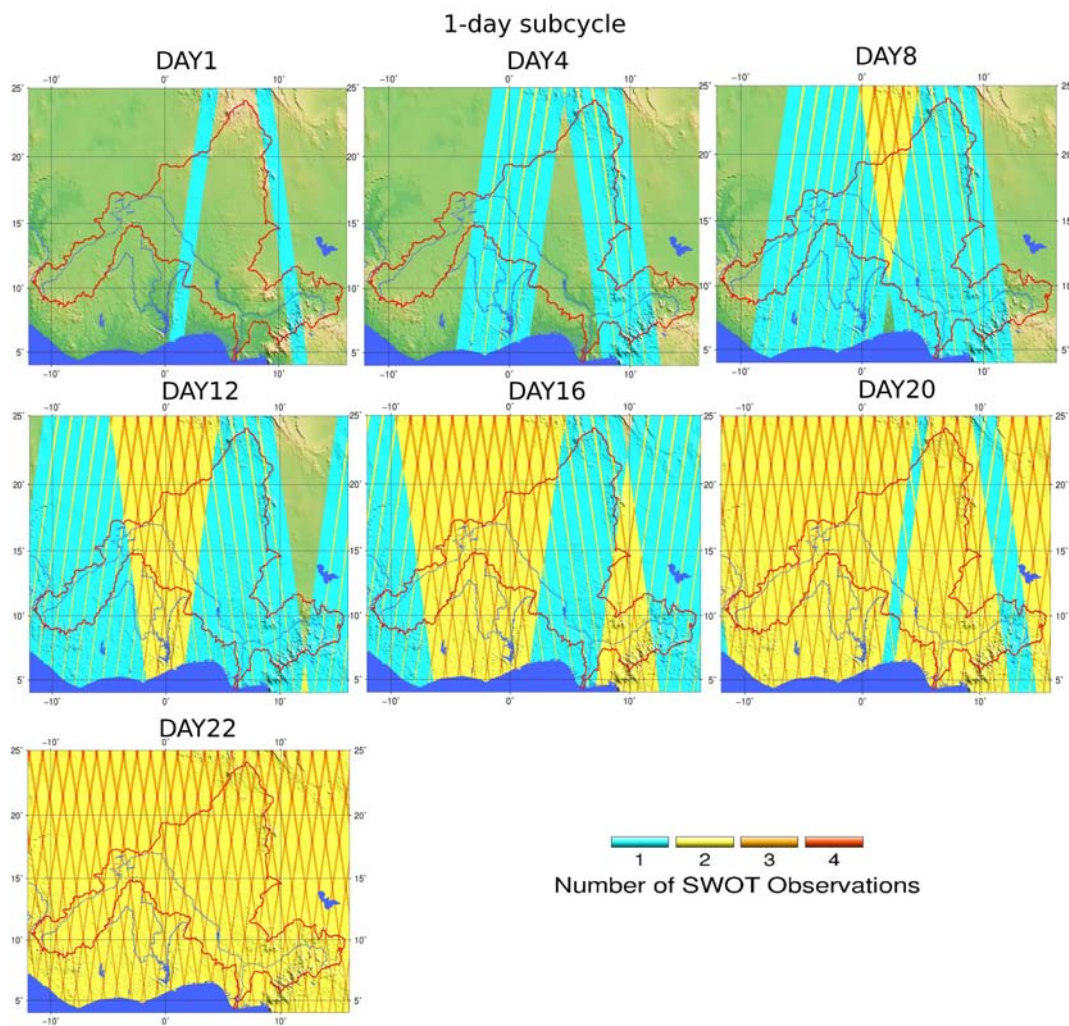


Figure 4.2: 1-day subcycle orbit coverage, data issued from the SWOT data simulator, Biancamaria, 2011.

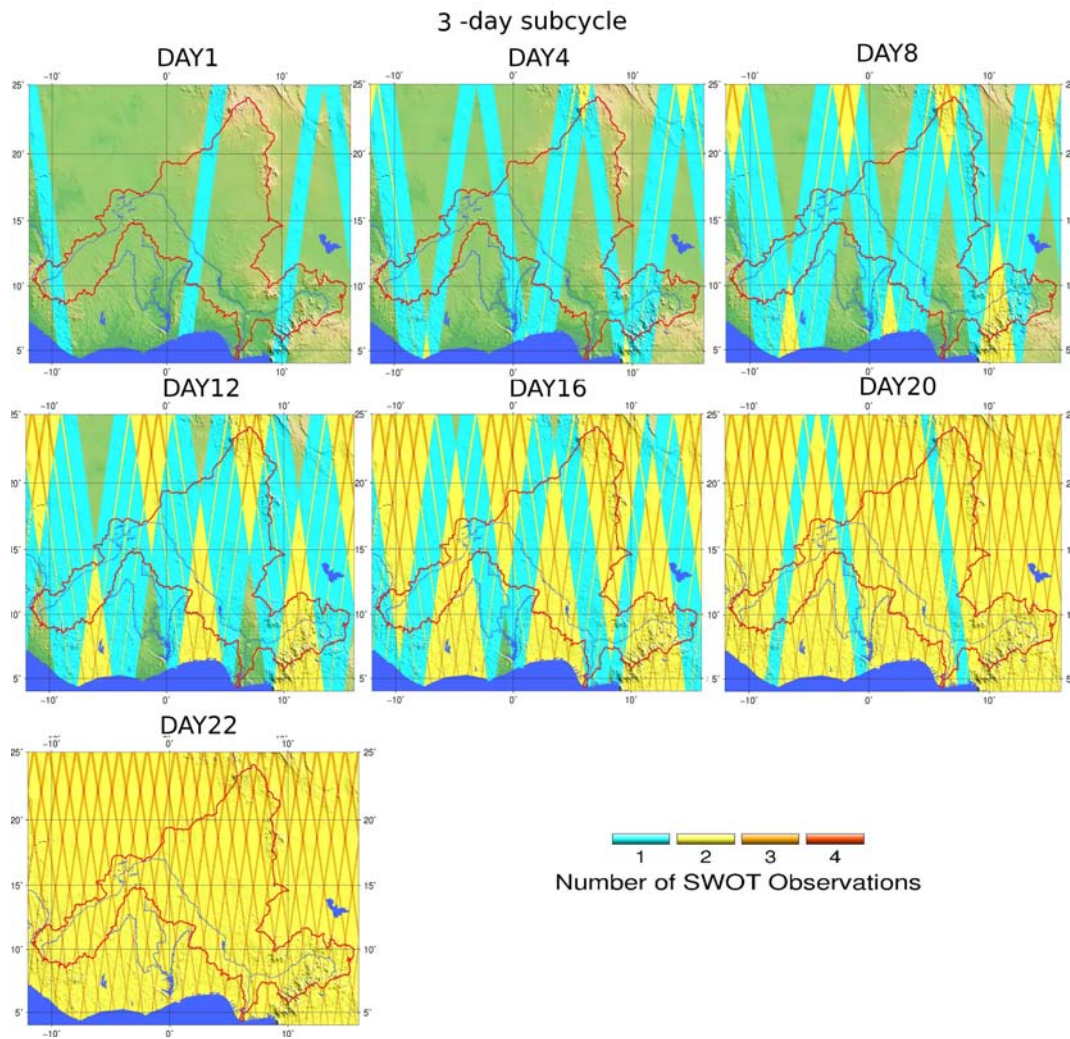


Figure 4.3: 3-day subcycle orbit coverage, data issued from the SWOT data simulator, Biancamaria, 2011.

the river bed leads to a better reproduction of surface water dynamics. There is a tendency to regard the selection of Manning coefficient as an arbitrary or intuitive process. Indeed, hydrodynamic models usually get input of Manning manually, using estimations based on visual interpretation of land cover. The roughness can also be described by geomorphologic relationships, related to an other parameter on which more information is known (river width for example). Both approaches can lead to significant errors in a large computational area with various land uses.

For the assimilation experiment, it was decided to consider the Manning coefficient over the Niger river as the control vector. The Niger river mask is built by assuming that all of the grid cells with a river width (which is an input parameter) superior to  $200m$  belong to the river bed, which corresponds to 110 pixels. The dimension of the control vector is then  $n = 110$ . Here, it is assumed that the modeling errors are only due to uncertainties in the Manning coefficient. The 'truth' is then constructed by integrating the ISBA-TRIP model, using a reference distribution of the Manning coefficient (Fig 4.4) as an input parameter. This 'truth' corresponds to the simulation noted as AQF in Chap. 3.

In order to create a corrupted run, and assuming that the modeling errors are only due to uncertainties in the Manning coefficient, a corrupted distribution of the Manning coefficient ( $n_{riv}$ ) is generated. The error on the Manning coefficient is described as following a Gaussian distribution, centered at 0, and with standard deviation equal to  $\sigma^b$ . An approximative error of 20% of the Manning coefficient is a reasonable range and  $\sigma^b$  is fixed to 20% of the mean value of the Manning coefficient over the river ( $\sigma^b = 20\%$  of 0.074). 110 new values of  $n_{riv}$  are obtained and gathered to form the background vector,  $\mathbf{x}_b$ . The corrupted simulation is then built by integrating the model, using  $\mathbf{x}_b$  as an input parameter.

The BLUE algorithm was chosen for the calculation of the analysis due to the low calculation cost of this method. Indeed, the matrice formulation is made possible due to the small dimensions of the analysis problem ( $110 \times 110$ ) which is computationally less fastidious than a minimization method. The linearity hypothesis is discussed in Section 4.2.3.3.

The aim of the assimilation is thus to use the SWOT observed water levels over a prescribed observation period (said assimilation cycle) in order to get an optimal corection of the Manning coefficient,  $n_{riv}$ , over the river mask. The impact of the assimilation on the model states (water levels, discharge, floods, water storage etc...) will then be quantified.

The main variables presented in the Table 4.1, and those playing a key role from Eq. 4.10 are redefined with more precision in Table 4.3.

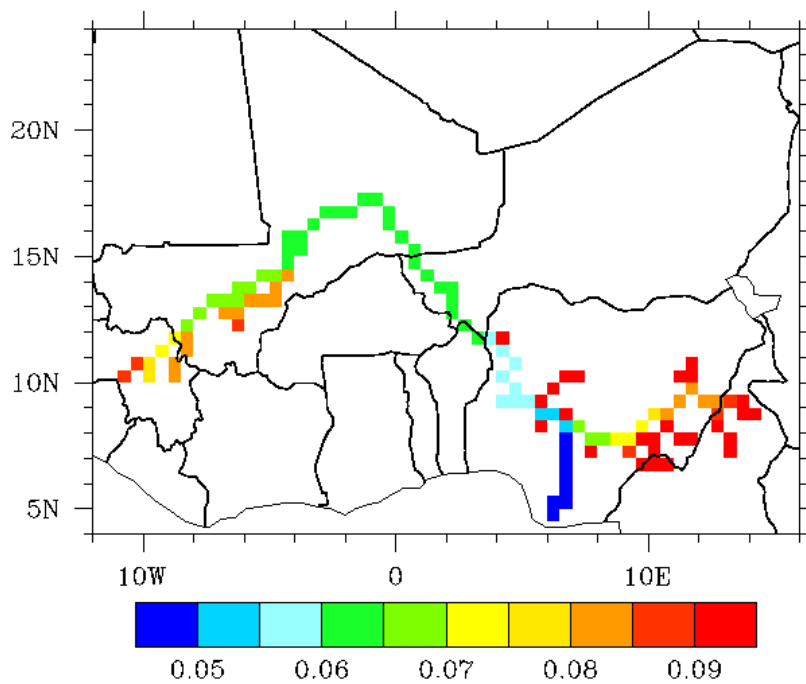


Figure 4.4: Distribution of the 'true' Manning coefficient over the river mask. This distribution of the Manning coefficient was used as an input parameter to run the ISBA-TRIP model in Chapter 3.

Symbol	Variable	Dimensions
$y^0$	Observation vector, containing the SWOT WL observations during the $N$ day assimilation window	$p$ (different for each assimilation cycle)
$x^b$	Background vector, containing the corrupted Manning coefficient over the river mask	$n = 110$
$x^a$	Analysis vector, containing the corrected values of the Manning coefficient over the river mask	$n = 110$
$M$	ISBA-TRIP (non linear)	
$H(x^b)$	ISBA-TRIP simulated water levels, using $x^b$ as an input parameter	$p$
$R$	Observation error covariance matrix (related to water levels)	$p \times p$
$B$	Background error covariance matrix (related to the Manning coefficient)	$n \times n$
$A$	Analysis error covariance matrix	$n \times n$
$\mathbf{H}$	Jacobian matrix of $H$ (sensitivity of ISBA-TRIP water levels to the Manning coefficient)	$n \times p$
$K$	Gain matrix	

Table 4.3: Principal variables, vectors and matrices used in the data assimilation of SWOT water levels. The assimilation window length is  $N$  days. The number  $p$  of observed water levels during the assimilation window changes for each cycle.

#### 4.2.4.2 Error covariance matrices

The uncertainties in the observations and in the model are statistically represented by the error vectors  $\varepsilon^0$  and  $\varepsilon^b$ . For the assimilation, it was assumed that these errors can be represented by Gaussian distributions, centered at 0, to be coherent with the BLUE hypothesis of unbiased errors. The standard deviation  $\sigma^0$  has to be determined ( $\sigma^b$  was already defined in Sect. 4.2.4.1).

##### Observation error covariances matrix

It is generally very difficult to estimate the observation errors. The errors in the observed SWOT water levels can be due to several reasons :

- error due to the satellite altitude
- baseline error
- instrument error

The estimation of these errors has been done within the framework of an ongoing PhD at LEGOS/CNES (Lion, 2012). They are defined as Gaussian errors, but not necessarily centered at 0, and they vary according to the location and the orbit. Before using these errors in the assimilation system, it was decided to fix  $\sigma^0$  to a simpler value, which varies for each assimilation window.  $\sigma^0$  is fixed to 20% of the average observed value of water level over the assimilation window (which should normally be larger than the real instrument error). The vector  $\varepsilon^0$  is thus defined by a Gaussian distribution centered at 0, and of standard deviation  $\sigma^0$ .

For the estimation of the observation errors covariance matrix,  $\mathbf{R}$ , it was assumed that the observation errors are not correlated along track which might not be the case in reality. However, this type of error is easier to represent, and it was chosen as a first step for the assimilation. The matrix  $\mathbf{R}$  is therefore a diagonal matrix, and each diagonal term is equal to  $(\sigma^0)^2$ .  $\mathbf{R}$  varies for every assimilation cycle, depending on the observed water levels.

##### Background error covariances matrix

This matrix represents the uncertainties related to the Manning coefficient. As said before, the Manning coefficient is a key parameter influencing the river dynamics, but its estimation is usually difficult. In ISBA-TRIP,  $n_{riv}$  is assumed to vary linearly with the river width,  $W$ , from 0.04 near the river mouth to 0.10 in the upstream grid cells :

$$n_{riv} = n_{min} + (n_{max} - n_{min}) \left( \frac{W_{mouth} - W}{W_{mouth} - W_{min}} \right) \quad (4.28)$$

where  $n_{max}$  and  $n_{min}$  are the maximum and the minimum values of the Manning friction factor (respectively equal to 0.10 and 0.04),  $W_{min}(m)$  is the minimum river width value and  $W_{mouth}(m)$  is the width of the mouth of the river. This relationship relies on geomorphologic relationships which are a reasonable approximation over the globe, but they are not always representative of the reality for a specific basin. The background error vector,  $\varepsilon^b$ , is described as a gaussian distribution, centered at 0. It is generally difficult to estimate the range of the background error since the 'truth' is usually unknown. However, in the context of an OSE, the true state of the model is known, as well as the input parameters. It was therefore decided to set the standard deviation  $\sigma^b$  to 20% of the average value of the Manning coefficient over the river. It is also assumed that the modeling errors are not correlated in space and the matrix  $\mathbf{B}$  is diagonal, the diagonal term being equal to  $(\sigma^b)^2$ . Unlike matrix  $\mathbf{R}$ , this matrix does not vary through the assimilation cycles.

#### 4.2.4.3 Jacobian matrix calculation

The observation operator,  $H$ , describes the relationship between the observations and the state variable. The hypothesis of linearized observation operator is needed in order to derive a rigorous algebraic expression for the optimal  $\mathbf{K}$ . In practice,  $H$  may not be linear, but it usually makes physical sense to linearize it in the vicinity of the background state (Bouttier and Courtier, 1999):

$$H(x) - H(\mathbf{x}_b) \approx \mathbf{H}(\mathbf{x} - \mathbf{x}_b) \quad (4.29)$$

The Jacobian matrix  $\mathbf{H}$ , is then defined (in the vicinity of the background state) as :

$$\mathbf{H} = \frac{\partial H}{\partial x} \quad (4.30)$$

The BLUE algorithm relies on the assumption that the observation operator  $H$ , is linear (or linearized). According to this assumption, for a variation of the Manning coefficient,  $\Delta x$ , the observation operator,  $H$ , can be expressed using a Taylor expansion (neglecting higher order terms):

$$H(x + \Delta x) = H(x) + \mathbf{H}\Delta x \quad (4.31)$$

The Jacobian matrix,  $\mathbf{H}$ , describes the variations of water levels induced by the variation of Manning coefficient and can be written using centered finite

differences :

$$\mathbf{H}_{ij} = \frac{\partial H}{\partial x_{|ij}} = \frac{H(x + \Delta x)_t - H(x - \Delta x)_t}{\Delta x_j} = \frac{\Delta y_i^+ - \Delta y_i^-}{\Delta x_j^+ + \Delta x_j^-} \quad (4.32)$$

$\Delta y_i^+$  and  $\Delta y_i^-$  represent the water level variations at pixel  $i$  related to variations  $\Delta x_j^+$  and  $\Delta x_j^-$  of the Manning coefficient at pixel  $j$ . Note that for this study, tests of linearity were done first for a non-centered finite difference scheme but it turned out to be more noisy. For this reason, the centered finite differences were used for this study. The calculation of  $\mathbf{H}$  requires multiple perturbed runs. Indeed, for an observation located at pixel  $i$ , the impact of a Manning variation at all of the pixels situated upstream of  $i$  is needed. However, for each assimilation cycle, all the pixels of the river mask are perturbed individually (and not only the pixels upstream of the observation) ie 220 runs are launched. This avoids the need to calculate the specific drainage area for each observed point, but can be optimized as a perspective to further improve the system in a future study.

Several tests were done to evaluate the linearity hypothesis. For a Manning distribution  $\mathbf{x}$ , the observation operator  $H$  can be written as :  $H(\mathbf{x}) = S \circ M(\mathbf{x})$  where  $S$  is assumed to be a linear operator. Then, the previous equation can be applied to the model integration,  $M$ , to test the assumption that :

$$M(x + \Delta x) \approx M(x) + \frac{dM}{dx} dx = M(x) + \frac{M(x + \Delta x) - M(x - \Delta x)}{2\Delta x} \Delta x \quad (4.33)$$

where  $M(x)$  is the model simulated water level for a Manning parameter equal to  $x$ . The higher order terms are neglected.  $\Delta x$  is thus a local perturbation of the Manning coefficient  $x$ . To test this assumption, the river Manning coefficient was globally perturbed as  $\Delta x = \pm 20\%$ . Since the linearity of the model might depends on the climatic conditions and variability, such as the rainfall, the perturbation is applied the first day of each month and the daily response of the model for the whole month starting from the day of perturbation is observed. Fig 4.5 shows the daily evolution of left and right members of Eq. 4.18, averaged over the river, for the year 2002. As seen in the figure, the two members coincide well for the whole year 2002. Moreover, in order to take into account each point individually (and not make an average), the water levels are plotted from the perturbed run as a function of the reference water levels (Fig.4.6). The lines corresponding to the functions  $y = x + 10\%x$  and  $y = x - 10\%x$  are represented in black on in Fig.4.6. The perturbed water levels evolve as a linear function of the reference water levels which confirms that the relationship between  $M(x + \Delta x)$  and  $M(x)$  is linear. This result is better observed for small values of the water level. For high values however, the perturbation stays relatively close to the  $|y = x|$  line (less than 8% which represents a deviation of about 60 cm for a

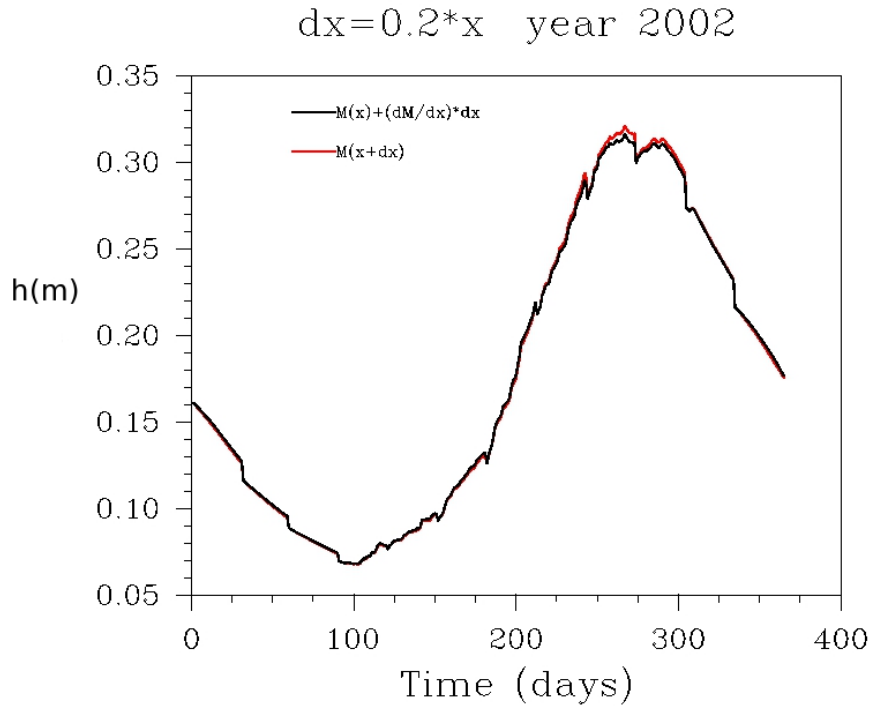


Figure 4.5: Daily evolution of the members 1 and 3 of equation 4.18, averaged over the basin.

8-meters water height). So on average over the river, the simulated water level response to a 20% global perturbation of the Manning coefficient is linear.

Another test was performed to test the linearity of the system. The perturbed distribution of the Manning coefficient (Sect. 4.2.3.4) is equal to the true Manning parameter,  $x^t$ , to which a spatially distributed Gaussian error centered at 0 and of standard deviation  $\sigma^b$  is added. Then, the same methodology as before is used, i.e. this gaussian perturbation is applied in the reference run every month of 2002. The differences of water levels between the two runs are observed to see if the model is able to keep the gaussian error pattern, which would be the case for a linear model. The probability distribution function of the water levels error between the reference run and the perturbed run is calculated for the whole period (Fig 4.7) and for each month (Fig 4.8). Fig 4.7 shows that the model globally keeps the Gaussian pattern of the error and the Gaussian center is also conserved. Moreover, Fig 4.8 shows the probability distribution function (pdf) of the water level differences for each month (for the 5 days following the perturbation). The Gaussian error pattern is more or less well captured depending on the period of the year. Indeed, the model has more difficulties to conserve the gaussian pattern of the error during the monsoon which might be due to

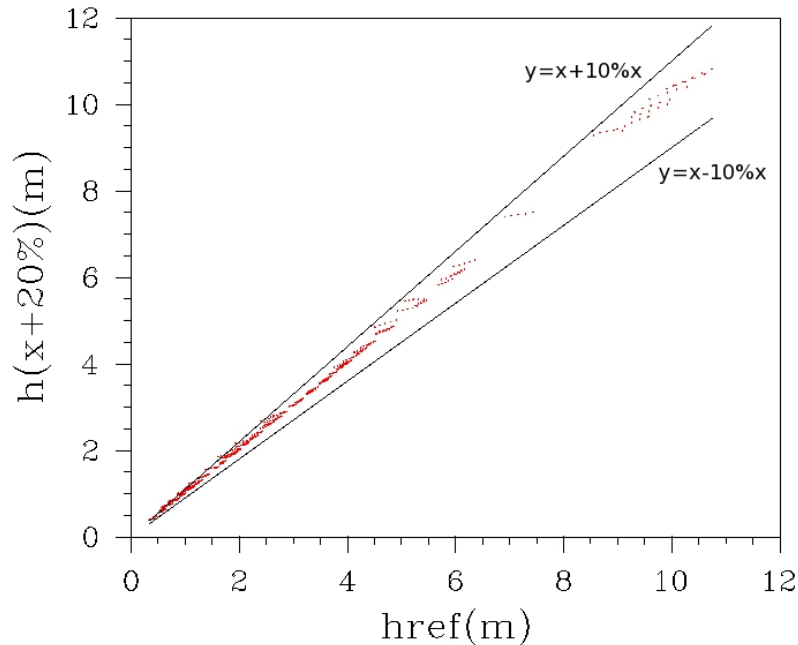


Figure 4.6: Perturbed water levels versus reference water levels for year 2002. The black lines represent the functions  $y = x + 10\%$  and  $y = x - 10\%$ .

its higher sensitivity to rainfall anomalies during this period. The center of the Gaussian is, however, always kept (except in September and October which are months of maximum floods which might induce some non-linearity).

#### 4.2.4.4 Perturbed run

As stated before, the background error of the Manning coefficient is expressed as a Gaussian centered at 0 with standard deviation  $\sigma^b$ . A perturbed distribution of Manning is built from the reference Manning coefficient by adding this Gaussian error to  $\mathbf{x}^t$ . The daily relative difference of water levels between the standard simulation AQ-F and the perturbed run, averaged over the year 2002 are shown in Fig.4.9. The relative difference is calculated only where the reference water level is greater than 2 meters to consider relatively significant water level differences. The differences of water levels are largely heterogeneous in space and amplitude, ranging from  $-60\%$  to  $100\%$ . Moreover, Fig 4.9b shows that the difference between the two simulations is greater than  $36\%$  all the year with maxima from January to June and during the monsoon.

The discharge is less impacted by the perturbation of the Manning coefficient than the river water levels (Fig.4.10), with a relative difference ranging from

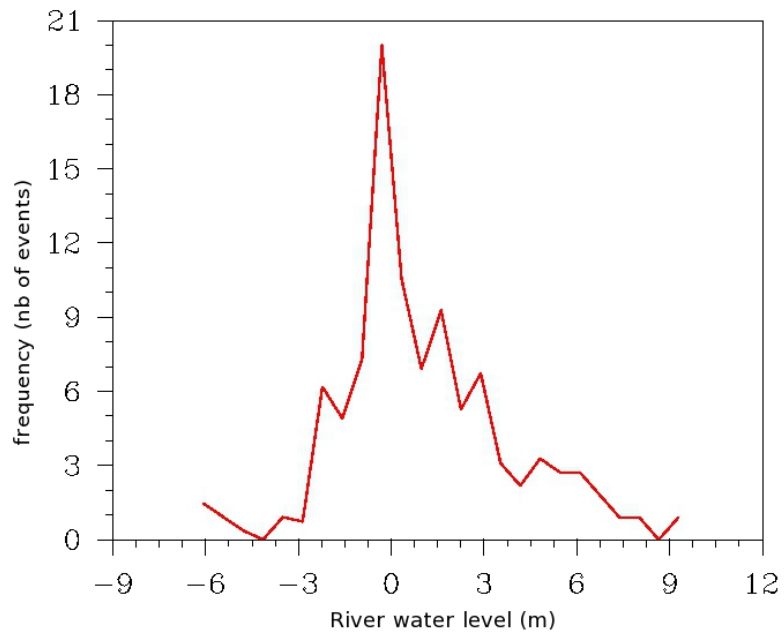


Figure 4.7: Probability distribution functions for the year 2002 of the difference of water levels between the perturbed and the reference run. The points considered are located on the river mask and the error in the 5 days following the application of the perturbations are considered.

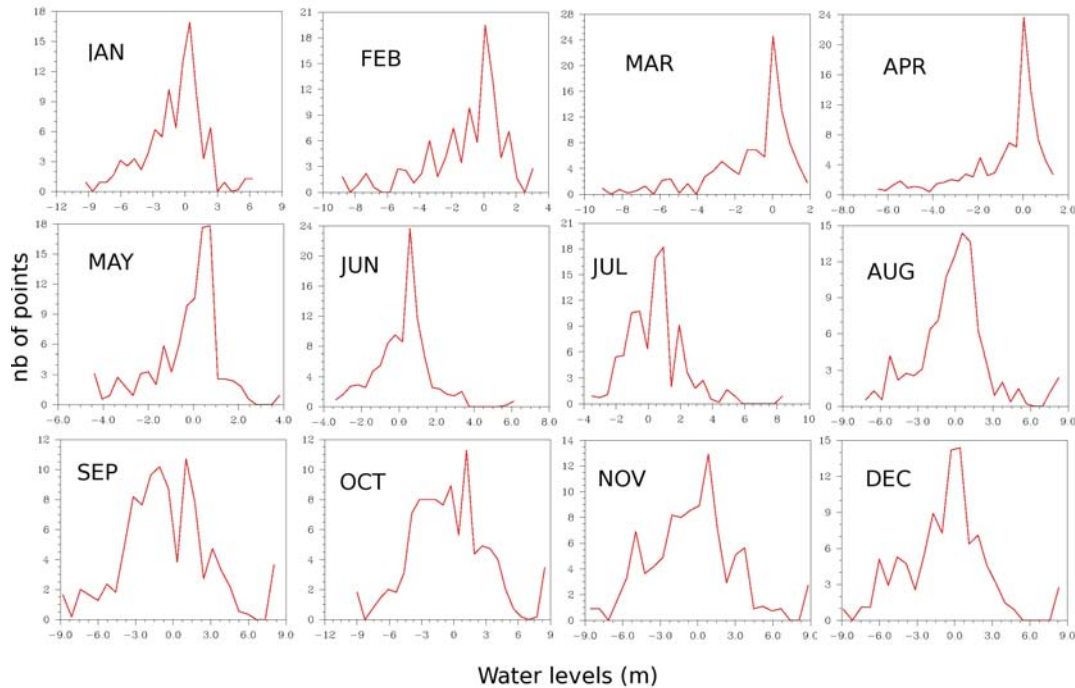


Figure 4.8: As in Fig.4.7, except the monthly values are shown.

−36% to 12%. Moreover, the spatial pattern of the relative difference between the reference and the perturbation is less heterogeneous than that observed for water levels. Indeed, it seems that the discharge of the river, is impacted 'zonally', and not individually pixel by pixel as for the water levels. The time evolution of the relative bias follows the same trajectory as for the water levels with maxima during the monsoon and from January to June (Figure 4.10).

The Figs 4.11 and 4.12 show respectively the simulated water levels and discharge in the 8 locations with observations examined in Chapter 3. In these figures, the most significant differences are observed at the same periods as mentioned previously.

From the previous figures, the perturbed distribution of  $n_{riv}$  created using a gaussian distribution centered at 0, leads to non-negligible differences in the simulated water heights and discharge. This will constitute the perturbed simulation, that will be corrected via assimilation. The impact of this correction on the Manning coefficient, but also on the water levels and discharge along the river, will be investigated.

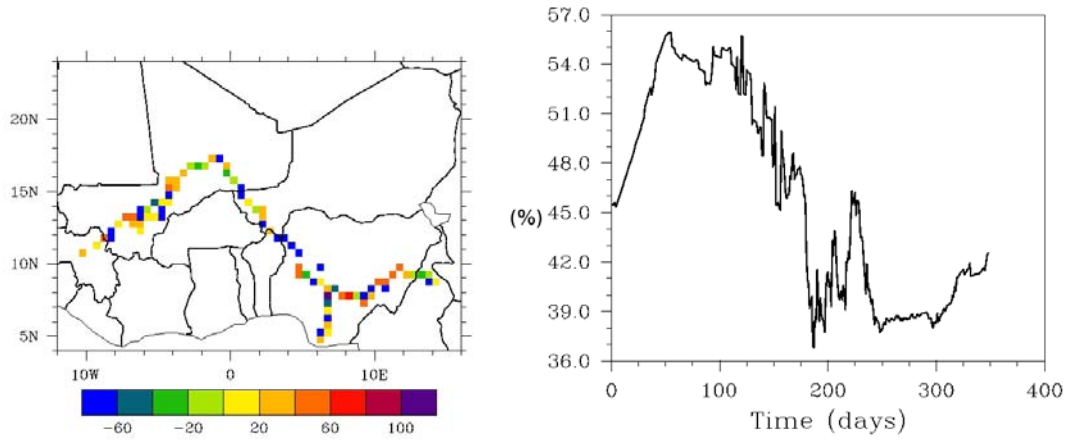


Figure 4.9: **Left** : Relative difference of simulated water levels between the reference and the perturbed simulations. The difference is calculated as the daily ratio  $\frac{h_{ref}-h_{pert}}{h_{ref}}$  and is averaged over the year 2002. This ratio is calculated only when  $h_{ref}$  is greater than 2 meters. **Right** : Time evolution of the relative difference of water levels between the reference and the perturbed simulations, averaged over the river mask.

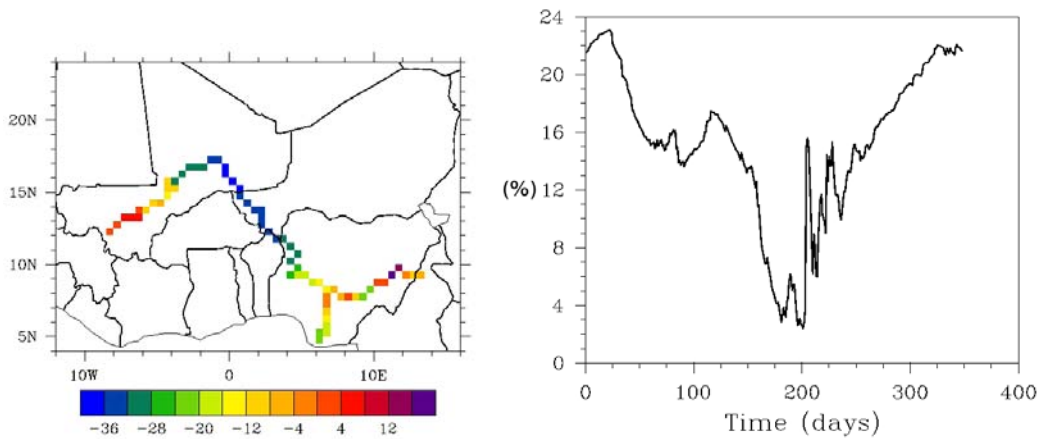


Figure 4.10: **Left** : Relative difference of simulated discharge between the reference and the perturbed simulations. The difference is calculated as the daily ratio  $\frac{q_{ref}-q_{pert}}{q_{ref}}$  and is averaged over the year 2002. This ratio is calculated only when  $q_{ref}$  is greater than  $800 \text{ m}^3/\text{s}$ . **Right** : Time evolution of the relative difference of discharge between the reference and the perturbed simulations, averaged over the river mask.

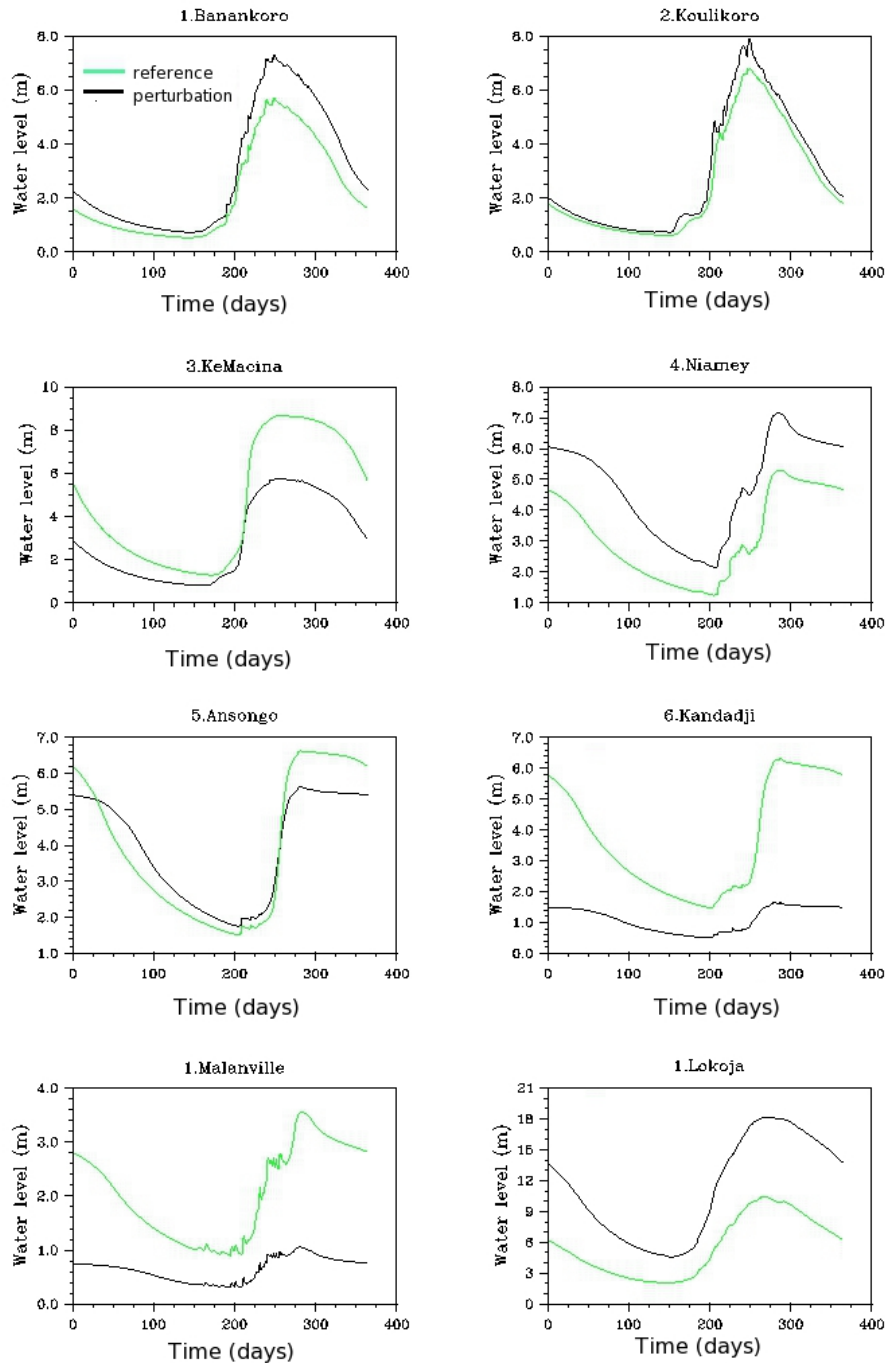


Figure 4.11: Time evolution of the reference and perturbed water heights over the year 2002.

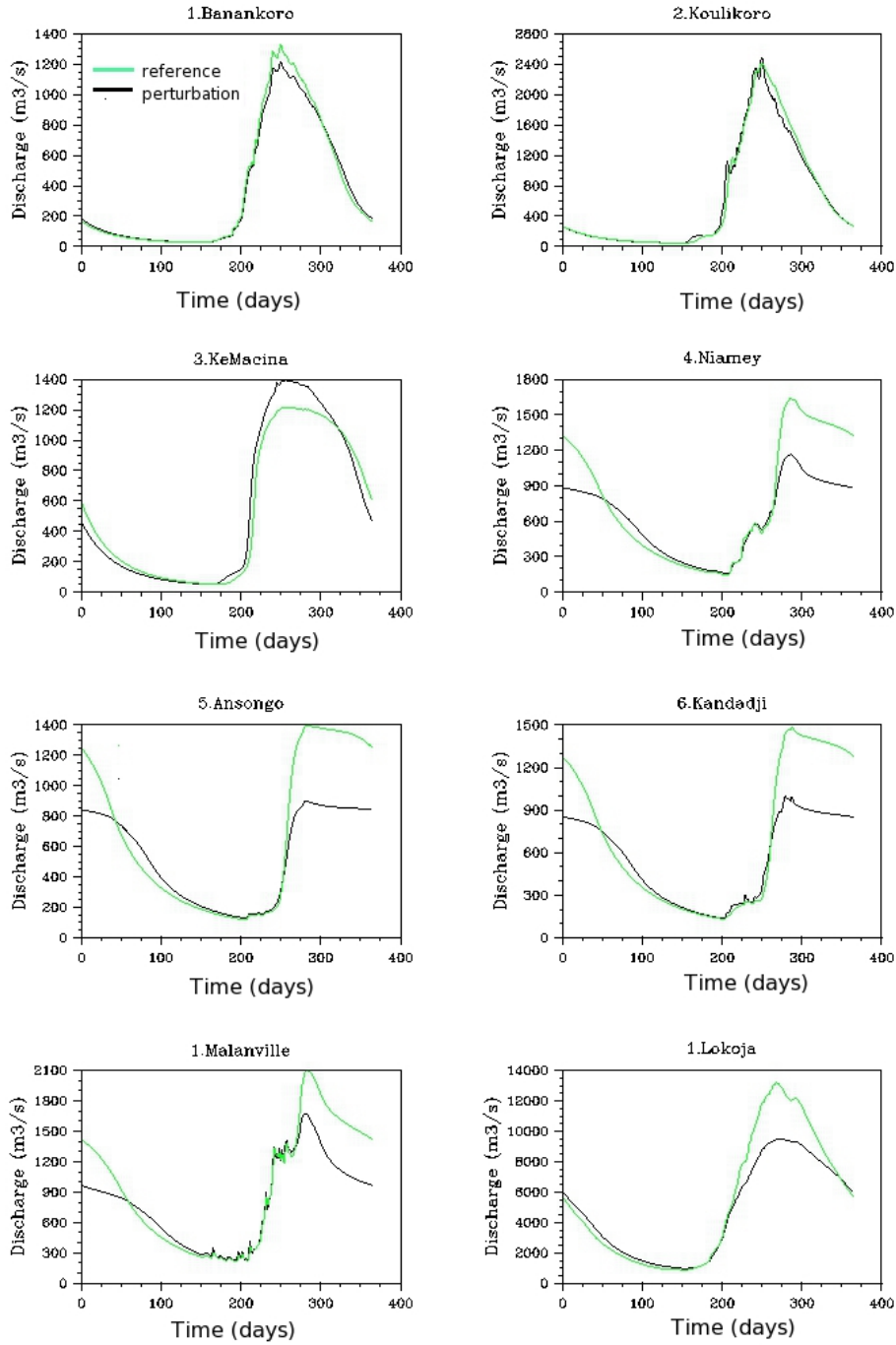


Figure 4.12: As in Fig.4.11, except for the discharge.

#### 4.2.4.5 Practical OSSE implementation

##### Methodology

The data assimilation methodology is summarized in Fig.4.13.

##### First assimilation cycle

First, a  $N$ -day assimilation window is considered. The reference run over  $N$  days is used in order to get the SWOT observations to which is added a gaussian error, centered at 0 with standard deviation  $\sigma^0$ , which will constitute the observation vector  $\mathbf{y}^0$ . The background vector,  $\mathbf{x}_b$ , consists in the 110 perturbed values of the Manning coefficient over the river mask (Figure 4.4). The model is integrated over the  $N$ -day period to obtain the equivalent water levels in the observation space  $H(\mathbf{x}_b)$ . To estimate the Jacobian matrix, 220 distributions of  $n_{riv}$  are created as required for the calculation of the centered finite differences. For each of these distributions, only one pixel of the control vector is modified with a perturbation of  $+\Delta x$  or  $-\Delta x$ . The model is integrated in order to obtain the corresponding  $\Delta y$  over the river. The terms of the Jacobian matrix,  $\mathbf{H}$ , is calculated using Eq. 4.17. The BLUE algorithm is then able to estimate the gain matrix  $\mathbf{K}$  and a corrected Manning vector,  $\mathbf{x}_a$ , which is used as an input to integrate the model over the same  $N$ -day period in order to obtain an analysis trajectory over  $[J - N, J - 1]$ .

##### Second and following cycles

At time  $J - 1$ , the analysis vector,  $\mathbf{x}_a$ , obtained from the previous assimilation cycle, is used as the new background vector for the following cycle over the period  $[J - 1, J - 1 + N]$ .  $\sigma^0$  is re-estimated according to the observations, but  $\sigma^b$  is constant in time. The method is then the same than for the previous cycle (220 perturbed runs, calculation of  $\mathbf{H}$ , get the anaysis trajectory), and for the successive cycles.

The longer the assimilation window, the more computationally expensive the Jacobian calculation will be. Indeed, the SWOT satellite will provide observations over the river every day (between 5 and 20 observations depending of the day of orbit). To be temporally coherent with the observations, 220 runs would be necessary every day of the assimilation window to calculate the Jacobian matrix. Indeed, as shown by the linearity tests, the impact of a Manning coefficient perturbation on the river partly depends on the environmental conditions

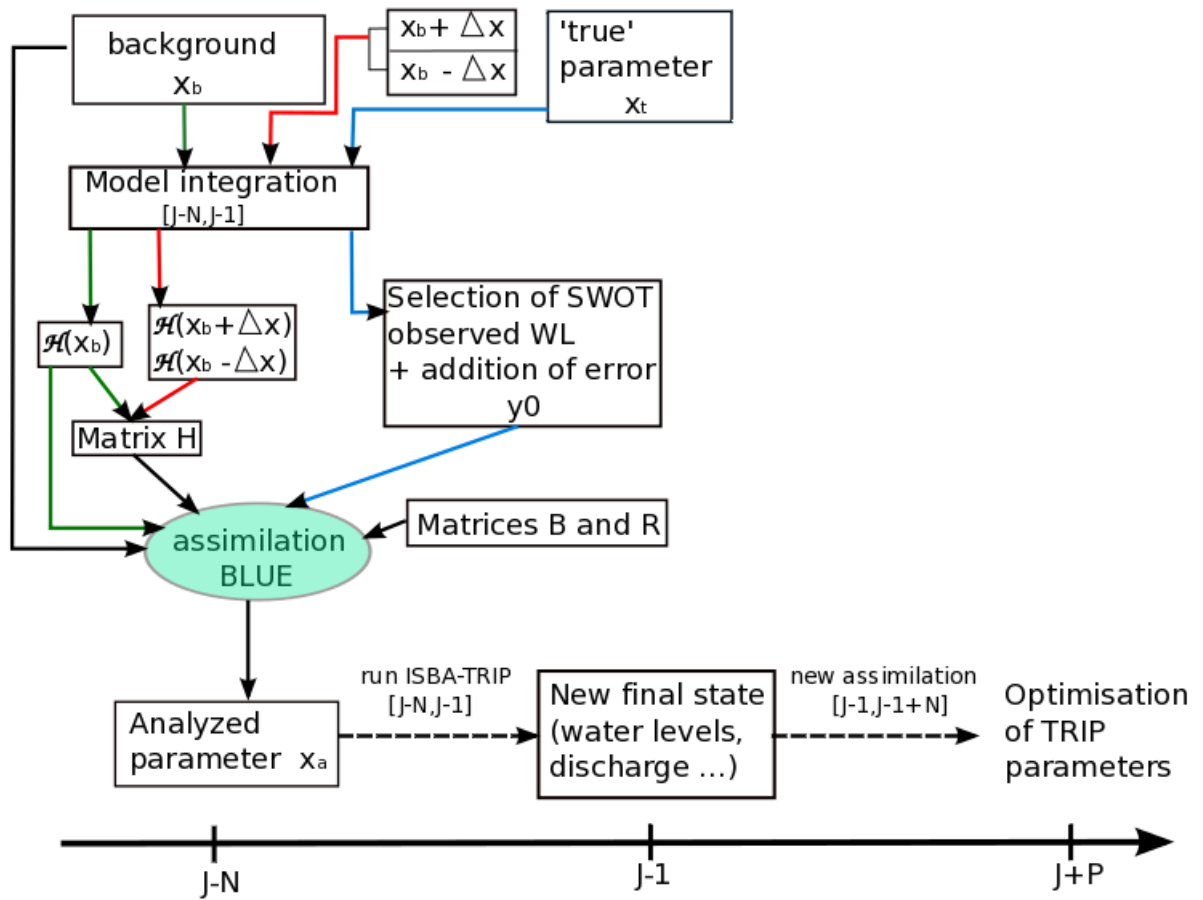


Figure 4.13: Schematic of the assimilation scheme used in this study.

(rain intensity for example). Therefore, in order to ensure the relevancy of the Jacobian matrix, the perturbation must be applied on the day of observation. To limit the number of simulations, it was decided to chose a relatively short assimilation window, i.e. 2 days. Moreover, the assumption was made that a perturbation at day 1 of the window, would have approximately the same impact over the window at day 2 of the window. This way, it is not necessary to launch  $2 \times 220$  runs for each cycle. The results were compared to a 1-day assimilation window experiment, and showed no significant degradation of the scores, while reducing the time of computation.

It is expected that after a number of cycles, the averaged Manning distribution over the river will tend towards an optimal value and stay constant. This is however not evident because the relatively simple physics of the hydrological model induces equifinality issues, i.e. that several solutions might simultaneously resolve the assimilation problem.

### **The OPALM coupling software**

O-PALM (Parallel Assimilation with a Lot of Modularity (Fouilloux and Piacentini, 1999; Buis et al., 2006)) is a dynamic coupling software, developed at CERFACS (Centre Européen de Recherche et Formation Avancée en Calcul Scientifique, <http://www.cerfacs>) within the Global change team. O-PALM (Open PALM) is particularly useful for implementing the assimilation scheme since it allows the concurrent execution and inter-communication of programs which have not been specifically designed for such a task. The exchange of data (such as the analysis, background vector and observations) between independant programs is then made easier thanks to the OPALM interface. The main qualities of the PALM coupler are its easy set-up, its flexibility, its performance round, its availability (open source), the simple updates and evolutions of the coupled application and the functions that it offers.

A basic application of PALM is made of one or several branches which can be launched separately at any time during the PALM simulation (see figure 4.14). These branches include different algorithms and/or programs which can inter-communicate via the dedicated PALM communications. The PALM software can be used with several programming languages such as fortran 90, 77, C and C++. The only PALM constraint is that the programs must include a specific header in order to be indentified. PALM includes a friendly-user interface, called PrePALM, which allows the development complex applications in an easy manner.

The main PALM features for data assimilation are :

- The coupling of independent numerical codes or subroutines such as DA related subroutines
- The intrusive behaviour of PALM in the code (ID card, easy insertion of palm commands in the code)
- The user-friendly HMI for an easy and modular implementation of DA related subroutines
- There are two levels of parallelism, allowing the best performances of the algorithm.
- The explicit time reference for the exchanged fields and the time interpolation utilities, allow a complete independence between the model time stepping and the observation frequency.
- The pre-defined algebra toolbox, providing the necessary linear algebra and minimization functions
- The easy accessibility to basic operators in the intern buffer

For more details about the OPALM coupler, see [http://www.cerfacs.fr/globc/PALM\\_WEB/](http://www.cerfacs.fr/globc/PALM_WEB/).

The PrePALM design of the assimilation scheme is presented in Fig. 4.14. It is made of a principal branch (light green), which represents the launching of the assimilation loop. During the simulation, this branch will call three other branches in order to generate  $x^b$  (light blue branch), the perturbed Manning distributions for the Jacobian calculation (green branch), the observation vector (red branch) and the analysis (dark blue branch). The exchanges of data are represented by the dashed lines. The ISBA-TRIP runs are launched by the principal branch on an external cluster.

## 4.2.5 Results

The results of the data assimilation method are presented in this Section. The assimilation window length is 2 days and the experiment is started on June 1st 2002, just before the beginning of the monsoon season. During one orbit of 22 days, there are about 53 SWOT tracks passing over the river for the 3-day subcycle orbit and 50 tracks for the 1-day subcycle.

### 4.2.5.1 Analysis of one assimilation cycle

Case of June 17th and 18th 2002

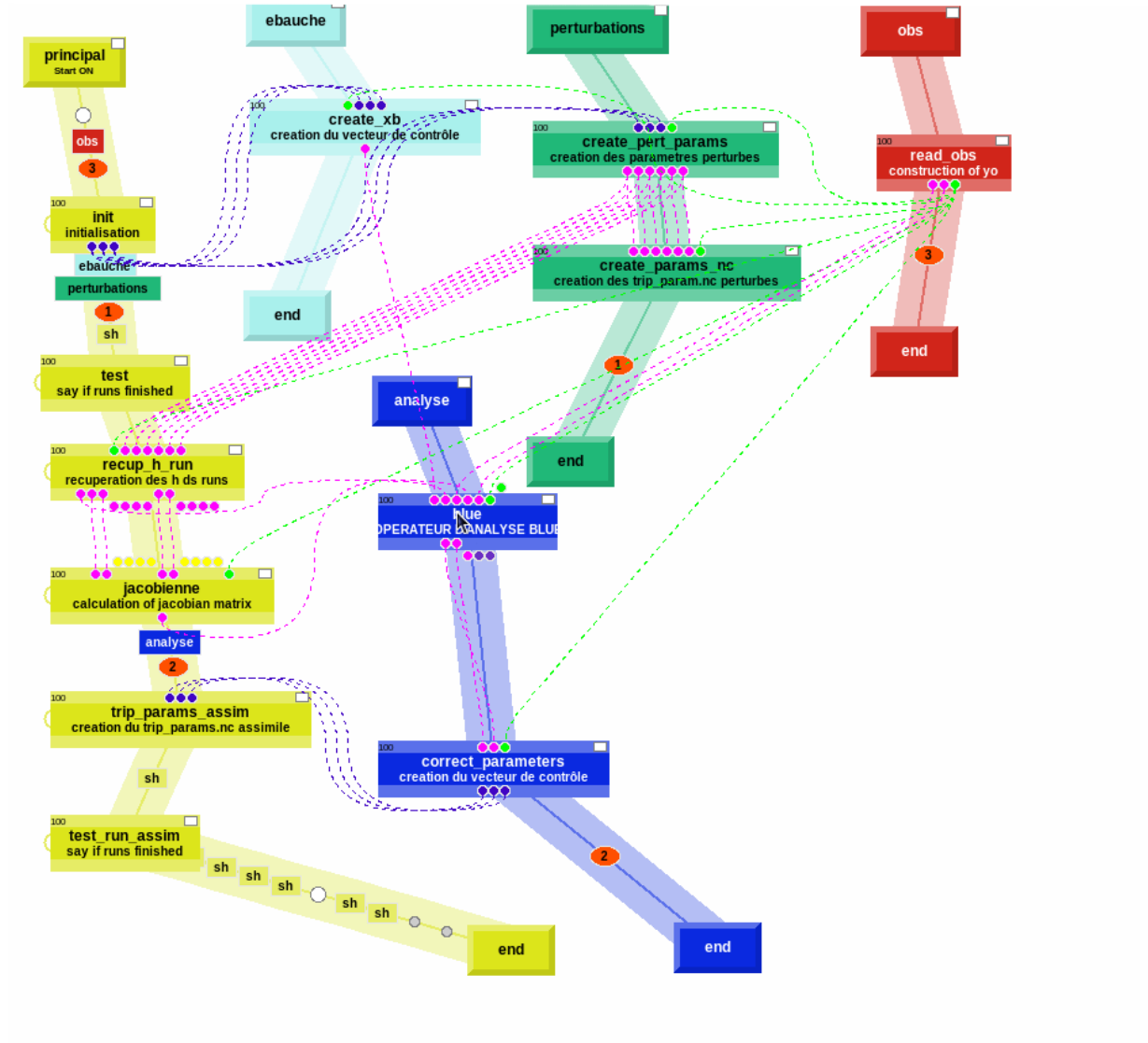


Figure 4.14: The ISBA-TRIP assimilation application designed with the PrePALM interface.

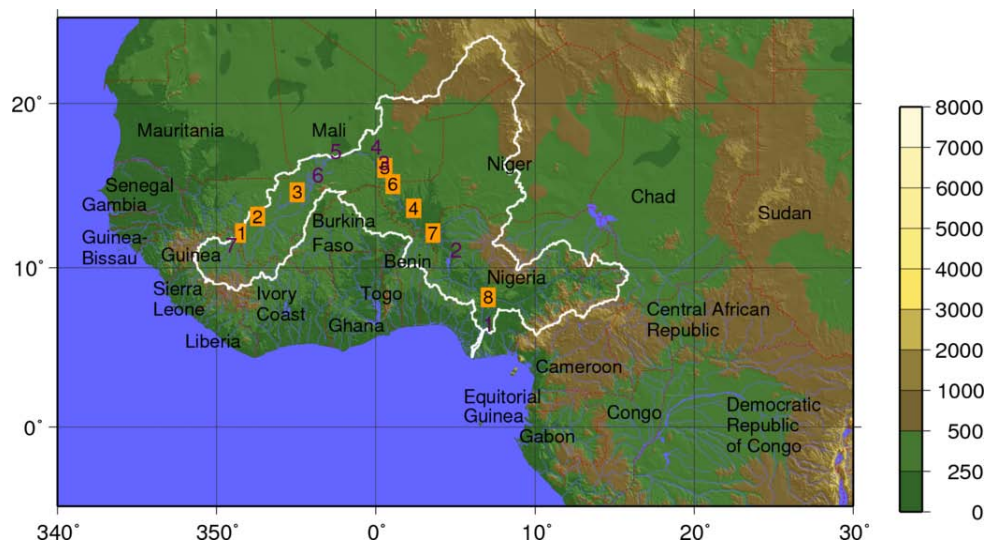


Figure 4.15: Niger river basin. The spatial resolution is  $0.5^\circ \times 0.5^\circ$ . The white contour is the delimitation of the Niger basin. The yellow squares are the stations where discharge observations are available: (1) Banankoro, (2) Koulikoro, (3) Ke Macina, (4) Niamey, (5) Ansongo, (6) Kandadji, (7) Malanville and (8) Lokoja. The purple figures are the sites where height change observations are used for evaluation. The legend indicates the elevation (m).

A single assimilation cycle is analysed in order to verify the coherence of the assimilation method. The tests are done for the 1-day subcycle orbit, on a day when the SWOT tracks are sparse over the basin (upstream and downstream of the river). The correction induced by the assimilation of the Manning coefficient, the water levels and the discharge, for one assimilation cycle is analysed.

Figure 4.16 shows the river pixels observed by the SWOT satellite (estimated by the simulator, Biancamaria, 2011) on June 17th (green) and June 18th (red). For these pixels, the water levels issued from the reference run will constitute the SWOT observed water levels for the assimilation cycle covering this two days period.

Fig 4.16-b shows the difference of relative bias between the *a priori* Manning coefficient (with no assimilation) and the corrected Manning coefficient (with assimilation). The relative bias is calculated as the ratio :

$$bias = \frac{(n_{riv_{with/withoutassi}} - n_{riv_{truth}})}{n_{riv_{truth}}}. \quad (4.34)$$

Positive values on the map (red) represent pixels where the analysed Manning coefficient is closer to the true coefficient than the *a priori* Manning coefficient. Negative values (blue) represent the opposite. First, note that the Manning coefficient is corrected upstream of the observations, which is coherent since only the pixels located upstream of the observed points will affect the water levels at these sites. Looking at Figs 4.16 b. and c., the Manning coefficient and water levels are generally improved (up to 12% for Manning and 6% for the water levels), and, in most cases, an improvement of Manning leads to an improvement of the water level, although to a lesser extent. However, as seen in Fig 4.16-d., the improvement of water levels does not necessary translate to an improvement of the discharge. Indeed, it is logically expected that a better estimation of the water levels would result in a better estimation of the discharge which is not always observed here.

#### 4.2.5.2 Impact of assimilation on water levels

Here the assimilation experiment is run from June 2002 to December 2003. First, the impact of assimilation on water levels is analysed. Table 4.4 gives the water level mean relative bias averaged over the entire river and at each of the 8 locations with gages. Fig 4.17 shows the water level relative bias averaged over the river versus time when i) there is no assimilation (black curve), ii) after 1-day subcycle orbit SWOT observation assimilation (green curve) and (iii) the 3-day subcycle orbit SWOT observation assimilation (blue curve). Finally, water level time series for i) the truth (red curves), ii) for no assimilation (black curves) and iii) for 1-day subcycle (green curves) and iv) 3-day subcycle (blue) orbits SWOT

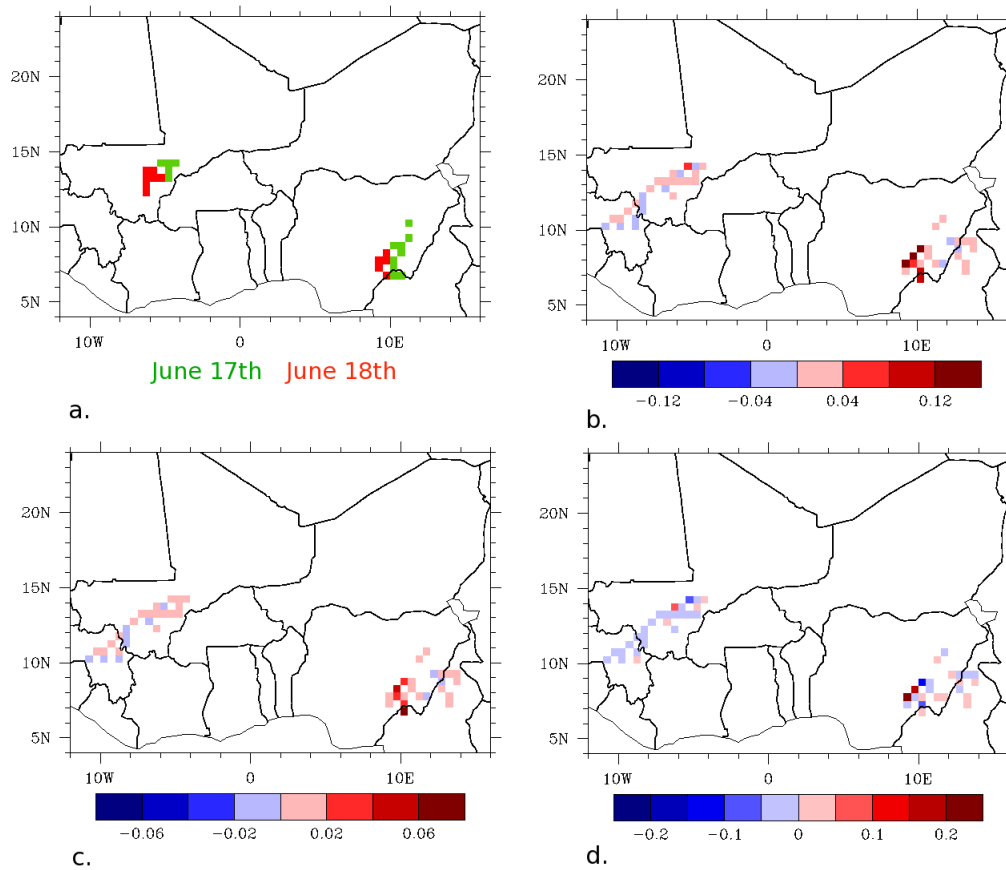


Figure 4.16: a. Map of the observed river pixels for June 17th (green) and June 18th (red). b. Difference of relative bias between the *a priori* Manning coefficient (with no assimilation) and the corrected Manning coefficient (with assimilation). The relative bias is calculated as the ratio  $\frac{(n_{riv\_with/without\_assim} - n_{riv\_truth})}{n_{riv\_truth}}$ . Positive values on the map (red) mean that the analysed Manning coefficient is closer to the true coefficient than the *a priori* Manning coefficient. Negative values (blue) mean that the *a priori* Manning coefficient is closer to the true Manning coefficient than the analysed Manning coefficient. c. Same as b. for water levels. d. Same as b. for discharge.

Location $n^\circ$	Riv Mean	1	2	3	4	5	6	7	8
No assi	0.45	0.35	0.17	0.36	0.55	0.16	0.69	0.68	1.1
3dsbc	0.12	0.09	0.25	0.11	0.17	0.12	0.12	0.1	0.09
1dsbc	0.12	0.19	0.1	0.11	0.12	0.13	0.07	0.12	0.18

Table 4.4: Water level relative bias averaged over the river and at the location of the 8 gages along the river (each gage is defined by its number specified inside the orange rectangles in Fig.4.15). The relative bias is calculated as the ratio  $((h_{with/withoutassi} - h_{obs,wot})/h_{obs,wot})$  where  $h$  is the water level(m).

observation assimilation are shown on Fig 4.18. From these results, the assimilation significantly improves the relative bias over the whole river (the relative bias is reduced more than three times with the assimilation) and at the 8 gages. The temporal evolution of water levels is also improved by the assimilation, especially in the locations situated downstream in the river. Indeed, in most of the 8 locations, the correction represents several meters (for a mean river depth of 8m over the river), and goes up to 9m at Lokoja. Moreover, there is almost no difference between the two orbits, with slightly better results for the 3-day subcycle orbit.

Fig 4.19 shows the daily distributed relative bias of water levels averaged over the period June 2002-December 2003 for the run with (a) no assimilation, (b) for a 1-day subcycle assimilation and (c) for a 3-day subcycle assimilation. As mentioned before the relative bias is globally improved with slightly better results downstream, close to the river mouth. The histograms in Figure 4.20 show the number of pixels contained in different ranges of relative bias going from 0 to 1.2. Without assimilation, the relative bias range over the river goes from 0 to 1.2. With assimilation, more than 90% of the river pixels have a relative bias smaller than 0.2 for both subcycles and no pixel has a relative bias higher than 0.5.

#### 4.2.5.3 Impact of assimilation on Manning coefficient

For the assimilation to be satisfactory, it is expected that the Manning coefficient, to which the correction is applied, will temporally tend towards the 'true' Manning coefficient. Indeed, since the Manning coefficient is spatially distributed, several combinations of this parameter might resolve the assimilation problem which is defined as the equifinality hypothesis. Fig 4.21 shows the Manning coefficient relative bias (averaged over the river) time series for the two orbits. The averaged relative bias of the Manning coefficient is significantly improved during the assimilation period and seems to converge to a stable value (about 0.19 for

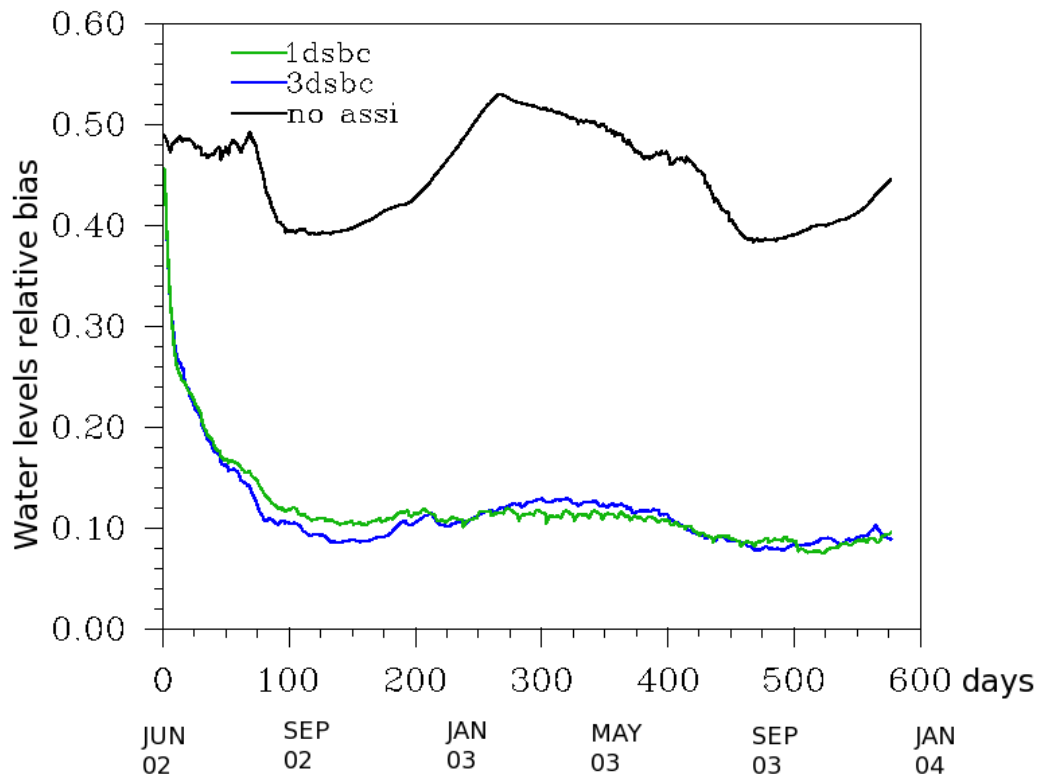


Figure 4.17: Water level relative bias averaged over the river versus time with no assimilation (black), with 1-day subcycle (orange) and 3-day subcycle (blue) orbits SWOT assimilation. The relative bias is calculated as the ratio  $((h_{with/withoutassi} - h_{obs_{swot}})/h_{obs_{swot}}$  where h is the water level(m).

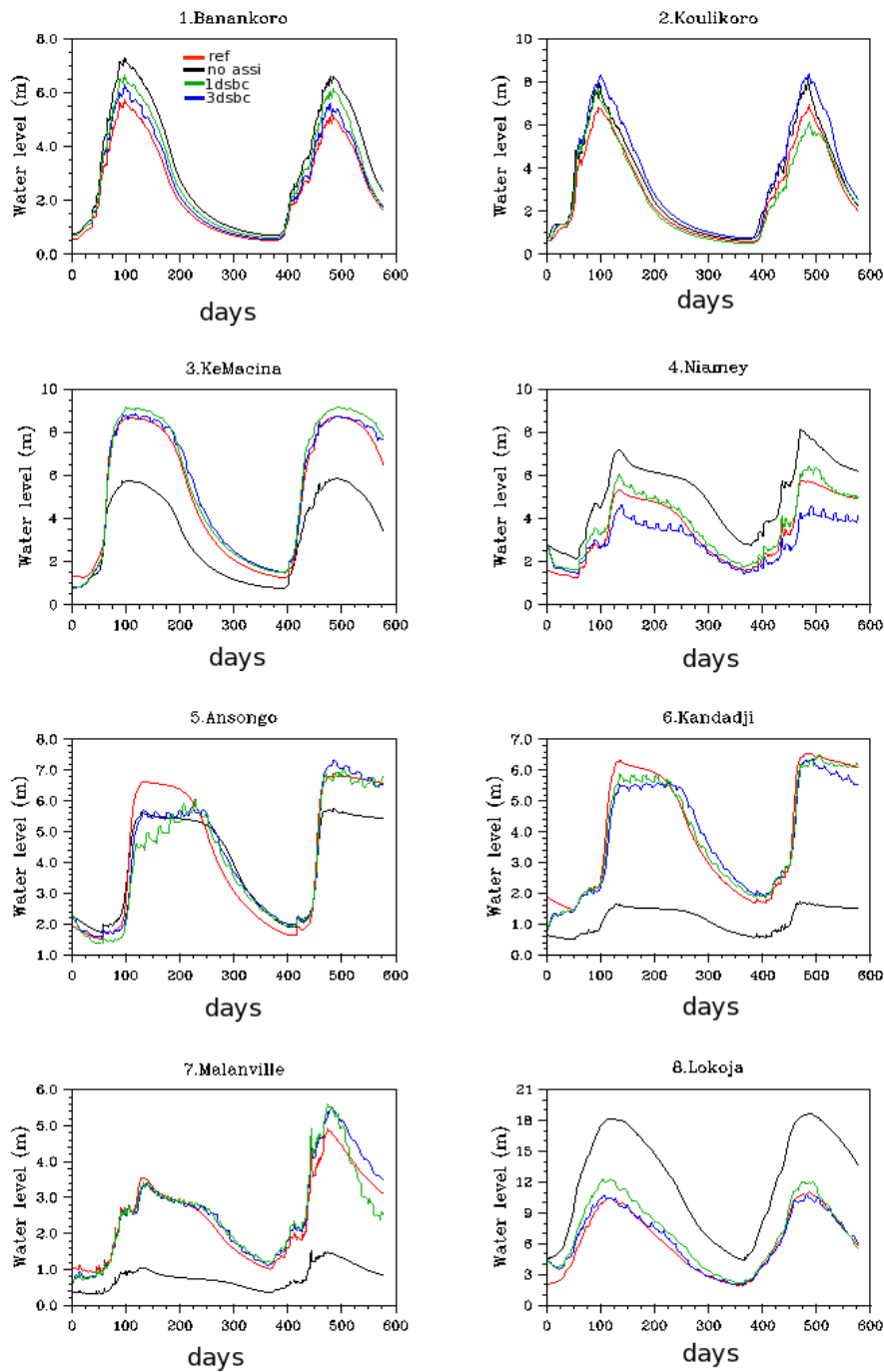


Figure 4.18: Time evolution of water levels at the location of the 8 gages for the "truth" (red curves), with no assimilation (black curves) and with assimilation of SWOT 1-day subcycle (green) and 3-day subcycle (blue) orbits observations.

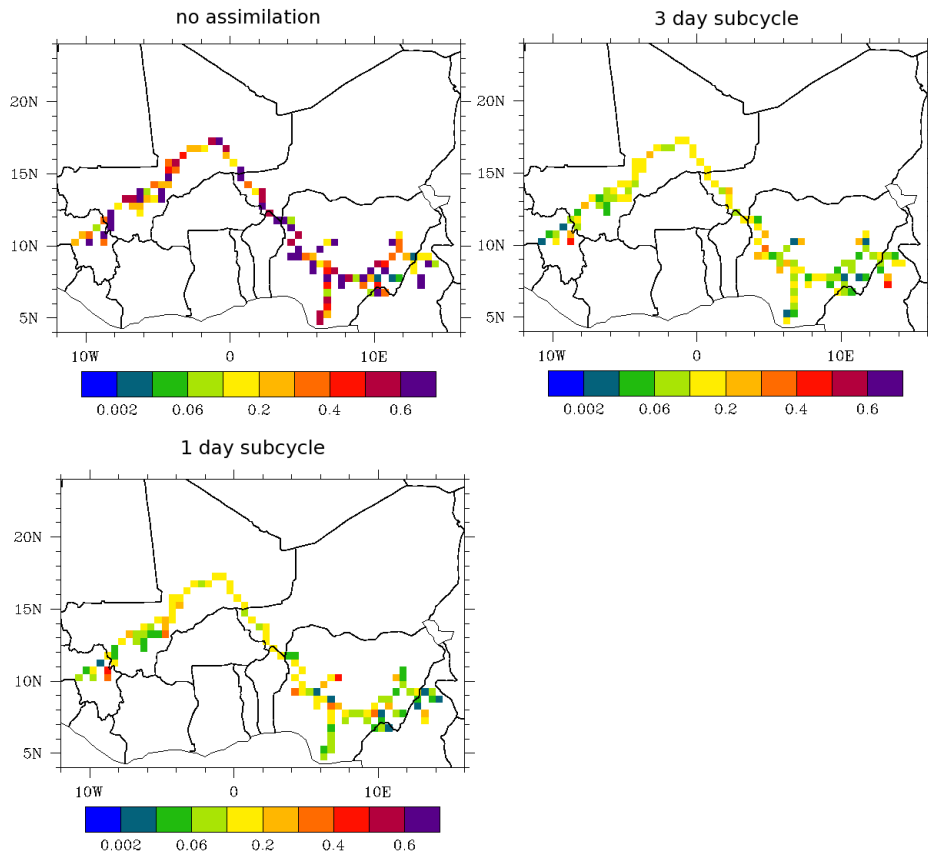


Figure 4.19: Spatial relative bias of water levels averaged over the period of assimilation.

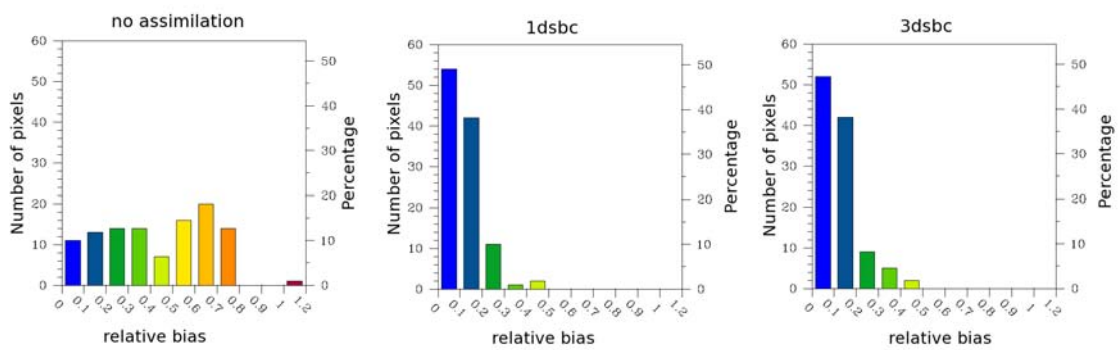


Figure 4.20: Number of pixels contained in different ranges of relative bias going from 0 to 1.2.

the 1-day subcycle orbit and 0.17 for the 3-day subcycle orbit), since the bias is not significantly changed from January 2003 until the end of the assimilation experiment. The method is then able to converge towards an optimal Manning coefficient which is globally closer to the true parameter than with no assimilation. As for the water levels, the 3-day subcycle orbit has a slightly better bias than the 1-day subcycle orbit.

The Manning coefficient temporal evolution at the 8 locations with gages is shown on Fig. 4.22.

The 1-day subcycle and 3-day subcycle orbit assimilations seem to converge globally to the same values, except in Ke Macina. Moreover, it appears that with a 3-day subcycle the Manning coefficient converges faster to its optimal value.

#### 4.2.5.4 Impact of assimilation on river discharge

Tab 4.5 presents discharge temporal mean relative bias averaged over the whole river and at the location of each gages. Fig 4.23 shows the relative bias averaged over the river versus time when there is no assimilation (black curve), after 1-day subcycle orbit SWOT observation assimilation (orange curve) and 3-day subcycle orbit SWOT observation assimilation (blue curve). Finally, the discharge time series for the truth (red curves), for no assimilation (black curves) and for 1-day subcycle (green curves) and 3-day subcycle (blue) orbits SWOT observation assimilation are shown in Fig 4.24. First, these results show that the assimilation also contributes to the improvement of the river discharge over the whole basin and at the 8 locations, although this improvement is less than that obtained for the water levels. Moreover, the impact of the assimilation on the discharge is more dependent on the studied season which was not the case for water levels. The improvement of water levels, although to a lesser extent than for the discharge can represent several hundreds of  $m^3.s^{-1}$  globally and about  $3000m^3.s^{-1}$  in Lokoja which is a significant improvement (see Fig. 4.24). At most of the 8 locations, the discharge with assimilation is better simulated for the second monsoon rainfall peak than for the first one which might be due to the propagation of the analysis during the assimilation. Also, the discharge with assimilation is more or less 'noisy' for both orbits, during the wet seasons. This is likely due to a higher sensitivity of discharge to a modification of the Manning coefficient during this period. The discharge is particularly well improved in Lokoja, i.e. the location situated the most downstream of the river which is a promising result for coupled land-ocean applications in which one of the principal roles of RRM is to provide temporal estimations of discharge at the river mouth. As for the water levels, there is almost no difference between the different orbits when discharge is considered.

Fig 4.25 shows the daily distributed relative bias of discharge averaged over

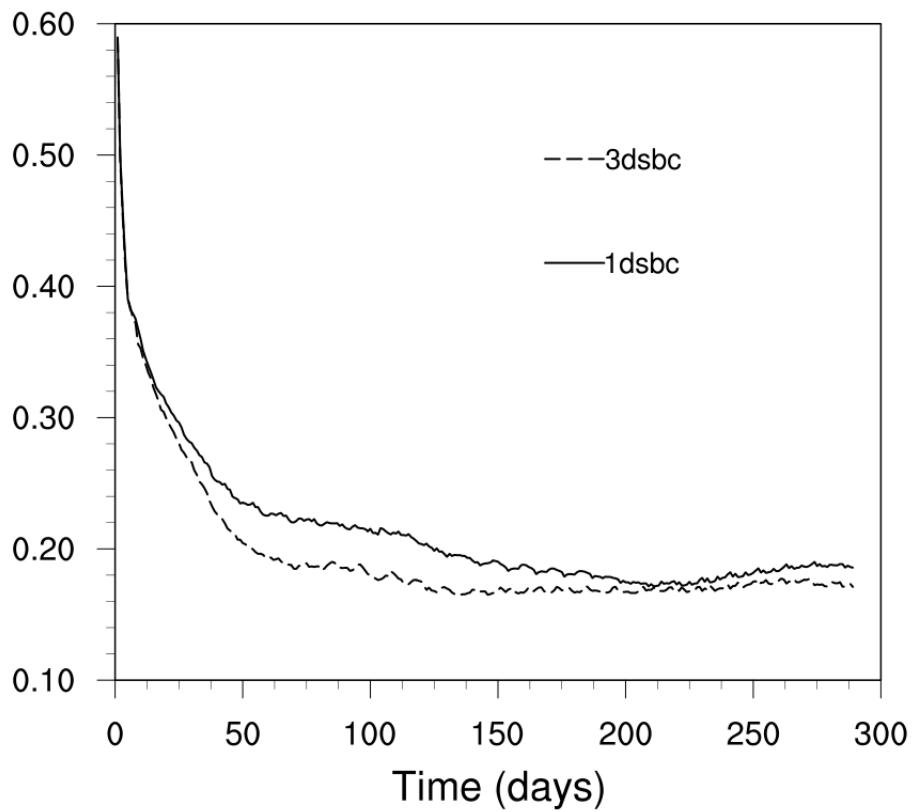


Figure 4.21: Manning coefficient relative bias averaged over the river versus time with 1-day subcycle (straight line) and 3-day subcycle (dashed line) orbits SWOT assimilation. The related bias is calculated as the ratio  $(n_{riv_{with/withoutassi}} - n_{riv_{truth}})/n_{riv_{truth}}$ , where  $n_{riv}$  is the Manning coefficient.

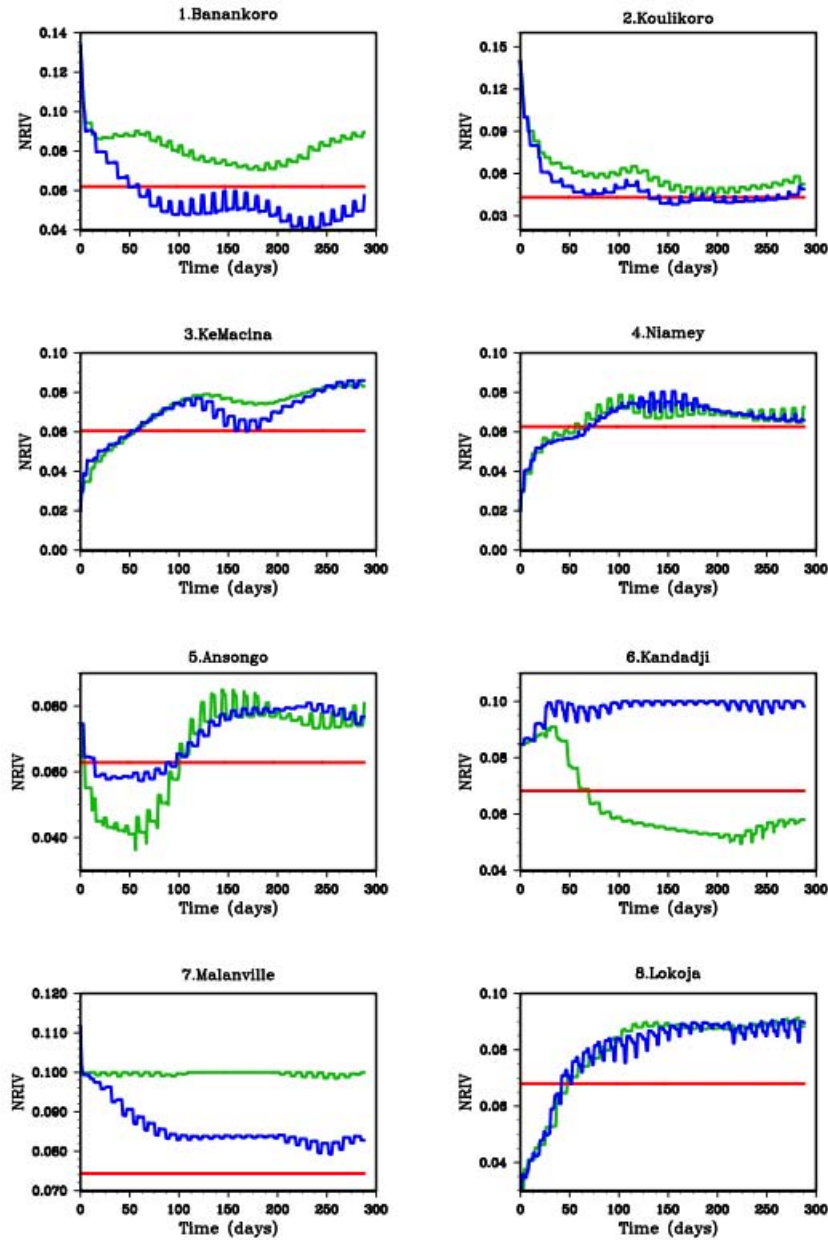


Figure 4.22: Manning coefficient versus assimilation cycles at the 8 locations with gages for the 3 day subcycle (blue) and 1 day subcycle (green) orbits. The true coefficient is in red.

Location $n^\circ$	Riv Mean	1	2	3	4	5	6	7	8
No assi	0.14	0.06	0.1	0.18	0.22	0.2	0.2	0.15	0.14
3dsbc	0.08	0.04	0.04	0.11	0.14	0.14	0.14	0.09	0.06
1dsbc	0.07	0.03	0.03	0.09	0.13	0.13	0.11	0.08	0.06

Table 4.5: Discharge relative bias averaged over the river and at location of the 8 gages along the river (each gage is defined by its number specified inside the orange rectangles on Fig.4.15). The relative bias is calculated as the ratio  $((q_{with/withoutassi} - q_{obs_{swot}})/q_{obs_{swot}}$  where  $q$  is the discharge( $m^3.s^{-1}$ ).

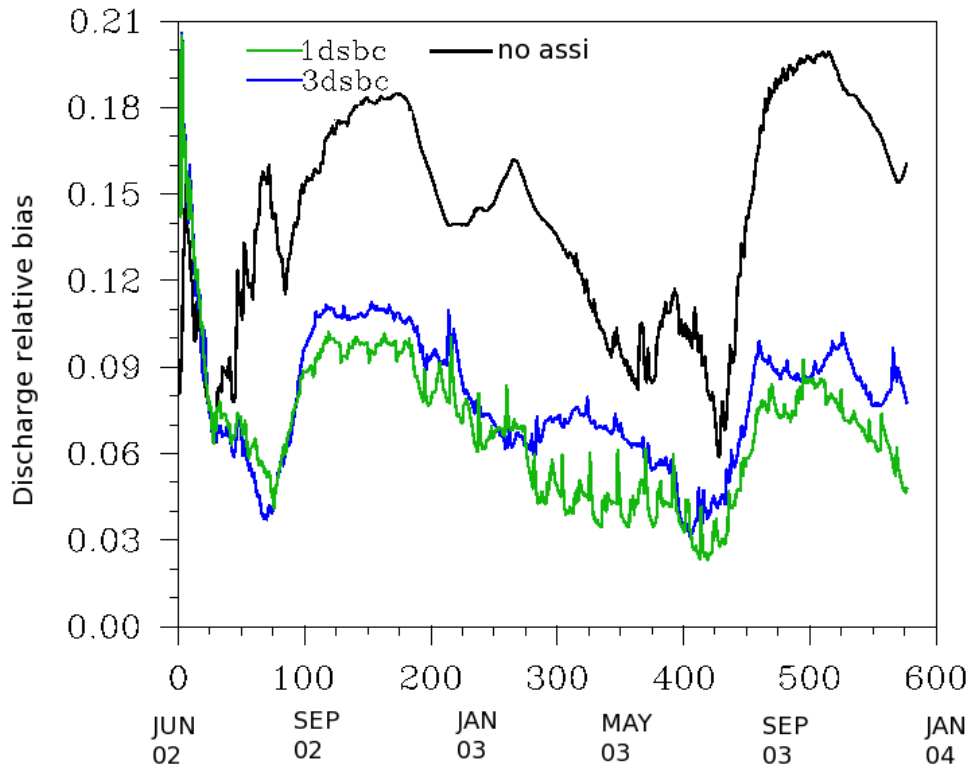


Figure 4.23: Discharge relative bias averaged over the river versus time with no assimilation (black), with 1-day subcycle (orange) and 3-day subcycle (blue) orbits SWOT assimilation. The relative bias is calculated as the ratio  $((q_{with/withoutassi} - q_{obs_{swot}})/q_{obs_{swot}}$  where  $q$  is the water level( $m^3.s^{-1}$ ).

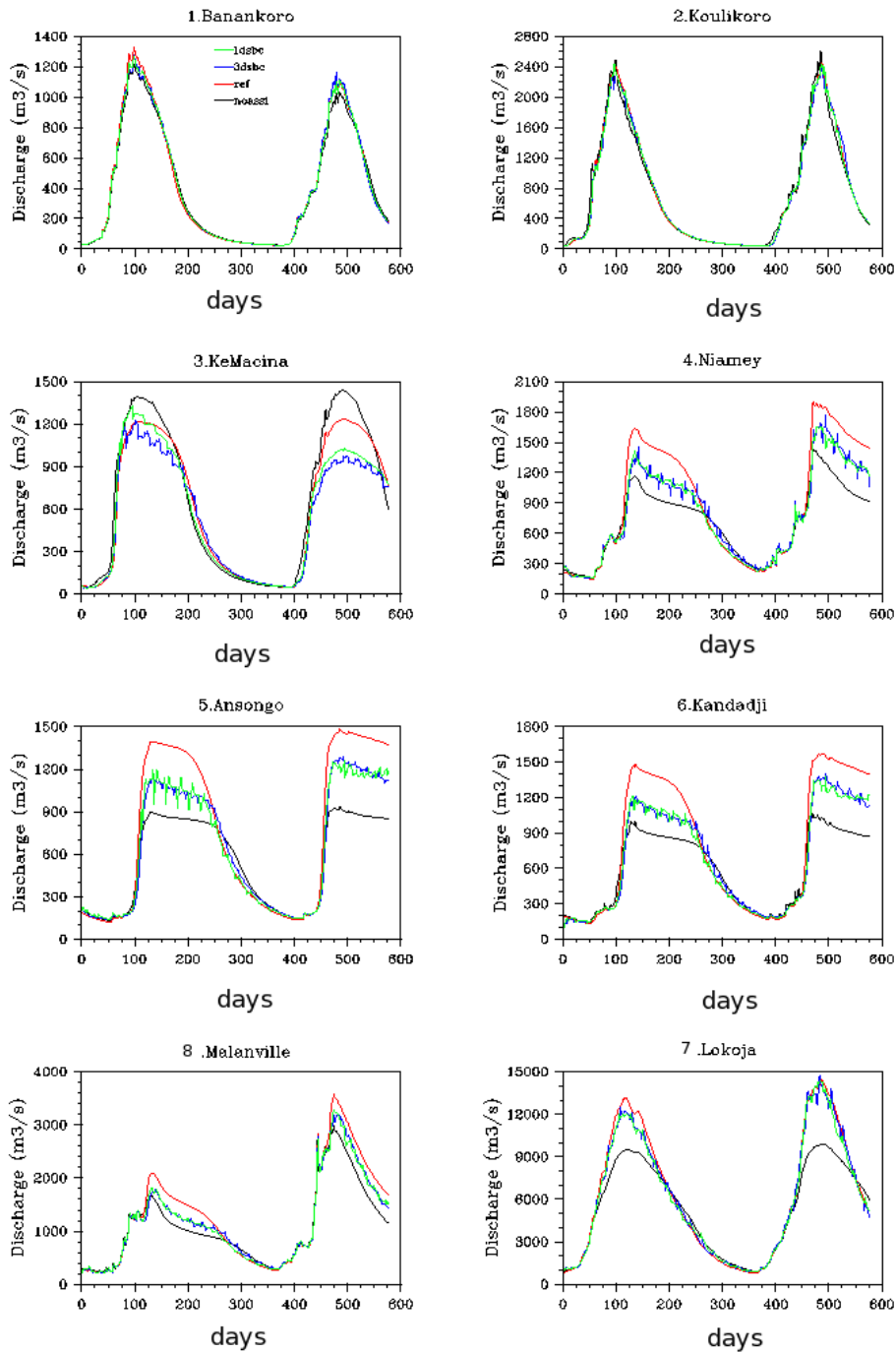


Figure 4.24: Time evolution of discharge at the location of the 8 gages for the "truth" (red curves), with no assimilation (black curves) and with assimilation of SWOT 1-day subcycle (green) and 3-day subcycle (blue) orbits observations.

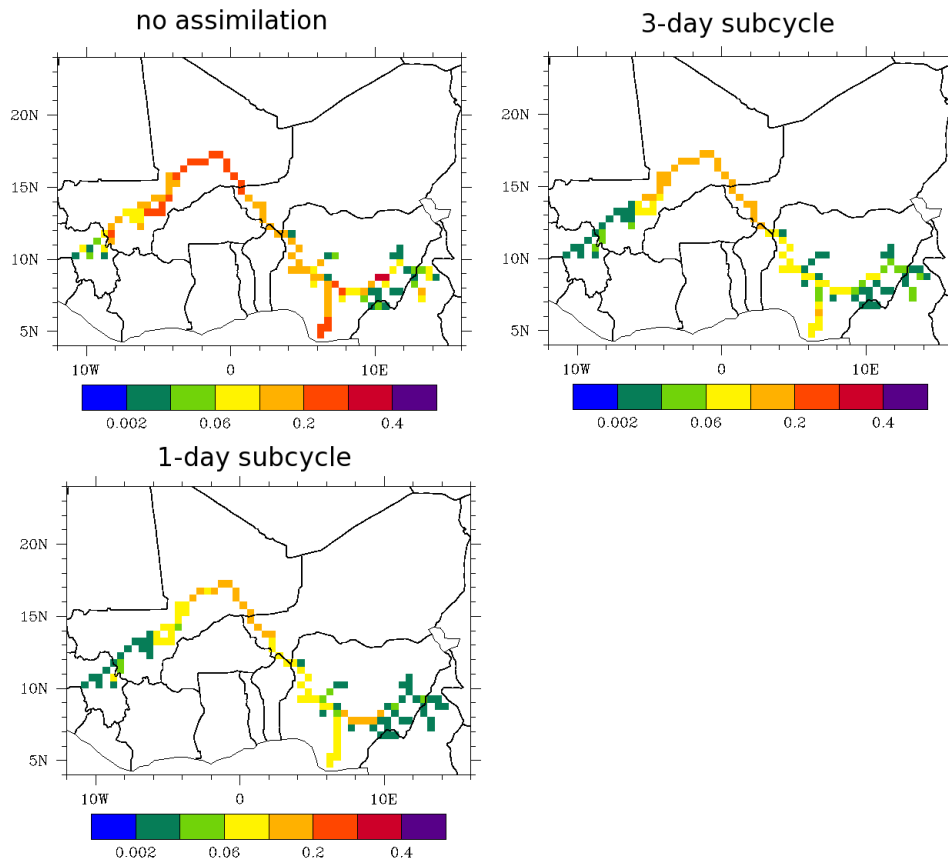


Figure 4.25: Relative bias of discharge averaged over the period of assimilation.

the period June 2002-December 2003 for the run with no assimilation (a), for a 1-day subcycle assimilation (b) and for a 3-day subcycle assimilation (c). The discharge relative bias is globally improved with better results over the inner delta for the 1-day subcycle orbit. Apart from that there is no significant difference between the two orbits. The histograms on Fig 4.26 show the number of pixels contained in different ranges of relative bias going from 0 to 0.4. Without assimilation, the relative bias range over the river goes from 0 to 0.4. With assimilation, all the pixels have a relative bias smaller than 0.2, 80% of them being less than 0.1.

To better understand the relationship between the water levels and the discharge, the flooded fraction time series at 2 locations (KeMacina and Lokoja) is shown on Fig. 4.27. In KeMacina, there was no flooded fraction before the assimilation while there was about 20% for the 'truth'. But the increase of the water level with the assimilation leads to a formation of floods, which is more coherent with the reference run. Moreover, the amplitude of the flooded fraction

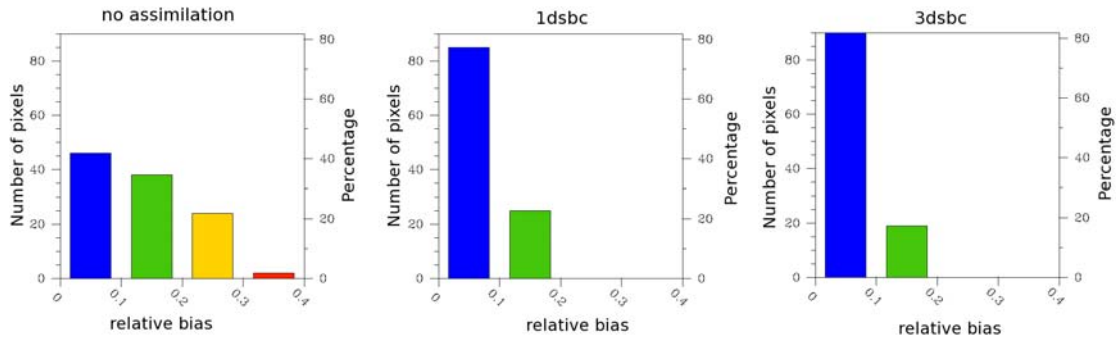


Figure 4.26: Number of pixels contained in different ranges of relative bias going from 0 to 0.4.

is well simulated with the assimilation. Another interesting case is observed in Lokoja, where the model simulates floodplains (25%) with no assimilation, which is not observed for the 'truth'. Here again, by reducing the water levels, the assimilation prevents this flooding from occurring. No floods are modeled at the other sites for the truth, the run with no assimilation or the run with assimilation, so these sites are not shown in Fig 4.27. These results are valuable since they show that the assimilation allows a correction of the flooding prediction in two major sites of the Niger basin. Indeed, Ke Macina is situated just upstream to the entrance of the inner delta region, while Lokoja is not far from the river outlet.

Also, the response of the discharge to a water level modification depends on whether there are floods or not. For example, at Ke Macina during the monsoon period, the water level is increased via assimilation, which causes a better fit with the reference. The increase of water level leads to the creation of floods in this particular region (the region was not flooded before assimilation) and to a decrease of the discharge. This is coherent with the results of Chapter 3, in which the introduction of floodplains leads to a reduction of the discharge. However, in the regions without floodplains, an increase of water level leads to an increase of the discharge (see Kandadji for example).

#### 4.2.5.5 Importance of analysis propagation

In the method presented here, the analysis issued from one assimilation cycle is propagated, since it is used as the control vector for the following assimilation cycle. To investigate the validity of this choice, an assimilation application for which the analysis is not propagated was launched over 90 cycles (180 days). Fig. 4.28 shows the temporal water levels for the truth (red), with no assimilation

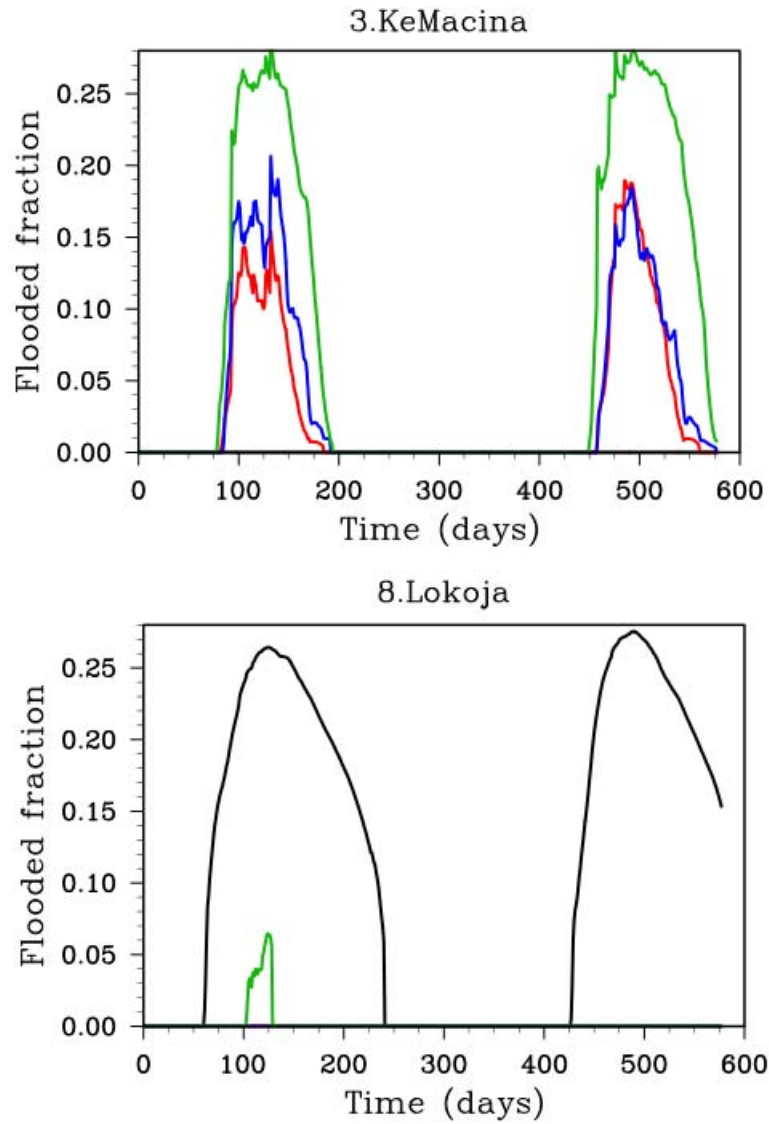


Figure 4.27: Flooded fraction versus time in Ke Macina and Lokoja, for the truth (red), with no assimilation (black), for 1dsbc (green) and 3dsbc (blue).

(black), with assimilation with propagation of the analysis (blue) and with no propagation of the analysis (green). With no propagation, the model seems to stay close to the simulation with no assimilation, since at each assimilation cycle, the information from the previous cycle is not known by the model. Moreover, in Fig 4.29, the evolution of the Manning coefficient in the eight locations is shown. It is seen that without the propagation of the correction through the assimilation cycles, there is no correction occurring in some stations when they were initially corrected in the assimilation with propagation of the analysis. This highlights the fact that, the method needs the information from previous cycles to optimize the parameter.

#### **4.2.5.6 Water storage variations**

For water resource management applications and for making reliable future water resource projections, global hydrologic models must be able to simulate the water storage variations in the continental reservoirs. It is then of interest to see if data assimilation can help to better simulate these water variations. Figs 4.30 and 4.31 show the relative water storage variations in the 5 principal continental reservoirs, averaged over the basin, every 10 and 30 days, for the truth (red), with no assimilation (black), with 1 day-subcycle (blue) and with 3-day subcycle (green). At every time step, only the pixels where the water storage is bigger than 5% of the water storage at the previous time (10 and 30 days before) are considered.

First, the flood and soil reservoirs show no differences between the runs, which means that Manning uncertainty do not impact significantly the storage variations of these reservoirs. Indeed, the water contained in the soil and in the floodplains is highly dependant on the rain intensity, and this source of uncertainties was not considered for the assimilation. In the river reservoir, the 10-day water storage variations with assimilation are noisy. However the 30-day water storage variations with assimilation better fit with the maxima and minima of the reference water storage anomalies than without assimilation. In the groundwater and aquifer reservoir, the simulations with assimilation generally better represent the water storage variations. From these results, the assimilation seems to be useful for better representing anomalies in the continental reservoirs, especially the groundwater and aquifer, which are subject to many uncertainties due to the lack of data. However, since the rain uncertainties were not considered to build the perturbed run, there is hardly any differences between the truth and the perturbation for reservoirs which are more sensitive to rain forcing such as flooded areas and soil moisture. It is therefore difficult to evaluate the skill of the method to better simulate these reservoirs water variations, at least at the basin scale.

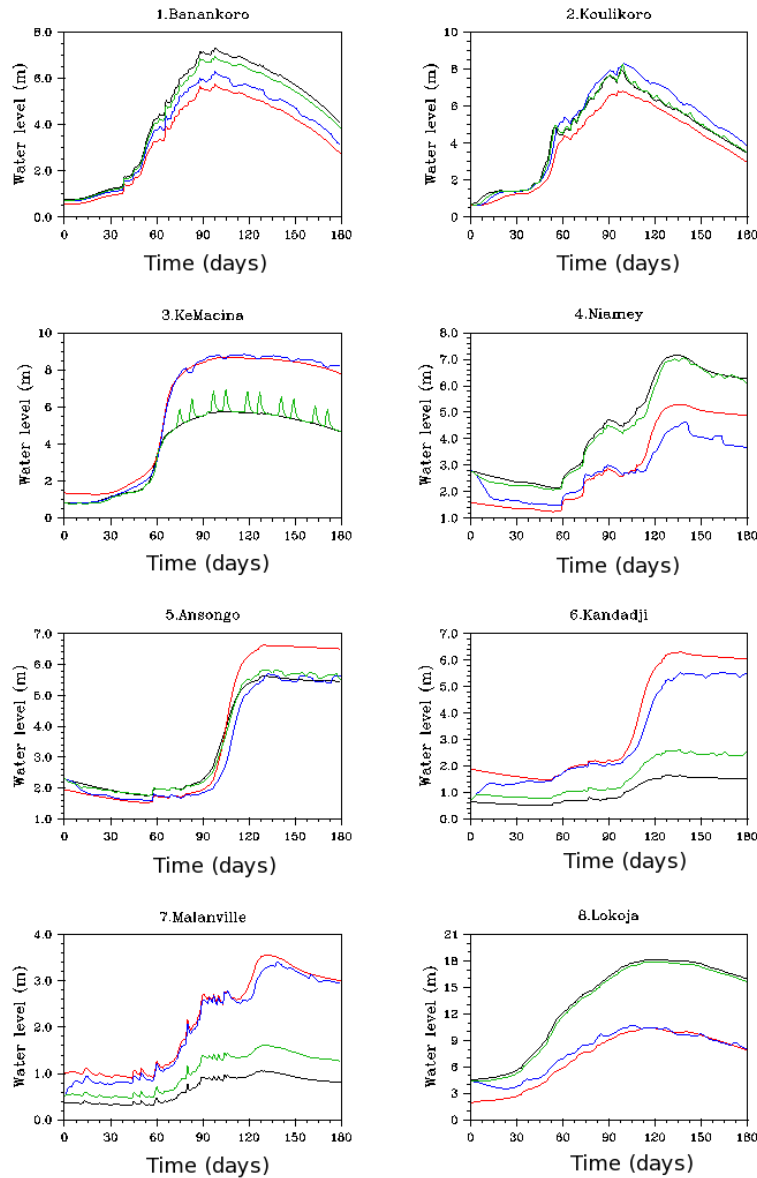


Figure 4.28: Time evolution of water elevations for the truth (red), with no assimilation (black), with assimilation without propagation of the analysis (green) and with propagation of the analysis (blue). The orbit subcycle is 3 days for both simulations with assimilation.

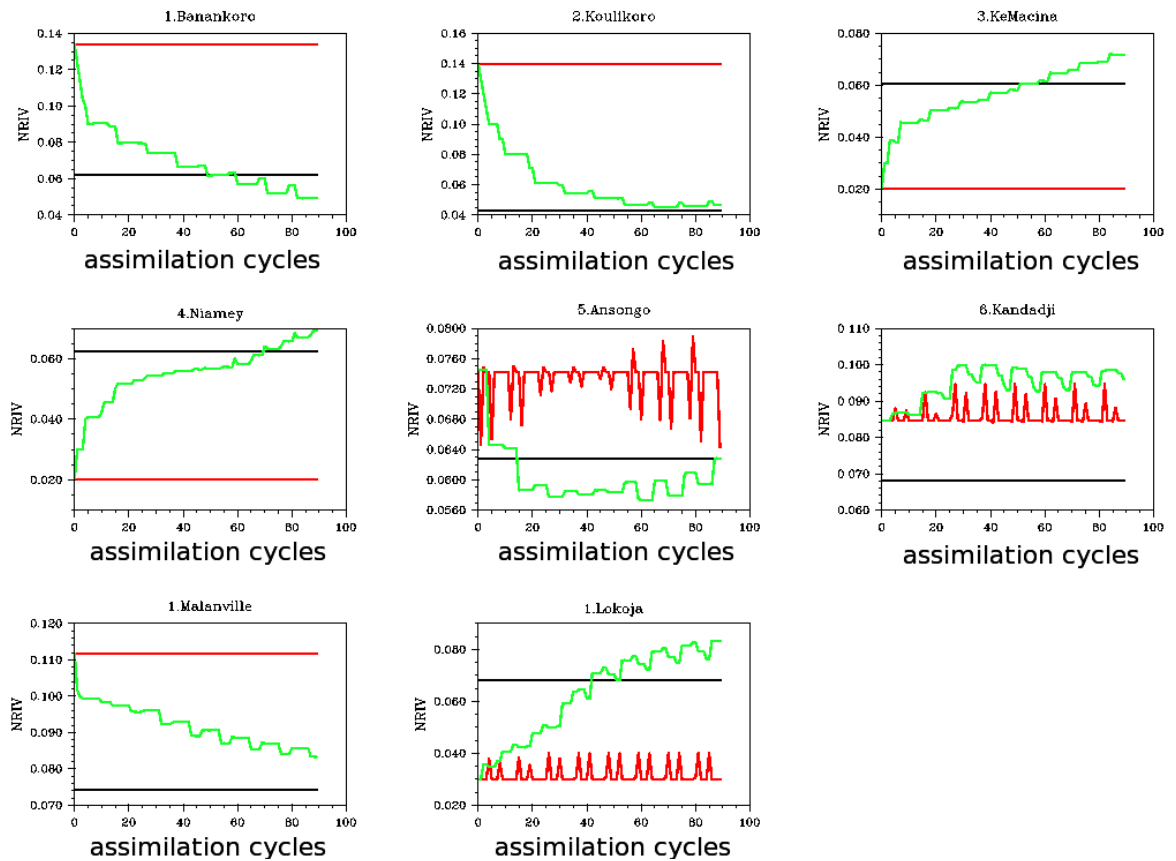


Figure 4.29: Time evolution of the Manning coefficient at the 8 locations with gages for the simulation with no propagation of the analysis (red) and with propagation of the analysis (green). The reference value of the Manning coefficient is in black.

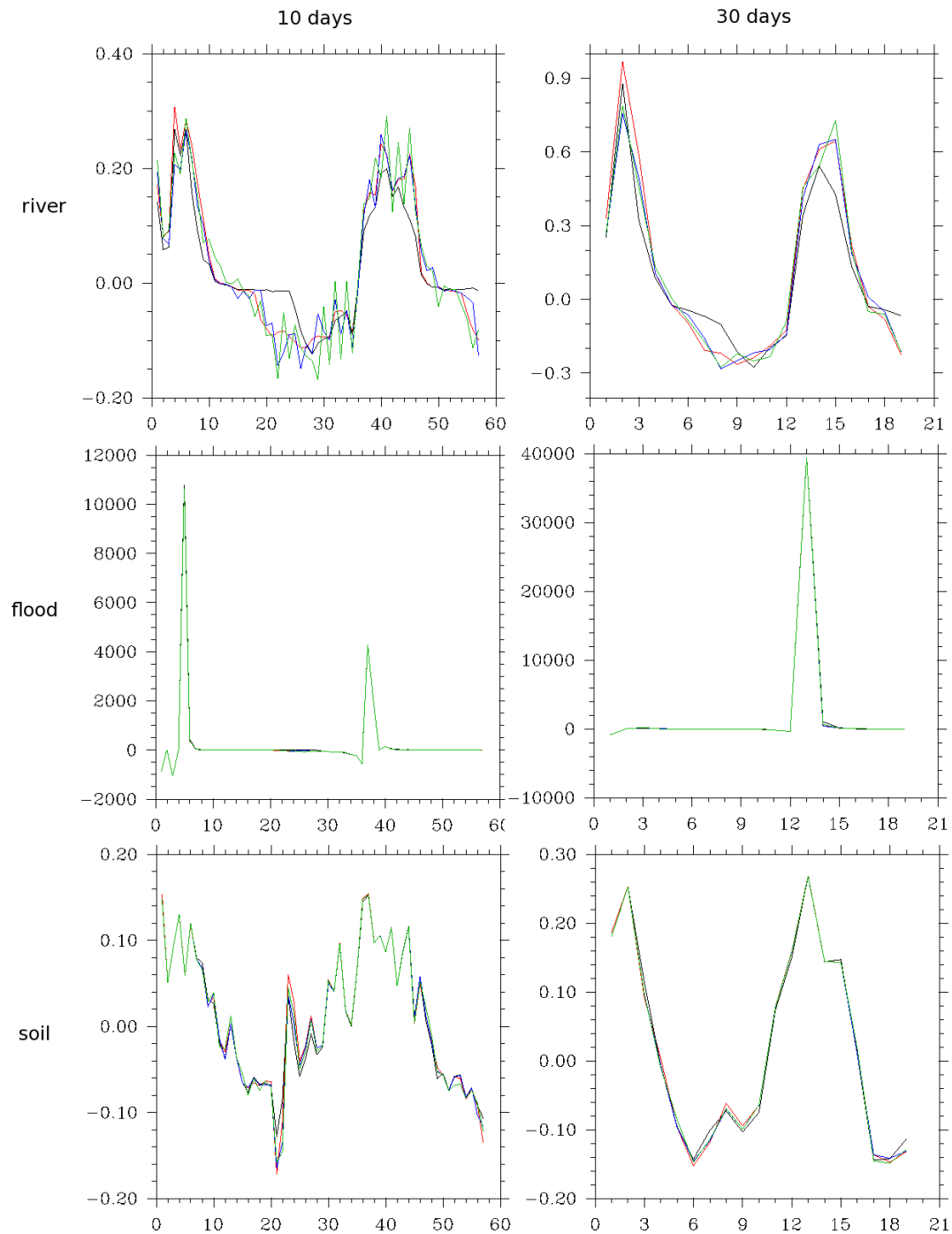


Figure 4.30: Water storage variations in the river the soil and the flood reservoirs for the truth (red), with no assimilation (black), with assimilation for the 1-day orbit subcycle (green) and for the 3-day subcycle (blue). The water storage variations are calculated every 10 days (left) and every 30 days (right).

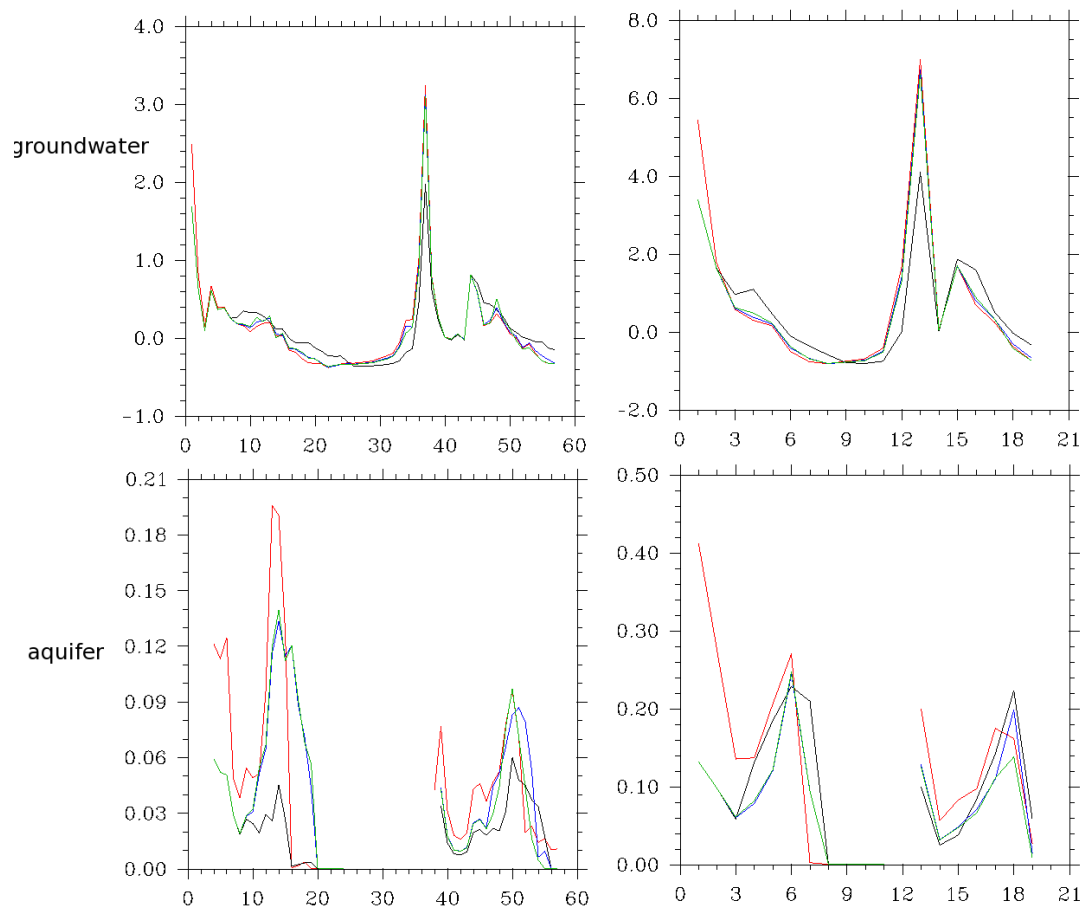


Figure 4.31: same as Fig. 4.30 for the groundwater and aquifer reservoirs.

The flooded fraction over the inner delta region is shown in Fig 4.32 Fig 4.32 shows the temporal evolution of flooded fraction averaged over the inner delta region for the truth (red), with no assimilation (black), with assimilation for a 1-day subcycle (green) and with a 3-day subcycle (blue). Only the pixels where the flooded fraction is more than 10% are considered. Fig 4.33 shows the frequency of events according to the flooded fraction value for the truth (a), with no assimilation (b), with assimilation for a 1-day subcycle (c) and with a 3-day subcycle (d). Here again, only the pixels with a flooded fraction higher than 10% (0.1 on horizontal axis) are considered. From Fig 4.32, the differences between the simulations are not obvious, even if it seems that during the first flood season, the averaged flooded fraction over the delta is too high with no assimilation which is not the case with assimilation. Starting the second flood season, the peak of flooded fraction is underestimated by the simulation with no assimilation, which is corrected with assimilation for 3-day subcycle but not for 1-day subcycle.

In Fig 4.33, it is seen that , without assimilation, the model does not simulate flooded fractions higher than 0.5, which represents about 8% of the flood events for the reference run. Moreover, without assimilation, the model tends to overestimate the occurrence of smaller events. This is corrected by the assimilation, with a slight tendency to surestimate flood intensity for the assimilation with the 3-day subcycle orbit, while the 1-day subcycle orbits leads to an excessive occurrence of flooded fractions contained in the [0.2-0.3] range.

According to these results, data assimilation permits a better simulation of the water storage variations and to better estimate the occurrence and intensity of flood events in the inner delta area.

### 4.3 Use of the optimal analysis for hydrologic forecasting

For future water resource projections, it is of interest to see if the optimal parameter obtained previously can be used for hydrologic prediction, ie over a period with no SWOT observations and thus, without assimilation. Figs 4.34 and 4.35 show the time evolution of the relative bias of water levels and discharge averaged over the river for the period 2002-2007. Figs 4.36 and 4.37 show the water levels and discharge versus time over the period 2002-2007. The relative bias of water levels is reduced by about 30 % over the entire simulation period. The improvement of the discharge, in a lesser extent, is especially observed during the monsoon seasons (around a 7% improvement).

This study shows that the assimilation method can be applied as a calibration experiment in order to get a better simulation over a longer period for a prediction

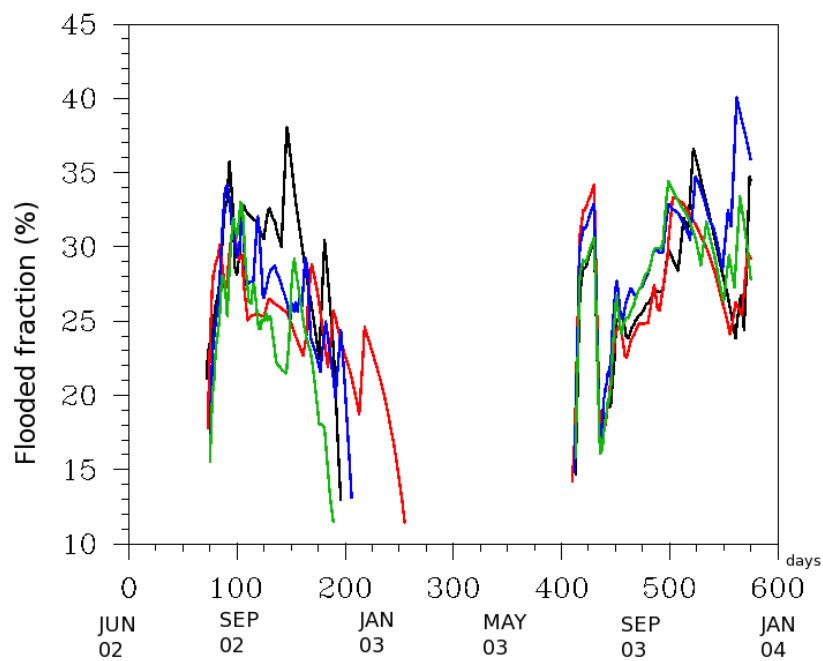


Figure 4.32: Time evolution of flooded fraction averaged over the inner delta region. Only the pixels with a flooded fraction higher than 10% are considered for the calculation.

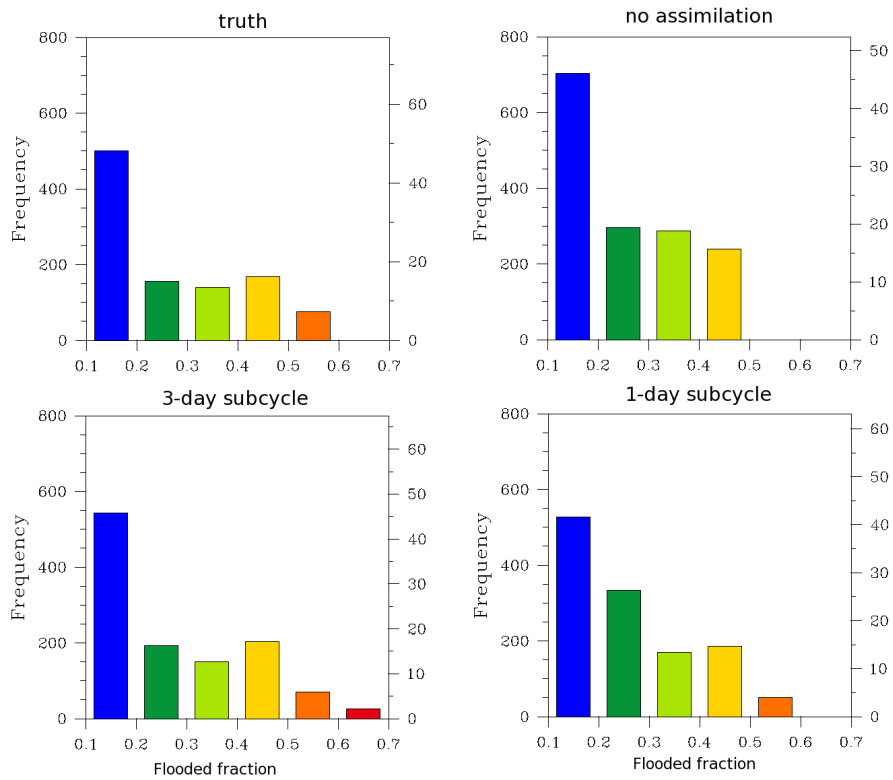


Figure 4.33: Frequency of flood events over the delta classified by intensity (flooded fraction). Only the pixels with a flooded fraction higher than 10% are considered for the calculation.

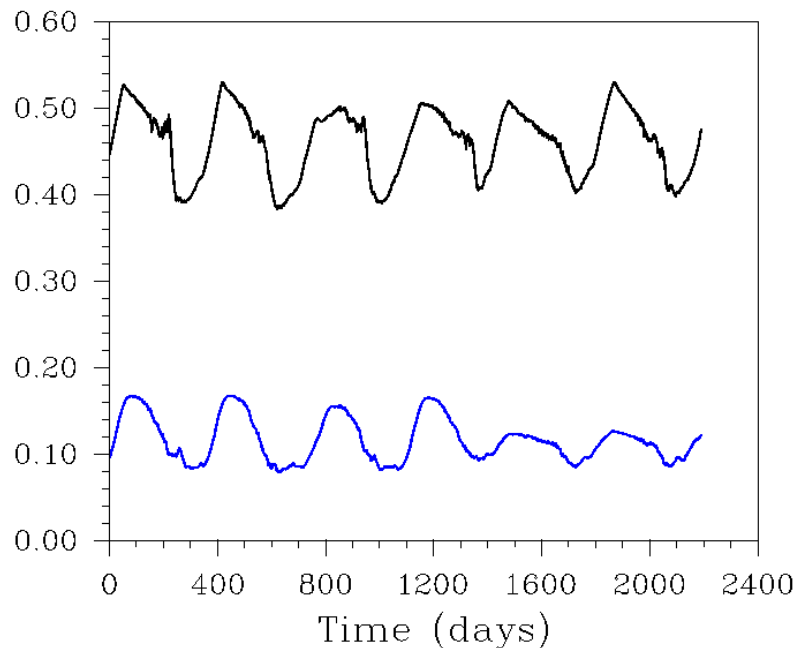


Figure 4.34: Time evolution of the water elevation bias for the truth (red), with the initial perturbed Manning coefficient (black) and with the optimal Manning coefficient obtained via assimilation (blue).

study.

## 4.4 Discussion

The optimization of the Manning coefficient using the proposed data assimilation methodology from June 2002 to December 2003 leads to a significant improvement of the water levels over the river, and also at the 8 locations with gages. Indeed, the relative bias of the water level is globally improved ( a 30 % reduction) and the amplitude of the water level is closer to the reference with assimilation than without assimilation. The relative bias of the Manning coefficient is also reduced (40% reduction) and it globally converges towards an optimal value despite potential problems related to equifinality. At some places however, the Manning is corrected after a large number of cycles so the question may be asked if other errors (related to other uncertainties) are not being corrected via the correction of the Manning. The discharge is also improved by the assimilation, but to a lesser extent than for the water levels (7%). Moreover, the method allows a better prediction of the occurrence and intensity of flood events

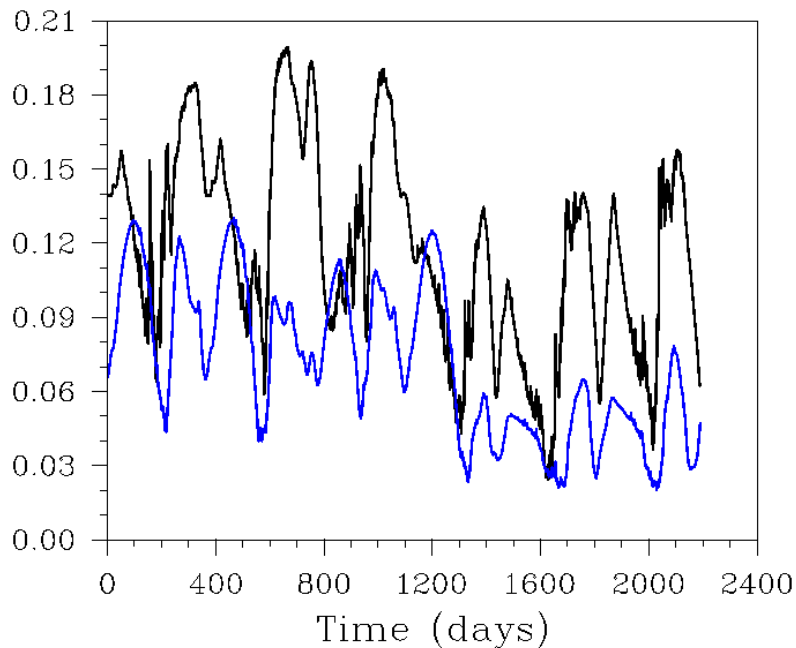


Figure 4.35: Same as Fig 4.34 for the discharge.

in the inner delta and showed skills to better simulate the maxima and minima of water storage anomalies in several continental reservoirs, especially the groundwater and the aquifer reservoirs, which evolution is difficult to observe.

This study is promising since, to our knowledge, no large scale assimilation applications exist for the optimization of spatially distributed hydrological parameters. It shows that SWOT observations would be useful for the improvement of CHSs hydrological parameters. A simulation over 2002-2007, using the optimal parameter from the assimilation experiment, showed that the method allows a better hydrologic forecasting of the Niger river hydrologic states, even after the calibration phase. This method could lead to a better representation of the water cycle in climate prediction applications, but could also be used for large scale water resource management applications. Finally, there is no significant difference between the two subcycle orbits used for this study, each one having better skill for certain situations. The temporal sampling is very different between the 1-day subcycle orbit and the 3-day subcycle orbit: the 1-day subcycle orbit will allow a daily (or even sub-daily) sampling for 11 days, but then there will be no observations for the remaining 11 days, leading to temporal gaps in the time series. The 3-day subcycle orbit will have 1 or 2 missing days every 2 to 3 days. While the 3-day subcycle orbit seems to be more appropriate for the hydrologic modeling of high latitude basins (Biancamaria et al., 2011), it does

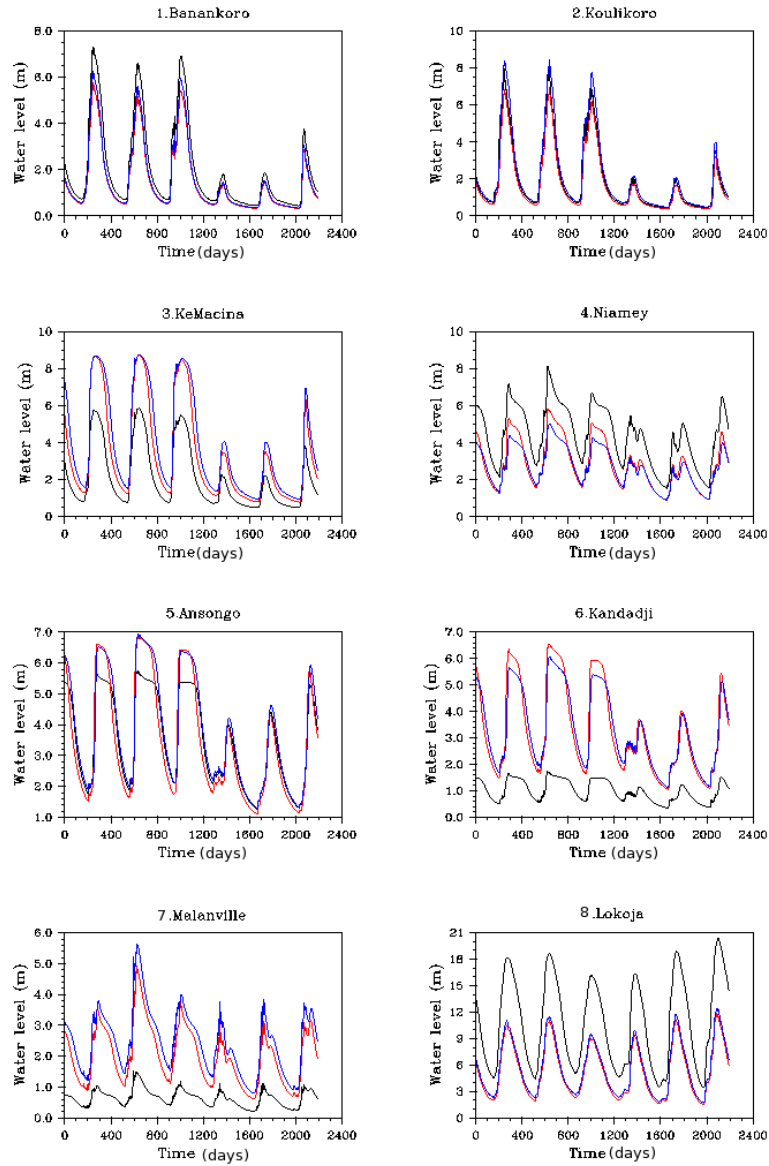


Figure 4.36: Time evolution of the water elevation for the truth (red), with the initial perturbed Manning coefficient (black) and with the optimal Manning coefficient obtained via assimilation (blue).

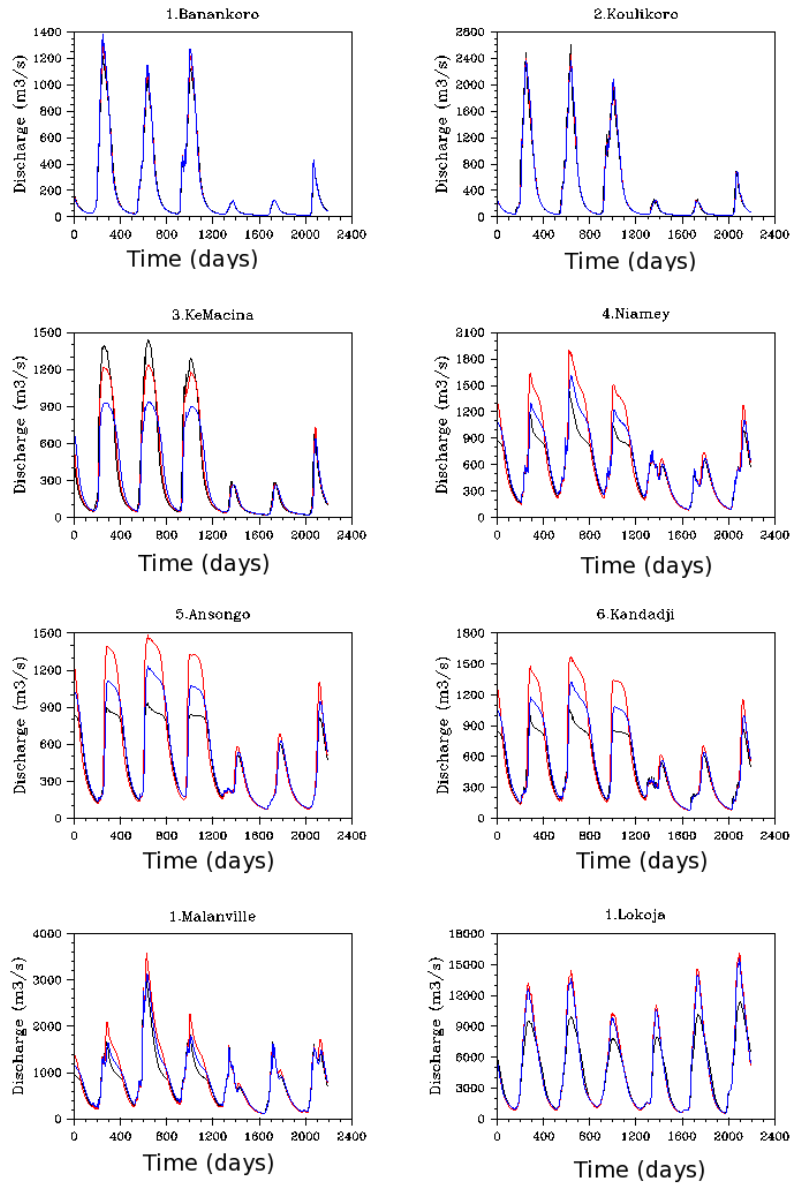


Figure 4.37: Same as Fig. 4.37 for the discharge.

not lead to a significant degree of improvement for a low latitude basin like the Niger river.

It should be noted that, this study has some limitations and many assumptions have been used. For example, the assumption of a white noise error for SWOT observations is probably too optimistic. Furthermore, no correlation along the swath has been considered. Estimating the satellite observations error sources has been the subject of several studies at the French spatial agency (CNES) in recent years. Initially, a white noise was introduced in the SWOT water level along track in order to represent the error due to satellite observations (Biancamaria et al., 2011). A PhD ongoing at LEGOS/CNES (Lion, 2012) presents methods to simulate, in a more realistic manner, different sources of SWOT satellite observation errors. These errors are said to be 'residual errors' which means that they appear during the satellite data treatment phase, mainly because of a poor knowledge of the satellite real state and position. These indirect errors are generally due to several factors such as the satellite altitude, the baseline, the roll and the phase. These errors are usually Gaussian but they not always have a mean value of 0. A perspective for improvement of the assimilation methodology proposed in this study, would be to introduce these errors into the assimilation system in order to get a more realistic estimation of SWOT observation errors and of the error covariance matrix  $\mathbf{B}$ . However, their introduction in the system is not obvious and could lead to a degradation of the errors due to the aforementioned Gaussian issue. Indeed, the Gaussian error distribution along SWOT tracks does not ensure that the error of the observation vector,  $\mathbf{y}^0$ , is Gaussian. Yet, the gaussianity of the observation error is a strong assumption of the BLUE and solutions must be found to get around this limitations.

The hypothesis that the Manning coefficient uncertainties are the only source of model errors is a very strong assumption since other errors, such as those related to precipitation uncertainties or the relatively simple ISBA-TRIP physics, can also be the sources of significant modeling errors. Also, it could be potentially interesting to perform the assimilation on an ensemble of perturbed runs in order to take into account several uncertainty scenarii. Thus, the estimation of the background modeling matrix could be done using an ensemble method (Evensen et al., 2004).

This method must be applied on other ISBA-TRIP parameters and on other large basins to evaluate its global application capability. Indeed, it is not ensured that a methodology that works for a specific basin is exportable to any other basin.

Finally, this study was done in the context of an observing system simulation experiment in which the truth was issued from a reference ISBA-TRIP simulation. This allows a validation of the methodology, but it does not ensure good functioning with real observations. Indeed, in the study presented here, the

truth and the perturbation are based on the same physical processes : this is not true when real data are used. Therefore, the assimilation should be applied using either real observations of water level, or water level issued from a different model, such as a model with higher resolution and a more detailed physics.

These proposed improvements aim at ensuring that the assimilation methodology is applicable in the real context of SWOT data assimilation.

## 4.5 Chapter conclusions and perspectives

This chapter presents a preliminary method to assimilate SWOT virtual water level in order to improve the ISBA-TRIP global hydrological model parameters. According to the sensitivity tests performed in Chapter 3, it was decided to apply the assimilation method to correct the Manning coefficient. This coefficient is a key parameter which impacts the dynamics of surface water, and thus the water level and discharge. However, its estimation is difficult and it is generally described in global scale models by geomorphologic relationships. In high resolution hydrological models, it is possible to 'tune' the model parameters in order to fit with observations. But, at the global scale this type of approach is limited by the lack of observed data. This study shows that the SWOT satellite data offer an alternative method to better calibrate large scale hydrologic models through assimilation. For this, an Observing System Simulation Experiment (OSSE) was done, using virtual SWOT observations of water levels. The SWOT virtual observations are generated using a reference ISBA-TRIP run. Then, a perturbed run is created, considering that the modeling uncertainties were only due to uncertainties with respect to the Manning coefficient. The Best Linear Unbiased estimator (BLUE) algorithm is then applied every 2 days (length of the assimilation window) to calculate a corrected Manning coefficient (analysis). The analysis is then considered as the new control vector for the following assimilation cycle. Thanks to this method, the estimation of an optimal spatially distributed Manning coefficient is possible. This Manning coefficient globally converges after an approximately 6 month period. This optimal distribution is closer to the true distribution than the perturbed one, showing that in this application, equifinality is not a limitation. This method gives promising a perspective for global scale applications, and it could be extended to other large basins. However, it is limited by its simple hypothesis and is still under improvement. For example, in this study, only the uncertainties related to the Manning coefficient were considered. Other sources of uncertainties could be considered for the assimilation, such as rainfall errors. Moreover, other modeling errors such as those from the ISBA parametrisation could be considered. To simplify the calculations, it was also considered that the observations and modeling errors were not correlated in space

and time which might not be realistic. The use of more realistic errors simulated in the framework of a PhD at LEGOS/CNES (Lion, 2012) is to be considered.

These preliminary results show that the method leads to a global reduction of 40% of the Manning bias over the river. This reduction significantly improves the water levels (the bias is reduced by 30% for the river) and, to a lesser degree, also improves the discharge (7% of reduction of the bias which can be significant for the Niger river considering that its mean annual discharge is  $6000m^3.s^{-1}$ ). Moreover, the biggest improvements were observed downstream of the river (Lokoja), which is a valuable result for climate applications which require estimation of the discharge at large rivers mouths. Another perspective consists in the application of this method to other TRIP parameters, or several parameters at a time. The correction of ISBA parameters, such as those controlling sub-grid runoff for example, is also planned but must be considered carefully as the impact on the river is less direct. Nonetheless, this will be addressed in the future. Before the satellite launch, the airSWOT airborne campaign will provide SWOT-like datasets of water level, which will allow a real SWOT data assimilation application, instead of the Observing system System experiment presented here. However, this airborne campaign will not cover the Niger basin, so the method must also be tested on other basins. Finally, the study showed that the method could be used to better forecast continental water storage anomalies and/or flood events occurrence and intensity in the inner delta, which are crucial issues for water resources management.



# Conclusion et perspectives

Parcourant 4180km des Hautes terres de Guinée jusqu'au Nigeria, le Niger est la principale source d'eau des millions de personnes qu'il approvisionne. Dans ces régions principalement rurales, où l'économie repose majoritairement sur des activités telles que l'agriculture et l'élevage, la disponibilité des ressources en eau est une condition essentielle au développement économique et social des populations. Pourtant ces dernières décennies, le bassin du Niger a souffert des aléas climatiques, donnant lieu à une forte augmentation d'évènements extrêmes telles que des inondations et des sécheresses. Pour limiter l'impact sur les populations de ces catastrophes naturelles, il est nécessaire de mieux comprendre les processus hydrologiques entrant en jeu dans le bassin du Niger. Ceux-ci sont fortement influencés par la mousson africaine, son intensité et sa variabilité. En retour, les eaux continentales sont susceptibles d'impacter l'atmosphère et le climat, au moins à l'échelle régionale. Du point de vue de la modélisation numérique, le bassin du Niger représente un challenge en raison de ses dimensions, mais surtout parce qu'il traverse des zones climatiques très diverses, allant d'une région quasi désertique dans la bande Sahélienne, vers une région très pluvieuse dans le golfe de Guinée. Le Niger passe notamment par le Delta intérieur du Niger, au Mali, large zone d'inondations et d'évaporation dont la dynamique impacte directement le débit du fleuve, mais aussi l'atmosphère via d'importants échanges d'énergie à la surface de ces plaines inondées. Enfin, le Niger rejoint l'océan par un large estuaire, où de nombreux affluents viennent booster le débit allant vers la côte. Une meilleure connaissance et gestion des ressources en eau dans cette région nécessite donc la maîtrise de processus hydrologiques et hydrodynamiques variés, actuellement fortement limitée par le manque de données mesurées ayant un bon recouvrement temporel et spatial. En effet, le contexte politico-économique empêche souvent la construction et/ou le maintien d'infrastructures permettant le suivi des eaux continentales. Depuis les années 70, des techniques spatiales sont développées afin d'acquérir des informations complémentaires et d'alimenter les modèles numériques. L'altimétrie classique, par exemple, a permis d'estimer les variations de hauteurs d'eau des lacs, en plus de son objectif principal qui est l'observation des océans. Dernièrement, des cartes globales et temporelles d'estimation des zones inondées ont été construites par l'exploitation de l'imagerie optique et radar (Papa et al., 2010). Cependant, les résolutions spatiales et temporelles limitées de ces techniques font qu'une grande partie des eaux continentales ne sont pas observées à l'heure actuelle. La mission spatiale SWOT, issue d'une collaboration internationale, constituera donc une avancée technologique majeure, en raison principalement de sa résolution spatiale encore jamais atteinte jusque là (50 à 100 mètres).

Le principal avantage de cette mission vient de l'utilisation d'un radar interférométrique appelé KaRIN (Ka-Band INterferometer pour radar interféromètre en bande Ka), donnant une trace au sol de 120km de large. Ainsi, avec sa large trace, le satellite SWOT couvrira tous les lacs, les rivières, réservoirs et océans de la terre au moins deux fois environ tous les 21 jours (jusqu'à 7 fois dans les hautes latitudes). Cependant, afin de préparer au mieux son lancement, prévu en 2019, les communautés scientifiques doivent déterminer comment ces données pourront être utilisées dans des régions et à des échelles variées.

Cette thèse se présente donc comme un travail de pré-lancement de la mission SWOT, dont le but est de déterminer la contribution des données satellites SWOT, à la modélisation hydrologique à grande échelle du bassin du Niger. Pour cela, il a d'abord fallu mettre en place une modélisation réaliste du bassin, à l'aide du modèle d'hydrologie continentale ISBA-TRIP, incluant un schéma de zones inondées (Decharme et al., 2011) et un réservoir simple d'aquifères profonds, développé durant cette thèse (Pedinotti et al., 2012). La simulation est effectuée sur la période 2002-2007 à une résolution spatiale de  $0.5^\circ$ . Au vu du nombre limité d'observations de débits le long du fleuve (8 sites de mesures ont été mis à notre disposition pour ce travail), il a fallu trouver d'autres données venant compléter notre connaissance de la dynamique des eaux de surface. Ces données sont choisies en fonction de leurs résolutions spatiale et temporelle qui doivent être suffisamment cohérentes avec la résolution du modèle et de leur période de recouvrement qui doit couvrir tout ou partie du temps de la simulation. Ainsi, plusieurs observations, dérivées de données satellites ont pu être utilisées pour évaluer le modèle (hauteurs d'eau, zones inondées, variations des stocks d'eau). De plus, plusieurs jeux de précipitation ont été pris en compte afin d'estimer leur compétence pour la modélisation hydrologique. Parmi 4 jeux de précipitations, deux d'entre eux (TRMM et RFE2) ont permis une bonne cohérence avec les observations et ont été gardés pour la suite de l'évaluation. Cette étude montre que le modèle, malgré sa relative simplicité, est capable de simuler les principaux processus hydrodynamiques du Niger. Le schéma de zones inondées permet une meilleure estimation du débit en aval du delta intérieur durant la mousson tandis que l'aquifère permet de mieux simuler les débits d'étiage. L'évaluation a aussi montré que le modèle est capable de simuler les principales zones d'inondations et d'estimer correctement les variations de stock d'eau sur le bassin. Enfin, une étude de sensibilité a aussi permis de mettre en évidence les paramètres sensibles du modèle, ce qui a constitué une étude préliminaire pour la deuxième phase de la thèse.

La deuxième phase de la thèse a consisté à déterminer comment les données SWOT pouvaient être utilisées dans le cadre de l'hydrologie globale. Plusieurs études ont montré que l'assimilation de données pouvait offrir des perspectives prometteuses d'amélioration des prévisions hydrologiques (Andreadis et al., 2007;

Biancamaria et al., 2011). Cependant, ces méthodes ne sont que peu utilisées dans le cadre de l'hydrologie à l'heure actuelle, et les études sont encore rares pour le moment, particulièrement à des échelles spatiales globales comme c'est le cas du modèle ISBA-TRIP. En effet, l'assimilation de données est souvent utilisée pour corriger l'état des modèles, ce qui ne peut pas être effectué dans le cadre de simulations climatiques pour lesquelles sont prévues les modèles de surface de grande échelle. Il a donc été décidé de mettre en place une méthode d'assimilation des données SWOT afin de réduire les incertitudes qui persistent sur certains paramètres d'entrée sensibles du modèle ISBA-TRIP. Cette méthode consiste à réaliser une expérience dite jumelle, très pratique lorsque l'on veut assimiler des observations qui n'existent pas encore comme c'est le cas pour les données du satellite SWOT. Le principe est donc de générer des données virtuelles de hauteur d'eau SWOT à la résolution du modèle, à l'aide d'une simulation de référence (cette simulation est appelée 'vérité'). Puis, en prenant en compte des incertitudes sur les paramètres du modèle, une simulation perturbée est créée. L'assimilation consiste alors à utiliser les observations SWOT afin de corriger les paramètres incertains en entrée du modèle et d'obtenir ainsi une meilleure représentation de certaines variables dynamiques telles que les hauteurs d'eau et le débit du fleuve. Après une étude de sensibilité, il a été décidé d'utiliser l'assimilation pour corriger un paramètre hydrologique important, le coefficient de Manning. Le coefficient de Manning décrit la propriété du sol à 'freiner' l'écoulement, c'est donc un coefficient de frottement. Difficile à estimer, il varie en fonction du type de sol et agit directement sur la vitesse de l'écoulement, c'est-à-dire sur le débit. Il agit également sur la formation des zones inondées. L'algorithme fournissant l'analyse à l'issue d'un cycle d'assimilation est le BLUE (Best Linear Unbiased Estimator). Cette étude, encore à un stade préliminaire, montre que l'assimilation de données permet une bien meilleure estimation des hauteurs d'eau (environ 30% de réduction du biais), et, en moindre proportions, des débits (7% de réduction du biais) sur la rivière. De plus, elle permet aussi une meilleure représentation de l'évolution des différents stocks d'eau continentale. Le biais du coefficient de Manning, en particulier, est nettement amélioré à l'issue de l'assimilation et semble converger vers une valeur optimale en dépit des problèmes d'équifinalité que suggère une telle étude. Il est aussi montré que l'assimilation permet une meilleure prédiction des inondations (occurrence, intensité) sur le delta intérieur du Niger. Enfin, le caractère prédictif de cette méthode est mis en évidence en utilisant le coefficient de Manning optimal obtenu lors de l'assimilation pour simuler l'hydrologie du bassin sur une période plus longue que celle de l'assimilation. Cependant, cette étude est encore dans une phase préliminaire et offre de nombreuses perspectives d'amélioration. Par exemple, elle suppose que les seules incertitudes de modélisation sont des erreurs sur l'estimation du coefficient de Manning alors que d'autres sources d'erreurs, telle

que la pluie, doivent être prises en compte. Aussi, cette méthode doit être étendue à d'autres paramètres incertains du système ISBA-TRIP, ainsi qu'à d'autres larges bassins du globe afin d'évaluer sa compétence pour des simulations globales.

La mission SWOT va permettre l'observation des lacs, fleuves et rivières à une résolution encore jamais atteinte à l'heure actuelle. Ces données vont constituer un outil important afin de mieux comprendre le cycle hydrologique global et de prévoir l'évolution future des ressources en eau. Sur le bassin du Niger, où le contexte politico-économique ne permet pas une bonne surveillance des réservoirs d'eau, elle permettra de faire progresser considérablement les connaissances hydrologiques et hydrodynamiques du bassin, offrant ainsi la possibilité d'une meilleure gestion des ressources, pour un moindre impact face au changement climatique.

With an approximate length of 4180 km (2600 miles) extending from the Guinea Highlands to the southern Nigerian coast, the Niger river is the main source of water for millions of people in West Africa. In these rural areas, the economy is largely based on activities such as agriculture and livestock farming, so water availability is critical for economic and social development. However, during the last several decades, the Niger basin has faced strong climate variability, leading to an increased number of extreme events such as drought and floods. Projections of greatly increased population in the Niger basin will also put even more pressure on the already limited resources. In order to limit the impact of extreme meteorological events on the population in the Niger basin, a better understanding of hydrological and hydrodynamic processes is required. These processes are conditioned by the intensity and variability of the West African Monsoon (WAM). Continental water storage and fluxes can then impact the atmosphere and climate, at least at the meso to regional scales. For numerical modelling, the Niger basin is a challenging region considering its large dimensions and the fact that it encounters very heterogeneous climatic conditions, from the semi-arid Sahelian zone to the relatively humid area adjacent to the Gulf of Guinea. Notably, the Niger river contains a vast inner delta which is seasonally flooded. These flooded areas are the source of significant evaporation which impacts the river discharge and the atmosphere. Finally, the Niger river joins the ocean through a large delta, where many tributaries contribute to a large increase of the discharge. A better knowledge and management of the water resources in this area requires a good understanding of the diverse hydrologic and hydrodynamic processes, but it is currently limited due to the lack of observations with sufficient spatial and temporal coverage. Indeed, the socio-economic context does not allow the construction and maintenance of the infrastructures needed for extensive continental water resource monitoring. Since the 1970's, remote sensing technologies have been developed in order to provide complementary information about surface water dynamics, and such data have also proven to be essential as input to and the evaluation of numerical models. Classic altimetry has permitted the estimation of lake and ocean water level variations, but such data is generally limited in terms of both spatial and temporal coverage. Recently, global maps of flooded areas over multi-year periods were built using optical and radar imagery (Papa et al., 2010). However, the spatial and temporal resolution of actual remote sensing techniques did not allow the monitoring of many continental water bodies. The SWOT satellite mission is a CNES-NASA joint project which represents a significant technological progress mainly due to its high spatial resolution (from 50 to 100m). The main advantage of this mission is the use of an interferometric radar known as KaRIN (Ka-band Interferometer) which will provide a 120 km swath. The large swath will be able to resolve all lakes, rivers, reservoirs and oceans areas wider than

100m at least twice every 21 days (up to 7 times during this period at high latitudes). In preparation for the satellite launch, scientists must determine how these data will be used considering different regions and different scales. This thesis is done within the framework of a SWOT satellite pre-launch study, and it aims at quantifying the potential contribution of SWOT satellite observations to global scale hydrological modelling with an application over the Niger basin. First, a reasonable modelling of the Niger river was set up and evaluated, using the ISBA-TRIP Continental Hydrologic System (CHS), which includes a flooding scheme (Decharme et al., 2011) and a deep aquifer reservoir (Pedinotti et al., 2012). The simulation was run over the period 2002-2007 at a 0.5 spatial resolution. Considering the limited number of discharge observations along the river (8 in-situ time series were available for this work), it was necessary to get complementary information describing the surface water dynamics. These data were selected considering their spatial and temporal resolution which must be coherent with those of the model, and which also cover the simulation period. Thus, several satellite datasets were used to evaluate the model (discharge, water level, flooded fraction, storage variations). Moreover, several rainfall datasets were used as forcing input in order to take rain uncertainties into account (at least to a first order). Among 4 precipitation fields, only 2 of them (TRMM and RFE2) lead to coherent simulations and were thus kept for the rest of the evaluation. This study has shown that, considering its relative simplicity, the model is able to reasonably simulate the major hydrodynamic processes of the Niger basin. The flooding scheme leads to a better representation of the discharge downstream of the inner delta area, while the aquifer reservoir permits a better simulation of the low flows. The evaluation also showed that the model is able to simulate the surface of the main flooded areas and to give good first-order estimates of the water storage variations. Finally, sensitivity were used to determine the most sensible set of input hydrological parameters.

The second phase of the thesis aimed at determining how the SWOT data can be used within the framework of global hydrological modelling. Several studies have shown that data assimilation gives promising perspectives for the improvement of hydrological predictions (Andreadis et al., 2007; Biancamaria et al., 2011). However, data assimilation (DA) is still rarely used for hydrology, especially at global scale. Indeed, DA is usually used to correct numerical model states (most often in meteorology to improve the initial state for a forecast) which can not be done within the framework of future climate simulations. It was then decided to build a SWOT observation assimilation method which will provide improved estimates of ISBA-TRIP input parameters. For this, an Observing System Simulation Experiment (OSSE) was done, using virtual SWOT observations of water levels which is useful within the framework of a pre-launch study because no observations exist yet. SWOT virtual water levels are then

generated on the model grid using a reference simulation (this simulation is considered as the 'truth'). Then, taking into account the errors due to parameter uncertainties, a perturbed simulation is created. Data assimilation consists in using SWOT virtual observations to improve the estimation of certain key model input parameters and to obtain a better estimation of hydrodynamical variables such as the water levels and the river discharge. Sensitivity tests were performed and it was decided to use the assimilation to correct a critical and difficult to define hydrological parameter, the Manning coefficient. The Manning coefficient quantifies how river-bed and floodplain roughness elements slow down the flow, and it can be considered as a drag coefficient. This spatially distributed parameter is not easy to estimate since it varies considerably in space and even in time. Moreover, it directly impacts the flow speed and thus the discharge. It is also very influential on the formation of floods. The algorithm used to provide the analysis after one assimilation cycle is the BLUE (Best Linear Unbiased Estimator). This preliminary study shows that DA is a promising method since it leads to a better estimation of river water levels (the averaged bias is reduced by 30%) and to a lesser extent, of the discharge (the bias is reduced by 7% over the river). Moreover, it allows a better representation of continental water storage variations. The Manning coefficient bias is also well improved and converges towards an optimal value despite potential problems related to equifinality. It is also shown that DA allows a better prediction of floods (occurrence, intensity) over the Niger inner delta. Finally, the optimal Manning coefficient obtained during the assimilation can be used for hydrological forecast over longer time periods than those of DA. However, this study is still in a preliminary phase and offers many perspectives for improvement. For example, only the errors related to the uncertainties on the Manning coefficient were considered to represent the modelling errors but other sources of uncertainties could be included such as those related to rainfall for example (as it was shown in the first part of this work that they can be significant). Also, this method must be applied to other key parameters (especially those which are hard to define from observations and are associated with considerable model sensitivity) and extended to other large basins to evaluate its skill for global applications. The SWOT mission will enable the monitoring of world lakes and rivers at an unprecedented resolution. These data will be a useful for obtaining a better understand the global hydrological cycle and for the prediction of the future evolution of continental fresh-water resources. Over the Niger basin where political and economical issues do not allow a robust monitoring of continental water reservoirs, SWOT will open the door to significant advances in the current knowledge of hydrologic and hydrodynamic processes over this basin. Finally, improved water resource management applications could be built based on the approaches presented herein in order to reduce the social and economic impact of climate change .



APPENDIX A

**A : Article published in HESS  
about ISBA-TRIP evaluation.**

---



## Evaluation of the ISBA-TRIP continental hydrologic system over the Niger basin using in situ and satellite derived datasets

V. Pedinotti<sup>1,2</sup>, A. Boone<sup>1</sup>, B. Decharme<sup>1</sup>, J. F. Crétaux<sup>3</sup>, N. Mognard<sup>3</sup>, G. Panthou<sup>4</sup>, F. Papa<sup>3</sup>, and B. A. Tanimoun<sup>5</sup>

<sup>1</sup>Groupe d'étude de l'atmosphère météorologique (GAME), URA1357, CNRS – Météo-France, Toulouse, France

<sup>2</sup>Centre National d'études spatiales (CNES), Toulouse, France

<sup>3</sup>Laboratoire d'Etudes en Géophysique et Océanographie Spatiales (LEGOS), Toulouse, France

<sup>4</sup>Laboratoire d'étude des Transferts en Hydrologie et Environnement (LTHE), Grenoble, France

<sup>5</sup>Autorité du Bassin du Niger (ABN), Niamey, Niger

*Correspondence to:* V. Pedinotti (vanessa.pedinotti@gmail.com)

Received: 30 September 2011 – Published in Hydrol. Earth Syst. Sci. Discuss.: 14 October 2011

Revised: 18 May 2012 – Accepted: 22 May 2012 – Published: 26 June 2012

**Abstract.** During the 1970s and 1980s, West Africa has faced extreme climate variations with extended drought conditions. Of particular importance is the Niger basin, since it traverses a large part of the Sahel and is thus a critical source of water for an ever-increasing local population in this semi arid region. However, the understanding of the hydrological processes over this basin is currently limited by the lack of spatially distributed surface water and discharge measurements. The purpose of this study is to evaluate the ability of the ISBA-TRIP continental hydrologic system to represent key processes related to the hydrological cycle of the Niger basin. ISBA-TRIP is currently used within a coupled global climate model, so that the scheme must represent the first order processes which are critical for representing the water cycle while retaining a limited number of parameters and a simple representation of the physics. To this end, the scheme uses first-order approximations to account explicitly for the surface river routing, the floodplain dynamics, and the water storage using a deep aquifer reservoir. In the current study, simulations are done at a 0.5 by 0.5° spatial resolution over the 2002–2007 period (in order to take advantage of the recent satellite record and data from the African Monsoon Multidisciplinary Analyses project, AMMA). Four configurations of the model are compared to evaluate the separate impacts of the flooding scheme and the aquifer on the water cycle. Moreover, the model is forced by two different rainfall datasets to consider the sensitivity of the model to rainfall input uncertainties. The model is evaluated using in situ discharge measurements as well as satellite derived flood extent, total continental water storage changes and river

height changes. The basic analysis of in situ discharges confirms the impact of the inner delta area, known as a significant flooded area, on the discharge, characterized by a strong reduction of the streamflow after the delta compared to the streamflow before the delta. In the simulations, the flooding scheme leads to a non-negligible increase of evaporation over large flooded areas, which decreases the Niger river flow by 15 % to 50 % in the locations situated after the inner delta as a function of the input rainfall dataset used as forcing. This improves the simulation of the river discharge downstream of the delta, confirming the need for coupling the land surface scheme with the flood model. The deep aquifer reservoir improves Niger low flows and the recession law during the dry season. The comparison with 3 satellite products from the Gravity Recovery and Climate Experiment (GRACE) shows a non negligible contribution of the deeper soil layers to the total storage (34 % for groundwater and aquifer). The simulations also show a non negligible sensitivity of the simulations to rain uncertainties especially concerning the discharge. Finally, sensitivity tests show that a good parameterization of routing is required to optimize simulation errors. Indeed, the modification of certain key parameters which can be observed from space (notably river height and flooded zones height changes and extent) has an impact on the model dynamics, thus it is suggested that improving the model input parameters using future developments in remote sensing technologies such as the joint CNES-NASA satellite project SWOT (Surface Water Ocean Topography), which will provide water heights and extent at land surface with an unprecedented 50–100 m resolution and precision.

## 1 Introduction

Over the past 5 decades, West Africa has faced extreme climate variations with extended extreme drought conditions most recently during the 70s and 80s (Ali and Lebel, 2009). In this region, precipitation is closely linked with the monsoon, and better understanding and prediction are needed for improved water resource management. With an approximate length of 4180 km (2600 miles), the Niger river is the largest river in West Africa. It starts in the Guinea Highlands in southeastern Guinea and ends in Nigeria, discharging through a massive delta into the Gulf of Guinea within the Atlantic Ocean. It is a significant source of water and food for West Africa which, as an agricultural region, is highly dependent on the water availability and management practices.

According to several studies (Coe, 1998; Andersen et al., 2005; Dadson et al., 2010), the seasonal and interannual cycle of the Niger river discharge is influenced by the hydrological processes, including overland processes (precipitation, evaporation, stream flows, floods, infiltration, etc.) and underground processes (groundwater and/or deep aquifer recharge). These processes are theorized to have feedbacks with the climate, rainfall variability and the carbon cycle (Houwelling et al., 1999; Matthews, 2000; Bousquet et al., 2006; Taylor, 2010; Taylor et al., 2011). Thus, a better parameterization of hydrological processes in atmospheric general circulation models (AGCMs) is necessary to obtain a better understanding of the feedbacks with the West African monsoon. This could then potentially translate into improved water resource management and climate prediction, at least at the regional scale (Gedney et al., 2000; Douville et al., 2000, 2003, 2004; Molod et al., 2004; Lawrence and Slater, 2007; Alkama et al., 2008).

Currently, the representation of the surface component of the hydrological cycle in AGCMs is done using continental hydrological systems (CHSs) composed of land surface models (LSMs), which provide the lower boundary conditions for heat, momentum and mass. Some AGCMs go further and include river routing models (RRMs) which are used to convert the runoff simulated by the LSMs into river discharge. RRM transfer the continental freshwater into the oceans at specific locations (as source terms for the ocean model component). The evaluation of LSM-RRM systems is therefore a crucial task. This is generally done using offline simulations driven by atmospheric forcing which is as realistic as possible. Such forcing data are usually generated using a combination of atmospheric model reanalysis or short term forecasts combined with satellite-based products which are calibrated or bias corrected using gauge data (Dirmeyer et al., 2006; Sheffield et al., 2006; Kim et al., 2009). These simulations are then evaluated with in situ river discharge data, which does not guarantee that the spatiotemporal distribution of water storage over and under the land surface is well represented. Over West Africa especially, measurement data are difficult to access due to geographical, geopolitical and economic issues. In this

context, satellite remote sensing techniques (Alsdorf and Lettenmaier, 2003; Alsdorf et al., 2007; Wigneron et al., 2003; Grippa et al., 2004) have become useful tools for hydrologic investigations. For instance, efforts have already been done to quantify the soil water content/groundwater using satellite data (Rodell et al., 2009; Grippa et al., 2011). Satellite altimetry has also been used for systematic monitoring of water levels in large rivers, lakes and floodplains and several studies have demonstrated the capability of using these sensors locally for estimating river discharge in large rivers, including the Amazon River (Leon et al., 2008; Calmant et al., 2008; Getirana et al., 2010), the Ganges-Brahmaputra (Papa et al., 2010a) or the Lake Chad basin (Coe and Birkett, 2004). Also, an advanced study of satellite altimetry by Enjolras and Rodriguez (2009) intended to derive water surface elevation of narrow river channels by using likelihood-estimation problem. In parallel, globally applicable remote sensing technique employing a suite of satellite observations has been developed and now provides estimates of the spatial and temporal dynamics of surface water extent at the global scale over the last 2 decades (Prigent et al., 2001, 2007; Papa et al., 2010b). In the future, the joint CNES-NASA Surface Water Ocean Topography (SWOT, to be launched in 2020) mission will measure the surface water height with an unprecedented resolution of 50 m over the globe (Alsdorf et al., 2007; Rodriguez, 2009). This will enable a global scale near real time monitoring of the majority of the worlds rivers, lakes and reservoirs with spatial resolution of about one hectare (Lee et al., 2010; Biancamaria et al., 2010). Such data should significantly accelerate the improvement of the representation of hydrology for global scale models.

The need for a better representation of the global water budget has resulted in numerous implementations of river routing schemes into LSMs, and they vary widely in their complexity and degree of calibration. For water management applications on the watershed scale, highly parameterized, geographically specific models can be used to provide accurate estimates of streamflow and reservoir status (Zagona et al., 2001; Dai and Labadie, 2001; Habets et al., 2008). For global scale applications, however, computationally efficient, easily parameterized, comparatively simple and physically-based routing methodologies are preferable. In fact, land waters are supposed to play an important role in the atmosphere and ocean dynamics (Alkama et al., 2008; Dirmeyer, 2000, 2001; Douville, 2000, 2003, 2004; Gedney et al., 2000; Koster et al., 2000, 2002; Lawrence and Slater, 2007; Molod et al., 2004). In AGCM applications, it is most important to close the water budget and get a good representation of the fluxes of water into the atmosphere and ocean. An early influential effort at large scale routing was done by Vorosmarty et al. (1989) who prepared a river routing network for the Amazon basin at a 0.5° resolution. Runoff produced by a water balance approach was routed through the network using a linear transfer model, with flow time calculated as a function of flow length, estimated subgrid scale sinuosity, and grid scale

velocities estimated on the basis of mean downstream discharge (Leopold et al., 1964). A similar linear transfer model was adopted by Miller et al. (1994) for application within the Goddard Institute for Space Studies (GISS) General Circulation Model (GCM) at the global scale. In their formulation, runoff produced by a GCM at  $4^\circ \times 5^\circ$  was routed to the ocean through a  $2^\circ \times 2.5^\circ$  network in which flow direction was determined by topography and velocity was a function of the slope. Because the scale of the implementation was quite coarse, slope based estimates of velocity were intentionally calculated to yield low values, providing an implicit correction for subgrid scale sinuosity and the time it would realistically take runoff to work its way through the river system. Sausen et al. (1994) implemented a linear routing scheme for the European Center Hamburg (ECHAM) GCM, with transport parameters semi-objectively calibrated to match observed flow in major gauged rivers. In a study of the Amazon River system, Costa and Foley (1997) adopted the velocity estimation procedure of Miller et al. (1994). As a refinement, they estimated the sinuosity coefficient independently for each tributary within the Amazon basin, and they adjusted velocities as a function of stream order. Costa and Foley (1997) further divided runoff into surface and sub-surface components and applied differential source retention times to each. Further variants on the Miller et al. (1994) approach include the global hydrological routing algorithm (HYDRA, Coe, 2000), which was implemented at a  $5^\circ$  resolution and included variability in surface waters, and made some adjustments to the Miller et al. (1994) method for calculating distributed velocities. Oki and Sud (1998) and Oki et al. (1999) continued this line of application through the development of the topographically corrected integrating pathways for routing models, TRIP (Total Runoff Integrating Pathways). Arora and Boer (1999) implemented a time-evolving velocity that depends on the amount of runoff generated in the GCM land grid, using Mannings equation to estimate flow velocities for a river channel with a rectangular section.

Decharme et al. (2008, 2011) used the TRIP approach to implement a flood routing scheme into the ISBA (Interaction Soil Biosphere Atmosphere)-TRIP CHS. The scheme accounts explicitly for the river routing, precipitation interception by the floodplains, the direct evaporation from the free water surface, and the possible re-infiltration into the soil in flooded areas. The regional and global evaluations of this scheme at a  $1^\circ$  by  $1^\circ$  spatial resolution emphasized the importance of floodplains in the continental part of the hydrologic cycle, through generally improved river discharges and a non-negligible increase of evapotranspiration. However, it was noticed that over some basins, including the Niger, the discharge was still overestimated (Decharme et al., 2011). A possible identified cause was that these regions might overlie large aquifers that can be relatively uncoupled to the river.

The difficulty of modelling the Niger basin and the current concerns about water resource management in West Africa

make the improved understanding of this basin a scientific and socio-economic challenge. Moreover, its role in climate change and its potential feedback with atmosphere are crucial issues. It is then important for a LSM to be able to reproduce the key components of the water cycle and their evolution which will enable the detection of big anomalies in climatologic applications. The purpose of this study is to evaluate the performance of the ISBA-TRIP CHS model, including a flooding scheme and a new simple aquifer reservoir, over the Niger basin using comparisons with in situ measurements as well as recently available satellite derived data from 2002–2007. This period covers the core observation period of the African Monsoon Multidisciplinary Analyses (AMMA) project (Redelsperger et al., 2006). More precisely, the model is run in 4 different configurations (with/without flooding scheme/aquifers) to evaluate the impact of floods and aquifers on the Niger basin model configuration.

In this study, we first examine the routing scheme and its ability to simulate discharge simulated by LSMs from the AMMA Land surface Model Intercomparison Project (ALMIP). For this, TRIP was run in offline mode (default made with no feedbacks with LSMs) with total runoff from 11 LSMs, including ISBA, as input data in order to explore the impact of routing alone on the river discharge. Secondly, we evaluate the ISBA-TRIP CHS model in fully coupled LSM-RRM mode in four different configurations using two rainfall datasets. The evaluation is done using a large variety of data consisting of gauging measurements for discharge and satellite-based products, such as water heights and flooded areas. The study also attempts to give quantitative estimates of the contribution of the different water budget components over the basin using satellite data. In Sect. 4, sensitivity tests were performed to determine the robustness of the model and where the greatest uncertainties exist with respect to model parameters. Finally, conclusions and perspectives are given in Sect. 5.

## 2 The ISBA-TRIP model

### 2.1 Review of the ISBA-TRIP model

ISBA is a state-of-the-art land surface model which calculates the time evolution of the surface energy and water budgets (Noilhan and Planton, 1989). In this paper, we use the 3-layer force-restore option (Boone et al., 1999). It includes a comprehensive sub-grid hydrology to account for the heterogeneity of precipitation, topography and vegetation in each grid cell. A TOPMODEL approach (Beven and Kirkby, 1979) has been used to simulate a saturated fraction,  $f_{\text{sat}}$ , where precipitation is entirely converted into surface runoff (Decharme et al., 2006). Infiltration is computed via two sub-grid exponential distributions of rainfall intensity and soil maximum infiltration capacity (Decharme and Douville, 2006).

The TRIP RRM was developed by Oki and Sud (1998) at the University of Tokyo. It was first used at Météo-France to convert the model simulated runoff into river discharge using a global river channel network at a  $1^\circ$  resolution. The original TRIP model is only based on a single surface prognostic reservoir,  $S$  (kg), whose discharge is linearly related to the river mass using a uniform and constant flow velocity.

In the ISBA-TRIP CHS, TRIP takes into account a simple groundwater reservoir,  $G$  (kg), which can be seen as a simple soil-water storage, and a variable stream flow velocity computed via the Mannings equation (Decharme et al., 2010; Appendix A). In addition, ISBA-TRIP includes a two-way flood scheme in which a flooded fraction,  $f_{\text{flood}}$ , of the grid cell can be determined (Decharme et al., 2008, 2011). The flood dynamics are described through the daily coupling between the ISBA land surface model and the TRIP river routing model, including a prognostic flood reservoir,  $F$  (kg). This reservoir fills when the river height exceeds the critical river bankfull height,  $h_c$  (m) (Appendix B). The flood interacts with the soil hydrology through infiltration,  $I_f$  ( $\text{kg s}^{-1}$ ), with the overlying atmosphere through precipitation interception  $P_f$  ( $\text{kg s}^{-1}$ ), and through free water surface evaporation  $E_f$  ( $\text{kg s}^{-1}$ ). These three terms are calculated by multiplying, respectively, the total infiltration, precipitation interception and water surface evaporation over the grid cell by the ratio of flooded area to the grid area. This results in a system of three prognostic equations:

$$\begin{cases} \frac{\partial G}{\partial t} = Q_{\text{sb}} - Q_{\text{out}}^G \\ \frac{\partial S}{\partial t} = Q_{\text{in}}^S + Q_{\text{out}}^G + (Q_{\text{out}}^F - Q_{\text{in}}^F) - Q_{\text{out}}^S \\ \frac{\partial F}{\partial t} = Q_{\text{in}}^F + (P_f - I_f - E_f) - Q_{\text{out}}^F \end{cases} \quad (1)$$

where  $Q_{\text{sb}}$  ( $\text{kg s}^{-1}$ ) is the deep drainage from ISBA,  $Q_{\text{out}}^G$  ( $\text{kg s}^{-1}$ ) the groundwater outflow,  $Q_{\text{in}}^S$  ( $\text{kg s}^{-1}$ ) the sum of the surface runoff from ISBA within the grid cell with the water inflow from the upstream neighboring grid cells, and  $Q_{\text{out}}^S$  ( $\text{kg s}^{-1}$ ) is the simulated discharge, while  $Q_{\text{in}}^F$  and  $Q_{\text{out}}^F$  ( $\text{kg s}^{-1}$ ) represent the flood inflow and outflow, respectively. See Appendix A and B for more details.

The global evaluation of the ISBA-TRIP CHS model at a  $1^\circ$  by  $1^\circ$  resolution suggested that the model may not take into account some important process such as the presence of large aquifers in certain regions (Decharme et al., 2011). Also, by comparing the chemical composition of river water and groundwater, Fontes et al. (1991) demonstrated that significant aquifer recharge occurs in the Niger Inland Delta region, especially during summer flooding. For these reasons, a simple linear aquifer reservoir was added to the model. This reservoir was built on the example of the groundwater reservoir,  $G$ , but with a significantly longer time delay factor,  $\tau_{\text{aq}}$  (s). This results in a new system of four prognostic equations:

$$\begin{cases} \frac{\partial G}{\partial t} = \alpha Q_{\text{sb}} - Q_{\text{out}}^G \\ \frac{\partial S}{\partial t} = Q_{\text{in}}^S + Q_{\text{out}}^G + (Q_{\text{out}}^F - Q_{\text{in}}^F) - Q_{\text{out}}^S \\ \frac{\partial F}{\partial t} = Q_{\text{in}}^F + (P_f - I_f - E_f) - Q_{\text{out}}^F \\ \frac{\partial Aq}{\partial t} = (1 - \alpha) Q_{\text{sb}} - Q_{\text{out}}^{Aq} \end{cases} \quad (2)$$

where  $\alpha$  represents the fraction of deep drainage going into the groundwater reservoir while the rest of the drainage ( $1 - \alpha$ ) goes into the aquifer. Unlike the groundwater reservoir, we assume that the aquifer reservoir local feedbacks are negligible, but contribute to the flow at the mouth of the river. The aquifer outflow  $Q_{\text{out}}^{Aq}$  ( $\text{kg s}^{-1}$ ) can be written as follows:

$$Q_{\text{out}}^{Aq} = \frac{Aq}{\tau_{Aq}}, \quad (3)$$

where  $\tau_{Aq}$  (s) is a constant and uniform time delay factor, which represents the characteristic timescale for the aquifer reservoir to drain laterally to the ocean (out of the basin). This simple approach is currently motivated mainly by the lack of data describing the water table, which would be required for a more detailed approach. Figure 1 illustrates the configuration of the ISBA-TRIP CHS model used in this study.

## 2.2 TRIP specific parameters

The baseline parameter values are presented in this section; the sensitivity of the model to these parameters will be investigated in a subsequent section. For the model evaluation, the time delay parameters for the groundwater and deep aquifer reservoirs are fixed to 30 days and 4 yr, respectively. The aquifer parameter  $\alpha$  is initially fixed at  $3/4$  (which implies that  $1/4$  of the drainage flows into the deep aquifer). The aquifer reservoir is defined equally in each pixel.

The river width is an important parameter because it modulates both the river flow speed and the floodplain dynamics. It is computed over the entire TRIP network via an empirical mathematical formulation that describes a simple geomorphologic relationship between  $W$  and the mean annual discharge at each river cross section (Knighton, 1998; Arora and Boer, 1999; Moody and Troutman, 2002; Decharme et al., 2011):

$$W = \max \left( 30, \beta \times Q_{\text{yr}}^{0.5} \right), \quad (4)$$

where  $Q_{\text{yr}}^{0.5}$  ( $\text{m}^3 \text{s}^{-1}$ ) is the annual mean discharge in each grid cell estimated using the global runoff database from Cogley (1979). As discussed in Decharme et al. (2011), the  $\beta$  coefficient can vary drastically from one basin to another (Knighton, 1998; Arora and Boer, 1999; Moody and Troutman, 2002). Decharme et al. (2011) proposed that  $\beta$  varies according to climatic zone and fixed  $\beta$  to 20 for monsoon

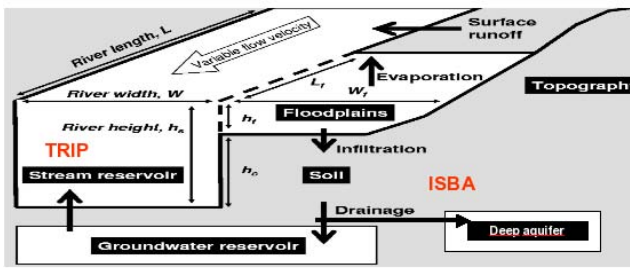


**Fig. 1.** Schematic representation of the ISBA/TRIP (Oki et al., 1999; Decharme, 2007) coupled system. The surface runoff calculated by the land surface model (ISBA) flows into the stream reservoir. The flood dynamic is described using a prognostic flood reservoir which fills when the river height exceeds a critical value and vice versa. The flood fraction is based on sub-grid topography. Finally, we add a linear aquifer reservoir so that the deep drainage is divided between the groundwater and the deep aquifer reservoirs.

basins and to 13 for semi-arid and arid basins. As the Niger river flows through both such climate zones, two different values are used within the Niger basin:  $\beta$  is 20 for the branch of the river going from the river mouth ( $5^\circ$  N) to  $12^\circ$  N and  $\beta$  is fixed to 10 for the remaining branch of the river. The spatial distribution of the river width is shown in Fig. 3a.

The key parameter for the floodplain parameterization is  $h_c$ , the critical river bankfull height (Decharme et al., 2008, 2011). In this study, as proposed by Decharme et al. (2011), it is computed according to the river width via a simple power function:

$$h_c = W^{1/3}. \quad (5)$$

The spatial distribution of  $h_c$  is shown in Fig. 3b. However, owing to both the uncertainties in this parameter and its impact on model results, sensitivity tests will be carried out using arbitrary  $h_c \pm 20\%$  (Decharme et al., 2008), leading to an increase or decrease in bankfull height up to 2 m.

Finally, as in Decharme et al. (2010), the Manning friction factor  $n_{riv}$  varied linearly and proportionally to  $W$  from 0.04 near the river mouth to 0.1 in the upstream grid cells (Fig. 3c):

$$n_{riv} = n_{min} + (n_{max} - n_{min}) \left( \frac{W_{mouth} - W}{W_{mouth} - W_{min}} \right), \quad (6)$$

where  $n_{riv}$  represents the Manning  $n$  factor of the grid cell,  $n_{max}$  and  $n_{min}$  the maximum and the minimum values of the Manning friction factor (respectively equal to 0.1 and 0.04),  $W_{min}$  (m) the minimum river width value and  $W_{mouth}$  (m) the width of the mouth in each basin of the TRIP network.

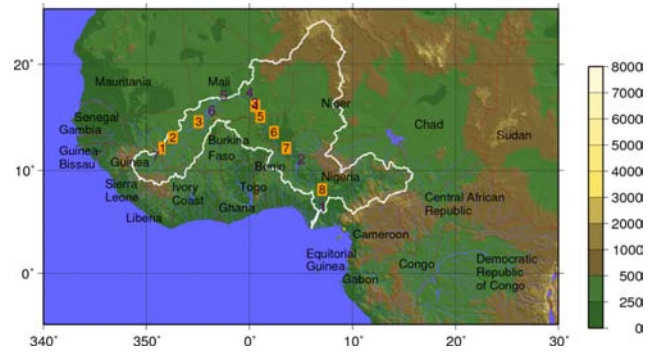


**Fig. 2.** ALMIP domain (stops at latitude  $20^\circ$  N). The spatial resolution is  $0.5^\circ \times 0.5^\circ$ . The white contour is the delimitation of the Niger basin. The yellow squares are the stations where discharge observations are available: (1) Banankoro (2) Koulikoro (3) Ke Macina (4) Niamey (5) Ansongo (6) Kandadji (7) Malanville (8) Lokoja. The purple figures are the sites where height change observations are used for evaluation. The legend indicates the topographical heights values (m).

### 3 Model setup and experimental design

#### 3.1 Methodology

In order to determine the impact of the flooding scheme on simulated discharges, the TRIP routing model is used in off-line mode, uncoupled from a LSM and without floodplains. ALMIP I, which is a part of the AMMA project, was motivated by an interest in fundamental scientific issues and by the societal need for improved prediction of the West African Monsoon (WAM) and its impacts on West African nations (Redelsperger et al., 2006). As part of this project, ALMIP I focused on better understanding land-atmosphere and hydrological processes over Western Africa (Boone et al., 2009). LSMs were run offline with prescribed atmospheric forcing consisting in a combination of observations, satellite products and atmospheric model output data. All of the LSMs used the same computational grid at a  $0.50^\circ$  spatial resolution (see the domain on Fig. 2). The advantage of using ALMIP data is that each LSM can simulate a different runoff response, therefore we use an ensemble of inputs. In the current study, 11 simulations are used over the 2002–2007 period. TRIP is used to compute daily outputs of discharges along the river and water mass storage for each activated reservoir.

In addition, the ISBA-TRIP CHS coupled model is used with and without the flooding scheme to quantify the impact of the scheme on the discharge and the surface energy budget. As the TRMM-3B42 rainfall (see next section for details) was used as forcing for the ALMIP experiment, the same forcing is used for the ISBA-TRIP CHS simulation with and without the flooding scheme. In the second part of this study, the deep aquifer reservoir is implemented into the ISBA-TRIP CHS model and deep drainage water is then distributed between deep soil layers and this aquifer reservoir

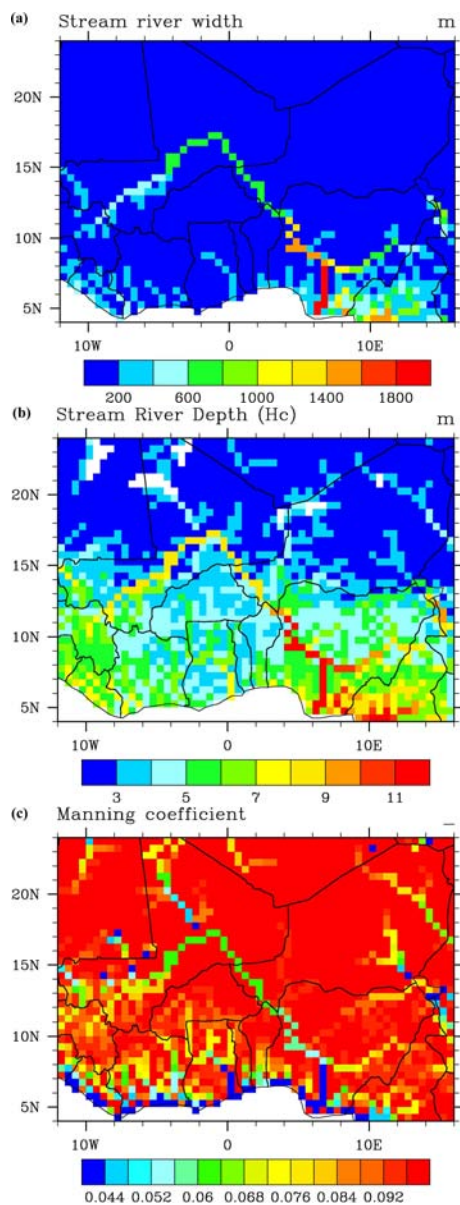


**Fig. 3.** Some TRIP parameters. Spatial distribution of the river width (up left), the river depth (up right) and the Manning coefficient (down).

(see details in Sect. 2). We then evaluate the ISBA-TRIP CHS model in four different configurations:

- no flooding scheme and no aquifer reservoir (NOAQNF);
- flooding scheme activated, no aquifer reservoir (NOAQF);
- no flooding scheme, insertion of aquifer reservoir (AQNF);
- flooding scheme activated, insertion of aquifer reservoir (AQF).

The model is run using two rainfall datasets (see next section for details) to take rain uncertainty into account in a simple manner, leading to 8 different simulations. Comparison with both in situ and remote sensing data will allow us to evaluate the simulated surface processes, the impact of the inclusion of floodplains and aquifers, and the ability of the model to estimate the river discharge.

### 3.2 Atmospheric forcing dataset to run ISBA-TRIP

The atmospheric state variables are based on the European Centre for Medium Range Forecasts (ECMWF) ECMWF numerical weather prediction (NWP) model forecasts for the years 2002–2007. The forcing variables consist in the air temperature, specific humidity, wind components at 10 m, and the surface pressure, all at a 3 h time step. Because of the importance of having accurate incoming radiation fluxes and precipitation, and because of the potentially significant errors in these variables derived from NWP models over this region (e.g. see Boone et al., 2009), merged satellite products are used. The downwelling longwave and shortwave radiative fluxes are provided by the LAND-SAF project (Geiger et al., 2008). Two products are used for rainfall forcing. The TRMM 3B42 product (Huffman et al., 2007) is used by default.

However, several studies have shown that RFE2 (Laws et al., 2004) produces rainfall over the Sahel agrees better with observed values than the other available rainfall products (e.g. Pierre et al., 2011), but it is at a time step which is not well adapted to land surface modelling (daily time step). Therefore, a second set of rainfall forcing data was created by disaggregating the daily RFE2 to a three hour timestep using the TRMM rainfall data. The monthly total RFE2 rainfall is well preserved using this simple downscaling method. This rain forcing is referred to as RFE-Hybrid (RFEH) herein. All of the simulations presented in this paper were done using the two datasets as forcing rainfall.

### 3.3 Evaluation datasets

Over the evaluation period (2002–2007), the simulated discharges are compared with daily gauge measurements along the Niger river from the Niger Basin Authority (ABN) as part of their Niger-HYCOS Project. These data are available in Koulikoro, Banankoro, Ke-Macina, Kandadji, Niamey, Ansongo, Malanville and Lokoja (see Fig. 2).

Satellite-derived inundation estimates are used to evaluate the spatial distribution and the time evolution of the flooded areas. Two different products are used. The first product is based on data from the MODIS multispectral imaging system installed onboard the Terra and Aqua satellites. In this study, the surface reflectance product (MOD09GHK) is used, which is defined as the reflectance that would be measured at the land surface if there were no atmosphere. The spatial resolution is 500 m for the corresponding MODIS images and

the coverage is global (Vermote et al., 2002). In order to detect open water and aquatic vegetation in arid and semi arid regions, a classification is performed using the fact that water surfaces do not reflect in the visible and near infra-red part of the spectrum. A threshold value has been estimated for reflectance in the MODIS frequency band-5 1230–1250 nm and for the NDVI index (Table 1) in order to delineate the shallow, sediment laden, and open water over the Inner Niger Delta, and also in order to distinguish between aquatic vegetation and vegetation on dry land. It has been assumed that small values of surface reflectance in band-5 characterize open water, independent of the NDVI index. When the surface reflectance in band-5 increases to the median value, depending on the NDVI index, it is assumed that there is a partial coverage of dry land by water, aquatic vegetation or vegetation on dry land. Finally, dry land is assumed when the NDVI is small and surface reflectance in band-5 is large. NDVI has been shown to be a robust index for monitoring temporal changes of the vegetation photosynthetic activity (Lyon et al., 1998; Lunetta et al., 2006). In the arid environment, a high level of vegetation photosynthetic activity can only be sustained by the presence of surface water or groundwater discharge. If dense enough, the aquatic vegetation and hydrophilic plants can mask underlying water and should be included in the estimate of the total area of the floodwaters. The NDVI ranges from negative values (open water) to  $>0.5$  for dense vegetation.

The second product consists in global estimates of the monthly distribution of surface water extent at about 25 km sampling intervals. These data were generated from complementary multiple satellite observations, including passive (Special Sensor Microwave Imager) and active (ERS scatterometer) microwaves along with visible and near infrared imagery (advanced very high resolution radiometer; AVHRR). These estimates were first developed over 1993–2000 (Prigent et al., 2007), adjusted and extended over 1993–2004 (Papa et al., 2010b) and recently recomputed for the entire period 1993–2007. This dataset has been extensively evaluated at the global scale (Papa et al., 2010b) and at river basin scale, including the Niger river (Papa et al., 2008). In the present study, this dataset is aggregated to a  $0.5^\circ$  resolution and referred to as PP. Because PP does not distinguish between the diverse anthropogenic and/or natural water bodies, while the ISBA-TRIP output must be compared only with flooded areas, two additional datasets are used to hybridize PP in order to conserve information on flood inter-annual variability only: the Global Lakes and Wetland Database (GLWD; Lehner and Döll, 2004) and the Monthly Irrigated and Rainfed Crop Areas (MIRCA2000; Portmann et al., 2010) database. The corresponding final product is named CPP in this study. The methodology is described in detail by Decharme et al. (2011), and so it is not detailed here.

Water height changes over the basin are evaluated using the HYDROWEB hydrological database ([http://www.legos.obs-mip.fr/en/equipes/gohs/resultats/i\\_hydroweb](http://www.legos.obs-mip.fr/en/equipes/gohs/resultats/i_hydroweb)).

The water level time series are based on altimetry measurements from ENVISAT satellite. Seven sites were chosen for the evaluation, one upstream of the Niger inner delta, four downstream of the delta and two in the delta. The data are available at a regular 35 days time step (with occasional missing data) from November 2002 to the end of 2007 (Calmant et al., 2008).

Total Water Storage (TWS) variations over the entire basin are evaluated using data from the Gravity Recovery and Climate Experiment (GRACE; Tapley et al., 2004). GRACE provides monthly TWS variation estimates based on highly accurate maps of the Earth's gravity field at monthly intervals at a resolution of approximately 300–400-km (Wahr et al., 2004; Swenson et al., 2003). The instrumentation and on-board instrument processing units are described in detail in Haines et al. (2003). Here, we used 60 months (from January 2003 to December 2007, excluding June 2003 and January 2004 because products are not available) of the Release 04 data produced by the Center for Space Research (CSR at The University of Texas in Austin), the Release 4.1 data produced by the Jet Propulsion Laboratory (JPL), and the GeoForschungsZentrum (GFZ) Release 04 (more details concerning GRACE data are available online at <http://grace.jpl.nasa.gov/data/>). The combination of these data with those datasets described in the previous paragraphs above will allow us to evaluate the distribution of water in the different TRIP reservoirs and to have a first estimation/validation of the aquifer water storage variations.

## 4 Results

### 4.1 Improvement of simulated discharges due to river flooding

The evaluation of the simulated river discharge is important for hydrological applications as well as for climate studies. Previous studies (Bonan, 1995; Coe et al., 2008; Decharme et al., 2008, 2011; Alkama et al., 2010; Dadson et al., 2010) have shown that the inclusion of a flooding scheme can impact the hydrological cycle by increasing the average evaporation and reducing the simulated discharge, which leads to a better estimation of the latter. Indeed, while an increasing number of LSMs used for large scale hydrological or GCM applications use river routing, most of these models do not represent floodplains. Flooded zones can be significant sources of evaporation and have a role of surface water storage, and their exclusion can result in an overestimation of the discharge for basins with significant annual flooding. To generalize this result, the TRIP RRM model was used in offline mode and without the flooding scheme (or aquifers) to convert simulated runoff and drainage from 11 LSMs into discharge. The LSMs considered for this study were part of the ALMIP I project (Boone et al., 2009). The Fig. 4 shows

**Table 1.** Threshold values used for the classification surface type used to monitor flood events. Band unit of reflectance is internal HDF-EOS data format specific to the Modis data and do not correspond to usual reflectance unit.

	Open water	Mix water/Dry land	Aquatic vegetation	Vegetation	Dry land
Band 5	<1200	>1200 & <2700	>1200 & <2700	>2700	>2700
NDVI	No test	<0.4	>0.4	>0.4	<0.4

the mean daily discharges simulated by the ALMIP models (black line) for several locations along the river. The blue range is the difference between the minimum and the maximum value of discharges simulated by the models and the red line is the observed discharge. The corresponding statistics are given in Table 2. Due to the bias in precipitations for years 2005 to 2007 (discussed in Sect. 4.4.), the statistics are calculated from 2002 to 2004 in order to better reflect the model performance.

In terms of observed discharge, there is a clear change of behaviour after the delta (Niamey, Ansongo, Kandadji, Malanville, Lokoja) compared to upstream of the delta (Banankoro, Koulikoro, Ke Macina). Indeed, the discharge before the delta is almost twice higher than downstream of the delta. This reflects the significant impact of the inner delta on the discharge amplitude due to the floodplains. The first 3 discharges on the Fig. 4 are located before the inner delta area (Banankoro, Koulikoro and Ke Macina). For these three locations, the discharge is reasonably represented by the ALMIP models. A bias in discharge is observed in 2005, 2006 and 2007 where the models simulate a smaller discharge compared to the previous years. This can be due to a bias in the rain forcing and will be discussed in Sect. 4.4. However, for the sites located downstream of the inner delta area (Niamey, Kandadji, Ansongo, Malanville and Lokoja) all of the ALMIP land surface models clearly overestimate the discharge leading to poor results compared to the three locations before the inner delta (see Table 2). In Malanville, the mean simulated discharge is around 5 times higher than that observed over this period. At the other sites (Niamey, Kandadji, Ansongo, and Lokoja), the mean simulated discharge is 2 to 2.8 times higher than observed. However, the variability of the discharge is generally well captured by the models as pointed out by the correlation scores (see Table 1). The green line represents the discharge simulated by the ISBA-TRIP CHS model with the flooding scheme activated. The results can be separated into three classes. First, in Banankoro and Koulikoro (before the inner delta), the discharge and thus the scores are not significantly changed, probably because no floods occur in these places. Second, after the inner delta (Niamey, Ansongo, Kandadji, Malanville and Lokoja), discharge has decreased considerably (50 %) in Niamey, Kandadji, Ansongo and Malanville and 26 % in Lokoja. The root mean square error (rms) has decreased considerably compared to the simulation without flooding scheme (see Table 2). Indeed, part of the water in the floodplains evaporates,

while part infiltrates into the flooded soil thereby reducing the stream reservoir water storage and discharge. The Nash-Sutcliffe coefficient or efficiency (eff) is also improved. Finally, in Ke Macina, the discharge is deteriorated by the addition of the flooding scheme. Among the sites before the inner delta, Ke Macina is the closest to the delta. It is likely that the model floods occur too soon upstream of the delta. This can be directly linked to a poor parametrisation or model parameter value (such as the river width) in this particular area. In the 3 locations upstream of the delta, there is a significant decrease of the simulated discharge in 2005, 2006 and 2007 which is not observed. This reduction of the discharge is observed for all the LSMs as well as for both configurations of ISBA-TRIP (with and without floods) and is more likely to be due to rainfall errors. This issue will be discussed in Sect. 4.4.

The impact of the flooding scheme on the surface energy budget was also investigated where the total evaporation includes evaporation from the soil and flooded areas and transpiration. The flooding scheme contributes to an increase in the evaporation mainly over the inland delta and in the southern part of the basin (+280 % with TRMM rainfall and +200 % with RFEH), which are areas which generally experience significant floods (see Sect. 4.2.2).

According to these results the floods occurring in the Niger inner delta region have an impact on the discharge, which is characterized by a decrease in its amplitude. The in situ discharge is among twice higher before the delta than after (Niamey, Ansongo, Kandadji and Malanville) and increases again when reaching the mouth of the river (Lokoja) where several tributaries join the Niger river. In addition, the flooding scheme allows a better simulation of the discharge after the delta, highlighting the importance of representing floodplains in LSMs. However, some model deficiencies remain, such as a bias of discharge in Ke Macina (possibly due to the previous cited reason), but also a bad reproduction of the recession flow during the dry season. In fact, the discharge remains relatively high during the dry season compared to the observations, which implies that there is too much water in the river. Several reasons for this can be identified, such as underestimated evaporation, an underestimation of the water in flooded areas or the neglect of aquifers. Anthropologic activities (dams, agriculture and water use for domestic consumption) are not explicitly accounted for and can also explain the bias between observed and simulated discharge, especially during the dry season when the population

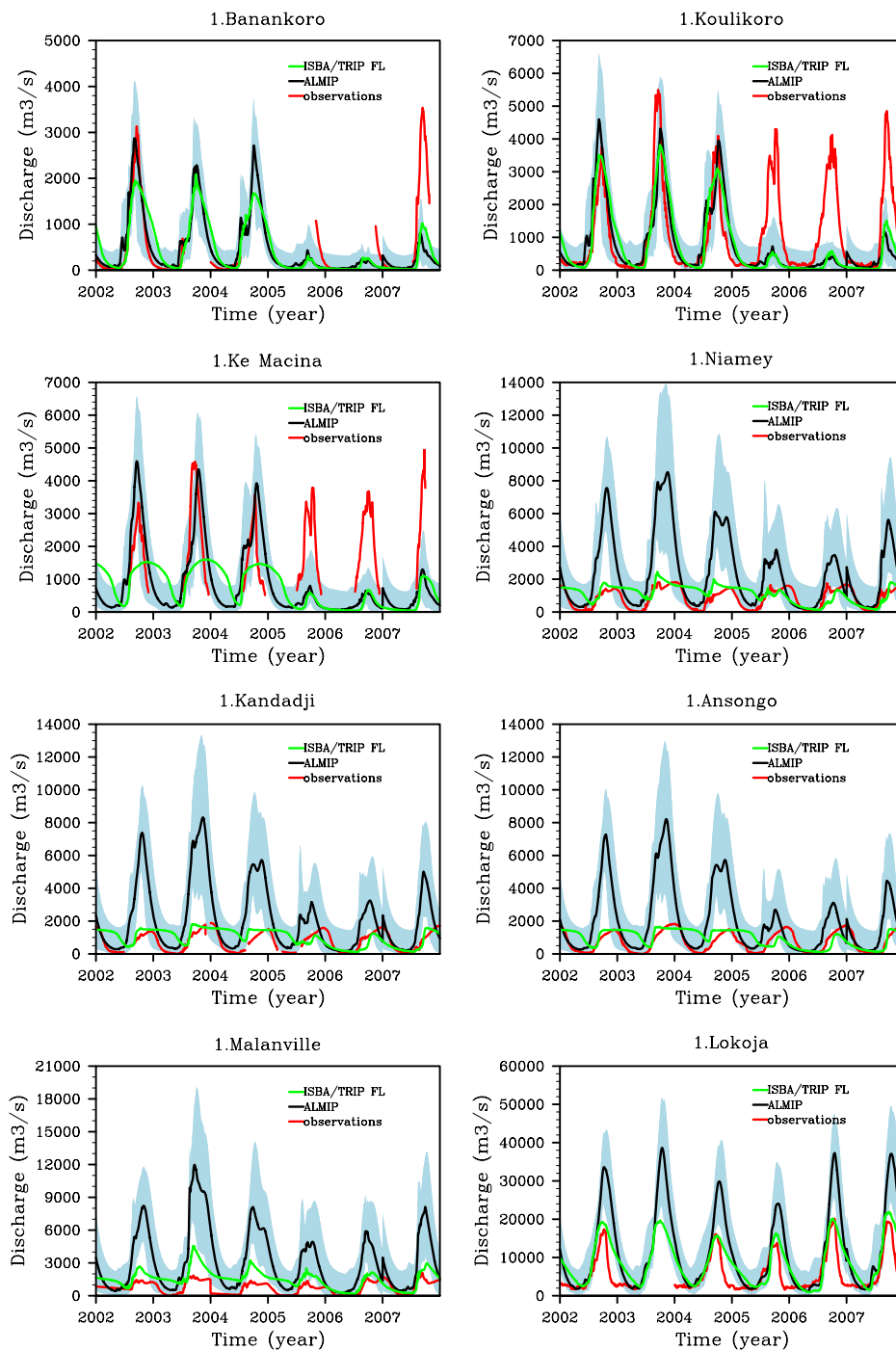


**Fig. 4.** Daily discharges (2002–2007) simulated by ALMIP LSMs without floods (average, black line) and by ISBA-TRIP using the flooding scheme (green). Observations are in red and the blue range is limited by the minimum and maximum discharge simulated by LSMs. The TRMM-3B42 rain product is used as forcing input.

might need to extract more water from the river due to the lack of rain. In order to investigate the impact of aquifers on the discharge, a relatively simple and linear aquifer reservoir was added to the model (see Sect. 2.1 for details). The next section will focus on 4 different configurations of the

ISBA-TRIP model and their respective impacts on some variables involved in the water cycle (discharge, water level changes, flooded fraction and total water storage). In order to take into account the rain uncertainties, two rainfall dataset are used as forcing (see Sect. 3.2 for details).

**Table 2.** Daily statistic scores of the discharge for the ALMIP LSMs and ISBA/TRIP with and without flooding from 2002 to 2004. TRMM-3B42 is used as forcing.

Corr.	Ban	Kou	KeM	Nia	Ans	Kan	Mal	Lok
ALMIP	0.97	0.83	0.5	0.8	0.73	0.73	0.82	0.78
ISBA–TRIP NF	0.98	0.9	0.7	0.76	0.73	0.74	0.75	0.81
ISBA–TRIP F	0.86	0.86	0.23	0.59	0.56	0.58	0.69	0.82
NS								
ALMIP	0.9	0.63	−0.2	−23.32	−23	−19.31	−62.42	−2.95
ISBA–TRIP NF	0.81	0.57	−0.95	−24.6	−22.9	−23.07	−57.08	−2.27
ISBA–TRIP F	0.69	0.7	−0.34	−0.52	−0.91	−0.37	−4.42	0.02
RMS								
ALMIP	0.58	0.76	0.6	3.54	4.04	3.61	5.25	1.66
ISBA–TRIP NF	0.81	0.81	0.76	3.63	4.36	3.93	5.03	1.51
ISBA–TRIP F	1.04	0.68	0.63	0.89	1.14	0.94	1.54	0.83

## 4.2 Separate impact of floods and aquifers on the Niger basin

### 4.2.1 Discharge

A fourth reservoir was added to the ISBA-TRIP model to represent deep aquifer processes (Sect. 2). This reservoir is supplied by a fraction of the soil drainage and it does not supply water back the river. Indeed, the model simulates too much water in the river, which could be due to the presence of large aquifers (Fontes et al., 1991; Decharme et al., 2011). Different values of the aquifer recharge factor ( $1-\alpha$ ) were tested and only the most relevant result is kept for the evaluation (see sensitivity tests in Sect. 4.6 for further details). In order to better understand the separated impacts of aquifers and floods, four different configurations of the model are tested in this study:

- no flooding scheme and no aquifer reservoir (NOAQNF);
- flooding scheme activated, no aquifer reservoir (NOAQF);
- no flooding scheme, insertion of aquifer reservoir (AQNF);
- flooding scheme activated, insertion of aquifer reservoir (AQF).

Two different rainfall datasets are also used as forcing: TRMM-3B42, already used in the ALMIP I project and in the previous section; and RFEH (see Sect. 3.2).

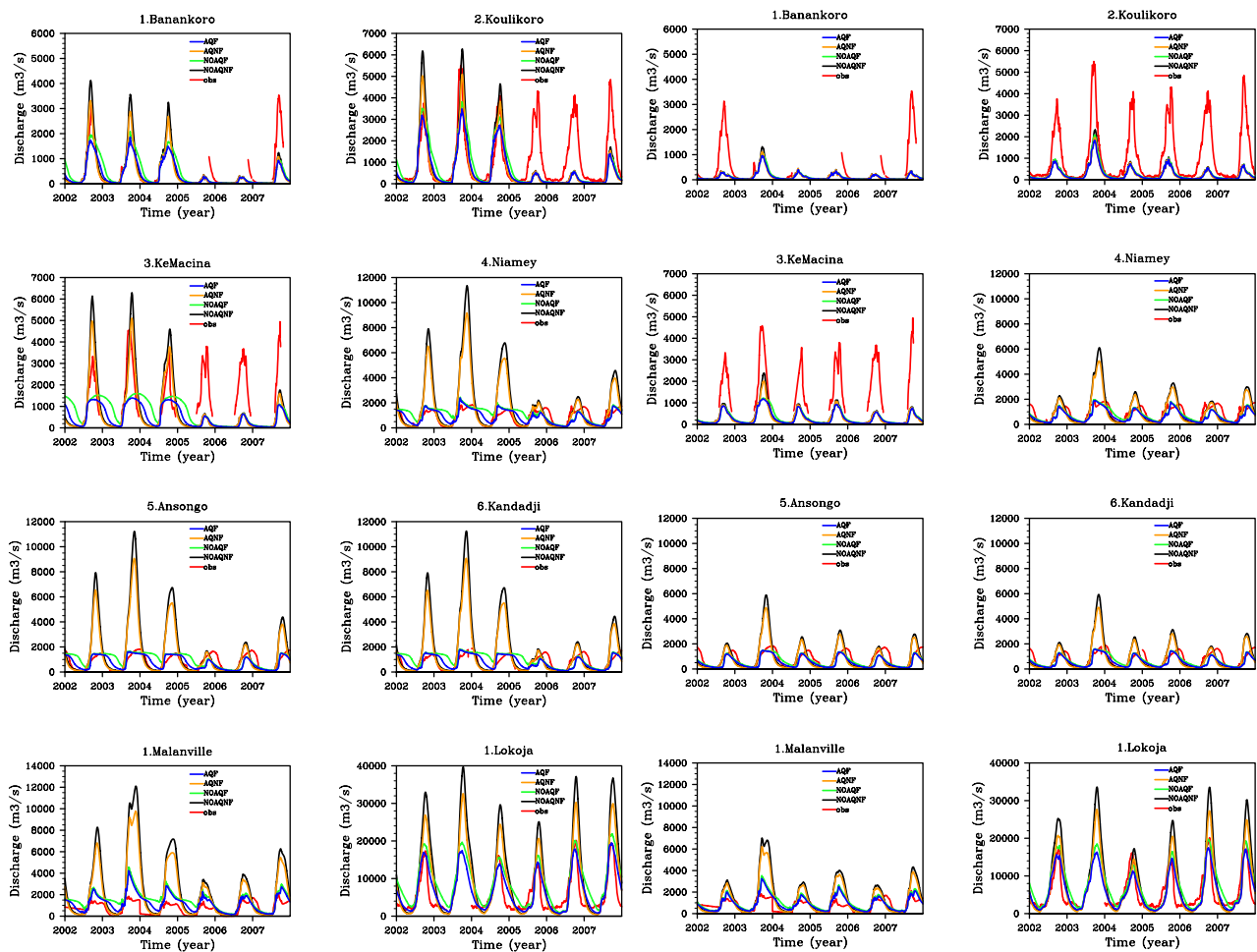
Figure 5 shows the simulated discharge for the 4 configurations when the model is forced by TRMM-3B42 and RFEH, respectively. Table 3 presents the statistical scores for each configuration and the best scores are in bold type. The statistics are generally better when both floods and aquifers are represented in the model, especially downstream of the inner delta when the model is forced by TRMM-3B42 (see

Table 3). Upstream of the delta, the Nash-Sutcliff coefficient and the RMS are generally better without aquifers with both forcing. With RFEH, the aquifers do not lead to a systematic improvement of the scores; however, they do not lead to a significant degradation either.

Before the inner delta, the introduction of aquifers impacts the discharge mostly by reducing the monsoon peak, resulting in a deterioration of the rms score. This deterioration might be due to the “simplicity” of the aquifer reservoir parametrisation. Indeed, the aquifer is homogeneously defined over all the domain and can generate biases in regions where this aquifer either does not exist or has a minor role.

Downstream of the inner delta, the aquifer impacts mostly the recession flow in two manners: it lengthens the period of maximum discharge and reduces the low flows. This results in a deterioration of the period except in Lokoja where the period and the recession law are improved (Fig. 5a). When the model is forced by TRMM, the presence of aquifers considerably improves the recession during the dry season. The reduction of low flows is explained by the fact that the river empties faster after the rainy season which results in a more realistic discharge during the dry season. In terms of statistics, the scores (ratio, rmse, eff) are similar or slightly deteriorated, except in Malanville and Lokoja where they are improved. The correlation score, however, is improved at all of the sites. The sensitivity of the model to the choice of the time delay factor  $\tau_{Aq}$  and the fraction  $\alpha$  will be presented in Sect. 5.

The scores are greatly improved by the addition of the flooding scheme for the locations situated downstream from the inner delta. The configuration with floods and aquifers generally leads to a good improvement of the scores in the sites located after the inner delta when the model is forced by the TRMM rainfall datasets. It is less obvious when the model is forced by RFEH rainfalls. However, when the aquifers deteriorate the scores, the deterioration is therefore small compared to the improvements (see Lokoja for example) and



**Fig. 5.** Daily discharges (2002–2007) simulated by ISBA-TRIP in the 4 different configurations of the model. Observations are in red. The TRMM-3B42 (2 left columns) and RFEH (2 right columns) rain product are respectively used as forcing input.

likely due to a bad parametrisation of aquifers in these regions. However, we recall that global applications do not aim at calibrating input parameters but at detecting the key processes which impact the evolution of the water cycle. Finally, we notice that all of the configurations poorly reproduce the discharge in 2005, 2006 and (to a lesser extent) in 2007.

To investigate the role of the inner delta over evaporation, we looked at the relative difference of total evaporation over the delta [ $13^{\circ}$  N– $16^{\circ}$  N;  $3^{\circ}$  W– $6^{\circ}$  W] between the simulations NOAQNPF and NOAQF when the model is forced by TRMM (the results are similar with RFEH). This is shown on Fig. 6 (blue solid line). Moreover, we added the relative difference of discharge between Niamey and Koulikoro (black solid line). Ke Macina is closer to the delta, but as many data are missing on this station, we looked at Koulikoro for the comparison. The dashed lines represent the absolute discharge in Niamey (green) and Koulikoro (red). During the monsoon, the observed discharge in Niamey is 40 to 80 % less than in Koulikoro, as noticed before. However, while the

discharge in Koulikoro decreases really fast at the end of the rainy season, the discharge in Niamey remains at its maximum value and even increases a little, resulting in a second peak of discharge. While the second peak corresponds to the flood signal of the upper Niger basin delayed by the inner delta and has been observed for decades, the first peak is likely related to increased contribution of the tributaries located downstream from the delta that appeared in the recent 10 to 15 yr (Amogu et al., 2010). The transition between the monsoon and the post-monsoon regime is also visible if we look at the total evaporation simulated with and without the flooding scheme over the delta. Indeed, during the monsoon, there is hardly any difference of evaporation between the two simulations. But, during the post-monsoon, the model including floodplains simulates 30 % more evaporation than without the flooding scheme. The floodplains intensify the creation of evaporation over the delta and the time correlation with the second peak of discharge in Niamey suggest that they also have an impact on the recession flow by

**Table 3.** Daily statistic scores of the discharge for the 4 configurations forced by TRMM-3B42 and RFEH from 2002 to 2004.

Corr. TRMM	Ban	Kou	KeM	Nia	Ans	Kan	Mal	Lok
NOAQNF	<b>0.98</b>	0.9	0.7	0.76	0.74	0.73	0.75	0.81
NOAQF	0.86	0.86	0.23	0.59	0.58	0.56	0.7	0.82
AQNF	0.97	<b>0.91</b>	<b>0.74</b>	0.76	0.73	0.72	<b>0.77</b>	0.83
AQF	0.94	0.9	0.43	<b>0.81</b>	<b>0.86</b>	<b>0.83</b>	0.73	<b>0.87</b>
Corr. RFEH								
NOAQNF	0.9	0.88	0.79	0.71	0.65	0.66	0.74	0.82
NOAQF	0.91	0.89	0.7	0.84	0.86	0.85	0.7	0.8
AQNF	0.89	0.9	<b>0.82</b>	0.7	0.63	0.65	<b>0.75</b>	0.83
AQF	<b>0.92</b>	<b>0.91</b>	0.78	<b>0.84</b>	<b>0.86</b>	<b>0.85</b>	0.74	<b>0.87</b>
NS TRMM								
NOAQNF	0.81	0.57	-0.94	-24.62	-23.07	-26.86	-57.08	-2.27
NOAQF	0.69	0.7	-0.34	-0.53	-0.36	-0.91	-4.42	0.02
AQNF	<b>0.94</b>	<b>0.8</b>	<b>0.17</b>	-14.83	-13.88	-16.76	-35.98	-0.59
AQF	0.82	0.31	-0.43	<b>0.49</b>	<b>0.64</b>	<b>0.41</b>	<b>-1.97</b>	<b>0.66</b>
NS RFEH								
NOAQ-NF	<b>-0.005</b>	<b>0.25</b>	<b>-0.58</b>	-2.58	-2.1	-2.85	-10.17	-0.06
NOAQ-F	-0.01	0.23	-1.09	<b>0.69</b>	<b>0.7</b>	<b>0.71</b>	-0.51	0.4
AQ-NF	-0.02	-0.17	-0.81	-1.41	-1.18	-1.71	-6.31	0.48
AQ-F	-0.03	0.15	-1.19	0.64	0.63	0.69	<b>0.008</b>	<b>0.7</b>
RMS TRMM								
NOAQNF	0.81	0.81	0.76	3.63	3.93	4.36	5.03	1.51
NOAQF	1.04	0.68	0.63	0.89	0.94	1.14	1.54	0.83
AQNF	<b>0.46</b>	0.56	<b>0.49</b>	2.85	3.48	2.45	4.01	1.05
AQF	0.79	<b>0.56</b>	0.65	<b>0.51</b>	<b>0.63</b>	<b>0.61</b>	<b>1.14</b>	<b>0.49</b>
RMS RFEH								
NOAQNF	<b>1.88</b>	<b>1.08</b>	<b>0.69</b>	1.36	1.41	1.62	2.2	0.86
NOAQF	1.88	1.1	0.79	<b>0.4</b>	<b>0.44</b>	<b>0.44</b>	0.81	0.65
AQNF	1.89	1.14	0.73	1.12	1.18	1.36	1.78	0.6
AQF	1.9	1.15	0.81	0.43	0.49	0.46	<b>0.66</b>	<b>0.45</b>

lengthening the period of maximum discharge. From 2005 to 2007, we notice a weaker evaporation over the delta than during previous years. This is coherent with the simulated discharge which is also very weak during these three years.

#### 4.2.2 Flooded areas

The quantification of wetland extent is an important step towards a better representation of surface water dynamics. In this study, the time and spatial distribution of wetlands were evaluated over the inner delta region, which is a large inundated area, and over the whole basin. Figure 7a and b show the time evolution of the mean monthly flooded fraction (in %) averaged over the inner delta region and over the Niger basin, respectively, with and without aquifers, when the model is forced by TRMM. Figure 7c and d present the same results when the model is forced by RFEH. Only the two configurations with and without aquifers are shown as there is no simulated flooded fraction without flooding scheme. The blue range on the Fig. 7a and c represents the interval between the minimum and the maximum Modis derived (JFC) flooded fraction. Over the delta, the simulated flooded fraction is generally included in this range, although it tends to be on the low end when the model is forced by

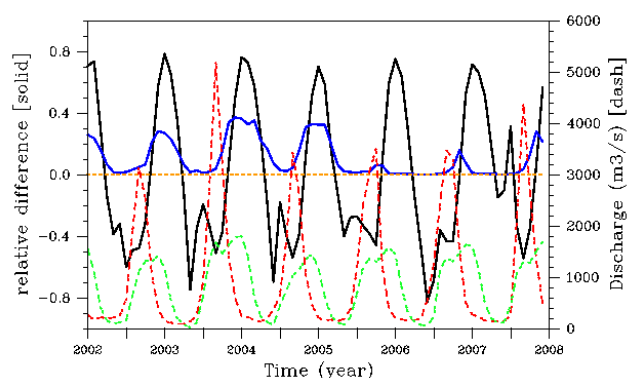


**Fig. 6.** Time evolution of the relative difference of simulated total evaporation between the simulation NOAQ-NF(1) and NOAQ-F(2) when the model is forced by TRMM-3B42 (solid blue line). The relative difference is the ratio  $((2) - (1)) / ((2) + (1))$ . Time evolution of the relative difference of observed discharge between Niamey and Koulikoro (solid black line). Time evolution of the discharge in Niamey (dashed green line) and Koulikoro (dashed red line).

RFEH. These results are reasonable since the Modis classification (JFC) fraction includes wetted vegetation and near-surface saturated soils. With both rainfall datasets, the presence of aquifers results in a reduction of flooded areas. But the impact of aquifers on the flooded fraction is more obvious for the simulation forced by TRMM rainfall. Indeed, the aquifers greatly improve the period of the floods. However, as shown in the figures, the CPP product is around 3 times higher than the modelled values over the basin and 10 times higher over the delta. This can be explained by the fact that the multi-satellite method can encounter some difficulties in accurately discriminating between very moist soils and standing open water, likely overestimating the actual fraction of inundations (Papa et al., 2010a, b). Model deficiencies may also explain this bias. They can be related to routing deficiencies due to a bad parametrization, or to LSMs deficiencies in the calculation of floodplains evaporation and/or infiltration.

Figure 8a and b show the time series of de-seasonalized anomalies (obtained by subtracting the 12-yr mean monthly value from individual months and then divided by the standard deviation) over the delta and over the basin, with and without aquifers, when the model is forced by TRMM. Figure 8c and d present the same results when the model is forced by RFEH. Over the delta, the Fig. 8a and c suggest that the model and the data are in good agreement in their time variations, with a better phasing between CPP and ISBA/TRIP. Over the basin, the CPP and model anomalies globally corroborate in phase and amplitude.

Figure 9a show the monthly relative CPP flooded fraction averaged over the period 2002–2007. The monthly values have been divided by the maximum monthly value over 2002–2007 to determinate the main observed flooded areas. According to these observations, the main inundations occur between July and December in three principal regions: the inner delta in Mali, the Northern Nigeria and the Southern basin. Figure 9b shows the monthly spatial correlation between CPP and ISBA-TRIP when the model is forced by TRMM with floods and aquifers. Over the 3 principal inundated regions, the correlation is bigger than 0.4. This correlation does not change significantly according to the configuration of the model.

The impact of general flooded areas over the evaporation was investigated. For this, only the grid cells with a flooded fraction higher than 15 % for the configuration NOAQF were considered. These cells represent 11 % of the basin if the model is forced by TRMM and 7 % of the basin if the model is forced by RFEH rainfalls. Figure 10 presents the averaged relative difference of total monthly evaporation simulated on these cells with (red) and without (blue) floodplains when the model is forced by TRMM. The evaporation on flooded areas is generally higher with the flooding scheme than without floods, especially during the monsoon and post-monsoon periods (20 to more than 50 % higher). The same observations are done for the simulations forced by RFEH.

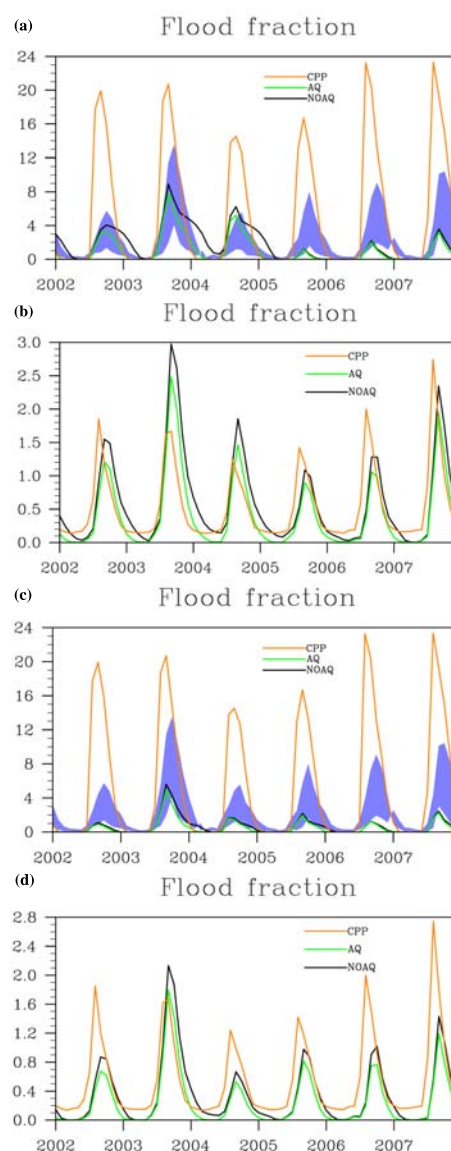


**Fig. 7.** (a) Time evolution of the mean monthly flooded fraction (in %) averaged over the inner delta region. The model is forced by TRMM-3B42. The blue range is the interval between the minimum and the maximum Modis classification (JFC) flooded fraction. (b) Time evolution of the mean monthly flooded fraction (in %) averaged over the basin. The model is forced by TRMM-3B42. (c) Time evolution of the mean monthly flooded fraction (in %) averaged over the inner delta region. The model is forced by RFEH. The blue range is the interval between the minimum and the maximum Modis classification (JFC) flooded fraction. (d) Time evolution of the mean monthly flooded fraction (in %) averaged over the basin. The model is forced by RFEH.

#### 4.2.3 River height change

To complete the evaluation of surface water dynamics, the river height time changes are compared to estimates from the HYDROWEB hydrological database developed by the

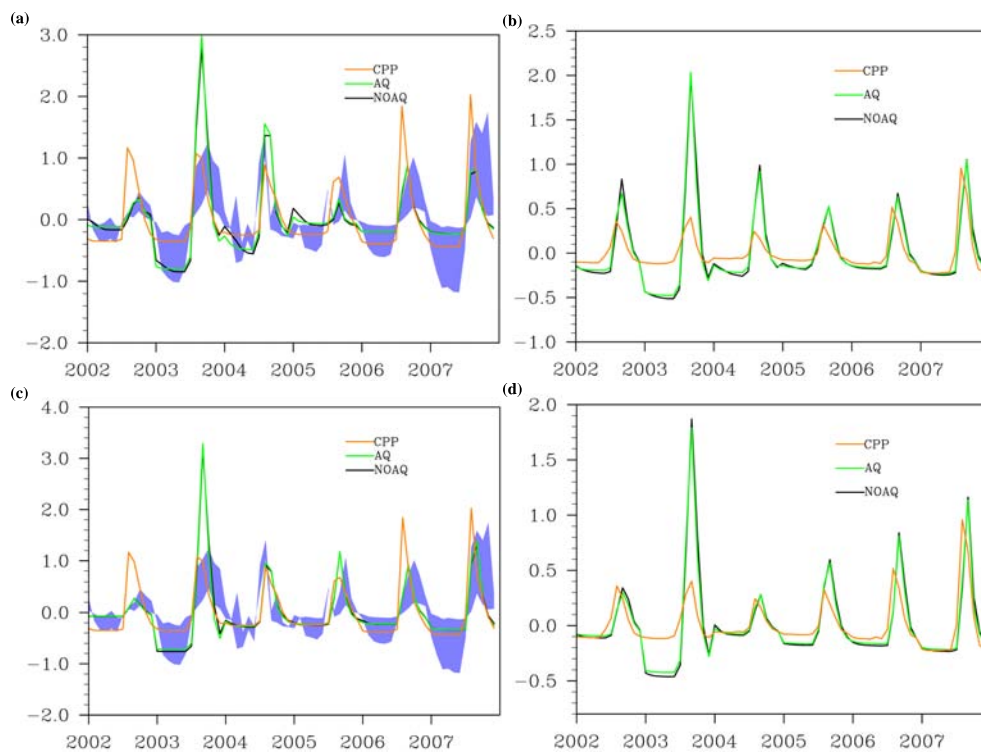


**Fig. 8.** (a) and (c) Time series of deseasonalized flood fraction anomalies (obtained by subtracting the 6-yr mean monthly value from individual months and then dividing by the standard deviation) over the delta. The blue range on the left figure delineates the maximum and minimum possible anomalies from Modis (JFC) products. The CPP product is orange. ISBA-TRIP without aquifers is in black and ISBA-TRIP with aquifers is in green. The TRMM-3B42 is used as forcing for (a) and RFEH is used for (c). (b) and (d) Time series of deseasonalized flood fraction anomalies (obtained by subtracting the 6-yr mean monthly value from individual months and then dividing by the standard deviation) over the basin. The CPP product is orange. ISBA-TRIP without aquifers is in black and ISBA-TRIP with aquifers is in green. The TRMM-3B42 is used as forcing for (b) and RFEH is used for (d).

LEGOS/GOHS (Calmant et al., 2008) which gives estimations of height changes at several points along the Niger river (Fig. 11). The seven locations used for comparison are noted in purple in Fig. 2. The bias error on the HYDROWEB water levels measures is estimated to be around 20 cm and the peaks of water height changes are within a range between 2 and 4 m. Since our interest is to be able to reproduce extreme events, this error is considered as reasonable for evaluating water height changes. The water level changes are represented in Fig. 11 for the four configurations when the model is forced by TRMM-3B42 rainfalls. The statistical scores are represented in Table 4 for the two rainfall datasets. The scores are generally improved by the presence of the flooding scheme. The addition of aquifers is more relevant when the model is forced by TRMM rainfall than RFEH. However, the scores are not greatly deteriorated by the presence of aquifers and considerably improved at the other sites. Without floodplains, the peaks of water height changes are overestimated. The model also overestimates the peaks of positive height changes which might be due to forcing anomalies (rain) or to model deficiencies. Indeed, the surface runoff stream function might be false in some areas

and, if overestimated, results in an overestimation of water height variation during rain events. Also, uncertainties in the river bed slope can also result in an overestimation of the water height changes in the valleys. Moreover, Yamazaki et al. (2011) showed the limitation of the kinematic wave approach. Indeed, when kinematic wave equation is used for discharge calculation, the predictability of water surface elevation becomes bad in flat river basins with floodplains. However, no attempt is made to calibrate these parameters here, which would be a long and difficult process and which is not necessary for use in a GCM.

### 4.3 Total terrestrial water storage

For global applications, it is of interest to evaluate the time evolution of total water storage (TWS) in LSMs and the contribution of each component to the total storage. Figure 12 shows the comparison between 3 GRACE satellite products that estimate the total water storage (TWS) change globally at  $1^\circ$  resolution (the blue range in the lower panels represents the difference between the maximum and minimum monthly observation values) and the water storage change in all of the

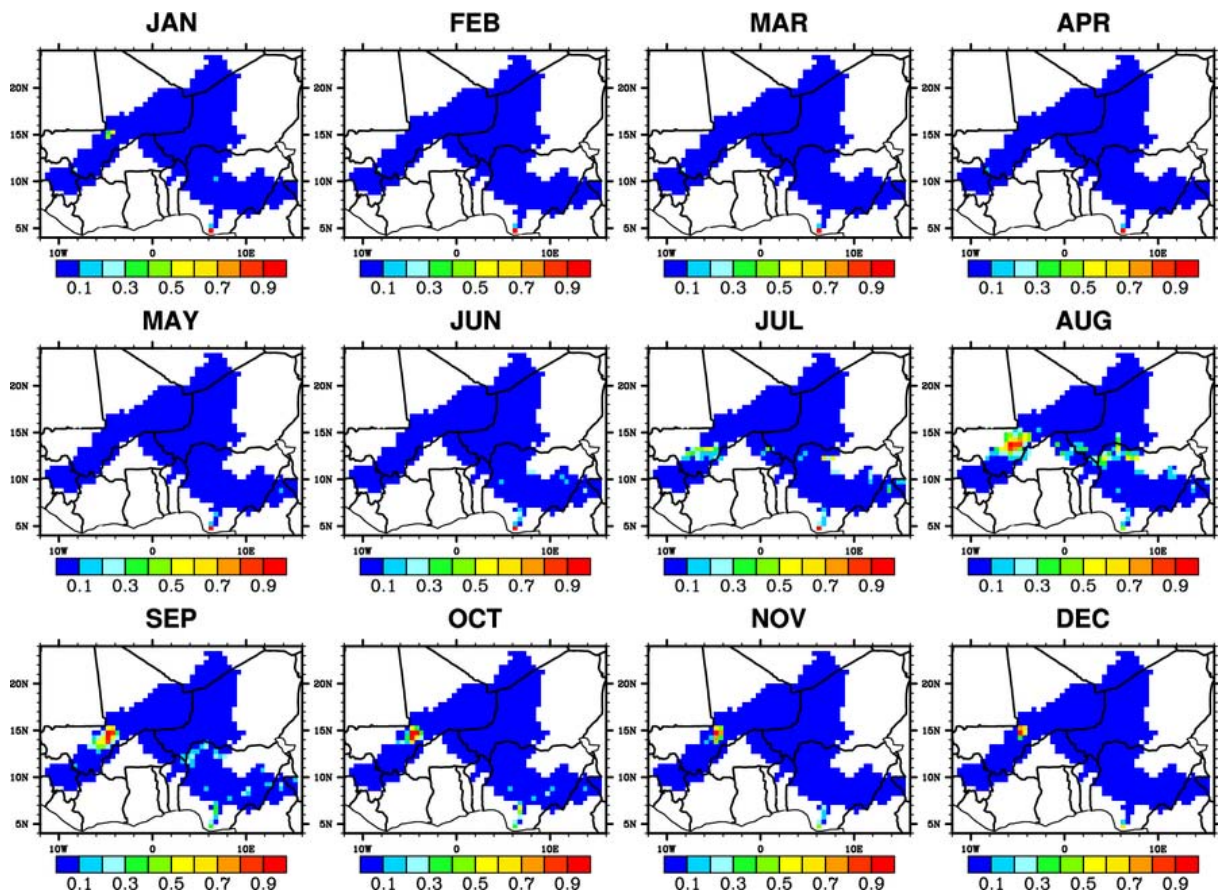


**Fig. 9a.** Spatial distribution of the normalized CPP flooded fraction averaged over 2002–2007 (the monthly value is divided by the maximum monthly value between 2002 and 2007).

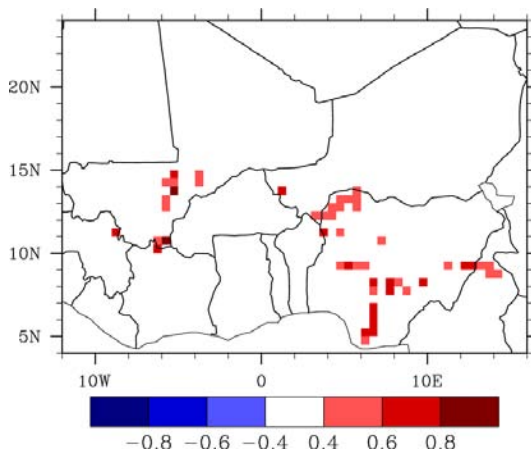


**Fig. 9b.** Spatial monthly correlation between ISBA-TRIP and CPP over 2002–2007.

reservoirs of the ISBA-TRIP model, averaged over the basin. The left panels represent the inter-annual variations (monthly means) and the right panels are the intra-annual variations (2003–2007 average for each month). The blue curve on the

**Table 4.** Correlations of the river height changes (from 2002 to 2007).

Corr. TRMM	1	2	3	4	5	6	7
NOAQNF	0.77	0.43	0.42	0.3	0.53	0.54	0.6
NOAQF	0.56	0.38	0.48	0.36	0.5	0.6	0.69
AQNF	<b>0.79</b>	0.38	0.41	0.3	0.54	0.53	0.61
AQF	0.7	<b>0.44</b>	<b>0.62</b>	<b>0.48</b>	<b>0.75</b>	<b>0.69</b>	<b>0.7</b>
Corr. RFEH							
NOAQNF	0.7	0.41	0.42	0.25	0.48	0.48	0.76
NOAQF	0.59	<b>0.43</b>	<b>0.65</b>	0.45	<b>0.69</b>	<b>0.76</b>	0.81
AQNF	<b>0.73</b>	0.39	0.41	0.24	0.49	0.48	0.79
AQF	0.68	0.4	0.63	<b>0.45</b>	0.67	0.74	<b>0.84</b>

lower panels represents the mean water storage change of the Niger basin in all of the ISBA-TRIP reservoirs. The upper panels contain the water storage change in each reservoir (averaged over the basin) and the middle panels present the time evolution of the rain, drainage, runoff and evaporation over the basin. On the figure, only the results for the configuration AQ-F forced by TRMM are shown but Table 5 presents the correlations for each configuration. The comparison of

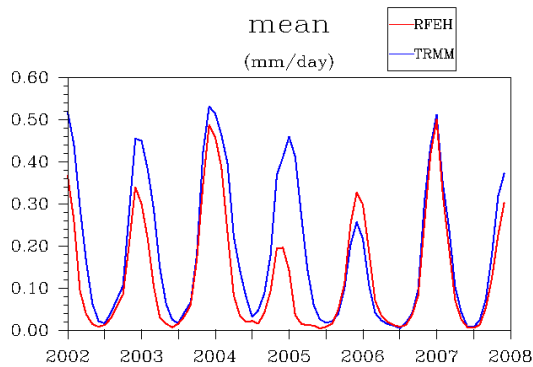


**Fig. 10.** Relative difference of evaporation between the two configurations NOAQ-NF and NOAQ-F. Only the cells with a monthly flooded fraction higher than 15 % over 2002–2007 are considered for the calculation.

ISBA-TRIP water storage change with the GRACE products over the Niger basin shows a very good correlation between the simulation and observations (more than 0.78) independently of the configuration considered. The contributions of each reservoir to the total water storage change appear in the Table 6 for the configuration AQ-F. Although the uppermost soil layers (approximately 1 to a few meters) comprise most of the total water storage change over the basin (49 %), the contribution of the other reservoirs, such as the groundwater and the aquifer, are not negligible (17 % each). The contribution of flooded zones is less (4 %), but since their impact on evaporation is not negligible, they must be considered also. These results emphasize the need for considering all such reservoirs in LSMs in order to close the water budget. Generally, studies compare the GRACE water storage change to the water storage change in the hydrologic soil layers only, i.e. the first soil meters (green curve in the last panel). However, this approximation is likely less valid for regions with significant storage in flooded zones and deeper soil layers since the contribution of these two reservoirs to the total water storage are not necessarily negligible.

#### 4.4 Rainfall comparison

A comparison of the rain datasets was done for every year. The averaged monthly ratio for every year  $(\text{TRMM} - \text{RFEH})/(\text{TRMM} + \text{RFEH})$ , which represents the relative bias of one dataset to the other, has been calculated when the monthly sum  $(\text{TRMM} + \text{RFEH})$  is bigger than 1mm/day. The most significant differences are observed during the monsoon period and visible on Fig. 13 which presents the previous ratio for the months of July, August and September 2002–2007. The basin is delimited by the black contour. Of note, significant differences are seen in the upper basin. From 2002 to 2004, the TRMM rainfall gives 20 to 80 % more rainfall than RFEH. This area is the main source

**Table 5.** Correlations of the model TWS with GRACE TWS (from 2002 to 2007).

Corr. TRMM	CSR	JPL	GFZ
NOAQ-NF	0.82	0.82	0.77
NOAQ-F	0.87	0.87	0.83
AQ-NF	0.84	0.83	0.79
AQ-F	0.87	0.86	0.82
Corr. RFEH			
NOAQ-NF	0.82	0.83	0.79
NOAQ-F	0.86	0.87	0.83
AQ-NF	0.83	0.84	0.8
AQ-F	0.86	0.86	0.83

**Table 6.** Contribution of the reservoirs for the configuration AQ-F forced by TRMM (%).

River	Soil	Floods	Aquifer	Groundwater
13	49	4	17	17

region for the river and this difference probably explains the fact that the discharge simulated when the model is forced by TRMM is generally bigger than the discharge when the model is forced by RFEH, in particular, when there is no flooding scheme (twice as large as than RFEH). Moreover, the discharge simulated using TRMM rainfall has a longer recession period, probably due to the fact that there is more water going from the floodplains to the river after the flooding season. Figure 13 also shows that in 2005, 2006 and 2007, the relative bias between the two datasets is no longer obvious. Looking at the discharge we can see that during these 2 yr, the two rainfall products produce a very similar discharge amplitude, which results in a big reduction of the discharge amplitude simulated by TRMM in comparison with previous years. One possible cause for the reduction in input rainfall is that the gauge analysis source was changed from the GPCC Monitoring analysis to the Climate Prediction Center (CPC) Climate Analysis and Monitoring System (CAMS) in May, 2005. This change was made to take advantage of the timeliness in CAMS, but in retrospect it introduced a discontinuity in the error characteristics of the gauge analysis (G. J. Huffman, personal communication, 2012).

#### 4.5 Aquifer storage

Over the Niger basin, it was noticed that the discharge was still overestimated (Decharme et al., 2011). A possible identified cause was that these regions might overlie large aquifers that can be relatively uncoupled to the river. The available data concerning the aquifer storage are generally very localized, making the comparison with such a global scale model not relevant. Figure 14 shows the repartition of the aquifer recharge over the basin when the model is forced by

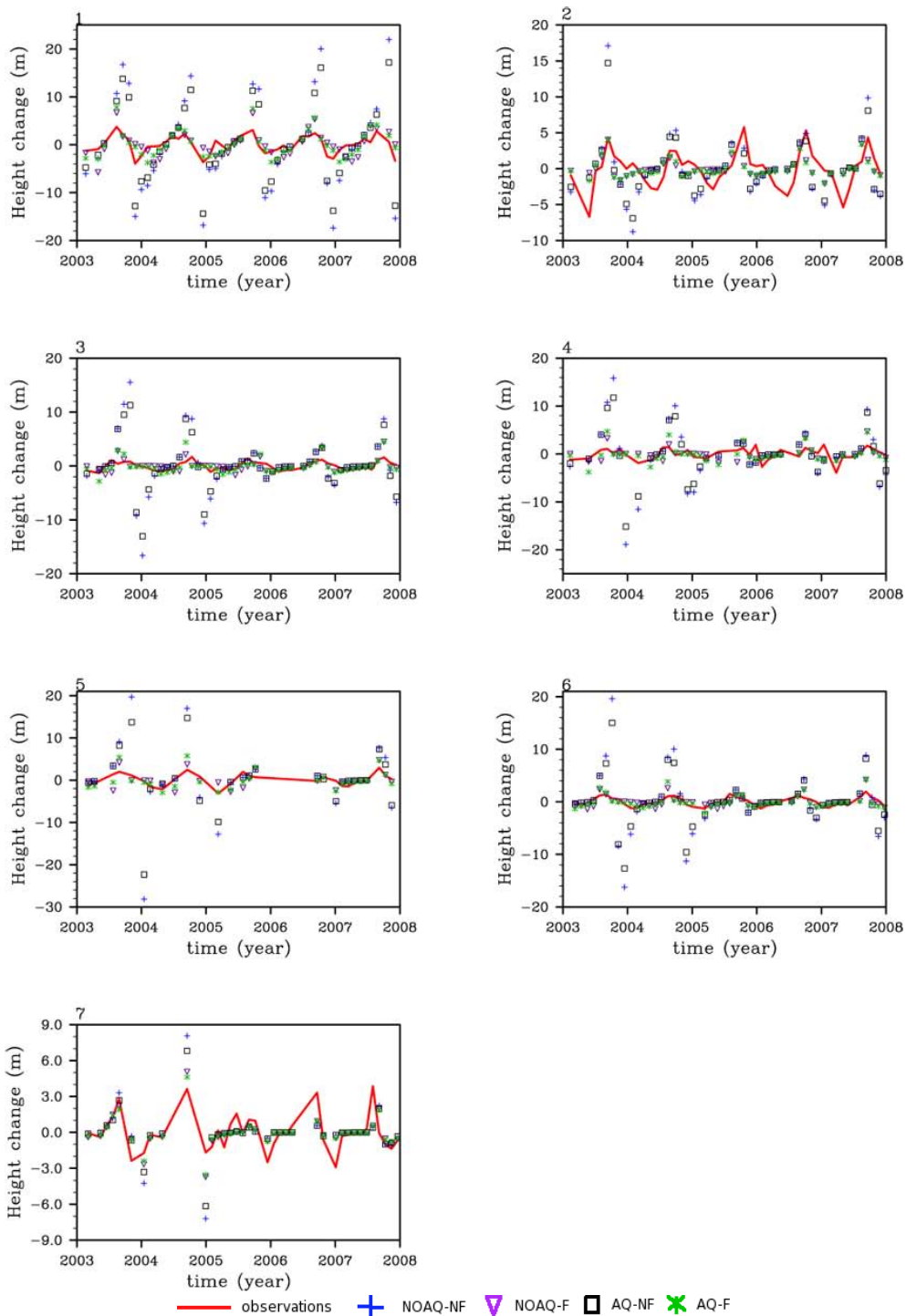


**Fig. 11.** Water level changes when the model is forced by TRMM.

RFEH. As expected, the aquifer recharge is very heterogeneous over the basin and follows rain patterns. There is also more aquifer recharge when the model is forced by TRMM than by RFEH. The aquifer reservoir is a relatively simple single-parameter linear reservoir and thus cannot represent high frequency fluctuations and distribution of the aquifer

recharge. However, the analysis of total water storage have shown that its contribution to this total storage is not negligible and must be taken into account to reproduce the evolution of the water budget.

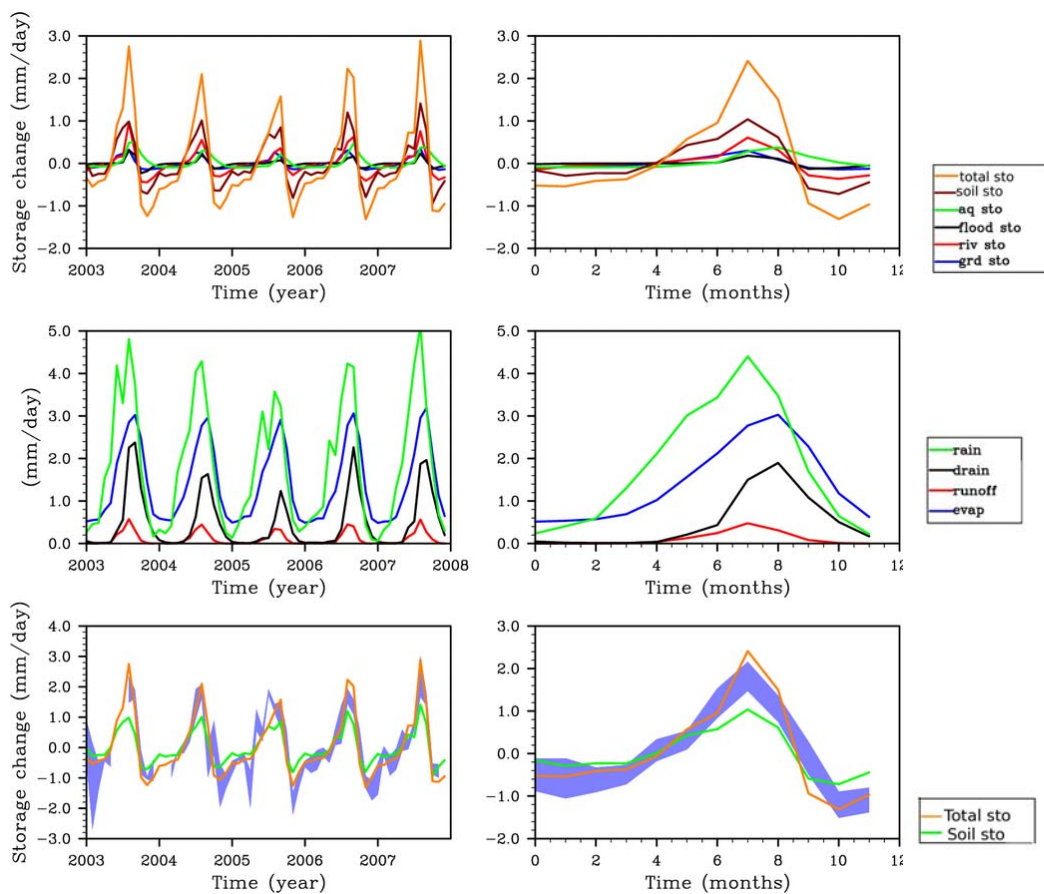


**Fig. 12.** Basin water storage change ( $\text{mm day}^{-1}$ ) of each reservoir (top). Time evolution of rain, runoff, drainage and evaporation over the basin (middle). Basin water storage change ( $\text{mm day}^{-1}$ ) in all reservoirs compared to GRACE datasets (down). The blue range is the difference between the maximum and the minimum GRACE products values. Left panels represent interannual variations (monthly averages) and right panels are the annual variations (each month is averaged over the whole 5 yr period).

#### 4.6 Sensitivity tests

Sensitivity tests were performed to determine the input parameters which have the most significant impact on the simulations. For global simulations, it is preferable that the model is not sensitive to too many parameters since tuning is a long and fastidious process at the global scale and spatially distributed global scale observational data is currently rather limited. Generally, physiographic relationships or the derivation of secondary parameters are preferred. The sensitivity of the ISBA-TRIP model to several key input parameters was investigated in this study in order to test their importance for a single regional scale basin. The Table 7 presents the key input parameters and the variations applied. The RFEH rainfall datasets were used for this study but the sensitivity tests using TRMM-3B42 rainfall datasets lead to the same tendencies with lesser extent when forced by RFEH. Both rainfall datasets were used for this study. However, as sensitivity tests generally lead to the same tendencies according to the rainfall dataset used as forcing, the different figures show the results for only one rain forcing.

The impact of the river critical height,  $h_c$ , on the simulated discharge was examined first. The river width  $W$  is kept at the default value. Increasing the critical height by 20 % leads to 5 % less flooded fraction over the inner delta and in the south of the basin. The evaporation also decreases over the flooded zones by 4 to 12 % (relative bias). Conversely, when decreasing the river height by 20 %, the flooded fraction is 5 % more over the same areas and the evaporation is increased by 14 to 24 %. The water height changes are also influenced by the critical height modification. Over the 7 virtual sites, an increase of  $h_c$  globally increases the water height changes (+30 %), while a decrease of  $h_c$  decreases the water height changes (−16 %). This can be explained by the fact that a river with a small  $h_c$  will be flooded earlier and the water will spread more rapidly over the surrounding area, making the river water level less sensitive to rain events. In terms of inter-annual discharge, increasing or decreasing  $h_c$ , respectively, increases or decreases the amplitude of the discharge by 5 to 15 % (Fig. 15a and b). However, the annual variability of the discharge is not changed by a modification

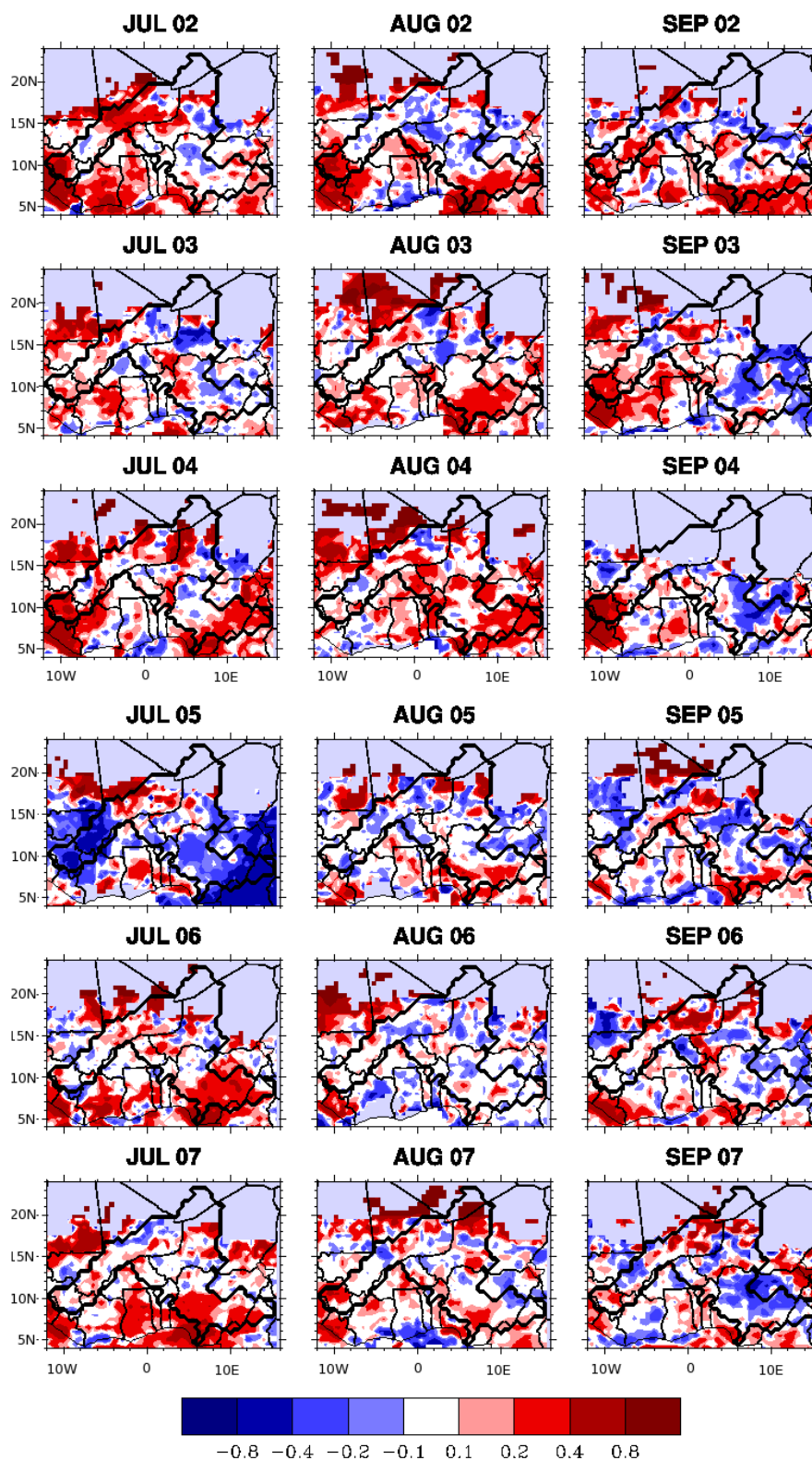


**Fig. 13.** Rainfall monthly averaged ratio  $(\text{TRMM} - \text{RFEH})/(\text{TRMM} + \text{RFEH})$ . The ratio is calculated only when the sum  $\text{TRMM} + \text{RFEH}$  is bigger than  $1 \text{ mm day}^{-1}$ .

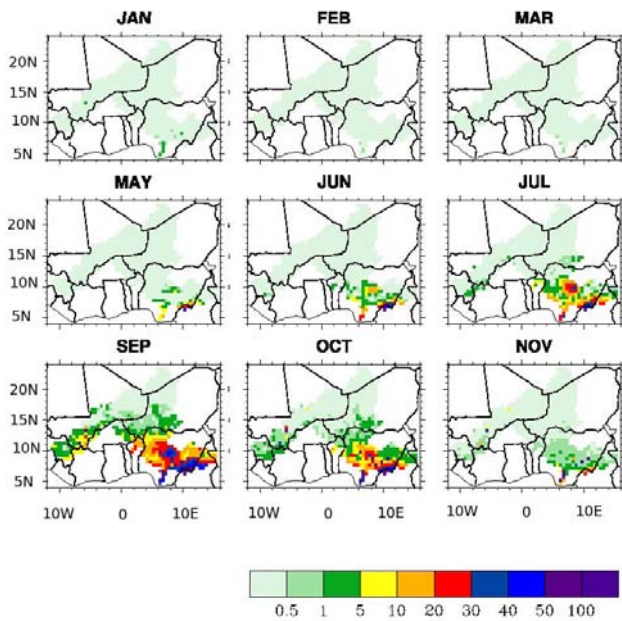


Fig. 14. Aquifer recharge distribution ( $\text{mm yr}^{-1}$ )

of the critical height. In Niamey, Ansongo and Kandadji, the increase of  $h_c$  leads to better statistical scores, which might suggest that the model overestimates the flood extend in these areas. In contrast, in Malanville, the scores are better when reducing the critical height, which suggests an underestimation of flooding at this site. In Lokoja however, the scores are better for the standard simulation. The impact of the river width,  $W$ , was also investigated. The critical height is not changed. Increasing  $W$  increases the amplitude of the discharge by around 6 %, while decreasing arbitrary  $W$  by 20 % decreases the discharge by 9 % (Fig. 15c and d). The water height changes vary differently according to the site. For example, for location 1 (see Fig. 2 for locations), a 20 % reduction of the river width reduces the mean water height changes by 35 % over the studied period. However, for locations 2, 4, 5, 6 and 7, the mean water height changes increase by 15 % to 28 % and there is no change for location 3. Indeed, water height changes depend on the topography which is modified with river width variations. The evaporation over the flooded areas is reduced by 3 to 9 % when  $W$  increases and increased by 4 to 16 % when  $W$  decreases. There are no significant impacts of  $W$  and  $h_c$  on the total water storage change. Indeed, the storage of the different reservoirs and the amount of drainage are only slightly changed by the modification of these parameters.

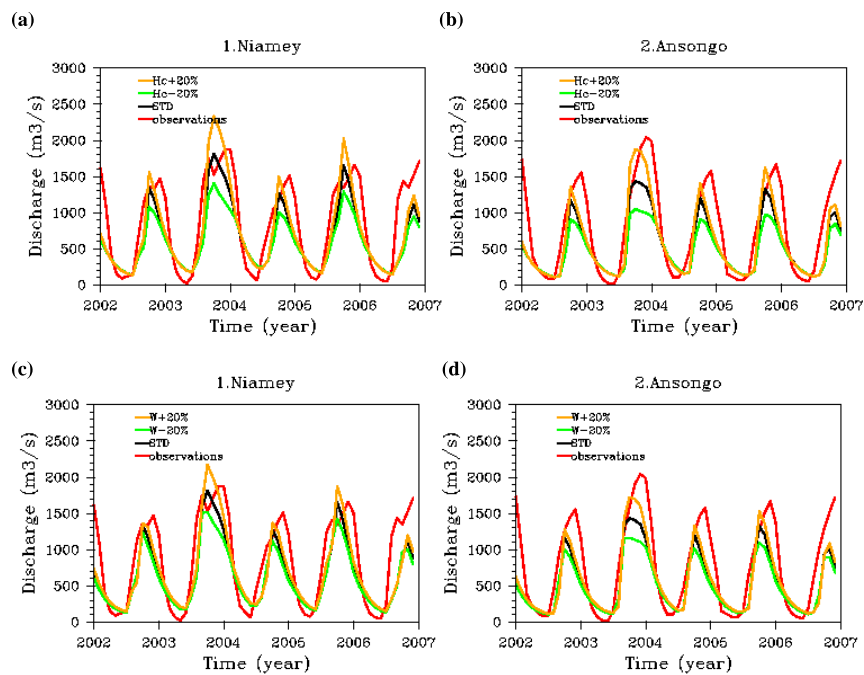
The mean value of the Manning coefficient,  $n_{\text{riv}}$ , is around 0.075 and most of the pixels have values above 0.06 (91 out of 110). Since the Niger basin covers a large area, the soil properties are very heterogeneous all over the basin, making it necessary to use spatial distributions of soil parameters. Two new distributions of  $n_{\text{riv}}$  were created and used to

Table 7. ISBA/TRIP key input parameters and the variations applied for sensitivity tests.

Case 1	$h_c$	Spatially distributed constant in time	a. +20 % b. –20 %
Case 2	$W$	Spatially distributed constant in time	a. +20 % b. –20 %
Case 2	$n_{\text{riv}}$	Spatially distributed constant in time	a. +20 % b. –40 %
Case 4	$\tau$	Constant in space and time	$\tau = 60; 90$
Case 5	$\tau_{\text{aq}}$	Constant in space and time	$\tau_{\text{aq}} = 1; 16$
Case 7	$\alpha$	Constant in space and time	$\alpha = \frac{1}{4}, \frac{1}{2}, \frac{3}{4}$

run the model: one distribution in which  $n_{\text{riv}}$  coefficient is arbitrary reduced by 40 % and the other one in which it is increased by 20 %. In order to keep a value included in a reasonable range (between 0.03 and 0.1), all the values out of this range after modification are set equal to the closest value in this range. Figure 16a shows the behaviour of the discharge for each distribution of  $n_{\text{riv}}$ . Increasing the Manning coefficient delays the response of the river to rain events. Indeed, small values of the coefficient speed the rise in water level and increase discharge amplitude. Also, the decrease of the discharge after the rainy season is faster when  $n_{\text{riv}}$  is smaller. We can also notice that when  $n_{\text{riv}}$  is bigger, the model is better able to dissociate the different rain events and two peaks of discharge appear. Flooded areas and evaporation are higher for large values of  $n_{\text{riv}}$  as the water flows more slowly in the river bed, generating smaller river height changes, and flooded areas empty to the river more slowly. The evaporation increases by 14 % over main evaporation areas when  $n_{\text{riv}}$  is 20 % higher and decreases by 18 % when it is 40 % smaller. Flooded areas are 15 % higher over the inner delta area when the Manning coefficient increases and 30 % smaller when it decreases. The increase of  $n_{\text{riv}}$  also delays the water height changes, while small values of  $n_{\text{riv}}$  decrease the peaks of river height changes. However, the impact of this coefficient on the water height change is more or less significant according to the observation sites, and for most of them this impact is not obvious. Finally, these modifications of  $n_{\text{riv}}$  have no significant impact on the total water storage change. Thus, the current distribution used in the model is the most reasonable according to the scores. The model is quite sensitive to Manning coefficient, which seems coherent. Since this coefficient is used for the calculation of the flow speed, it will impact the discharge, but also the creation of floods.

We also investigated the impact of increasing the groundwater reservoir's time delay factor on discharge, which extends the time of exchange between the groundwater reservoir and the river. Decharme et al. (2010) estimated that a time delay factor of the order of 30–60 days is generally



**Fig. 15.** Impact of modifications of the critical height  $h_c$  (a and b, up) and of the river width  $W$  (c and d, down) on the discharge (RFEH is used as forcing). The standard run stands for the simulation AQ-F with standard parameters (used for the simulations in previous sections).

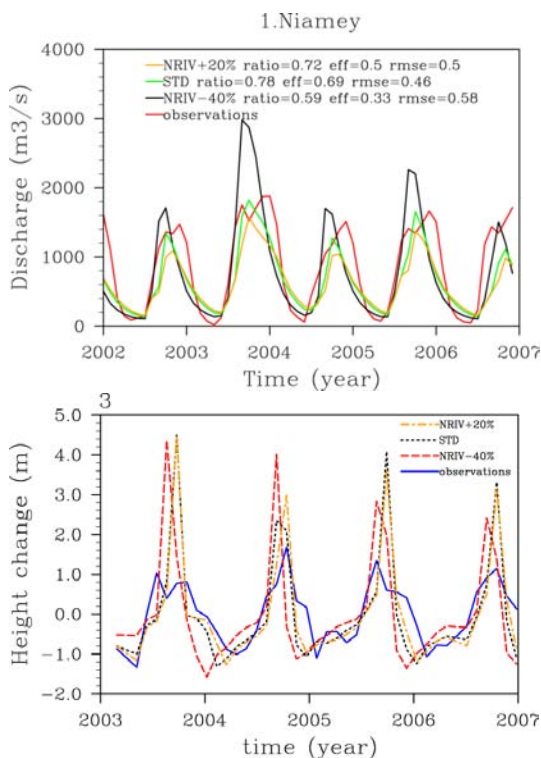


**Fig. 16.** Impact of the Manning coefficient on the river discharges and on the river height changes (RFEH is used as forcing). The standard run stands for the simulation AQ-F with standard parameters (used for the simulations in previous sections).

suitable for global simulations. The increase of  $\tau$  impacts the discharge on the descending phase by deteriorating the recession law. The scores are not significantly changed by the increase of  $\tau$ . The total water storage is not highly dependant on  $\tau$  either (the mean variation represents about 5 % of the mean water storage change). However, previous results emphasized that this parameter is important since it increases the residence time of water storage in the basin and allows a more realistic simulation of the discharge.

Finally, we investigated the impact of parameter related to the aquifers. The reduction of the distribution factor  $\alpha$  (which means an increase of the water going to the aquifer) decreases the discharge amplitude before the inner delta and accelerate the recession of the discharges after the inner delta (see Fig. 17). The scores are not significantly changed by the value of  $\alpha$  when the model is forced by RFEH and experience only few changes when forced by TRMM-3B42. The aquifer reservoir time delay factor has also no impact on the discharge as aquifers are assumed to be too deep and too slow to impact directly the river discharge. Modifications of  $\tau_{Aq}$  have a negligible impact on the total water storage of the basin (the mean variation represents less than 10 % of the mean water storage change). However, the simulation is done over a relatively short period (5 yr) over which the aquifer time delay factor might be less significant. Over longer periods of time, as for example for climatic studies, it is possible that water storage by aquifers and water discharge to the ocean has a significant impact on the water budget, and thus  $\tau_{Aq}$  could be one key parameter contributing to the water balance.

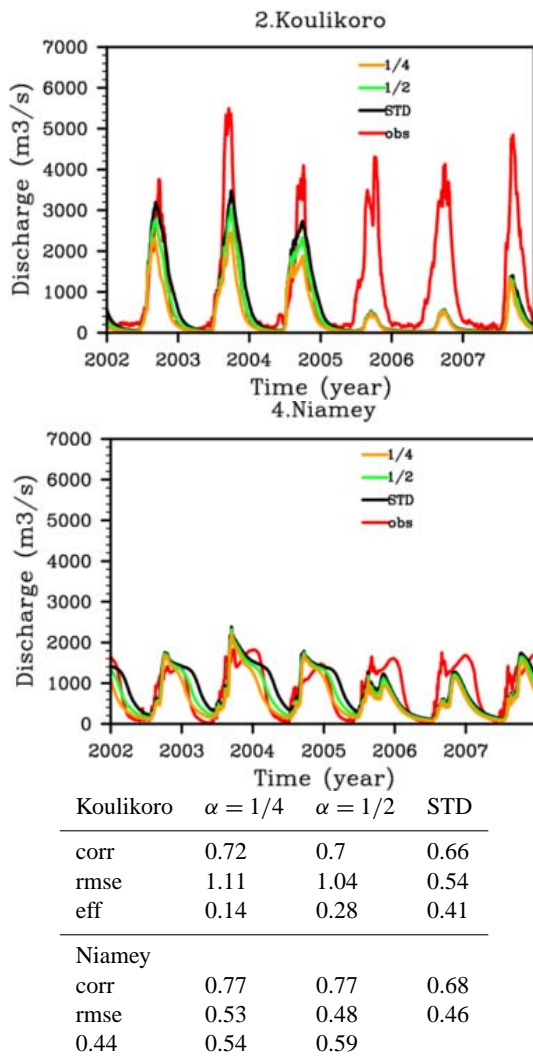


**Fig. 17.** Impact of aquifer distribution factor  $\alpha$  on the discharge (TRMM is used as forcing). The standard run stands for the simulation AQ-F with standard parameters (used for the simulations in previous sections).

**5 Discussion**

The presented study investigated the impact of a linear flooding scheme and a simple aquifer storage on the simulation of the Niger basin. The flooding scheme decreases streamflow and increases evaporation over flooded areas. The impacts of floods on the water fluxes and storage terms are found to be coherent with other studies (Coe et al., 2008; Decharme et al., 2008, 2011; Dadson et al., 2010), thus we further emphasize the need for representing these processes in GCMs. Moreover, the observed data from the ABN have shown a clear change of behaviour of the discharge after the inner delta compared to the discharge before the delta (the discharge is almost divided by two), highlighting the role of the delta in the discharge reduction. This is coherent with the impact of the flooding scheme on the simulated discharge (divided by

two after inclusion of floodplains in the model). However, it seems that in ISBA-TRIP, floods occur too early upstream of the delta, as suggested by the results in Ke Macina where the simulated discharge starts to be reduced while it is not the case in the observations. This might be due to poor values of the river parameters, such as river width in this particular region. The aquifer reservoir reduces the low flows and impacts the recession law, especially when the model is forced by TRMM. Moreover, its contribution to the total water budget is not negligible, and thus the consideration of aquifer processes is necessary to better simulate the evolution of the water cycle components. And indeed, several studies qualitatively suggest the presence of a deep water storage reservoir.

The results also suggest that the coupled land surface and river routing model provides a reasonable estimation of inland hydrological processes of the Niger basin when the flood scheme is activated and a deep aquifer is considered. Several diverse datasets have been used for model evaluation such as river discharge, spatial and temporal evolution of flooded areas and water height changes measured by satellite. These data provide basic constraints for estimating the sub-surface water storage and dynamics, but also the shallow soil water content and the groundwater storage, which are linearly related to the surface water. The comparison with GRACE total water storage dataset also show a good ability of the model to reproduce the evolution of total inland water.

Evapotranspiration is the remaining water budget component, but large scale observations are not available. The evaluation of this variable has been done within the context of several other studies. The ISBA surface temperature was evaluated using brightness temperatures from AMSR (de Rosnay et al., 2009), which is related to the surface energy budget and near surface soil moisture; and the monthly sensible heat fluxes aggregated from local scale observations to the ALMIP grid square were evaluated for a semi-arid region within the Niger basin (net radiation was imposed, thus monthly Bowen ratios can be estimated; Boone et al., 2009). Finally, regional scale water budget studies were performed over West Africa using ISBA evaporation estimates (Meynadier et al., 2010). All of the aforementioned studies imply that monthly scale evaporation estimates are reasonable.

Moreover, Mahe et al. (2009), estimated the water losses of the inner delta of the Niger river and their evolution from 1924 to 1996. They estimated the total evapotranspiration from the delta to be about 800 mm yr<sup>-1</sup> over the period 1924–1996, varying between 400 mm yr<sup>-1</sup> (1984) and 1300 mm yr<sup>-1</sup> (1924). The total evapotranspiration calculated by ISBA over the period 2002–2006 is 662 mm yr<sup>-1</sup>, which is contained in the range estimated by the previous study. They also related the water losses in the delta to the expansion of the floodplains, highlighting the importance of considering floods in a LSM.

However, some model deficiencies remain and can be due to different factors:

- A bias in the runoff and drainage calculated by the LSM. Further improvements could be obtained by calibrating the relevant parameters, but such a procedure is not relevant to GCM modelling.
- An over-simplified routing model. Indeed, global scale routing models are generally parametrized by geomorphologic relationships, which is not always realistic. Spatially distributed basin-specific parameters would undoubtedly improve the simulations.
- Rain biases can also be the origine of model biases. In this study, we have seen that the generally accepted two best rainfall datasets over this region give significantly different results.

Sensitivity tests have shown that a good routing model is required to optimize the simulation errors. For example, Fig. 15 shows that while increasing  $h_c$  in Niamey, Kandadji and Ansongo would improve the simulation score, it would have the opposite effect in Malanville. Thus, improvements in remote sensing technologies should help to create maps of spatial and temporal evolution of inland waters (river width, flooded areas expansion, river height) and thus compensate the lack of in situ measurements. These data will then either be used as input data and replace geomorphologic relations used currently to describe these parameters, or they will be assimilated into the model to correct simulation errors.

In GCMs, the input parameters, such as the Manning coefficient, critical height, river width and depth, are defined by empirical relationships which might not give the best results for all modelled basins, since the main objective of such parameterizations is to give the best overall global results. However, for regional or basin scale studies, these relationships lead to non-negligible known errors which could be reduced using satellite data. Indeed, satellite data could be used to spatially distribute parameters by basin and then could contribute to the development of a global database describing the major river characteristics, at least the stream width and the river bankfull height. This is an important step if GCM climate scenario output is to be used for water resource management at the regional scale.

Input rainfall uncertainties can also be the cause of biases in the simulations, as shown in Sect. 4.1 where the model, forced by two different rain datasets, gives significantly different results. In this paper, only the TRMM-3B42 and TRMM-RFE2-hybrid rain dataset, RFEH, were used for the bulk of the validation. However, other rain datasets were used as input rainfall to run the ISBA-TRIP model, such as PERSIANN (Precipitation Estimation from Remotely Sensed Information using Artificial Neural Networks, <http://chrs.web.uci.edu/persiann/>) from the Center for hydrometeorology and remote sensing (CHRS) and CMORPH (CPC MORPHing technique, <http://www.cpc.ncep.noaa.gov/products/janowiak/cmorph.shtml>) from the United States National Oceanic and Atmospheric Administration (NOAA).

The results of the simulations using both of these rainfall datasets showed a significant overestimation of the discharge (about 5 times higher than with the RFEH forcing for both CMORPH and PERSIANN forcing, and twice higher for the TRMM forcing) at all discharge observation sites, even with the representation of floods and aquifers. This is consistent with the work of Pierre et al. (2011) who showed that CMORPH dataset clearly overestimates precipitations over the Sahel. Improved spatially distributed remotely sensed datasets which are more precise for hydrological applications are thus needed.

## 6 Conclusions and perspectives

This study describes the evaluation of the ISBA-TRIP Continental Hydrologic System (CHS) over the Niger river basin, using a prognostic flooding scheme and a linear deep aquifer reservoir. The simulations are done at a  $0.5^\circ$  by  $0.5^\circ$  resolution over the 2002–2007 period. The flood scheme accounts explicitly for the precipitation interception by the floodplains, the direct evaporation from the free water surface and the possible re-infiltration into the soil. The deep aquifer reservoir has no feedback with the river locally and drains water to the river mouth over a comparatively long timescale. The model has been developed for use in climate model applications (coupled to the ARPEGE RCM and GCM at Météo France) where the representation of processes such as evaporation from the continental surface and freshwater fluxes to the ocean are fundamental to the global water budget. These applications especially aim at detecting strong anomalies in the future climate, and for this reason we focused on evaluating the ability of the model to reproduce inland waters anomalies. The model was run in four different configurations to evaluate the separated impacts of the flooding scheme and the aquifer reservoir on the modelisation of the Niger basin. Moreover, two different rainfall were used as forcing in order to take into account the impact of rain uncertainties on the simulations. The evaluation is done using a large variety of data, consisting of gauging measurements and satellite-derived products. This allows the spatially distributed evaluation of the separation of the water storage into its different components and it gives a first estimate of aquifer dynamics over the basin.

Considering the relative simplicity of the routing channel, the model provides a good estimation of the surface water dynamics: the spatio-temporal variability of the flooded areas, the river discharge and the river water height changes. The flooding scheme leads to an increase of evaporation and reduction of discharge after the inner delta area, testifying for the need to incorporate flood representations into land surface models (LSMs). The behaviour of the observed discharge also suggest an impact of the inner delta, known as an important flooded area, on the discharge. The aquifer reservoir impacts the representation of both low flows and the

recession law during the dry season. Note that recently an option to include a detailed representation of aquifers has been introduced into the ISBA-TRIP CHS (Vergnes et al., 2012). However, the quality of the input and observational data required to evaluate the scheme is currently lacking over the Niger basin. For this reason we have opted for a more simple linear reservoir approach in this study (consistent with the other TRIP reservoirs). However, the possible link between river height and aquifer storage will be explored using remotely sensed data in future work. The comparisons with GRACE total water storage change (GFZ, CSR and JPL) were used to evaluate the ability of the model to reproduce the evolution of the total inland water, and good overall agreement of total water stored with GRACE was found. Finally, the use of two different rainfall datasets as forcing has shown the sensitivity of the model to rain uncertainties.

Despite the fact that the main features of the river dynamics and water budget terms are represented reasonably well by this relatively simple system, some simulation deficiencies remain. For example, the model has a difficulty in terms of reproducing the discharge during the low flow period or the two annual peaks of discharge (only one peak is reproduced by the model). These deficiencies might be due to precipitation uncertainties or LSM errors (in terms of sub-grid runoff, evaporation and soil water transfer physics, input LSM physiographic parameters such as vegetation indices, soil texture and depth, etc.): but the focus in this study is mainly on river, floodplain and aquifer dynamics. Precipitation uncertainties were briefly touched upon by using different input forcings, but few currently available rainfall products are good enough to be useful for hydrological modelling studies over this region (notably owing to large biases). Regarding the RRM errors, Decharme et al. (2011) have discussed the questionable aspects of the flooding scheme such as the empirical computation of the river width, the choice of the river bankfull height, the simplified geometry of river stream and flood reservoirs, or the use of the Manning's formula for computing the mass transfer between them. Moreover, sensitivity tests have shown the non-negligible impact of some of the parameter values on simulations. However, the model has been developed for global climate applications at low resolutions and must be as robust as possible to be applicable at global scale, and therefore has a limited number of tunable parameters. However, upcoming advances in remote sensing technologies should permit an optimization of the spatially distributed parameters of the model. In fact, forcing uncertainties, especially rain uncertainties, represent a limitation for model tuning at this scale. Moreover, they can compensate the non-representation of lakes and large ponds.

A global database describing the basin characteristics such as the river width and the bankfull height would be of great interest for improving the model simulations. This likely depends heavily on advances in remote sensing technologies, which should help to get maps of spatial and temporal evolution of inland waters (river width, flooded areas expansion,

river height, etc.) and thus compensate for the lack of in situ measurements at the global scale. The joint CNES-NASA satellite project SWOT will provide water heights and extent at land surface with an unprecedented 50–100 m resolution and precision (centimetric accuracy when averaged over areas of 1 km; Durand et al., 2010). These data will then either be used as input data and replace geomorphologic relations used currently to describe surface parameters, or they will be assimilated into the model to correct model errors. Indeed, a small number of recent studies have begun to quantify the benefits of such a mission for land surface hydrology. For this purpose, synthetic water elevation data were created using the JPL Instrument Simulator (Rodriguez and Moller, 2004) and assimilated into CHS systems (Durand et al., 2008; Biancamaria et al., 2010). In all of these studies, the assimilation of synthetically generated SWOT measurements helped to reduce model errors and improved river discharge simulation. Other studies have used SWOT simulated data as inputs in algorithms to obtain estimates of river depth and discharge (Andreadis et al., 2007; Durand et al., 2010; Biancamaria et al., 2010, 2011). These preliminary results are promising and show the current need for such a mission, and the potential for improving the representation of hydrological processes in current models. Consequently, the next step of this work will consist of integrating synthetic SWOT data into a suitable assimilation system to determine their impact on the simulated discharge using the ISBA-TRIP CHS described herein.

## Appendix A

### The TRIP river discharge and groundwater outflow

The river discharge simulated by TRIP (Eq. 1) is computed using a streamflow variable velocity,  $v$  ( $\text{m s}^{-1}$ ), and via the Manning's formula:

$$Q_{\text{out}}^S = \frac{v}{L} S \quad \text{with} \quad v = \frac{\kappa}{n_{\text{riv}}} R^{2/3} s^{1/2}, \quad (\text{A1})$$

where  $L$  (m) is the river length that takes into account a meandering ratio of 1.4 as proposed by Oki and Sud (1998),  $s$  ( $\text{m m}^{-1}$ ) is the downstream river height loss per unit length approximated as the river bed slope,  $R$  (m) the hydraulic radius,  $\kappa$  ( $\text{m}^{-3} \text{s}^{-1}$ ) a constant equal to 1, and  $n_{\text{riv}}$  the dimensionless Manning friction factor which varies from the upstream part to the mouth of each basin. The river bed slope is indeed a critical parameter to compute velocity via the Manning formula. The STN-30p Digital Elevation Model (DEM) provided at  $0.5^\circ \text{C}$  by  $0.5^\circ \text{C}$  resolution by the ISLSCP2 database (<http://www.gewex.org/islscpdata.htm>) has been used. The STN-30p DEM was heavily edited to represent the actual elevation along the river network on a global scale, based on the aggregated HYDRO1 K DEM at 1 km resolution. Further adjustments were made to eliminate some of the unrealistic rapid slope changes in the STN-30p

DEM along the global river network. Yamazaki et al. (2009), included a realistic sub-grid-scale topography for a more reasonable representation of the river height loss. This inclusion could be considered as a possible improvement of the representation of the river bed slope in the TRIP model. The hydraulic radius is related to the stream water depth,  $h_s$  (m), calculated from the stream water mass,  $S$  (kg), assuming a rectangular river cross-section (Arora and Boer, 1999):

$$R = \frac{W h_s}{W + 2 h_s} \quad \text{where} \quad h_s = \frac{S}{L W \rho_W}, \quad (\text{A2})$$

where  $\rho_W$  ( $\text{kg m}^{-3}$ ) is the water density, and  $W$  (m) the bankfull river width.

The TRIP groundwater outflow (Eq. 1) is computed using the following simple linear relationship proposed by Arora and Boer (1999):

$$Q_{\text{out}}^G = \frac{G}{\tau} \quad (\text{A3})$$

where  $\tau$  (s) is an uniform and constant time delay factor of the groundwater reservoir which is fixed to 30 days. This groundwater reservoir does not represent the groundwater dynamics but only delays the groundwater flow contribution to the surface river reservoir within a particular grid cell: the deep drainage is fed into the surface reservoir with a time delay factor of  $\tau$ . More details can be found in Decharme et al. (2010).

## Appendix B

### The ISBA-TRIP flood model

As shown in Fig. 1, a simplified rectangular geometry is assumed in TRIP to represent the cross section between the floodplain and the river reservoirs in each grid cell. River flooding arises when the water height of the stream reservoir is higher than the critical bankfull height,  $h_c$  (m), and the flood outflow and inflow from this reservoir (Eq. 1) are given by:

$$\begin{cases} Q_{\text{in}}^F = \frac{v_{\text{in}}}{W + W_f} M_f \\ Q_{\text{out}}^F = \frac{v_{\text{out}}}{W + W_f} \min(M_f, F), \end{cases} \quad (\text{B1})$$

where  $W_f$  (m) is the floodplain width, and  $M_f$  (kg) the potential inflow (positive  $M_f$ ) or outflow (negative  $M_f$ ). This outflow assumes an equilibrium state between the stream and the floodplain water depth:

$$M_f = \rho_W L_f W (h_s - h_c - h_f), \quad (\text{B2})$$

where  $L_f$  (m) and  $h_f$  (m) are the length along the river and the depth of the floodplains,  $h_s$  (m) the water height of the stream reservoir, and  $h_c$  (m) the critical bankfull river height.  $W + W_f$  represents the distance covered by  $M_f$  from the

stream to the floodplains or conversely.  $v_{\text{in}}$  and  $v_{\text{out}}$  ( $\text{m s}^{-1}$ ) are the flood inflow and outflow velocities, respectively, computed using the Manning's formula:

$$v_{\text{in,out}} = \frac{s_{\text{in,out}}^{1/2}}{n_f} R_{\text{in,out}}^{2/3}, \quad (\text{B3})$$

where  $n_f$  is the Manning roughness coefficient for the floodplains that varies according to the vegetation type (Decharme et al., 2011), while  $s_{\text{in,out}}$  ( $\text{m m}^{-1}$ ) and  $R_{\text{in,out}}$  (m) are the inflow (or outflow) slope and hydraulic radius, respectively, at the interface between the floodplain and the river stream.

The flood inflow and outflow velocities computed using the Manning's formula require the hydrological slope between the floodplain and the river stream:

$$\begin{cases} s_{\text{in}} = \frac{\max(0, h_s - h_c - h_f)}{(W + W_f)/2} \\ s_{\text{out}} = \frac{\max(0, h_f + h_c - h_s)}{(W + W_f)/2}. \end{cases} \quad (\text{B4})$$

They also require the hydraulic radius assumed rectangular and calculated as follows:

$$\begin{cases} R_{\text{in}} = \frac{L_f \times \max(0, h_s - h_c)}{L_f + 2 \times \max(0, h_s - h_c)} \\ R_{\text{out}} = \frac{L_f h_f}{L_f + 2 h_f}, \end{cases} \quad (\text{B5})$$

where  $W_f$  (m),  $L_f$  (m) and  $h_f$  (m) are the width, the length and the depth (respectively) of the floodplains,  $h_s$  (m) the water height of the stream reservoir,  $h_c$  (m) the critical height of the river bed, and  $W$  (m) the stream river width. The  $h_f$  is calculated in each grid-cell with the help of the actual distribution of the local height,  $h_i$  (m), determined at a 1 km by 1 km resolution. The assumption is that each pixel,  $i$ , represents a sub-basin into a given grid-cell that can be potentially flooded. Each subbasin has a triangular form and is associated with a fraction,  $f_i$ , of the grid cell area,  $A$ . The  $h_i$  is computed using the local slope,  $\tau_i$  ( $^\circ$ ) and flow direction data given by the HYDRO1 K dataset (Verdin and Greenlee, 1996):

$$h_i = l \sqrt{\alpha_i} \tan\left(\frac{\sigma_i \pi}{180}\right), \quad (\text{B6})$$

where  $l$  (m) is the characteristic length of one pixel equal to 1000 m, and  $\alpha_i$  is equal to 1 if the local flow direction is north, south, east, or west, and to 2 elsewhere. Therefore, for each  $h_i$  a potential mass of flood,  $V(h_i)$  (kg), can be simply calculated using a discrete equation:

$$V(h_i) = \rho_w \sum_0^i V_i \quad \text{where} \quad V_i = \frac{A f_i h_i}{2}. \quad (\text{B7})$$

The sub-grid distributions of the flooded fraction and the flood depth allow to determine  $f_{\text{flood}}$ , and  $h_f$  at each time step and in each grid-cell via the comparison between the water mass into the floodplain reservoir,  $F$ , computed by TRIP

(Eq. 4) and the sub-grid distribution of this potential mass  $V(h_i)$ :

$$F = V(h_i) \Rightarrow \begin{cases} f_{\text{flood}} = \sum_0^i f_i \\ h_f = h_i. \end{cases} \quad (\text{B8})$$

When  $f_{\text{flood}}$  is known within the grid cell,  $W_f$  and  $L_f$  are simply calculated as follow:

$$\begin{cases} L_f = \max(0.001, r\sqrt{f_{\text{flood}}A}) \\ W_f = \frac{A_{f_{\text{flood}}}}{L_f}, \end{cases} \quad (\text{B9})$$

where  $r$  is the meandering ratio fixed to 1.4 as recommended by Oki and Sud (1998).

Finally, the precipitation interception by the floodplains,  $P_f$ , the re-infiltration,  $I_f$ , and the direct free water surface evaporation,  $E_f$ , (Eq. 1) are estimated by ISBA.  $I_f$  occurs if the flooded fraction,  $f_{\text{flood}}$ , calculated according to the sub-grid topography (Decharme et al., 2011), is superior to the soil saturated fraction,  $f_{\text{sat}}$ , and depends on the soil maximum infiltration capacity. In other words, the floodplains cannot infiltrate the fraction of the grid-cell for which the soil is saturated. To a first approximation, it allows to simply represent the fact that the actual floodplains evolve according to the presence of shallow aquifer and water table depth variations. More details can be found in Decharme et al. (2011).

## Appendix C

### List of acronyms.

AGCM	Atmospheric General Circulation Models
ALMIP	AMMA Land Surface Model Intercomparison
AMMA	African Monsoon Multidisciplinary Analysis
CHS	Continental Hydrologic System
GRACE	Gravity Recovery and Climate Experiment
HYCOS	Hydrologic Observation System
ISBA	Interactions Sol-Biosphère-Atmosphère
Land-SAF	Land Satellite Application Facility
LSM	Land Surface Model
MODIS	Moderate Resolution Imaging Spectroradiometer
NDVI	Normalized Difference Vegetation Index
RFE2	Rainfall Estimates version 2.0
RFEH	RFE-Hybrid
RRM	River Routing Model
SWOT	Surface Water Ocean Topography
TRIP	Total Runoff Integrating Pathways
TRMM	Tropical Rainfall Measuring Mission

*Acknowledgements.* This work is supported by the African Monsoon Multidisciplinary Analysis (AMMA) project and the Surface Water Ocean Topography (SWOT) satellite mission project of the “Centre National d’Etudes Spatiales” (CNES). The diverse studies presented in this paper would not have been possible without the valuable contribution of the “Autorité du Bassin du Niger” (ABN) and Catherine Prigent from the “Laboratoire d’Etudes du Rayonnement et de la Matière en Astrophysique”.

Edited by: Y. Fan



The publication of this article is financed by CNRS-INSU.

## References

- Ali, A. and Lebel, T.: The Sahelian standardized rainfall index revisited, *Int. J. Climatol.*, 29, 1705–1714, 2009.
- Alkama, M. R., Kageyama, M., Ramstein, G., Marti, O., Ribstein, P., and Swingedouw, D.: Impact of a realistic river routing in coupled ocean-atmosphere simulations of the Last Glacial Maximum climate, *Clim. Dynam.*, 30, 855–869, 2008.
- Alkama, R., Decharme, B., Douville, H., Becker, M., Cazenave, A., Sheffield, J., Voldoire, A., Tyteca, S., and Le Moigne, P.: Global evaluation of the ISBA/TRIP continental hydrological system, Part 1: Comparison to GRACE terrestrial water storage estimates and in situ river discharges, *J. Hydrometeorol.*, 11, 583–600, 2010.
- Alsdorf, D. E. and Lettenmaier, D. P.: Tracking fresh water from space, *Science*, 301, 5639, doi:10.1126/science.1089802, 2003.
- Alsdorf, D. E., Rodriguez, E., and Lettenmaier, D. P.: Measuring surface water from 593 space, *Rev. Geophys.*, 45, RG2002, doi:10.1029/2006RG000197, 2007.
- Amogu, O., Descroix, L., Yero, K. S., Le Breton, E., Mamadou, I., Ali, A., Vischel, T., Bader, J., Moussa, I. B., Gautier, E., Boubkraoui, S., and Belleudy, P.: Increasing River Flows in the Sahel?, *Water*, 2, 170–199, 2010.
- Andersen, I., Dione, O., Jarosewich-Holder, M., and Olivry, J. C.: The Niger river basin: A vision for sustainable management, World Bank Publications, 2005.
- Andreadis, K. M., Clark, E. A., Lettenmaier, D. P., and Alsdorf, D. E.: Prospects for river discharge and depth estimation through assimilation of swath-altimetry into a raster-based hydrodynamics model, *Geophys. Res. Lett.*, 34, L10403, doi:10.1029/2007GL029721, 2007.
- Arora, V. K. and Boer, G. J.: A variable velocity flow routing algorithm for GCMs, *J. Geophys. Res.*, 104, 30965–30979, doi:10.1029/1999JD900905, 1999.
- Beven, K. J. and Kirkby, M. J.: A physically-based variable contributing area model of basin hydrology, *Hydrol. Sci. Bull.*, 24, 43–69, 1979.

- Biancamaria, S., Andreadis, K. M., Durand, M., Clark, E. A., Rodriguez, E., Mognard, N. M., Alsdorf, D. E., Lettenmaier, D. P., and Oudin, Y.: Preliminary Characterization of SWOT Hydrology Error Budget and Global Capabilities, *IEEE J. Sel. Top. Appl.*, 3, 6–19, doi:10.1109/JSTARS.2009.2034614, 2010.
- Biancamaria, S., Durand, M., Andreadis, K. M., Bates, P. D., Boone, A., Mognard, N. M., Rodriguez, E., Alsdorf, D. E., Lettenmaier, D. P., and Clark, E. A.: Assimilation of virtual wide swath altimetry to improve Arctic river modeling, *Remote Sens. Environ.*, 115, 373–381, 2011.
- Bonan, G. B.: Sensitivity of a GCM to inclusion of inland water surfaces, *J. Climate*, 8, 2691–2704, doi:10.1175/1520-0442(1995)008<2691:SOAGST>2.0.CO;2, 1995.
- Boone, A., Calvet, J.-C., and Noilhan, J.: Inclusion of a Third Soil Layer in a Land-Surface Scheme using the Force-Restore method, *J. Appl. Meteorol.*, 38, 1611–1630, 1999.
- Boone, A., de Rosnay, P., Basalmo, G., Beljaars, A., Chopin, F., Decharme, B., Delire, C., Ducharme, A., Gascoïn, S., Grippa, M., Guichard, F., Gusev, Y., Harris, P., Jarlan, L., Kergoat, L., Mougin, E., Nasonova, O., Norgaard, A., Orgeval, T., Ottlé, C., Pocard-Leclercq, I., Polcher, J., Sandholt, I., Saux-Picart, S., Taylor, C., and Xue, Y.: The AMMA Land Surface Model Intercomparison Project, *B. Am. Meteorol. Soc.*, 90, 1865–1880, doi:10.1175/2009BAMS2786.1, 2009.
- Bousquet, P., Ciais, P., Miller, J. B., Dlugokencky, E. J., Hauglustaine, D. A., Prigent, C., Van der Werf, G. R., Peylin, P., Brunke, E. G., Carouge, C., Langenfelds, R. L., Lathiere, J., Papa, F., Ramonet, M., Schmidt, M., Steele, L. P., Tyler, S. C., and White, J.: Contribution of anthropogenic and natural sources to atmospheric methane variability, *Nature*, 443, 439–443, doi:10.1038/nature05132, 2006.
- Calmant, S., Seyler, F., and Cretaux, J. F.: Monitoring Continental Surface Waters by Satellite Altimetry, *Surv. Geophys.*, 29, 247–269, 2008.
- Coe, M. T.: A linked global model of terrestrial processes: Simulation of modern rivers, 781 lakes and wetlands, *J. Geophys. Res.*, 103, 8885–8899, 1998.
- Coe, M. T.: Modeling terrestrial hydrological systems at the continental scale: Testing the accuracy of an atmospheric GCM, *J. Climate*, 13, 686–704, doi:10.1175/1520-0442(2000)013<0686:MTHSAT>2.0.CO;2, 2000.
- Coe, M. T. and Birkett, C. M.: Calculation of river discharge and prediction of lake Height from satellite radar altimetry: example of the lake Chad basin, *Water Resour. Res.*, 40, W10205, doi:10.1029/2003WR002543, 2004.
- Coe, M. T., Costa, M. H., and Howard, E. A.: Simulating the surface waters of the Amazon River basin: impact of new river geomorphic and flow parameterizations, *Hydrol. Process.*, 22, 2542–2553, doi:10.1002/hyp.6850, 2008.
- Cogley, J. G.: The albedo of water as a function of latitude, *Mon. Weather Rev.*, 107, 775–781, doi:10.1175/1520-0493(1979)107<0775:TAOWAA>2.0.CO;2, 1979.
- Costa, M. H. and Foley, J. A.: Water balance of the Amazon Basin: Dependence on vegetation cover and canopy conductance, *J. Geophys. Res.*, 102, 973–989, doi:10.1029/97JD01865, 1997.
- Dadson, S. J., Ashpole, I., Harris, P., Davies, H. N., Clark, D. B., Blyth, E., and Taylor, C. M.: Wetland inundation dynamics in a model of land surface climate: Evaluation in the Niger inland delta region, *J. Geophys. Res.*, 115, D23114, doi:10.1029/2010JD014474, 2010.
- Dai, T. and Labadie, J. W.: River basin network model for integrated water quantity/quality management, *J. Water Resour. Pl.-ASCE*, 127, 295–305, 2001.
- de Rosnay, P., Drusch, M., Boone, A., Balsamo, G., Decharme, B., Harris, P., Kerr, Y., Pellarin, T., Polcher, J., and Wigneron, J.-P.: AMMA Land Surface Model Intercomparison Experiment coupled to the Community Microwave Emission Model: ALMIP-MEM, *J. Geophys. Res.*, 114, D05108, doi:10.1029/2008JD010724, 2009.
- Decharme, B.: Influence of runoff parameterization on continental hydrology: Comparison between the Noah and the ISBA land surface models, *J. Geophys. Res.*, 112, D19108, doi:10.1029/2007JD008463, 2007.
- Decharme, B. and Douville, H.: Introduction of a sub-grid hydrology in the ISBA land surface model, *Clim. Dynam.*, 26, 65–78, 2006.
- Decharme, B., Douville, H., Boone, A., Habets, F., and Noilhan, J.: Impact of an exponential profile of saturated hydraulic conductivity within the ISBA LSM: simulations over the Rhône basin, *J. Hydrometeorol.*, 7, 61–80, 2006.
- Decharme, B., Douville, H., Prigent, C., Papa, F., and Aires, F.: A new river flooding scheme for global climate applications: Offline evaluation over South America, *J. Geophys. Res.*, 113, D11110, doi:10.1029/2007JD009376, 2008.
- Decharme, B., Alkama, R., Douville, H., Becker, M., and Cazenave, A.: Global evaluation of the ISBA-TRIP continental hydrological system, Part II: Uncertainties in river routing simulation related to flow velocity and groundwater storage, *J. Hydrometeorol.*, 11, 601–617, 2010.
- Decharme, B., Alkama, R., Papa, F., Faroux, S., Douville, H., and Prigent, C.: Global off-line evaluation of the ISBA-TRIP flood model, *Clim. Dynam.*, 38, 1389–1412, doi:10.1007/s00382-011-1054-9, in press, 2011.
- Dirmeyer, P. A.: Using a global soil wetness dataset to improve seasonal climate simulation, *J. Climate*, 13, 2900–2922, 2000.
- Dirmeyer, P. A.: Climate drift in a coupled landatmosphere model. *J. Hydrometeorol.*, 2, 89–100, 2001.
- Dirmeyer, P. A., Gao, X., Zhao, M., Guo, Z., Oki, T., and Hanasaki, N.: GSWP-2: Multimodel analysis and implications for our perception of the land surface, *B. Am. Meteorol. Soc.*, 87, 1381–1397, 2006.
- Douville, H.: Assessing the influence of soil moisture on seasonal climate variability with AGCMs, *J. Hydrometeorol.*, 4, 1044–1066, 2003.
- Douville, H.: Relevance of soil moisture for seasonal atmospheric predictions: Is it an initial value problem?, *Clim. Dynam.*, 22, 429–446, 2004.
- Douville, H., Planton, S., Royer, J. F., Stephenson, D. B., Tyteca, S., Kergoat, L., Lafont, S., and Betts, R. A.: Importance of vegetation feedbacks in doubled-CO<sub>2</sub> climate experiments, *J. Geophys. Res.*, 105, 14841–14861, 2000.
- Dunn, C. E., Bertiger, W., Bar-Sever, Y., Desai, S., Haines, B., Kuang, D., Franklin, G., Harris, I., Kruizinga, G., Meehan, T., Nandi, S., Nguyen, D., Rogstad, T., Thomas, J. B., Tien, J., Romans, L., Watkins, M., Wu, S.-C., Bettadpur, S., and Kim, J.: Instrument of GRACE:GPS augments gravity measurements, application challenge, *GPS World*, 2003.

- Durand, M., Andreadis, K. M., Alsdorf, D. E., Lettenmaier, D. P., Moller, D., and Wilson, M.: Estimation of bathymetric depth and slope from data assimilation of swath altimetry into a hydrodynamic model, *Geophys. Res. Lett.*, 35, L20401, doi:10.1029/2008GL034150, 2008.
- Durand, M., Rodriguez, E., Alsdorf, D. E., and Trigg, M.: Estimating River Depth From Remote Sensing Swath Interferometry Measurements of River Height, Slope, and Width, *IEEE J. Sel. Top. Appl.*, 3, 20–31, doi:10.1109/JSTARS.2009.2033453, 2010.
- Enjolras, V. M. and Rodriguez, E.: Using altimetry waveform data and ancillary information from SRTM, Landsat, and MODIS to retrieve river characteristics, *IEEE T. Geosci. Remote.*, 47, 1869–1881, 2009.
- Fontes, J.-C., Andrews, J. N., Edmunds, W. M., Guerre, A., and Travi, Y.: Paleorecharge by the Niger River (Mali) deduced from groundwater geochemistry, *Water Resour. Res.*, 27, 199–214, 1991.
- Gedney, N., Cox, P. M., Douville, H., Polcher, J., and Valdes, J. P.: Characterizing GCM land surface schemes to understand their responses to climate change, *J. Climate*, 13, 3066–3079, 2000.
- Geiger, B., Meurey, C., Lajas, D., Franchistéguy, L., Carrer, D., and Roujean, J.-L.: Near real-time provision of downwelling short-wave radiation estimates derived from satellite observations, *Meteorol. Appl.*, 15, 411–420, 2008.
- Getirana, A. C. V., Bonnet, M.-P., Rotunno, O. C., Collischonn, W., Guyot, J. L., Seyler, F., and Mansur, W. J.: Hydrological modelling and water balance of the Negro River basin: evaluation based on in situ and spatial altimetry data, *Hydrol. Process.*, 24, 3219–3236, 2010.
- Grippa, M., Mognard, N. M., Letoan, T., and Josberger, E. G.: Siberia snow depth climatology from SSM/I data using a combined dynamic and static algorithm, *Remote Sens. Environ.*, 93, 30–41, 2004.
- Grippa, M., Kergoat, L., Frappart, F., Araud, Q., Boone, A., de Rosnay, P., Lemoine, J.-M., Gascoïn, S., Balsamo, G., Ottlé, C., Decharme, B., Saux-Picart, S., and Ramillien, G.: Land water storage variability over West Africa estimated by GRACE and land surface models, *Water Resour. Res.*, 47, W05549, doi:10.1029/2009WR008856, 2011.
- Habets, F., Boone, A., Champeaux, J.-L., Etchevers, P., Franchistéguy, L., Leblois, E., Ledoux, E., Le Moigne, P., Martin, E., Morel, S., Noilhan, J., Quintana Segui, P., Rousset-Regimbeau, F., and Viennot, P.: The SAFRAN-ISBA-MODCOU hydrometeorological model applied over France, *J. Geophys. Res.*, 113, D06113, doi:10.1029/2007JD008548, 2008.
- Haines, B., Dunn, C., Kim, J., Bar-Sever, Y., Desai, S., Kuang, D., Franklin, G., Harris, I., Kruizinga, G., Meehan, T., Nandi, S., Nguyen, D., Rogstad, T., Thomas, J. B., Tien, J., Romans, L., Watkins, M., Wu, S. C., Bettadpur, S., and Bertiger, W.: Instrument of GRACE: GPS augments gravity measurements, *GPS World*, 14, 16–28, 2003.
- Houweling, S., Kaminski, T., Dentener, F., Lelieveld, J., and Heinemann, M.: Inverse modeling of methane sources and sinks using adjoint of a global transport model, *J. Geophys. Res.*, 104, 26137–26160, doi:10.1029/1999JD900428, 1999.
- Huffman, G. J., Adler, R. F., Bolvin, D. T., Gu, G., Nelkin, E. J., Bowman, K. P., Hong, Y., Stocker, E. F., and Wolff, D. B.: The TRMM Multisatellite Precipitation Analysis (TMPA): Quasiglobal, multiyear, combined-sensor precipitation estimates at fine scales, *J. Hydrometeorol.*, 8, 3855, doi:10.1175/JHM560.1, 2007.
- Kim, H., Yeh, P. J.-F., Oki, T., and Kanae, S.: Role of rivers in the seasonal variations of terrestrial water storage over global basins, *Geophys. Res. Lett.*, 36, L17402, doi:10.1029/2009GL039006, 2009.
- Koster, R. D., Suarez, M., Ducharme, A., Stieglitz, M., and Kumar, P.: A catchment-based approach to modeling land surface processes in a general circulation model. Part I: Model structure, *J. Geophys. Res.*, 105, 24809–24822, 2000.
- Koster, R. D., Dirmeyer, P. A., Hahmann, A. N., Ijpelaar, R., Tyahla, L., Cox, P., and Suarez, M. J.: Comparing the degree of land-atmosphere interaction in four atmospheric general circulation models, *J. Hydrometeorol.*, 3, 363–375, 2002.
- Knighton, E.: *Fluvial forms and processes: A new perspective*, Edward Arnold, London, 383 pp., 1998.
- Lawrence, D. M. and Slater, A. G.: Incorporating organic soil into a global climate model, *Clim. Dynam.*, 30, 145–160, 2007.
- Laws, K. B., Janowiak, J. E., and Huffman, J. G.: Verification of rainfall estimates over Africa using RFE, NASA MPA-RT and CMORPH, AMS 18th Conference on Hydrology, Seattle, Washington, 2004.
- Lee, H., Durand, M., Jung, H. C., Alsdorf, D., Shum, C. K., and Sheng, Y.: Characterization of surface water storage changes in Arctic lakes using simulated SWOT measurements, *Int. J. Remote Sens.*, 31, 3931–3953, 2010.
- Lehner, B. and Döll, P.: Development and validation of a global database of lakes, 881 reservoirs and wetlands, *J. Hydrol.*, 296, 1–22, 2004.
- Leon, J. G., Calmant, S., Seyler, F., Bonnet, M.-P., Cauhopé, M., Frappart, F., Filizola, N., and Fraizy, P.: Rating curves and estimation of average water depth at the upper Negro River based on satellite altimeter data and modeled discharges, *J. Hydrol.*, 328, 481–496, 2008.
- Leopold, L. B., Wolman, M. G., and Miller, J. P.: *Fluvial Processes in Geomorphology*, W. H. Freeman, New York, 1964.
- Lunetta, R. S., Knight, J. F., Ediriwickrema, J., Lyon, J. G., and Worthy, L. D.: Land-cover change detection using multi-temporal MODIS NDVI data, *Remote Sens. Environ.*, 105, 142–154, 2006.
- Lyon, J. G., Yuan, D., Lunetta, R. S., and Elvidge, C. D.: A change detection experiment using vegetation indices, *Photogramm. Eng. Rem. S.*, 64, 143–150, 1998.
- Mahe, G., Bamba, A., Soumaguel, A., Orange, D., and Olivry, J.-C.: Water losses in the inner delta of the River Niger: water balance and flooded area, *Hydrol. Process.*, 23, 3157–3160, doi:10.1002/hyp.7389, 2009.
- Matthews, E.: *Wetlands, in Atmospheric Methane: Its Role in the Global Environment*, edited by: Khalil, M. A. K., Springer, New York, 202–233, 2000.
- Meynadier, R., Bock, O., Guichard, F., Boone, A., Roucou, P., and Redelsperger, J.-L.: The West African Monsoon water cycle. Part I: a hybrid water budget dataset, *J. Geophys. Res.*, 115, D19106, doi:10.1029/2010JD013917, 2010.
- Miller, J. R., Russell, G. L., and Caliri, G.: Continental scale river flow in climate models, *J. Climate*, 7, 914–928, doi:10.1175/1520-0442(1994)007<0914:CSRFC<sub>2</sub>.0.CO;2, 1994.

- Molod, A., Salmun, H., and Waugh, D.: The Impact on a GCM Climate of an Extended Mosaic Technique for the Land – Atmosphere Coupling, *J. Climate*, 17, 3877–3891, 2004.
- Moody, J. A. and Troutman, B. M.: Characterization of the spatial variability of channel morphology, *Earth Surf. Proc. Land.*, 27, 1251–1266, 2002.
- Noilhan, J. and Planton, S.: A simple parameterization of land surface processes for meteorological models, *Mon. Weather Rev.*, 117, 536–549, doi:10.1175/1520-0493(1989)117;0536:ASPOLS<sub>2</sub>.0.CO;2, 1989.
- Oki, T. and Sud, Y. C.: Design of total runoff integrating pathways (TRIP), *Earth Interact.*, 2, 136, doi:10.1175/1087-3562(1998)002;0001:DOTRIP<sub>2</sub>.3.CO;2, 1998.
- Oki, T., Nishimura, T., and Dirmeyer, P.: Assessment of annual runoff from land surface models using Total Runoff Integrating Pathways (TRIP), *J. Meteorol. Soc. Jpn.*, 77, 235–255, 1999.
- Papa, F., Guntner, A., Frappart, F., Prigent, C., and Rossow, W. B.: Variations of surface water extent and water storage in large river basins: A comparison of different global data sources, *Geophys. Res. Lett.*, 35, L11401, doi:10.1029/2008GL033857, 2008.
- Papa, F., Durand, F., Rossow, W. B., Rahman, A., and Bala, S. K.: Satellite altimeter derived monthly discharge of the Ganga Brahmaputra River and its seasonal to interannual variations from 1993 to 2008, *J. Geophys. Res.*, 115, C12013, doi:10.1029/2009JC006075, 2010a.
- Papa, F., Prigent, C., Aires, F., Jimenez, C., Rossow, W. B., and Matthews, E.: Interannual variability of surface water extent at the global scale, 1993–2004, *J. Geophys. Res.-Atmos.*, 115, D12111, doi:10.1029/2009JD012674, 2010b.
- Pierre, C., Bergametti, G., Marticorena, B., Mougin, E., Lebel, T., and Ali, A.: Pluriannual comparisons of satellite based rainfall products over the Sahelian belt for seasonal vegetation modelling, *J. Geophys. Res.*, 116, D18201, doi:10.1029/2011JD016115, 2011.
- Portmann F. T., Siebert, S., and Döll, P.: Global monthly irrigated and rainfed crop areas 926 around the year 2000: A new high-resolution data set for agricultural and hydrological 927 modeling. *Global Biogeochem. Cy.*, 24, GB1011, doi:10.1029/2008GB003435, 2010.
- Prigent, C., Matthews, E., Aires, F., and Rossow, W. B.: Remote sensing of global wetland dynamics with multiple satellite data set, *Geophys. Res. Lett.*, 28, 4631–4634, 2001.
- Prigent, C., Papa, F., Aires, F., Rossow, W. B., and Matthews, E.: Global inundation dynamics inferred from multiple satellite observations, 1993–2000, *J. Geophys. Res.*, 112, D12107, doi:10.1029/2006JD007847, 2007.
- Redelsperger, J.-L., Thorncroft, C. D., Diedhiou, A., Lebel, T., Parker, D. J., and Polcher, J.: African Monsoon Multidisciplinary Analysis: An international research project and field campaign, *B. Am. Meteorol. Soc.*, 87, 1739–1746, 2006.
- Roddel, M., Velicogna, I., and Famiglietti, J. S.: Satellite-based estimates of groundwater depletion in India, *Nature*, 460, 999–1003, doi:10.1038/nature08238, 2009.
- Rodriguez, E.: SWOT science requirements Document, JPL document, Initial release, 2009.
- Rodriguez, E. and Moller, D.: Measuring surface water from space, *Eos Trans. AGU*, 85, Fall Meet. Suppl., Abstract H22C-08, 2004.
- Sausen, R., Schubert, S., and Dumenil, L.: A model of river runoff for use in coupled atmosphere ocean models, *J. Hydrol. Amsterdam*, 155, 337–352, doi:10.1016/0022-1694(94)90177-5, 1994.
- Sheffield, J., Goteti, G., and Wood, E. F.: Development of a 50-year high-resolution global data set of meteorological forcings for land surface modeling, *J. Climate*, 19, 3088–3111, 2006.
- Swenson, S., Wahr, J., and Milly, P.: Estimated accuracies of regional water storage variations inferred from the Gravity Recovery and Climate Experiment (GRACE), *Water Resour. Res.*, 39, 1223, doi:10.1029/2002WR001808, 2003.
- Tapley, B. D., Bettadpur, S., Ries, J. C., Thompson, P. F., and Watkins, M. M.: GRACE measurements of mass variability in the Earth system, *Science*, 305, 503–505, 2004.
- Taylor, C. M.: Feedbacks on precipitation from an African wetland, *Geophys. Res. Lett.*, 37, L05406, doi:10.1029/2009GL041652, 2010.
- Taylor, C. M., Gounou, A., Guichard, F., Harris, P. P., Ellis, R. J., Couvreur, F., and De Cauwe, M.: Frequency of Sahelian storm initiation enhanced over mesoscale soil-moisture patterns, *Nat. Geosci.*, 4, 430–433, doi:10.1038/ngeo1173, 2011.
- Verdin, K. L. and Greenlee, S. K.: Development of continental scale digital elevation models and extraction of hydrographic features, in: *Proceedings, Third International Conference/Workshop on Integrating GIS and Environmental Modeling*, Santa Fe, New Mexico, 21–26 January 1996, National Center for Geographic Information and Analysis, Santa Barbara, California, 1996.
- Vergnes, J.-P., Decharme, B., Alkama, R., Martin, E., Habets, F., and Douville, H.: A Simple Groundwater Scheme for Hydrological and Climate Applications: Description and Off-line Evaluation over France, *J. Hydrometeorol.*, online first: doi:10.1175/JHM-D-11-0149.1, 2012.
- Vermote, E., El Sallouss, N., and Justice, C. O.: Atmospheric correction of MODIS data in the visible to near infrared: first results, *Remote Sens. Environ.*, 83, 97–111, 2002.
- Vorosmarty, C. J., Moore III, B., Grace, A. L., Gildea, M. P., Melillo, J. M., Peterson, B. J., Rastetter, E. B., and Steudler, P. A.: Continental scale models of water balance and fluvial transport: An application to South America, *Global Biogeochem. Cy.*, 3, 241–265, doi:10.1029/GB003i003p00241, 1989.
- Wahr, J., Swenson, S., Zlotnicki, V., and Velicogna, I.: Time-variable gravity from GRACE: First results, *Geophys. Res. Lett.*, 31, L11501, doi:10.1029/2004GL019779, 2004.
- Wigneron, J. P., Calvet, J. C., Pellarin, T., Van de Griend, A., Berger, M., and Ferrazzoli, P.: Retrieving near-surface soil moisture from microwave radiometric observations: current status and future plans, *Remote Sens. Environ.*, 85, 489–506, 2003.
- Yamazaki, D., Oki, T., and Kanae, S.: Deriving a global river network map and its sub-grid topographic characteristics from a fine-resolution flow direction map, *Hydrol. Earth Syst. Sci.*, 13, 2241–2251, doi:10.5194/hess-13-2241-2009, 2009.
- Yamazaki, D., Kanae, S., Kim, H., and Oki, T.: A physically-based description of floodplain inundation dynamics in a global river routing model. *Water Resour. Res.* 47, W04501, doi:10.1029/2010WR009726, 2011.
- Zagona, E. A., Fulp, T. J., Shane, R., Magee, T., and Goranflo, H. M.: RiverWare: A generalized tool for complex reservoir system modeling, doi:10.1111/j.1752-1688.2001.tb05522.x, 2001.

# Bibliography

- [Adler *et al.* 2000] Adler R. F., G. J. Huffman, D. T. Bolvin, S. Curtis and E. J. Nelkin. *Tropical Rainfall Distributions Determined Using TRMM Combined with Other Satellite and Rain Gauge Information*. Journal of Applied Meteorology, vol. 39, no. 12, pages 2007–2023, 2000.
- [Al Nakshabandi & Kohnke 1965] Al Nakshabandi G. and H. Kohnke. *Thermal conductivity and diffusivity of soils as related to moisture tension and other physical properties*. Agricultural Meteorology, vol. 2, pages 271–279, 1965.
- [Alapaty *et al.* 1997] Alapaty K., J. E. Pleim, S. Raman, D. S. Niyogi and D. W. Byun. *Simulation of Atmospheric Boundary Layer Processes Using Local and Nonlocal-Closure Schemes*. Journal of Applied Meteorology, vol. 36, no. 3, pages 214–233, 1997.
- [Ali & Lebel 2009] Ali A. and T. Lebel. *The Sahelian standardized rainfall index revisited*. International Journal of Climatology, vol. 29, no. 12, pages 1705–1714, 2009.
- [Alkama *et al.* 2008] Alkama R., M. Kageyama, G. Ramstein, O. Marti, P. Ribstein and D. Swingedouw. *Impact of a realistic river routing in coupled ocean–atmosphere simulations of the Last Glacial Maximum climate*. Climate Dynamics, vol. 30, no. 7–8, pages 855–869, 2008.
- [Alkama *et al.* 2010] Alkama R., B. Decharme, H. Douville, M. Becker, A. Cazenave, J. Sheffield, A. Voldoire, S. Tyteca and P. Le Moigne. *Global Evaluation of the ISBA-TRIP Continental Hydrological System. Part I: Comparison to GRACE Terrestrial Water Storage Estimates and In Situ River Discharges*. Journal of Hydrometeorology, vol. 11, no. 3, pages 583–600, 2010.
- [Alpatev 1954] Alpatev A. Moisture exchange in cultivated crops. Gidrometeoizdat édition, 1954.
- [Alsdorf *et al.* 2007] Alsdorf D. E., E. Rodríguez and D. P. Lettenmaier. *Measuring surface water from space*. Reviews of Geophysics, vol. 45, no. 2, 2007.
- [Alsdorf 2003] Alsdorf D. E. *Tracking Fresh Water from Space*. Science, vol. 301, no. 5639, pages 1491–1494, 2003.

- [Amogu *et al.* 2010] Amogu O., L. Descroix, K. S. Yéro, E. Le Breton, I. Mammadou, A. Ali, T. Vischel, J.-C. Bader, I. B. Moussa, E. Gautier, S. Boubkraoui and P. Belleudy. *Increasing River Flows in the Sahel?* Water, vol. 2, no. 2, pages 170–199, 2010.
- [Andersen *et al.* 2002] Andersen J., I. Sandholt, K. H. Jensen, J. C. Refsgaard and H. Gupta. *Perspectives in using a remotely sensed dryness index in distributed hydrological models at the river-basin scale.* Hydrological Processes, vol. 16, no. 15, pages 2973–2987, 2002.
- [Andersen *et al.* 2005] Andersen I., O. Dione, M. Jarosewich-Holder and J.-C. Olivry. *The niger river basin: A vision for sustainable management.* World Bank, Washington, DC, 2005.
- [Andreadis *et al.* 2007] Andreadis K. M., E. A. Clark, D. P. Lettenmaier and D. E. Alsdorf. *Prospects for river discharge and depth estimation through assimilation of swath-altimetry into a raster-based hydrodynamics model.* Geophysical Research Letters, vol. 34, no. 10, 2007.
- [André *et al.* 1986] André J.-C., J.-P. Goutorbe and A. Perrier. *HAPEX - MOBILHY: A Hydrologic Atmospheric Experiment for the Study of Water Budget and Evaporation Flux at the Climatic Scale.* Bulletin of the American Meteorological Society, vol. 67, no. 2, pages 138–144, 1986.
- [Arora & Boer 1999] Arora V. K. and G. J. Boer. *A variable velocity flow routing algorithm for GCMs.* Journal of Geophysical Research, vol. 104, no. D24, page 30965, 1999.
- [Arora 2002] Arora V. *Modeling vegetation as a dynamic component in soil-vegetation-atmosphere transfer schemes and hydrological models.* Reviews of Geophysics, vol. 40, no. 2, page 1006, 2002.
- [Avisar & Pielke 1989] Avisar R. and R. A. Pielke. *A Parameterization of Heterogeneous Land Surfaces for Atmospheric Numerical Models and Its Impact on Regional Meteorology.* Monthly Weather Review, vol. 117, no. 10, pages 2113–2136, 1989.
- [Barbé & Lebel 1997] Barbé L. L. and T. Lebel. *Rainfall climatology of the HAPEX-Sahel region during the years 1950–1990.* Journal of Hydrology, vol. 188–189, pages 43–73, 1997.
- [Barnett *et al.* 1989] Barnett T. P., L. Dümenil, U. Schlese, E. Roeckner and M. Latif. *The Effect of Eurasian Snow Cover on Regional and Global Climate Variations.* Journal of the Atmospheric Sciences, vol. 46, no. 5, pages 661–686, 1989.

- [Bergkamp 1998] Bergkamp G. *A hierarchical view of the interactions of runoff and infiltration with vegetation and microtopography in semiarid shrublands*. CATENA, vol. 33, no. 3-4, pages 201–220, 1998.
- [Betts *et al.* 1997] Betts R. A., P. M. Cox, S. E. Lee and F. I. Woodward. *Contrasting physiological and structural vegetation feedbacks in climate change simulations*. , Published online: 19 June 1997; | doi:10.1038/42924, vol. 387, no. 6635, pages 796–799, 1997.
- [Beven & Kirkby 1979] Beven K. and M. Kirkby. *A physically-based variable contributing area model of basin hydrology*. Hydrological Sciences Bulletin, vol. 24, no. 1, pages 43–69, 1979.
- [Bhumralkar 1975] Bhumralkar C. M. *Numerical Experiments on the Computation of Ground Surface Temperature in an Atmospheric General Circulation Model*. Journal of Applied Meteorology, vol. 14, no. 7, pages 1246–1258, 1975.
- [Biancamaria *et al.* 2010] Biancamaria S., K. M. Andreadis, M. Durand, E. A. Clark, E. Rodriguez, N. M. Mognard, D. E. Alsdorf, D. P. Lettenmaier and Y. Oudin. *Preliminary Characterization of SWOT Hydrology Error Budget and Global Capabilities*. IEEE Journal of Selected Topics in Applied Earth Observations and Remote Sensing, vol. 3, no. 1, pages 6–19, 2010.
- [Biancamaria *et al.* 2011] Biancamaria S., M. Durand, K. Andreadis, P. Bates, A. Boone, N. Mognard, E. Rodríguez, D. Alsdorf, D. Lettenmaier and E. Clark. *Assimilation of virtual wide swath altimetry to improve Arctic river modeling*. Remote Sensing of Environment, vol. 115, no. 2, pages 373–381, 2011.
- [Blackadar 1976] Blackadar A. *Modeling Nocturnal Boundary-Layer*. Bulletin of the American Meteorological Society, vol. 57, no. 5, pages 631–631, 1976.
- [Bock *et al.* 2011] Bock O., F. Guichard, R. Meynadier, S. Gervois, A. Agustí-Panareda, A. Beljaars, A. Boone, M. Nuret, J.-L. Redelsperger and P. Roucou. *The large-scale water cycle of the West African monsoon*. Atmospheric Science Letters, vol. 12, no. 1, pages 51–57, 2011.
- [Bonan 1995] Bonan G. B. *Sensitivity of a GCM Simulation to Inclusion of Inland Water Surfaces*. Journal of Climate, vol. 8, no. 11, pages 2691–2704, 1995.

- [Boone & Etchevers 2001] Boone A. and P. Etchevers. *An Intercomparison of Three Snow Schemes of Varying Complexity Coupled to the Same Land Surface Model: Local-Scale Evaluation at an Alpine Site*. Journal of Hydrometeorology, vol. 2, no. 4, pages 374–394, 2001.
- [Boone & Wetzel 1996] Boone A. and P. J. Wetzel. *Issues related to low resolution modeling of soil moisture: experience with the PLACE model*. Global and Planetary Change, vol. 13, no. 1-4, pages 161–181, 1996.
- [Boone *et al.* 1999] Boone A., J.-C. Calvet and J. Noilhan. *Inclusion of a Third Soil Layer in a Land Surface Scheme Using the Force-Restore Method*. Journal of Applied Meteorology, vol. 38, no. 11, pages 1611–1630, 1999.
- [Boone *et al.* 2000] Boone A., V. Masson, T. Meyers and J. Noilhan. *The Influence of the Inclusion of Soil Freezing on Simulations by a Soil-Vegetation-Atmosphere Transfer Scheme*. Journal of Applied Meteorology, vol. 39, no. 9, pages 1544–1569, 2000.
- [Boone *et al.* 2004] Boone A., F. Habets, J. Noilhan, D. Clark, P. Dirmeyer, S. Fox, Y. Gusev, I. Haddeland, R. Koster, D. Lohmann, S. Mahanama, K. Mitchell, O. Nasonova, G.-Y. Niu, A. Pitman, J. Polcher, A. B. Shmakin, K. Tanaka, B. van den Hurk, S. V erant, D. Verseghy, P. Viterbo and Z.-L. Yang. *The Rh one-Aggregation Land Surface Scheme Intercomparison Project: An Overview*. Journal of Climate, vol. 17, no. 1, pages 187–208, 2004.
- [Boone *et al.* 2009a] Boone A., A. C. V. Getirana, J. Demarty, B. Cappelaere, S. Galle, M. Grippa, T. Lebel, E. Mougin, C. Peugeot and T. Vischel. *AMMA Land Surface Model Intercomparison Project Phase 2 (ALMIP-2)*. Gewex News, 2009.
- [Boone *et al.* 2009b] Boone A., B. Decharme, F. Guichard, P. de Rosnay, G. Balsamo, A. Beljaars, F. Chopin, T. Orgeval, J. Polcher, C. Delire, A. Ducharne, S. Gascoin, M. Grippa, L. Jarlan, L. Kergoat, E. Mougin, Y. Gusev, O. Nasonova, P. Harris, C. Taylor, A. Norgaard, I. Sandholt, C. Ottl e, I. Poccard-Leclercq, S. Saux-Picart and Y. Xue. *The AMMA Land Surface Model Intercomparison Project (ALMIP)*. Bulletin of the American Meteorological Society, vol. 90, no. 12, pages 1865–1880, 2009.
- [Boone *et al.* 2010] Boone A. A., I. Poccard-Leclercq, Y. Xue, J. Feng and P. Rosnay. *Evaluation of the WAMME model surface fluxes using results from the AMMA land-surface model intercomparison project*. Climate Dynamics, vol. 35, no. 1, pages 127–142, 2010.

- [Bosilovich & Sun 1995] Bosilovich M. G. and W.-Y. Sun. *Formulation and verification of a land surface parameterization for atmospheric models*. Boundary-Layer Meteorology, vol. 73, no. 4, pages 321–341, 1995.
- [Bousquet *et al.* 2006] Bousquet P., P. Ciais, J. B. Miller, E. J. Dlugokencky, D. A. Hauglustaine, C. Prigent, G. R. Van der Werf, P. Peylin, E.-G. Brunke, C. Carouge, R. L. Langenfelds, J. Lathière, F. Papa, M. Ramonet, M. Schmidt, L. P. Steele, S. C. Tyler and J. White. *Contribution of anthropogenic and natural sources to atmospheric methane variability*. Nature, vol. 443, no. 7110, pages 439–443, 2006.
- [Bouttier & Courtier ] Bouttier F. and P. Courtier. *Data assimilation concepts and methods*.
- [Braud *et al.* 1993] Braud I., J. Noilhan, P. Bessemoulin, P. Mascart, R. Haverkamp and M. Vauclin. *Bare-ground surface heat and water exchanges under dry conditions: Observations and parameterization*. Boundary-Layer Meteorology, vol. 66, no. 1-2, pages 173–200, 1993.
- [Brooks & Corey 1966] Brooks R. and A. Corey. *Properties of Porous Media Affecting Fluid Flow*. Journal of the Irrigation and Drainage Division, vol. 92, no. 2, pages 61–90, 1966.
- [Budyko 1958] Budyko M. I. The heat balance of the earth's surface. U.S. Dept. of Commerce, Weather Bureau, 1958.
- [Buermann *et al.* 2001] Buermann W., J. Dong, X. Zeng, R. B. Myneni and R. E. Dickinson. *Evaluation of the Utility of Satellite-Based Vegetation Leaf Area Index Data for Climate Simulations*. Journal of Climate, vol. 14, no. 17, pages 3536–3550, 2001.
- [Buis *et al.* 2006] Buis S., A. Piacentini and D. Declat. *PALM: a computational framework for assembling high-performance computing applications*. Concurrency and Computation-Practice & Experience, vol. 18, no. 2, pages 231–245, 2006.
- [Calmant *et al.* 2008] Calmant S., F. Seyler and J. F. Cretaux. *Monitoring Continental Surface Waters by Satellite Altimetry*. Surveys in Geophysics, vol. 29, no. 4-5, pages 247–269, 2008.
- [Calvet & Soussana 2001] Calvet J.-C. and J.-F. Soussana. *Modelling CO<sub>2</sub>-enrichment effects using an interactive vegetation SVAT scheme*. Agricultural and Forest Meteorology, vol. 108, no. 2, pages 129–152, 2001.

- [Calvet *et al.* 1998] Calvet J.-C., J. Noilhan and P. Bessemoulin. *Retrieving the Root-Zone Soil Moisture from Surface Soil Moisture or Temperature Estimates: A Feasibility Study Based on Field Measurements*. Journal of Applied Meteorology, vol. 37, no. 4, pages 371–386, 1998.
- [Campo *et al.* 2006] Campo L., F. Caparrini and F. Castelli. *Use of multi-platform, multi-temporal remote-sensing data for calibration of a distributed hydrological model: an application in the Arno basin, Italy*. Hydrological Processes, vol. 20, no. 13, pages 2693–2712, 2006.
- [Casenave & Valentin 1992] Casenave A. and C. Valentin. *A runoff capability classification system based on surface features criteria in semi-arid areas of West Africa*. Journal of Hydrology, vol. 130, no. 1-4, pages 231–249, 1992.
- [Charney *et al.* 1975] Charney J., P. H. Stone and W. J. Quirk. *Drought in the Sahara: A Biogeophysical Feedback Mechanism*. Science, vol. 187, no. 4175, pages 434–435, 1975.
- [Chen & Kumar 2001] Chen J. and P. Kumar. *Topographic Influence on the Seasonal and Interannual Variation of Water and Energy Balance of Basins in North America*. Journal of Climate, vol. 14, no. 9, pages 1989–2014, 2001.
- [Clapp & Hornberger 1978] Clapp R. B. and G. M. Hornberger. *Empirical equations for some soil hydraulic properties*. Water Resources Research, vol. 14, no. 4, page 601, 1978.
- [Coe & Birkett 2004] Coe M. T. and C. Birkett. *Calculation of river discharge and prediction of lake height from satellite radar altimetry: Example for the Lake Chad basin*. Water Resources Research, vol. 40, no. 10, 2004.
- [Coe *et al.* 2008] Coe M. T., M. H. Costa and E. A. Howard. *Simulating the surface waters of the Amazon River basin: impacts of new river geomorphic and flow parameterizations*. Hydrological Processes, vol. 22, no. 14, pages 2542–2553, 2008.
- [Coe 1998] Coe M. T. *A linked global model of terrestrial hydrologic processes: Simulation of modern rivers, lakes, and wetlands*. Journal of Geophysical Research, vol. 103, no. D8, page 8885, 1998.
- [Coe 2000] Coe M. T. *Modeling Terrestrial Hydrological Systems at the Continental Scale: Testing the Accuracy of an Atmospheric GCM*. Journal of Climate, vol. 13, no. 4, pages 686–704, 2000.

- [Cogley 1979] Cogley J. G. *The Albedo of Water as a Function of Latitude*. Monthly Weather Review, vol. 107, no. 6, pages 775–781, 1979.
- [Cohen & Rind 1991] Cohen J. and D. Rind. *The Effect of Snow Cover on the Climate*. Journal of Climate, vol. 4, no. 7, pages 689–706, 1991.
- [Collischonn *et al.* 2008] Collischonn B., W. Collischonn and C. E. Morelli Tucci. *Daily hydrological modeling in the Amazon basin using TRMM rainfall estimates*. Journal of Hydrology, vol. 360, no. 1-4, pages 207–216, 2008.
- [Costa & Foley 1997] Costa M. H. and J. A. Foley. *Water balance of the Amazon Basin: Dependence on vegetation cover and canopy conductance*. Journal of Geophysical Research, vol. 102, no. D20, page 23973, 1997.
- [Cox *et al.* 1999] Cox P. M., R. A. Betts, C. B. Bunton, R. L. H. Essery, P. R. Rowntree and J. Smith. *The impact of new land surface physics on the GCM simulation of climate and climate sensitivity*. Climate Dynamics, vol. 15, no. 3, pages 183–203, 1999.
- [Crow & Ryu 2009] Crow W. T. and D. Ryu. *A new data assimilation approach for improving runoff prediction using remotely-sensed soil moisture retrievals*. Hydrol. Earth Syst. Sci., vol. 13, no. 1, pages 1–16, 2009.
- [Dadson *et al.* 2010] Dadson S. J., I. Ashpole, P. Harris, H. N. Davies, D. B. Clark, E. Blyth and C. M. Taylor. *Wetland inundation dynamics in a model of land surface climate: Evaluation in the Niger inland delta region*. Journal of Geophysical Research, vol. 115, no. D23, 2010.
- [Dai & Labadie 2001] Dai T. and J. W. Labadie. *River Basin Network Model for Integrated Water Quantity/Quality Management*. Journal of Water Resources Planning and Management, vol. 127, no. 5, pages 295–305, 2001.
- [de Rosnay *et al.* 2009] de Rosnay P., M. Drusch, A. Boone, G. Balsamo, B. Decharme, P. Harris, Y. Kerr, T. Pellarin, J. Polcher and J.-P. Wigneron. *AMMA Land Surface Model Intercomparison Experiment coupled to the Community Microwave Emission Model: ALMIP-MEM*. Journal of Geophysical Research, vol. 114, no. D5, 2009.
- [Deardorff 1977] Deardorff J. W. *A Parameterization of Ground-Surface Moisture Content for Use in Atmospheric Prediction Models*. Journal of Applied Meteorology, vol. 16, no. 11, pages 1182–1185, 1977.

- [Deardorff 1978] Deardorff J. W. *Efficient prediction of ground surface temperature and moisture, with inclusion of a layer of vegetation*. Journal of Geophysical Research, vol. 83, no. C4, page 1889, 1978.
- [Decharme & Douville 2006] Decharme B. and H. Douville. *Introduction of a sub-grid hydrology in the ISBA land surface model*. Climate Dynamics, vol. 26, no. 1, pages 65–78, 2006.
- [Decharme & Douville 2007] Decharme B. and H. Douville. *Global validation of the ISBA sub-grid hydrology*. Climate Dynamics, vol. 29, no. 1, pages 21–37, 2007.
- [Decharme *et al.* 2006] Decharme B., H. Douville, A. Boone, F. Habets and J. Noilhan. *Impact of an Exponential Profile of Saturated Hydraulic Conductivity within the ISBA LSM: Simulations over the Rhône Basin*. Journal of Hydrometeorology, vol. 7, no. 1, pages 61–80, 2006.
- [Decharme *et al.* 2008] Decharme B., H. Douville, C. Prigent, F. Papa and F. Aires. *A new river flooding scheme for global climate applications: Off-line evaluation over South America*. Journal of Geophysical Research, vol. 113, no. D11, 2008.
- [Decharme *et al.* 2010] Decharme B., R. Alkama, H. Douville, M. Becker and A. Cazenave. *Global Evaluation of the ISBA-TRIP Continental Hydrological System. Part II: Uncertainties in River Routing Simulation Related to Flow Velocity and Groundwater Storage*. Journal of Hydrometeorology, vol. 11, no. 3, pages 601–617, 2010.
- [Decharme *et al.* 2011] Decharme B., R. Alkama, F. Papa, S. Faroux, H. Douville and C. Prigent. *Global off-line evaluation of the ISBA-TRIP flood model*. Climate Dynamics, vol. 38, no. 7-8, pages 1389–1412, 2011.
- [Decharme 2007] Decharme B. *Influence of runoff parameterization on continental hydrology: Comparison between the Noah and the ISBA land surface models*. Journal of Geophysical Research, vol. 112, no. D19, 2007.
- [Delire *et al.* 1997] Delire C., J.-C. Calvet, J. Noilhan, I. Wright, A. Manzi and C. Nobre. *Physical properties of Amazonian soils: A modeling study using the Anglo-Brazilian Amazonian Climate Observation Study data*. Journal of Geophysical Research, vol. 102, no. D25, page 30119, 1997.
- [Descroix *et al.* 2008] Descroix L., J. González Barrios, D. Viramontes, J. Poulenard, E. Anaya, M. Esteves and J. Estrada. *Gully and sheet erosion on subtropical mountain slopes: Their respective roles and the scale effect*. CATENA, vol. 72, no. 3, pages 325–339, 2008.

- [Dewey 1977] Dewey K. *Daily Maximum and Minimum Temperature Forecasts and Influence of Snow Cover*. Monthly Weather Review, vol. 105, no. 12, pages 1594–1597, 1977.
- [Dickinson & Henderson-Sellers 1988] Dickinson R. E. and A. Henderson-Sellers. *Modelling tropical deforestation: A study of GCM land-surface parametrizations*. Quarterly Journal of the Royal Meteorological Society, vol. 114, no. 480, pages 439–462, 1988.
- [Dirmeyer *et al.* 1999] Dirmeyer P. A., A. J. Dolman and N. Sato. *The Pilot Phase of the Global Soil Wetness Project*. Bulletin of the American Meteorological Society, vol. 80, no. 5, pages 851–878, 1999.
- [Dirmeyer *et al.* 2006] Dirmeyer P. A., X. Gao, M. Zhao, Z. Guo, T. Oki and N. Hanasaki. *GSWP-2: Multimodel Analysis and Implications for Our Perception of the Land Surface*. Bulletin of the American Meteorological Society, vol. 87, no. 10, pages 1381–1397, 2006.
- [Dirmeyer 2000] Dirmeyer P. A. *Using a Global Soil Wetness Dataset to Improve Seasonal Climate Simulation*. Journal of Climate, vol. 13, no. 16, pages 2900–2922, 2000.
- [Dirmeyer 2001] Dirmeyer P. A. *Climate Drift in a Coupled Land–Atmosphere Model*. Journal of Hydrometeorology, vol. 2, no. 1, pages 89–100, 2001.
- [Dolman & Gregory 1992] Dolman A. J. and D. Gregory. *The parametrization of rainfall interception in GCMs*. Quarterly Journal of the Royal Meteorological Society, vol. 118, no. 505, pages 455–467, 1992.
- [Douville & Royer 1996a] Douville H. and J.-F. Royer. *Influence of the temperate and boreal forests on the Northern Hemisphere climate in the Météo-France climate model*. Climate Dynamics, vol. 13, no. 1, pages 57–74, 1996.
- [Douville & Royer 1996b] Douville H. and J. F. Royer. *Sensitivity of the Asian summer monsoon to an anomalous Eurasian snow cover within the Météo-France GCM*. Climate Dynamics, vol. 12, no. 7, pages 449–466, 1996.
- [Douville *et al.* 1995] Douville H., J. F. Royer and J. F. Mahfouf. *A new snow parameterization for the Météo-France climate model*. Climate Dynamics, vol. 12, no. 1, pages 21–35, 1995.
- [Douville *et al.* 1999] Douville H., E. Bazile, P. Caille, D. Giard, J. Noilhan, L. Peirone and F. Taillefer. *Global Soil Wetness Project: Forecast and*

- assimilation experiments performed at Meteo-France*. Journal of the Meteorological Society of Japan, vol. 77, no. 1B, pages 305–316, 1999.
- [Douville *et al.* 2000] Douville H., S. Planton, J.-F. Royer, D. B. Stephenson, S. Tyteca, L. Kergoat, S. Lafont and R. A. Betts. *Importance of vegetation feedbacks in doubled-CO<sub>2</sub> climate experiments*. Journal of Geophysical Research, vol. 105, no. D11, page 14841, 2000.
- [Douville 2003] Douville H. *Assessing the Influence of Soil Moisture on Seasonal Climate Variability with AGCMs*. Journal of Hydrometeorology, vol. 4, no. 6, pages 1044–1066, 2003.
- [Douville 2004] Douville H. *Relevance of soil moisture for seasonal atmospheric predictions: Is it an initial value problem?* Climate Dynamics, vol. 22, no. 4, pages 429–446, 2004.
- [Drusch *et al.* 2009] Drusch M., K. Scipal, P. de Rosnay, G. Balsamo, E. Andersson, P. Bougeault and P. Viterbo. *Towards a Kalman Filter based soil moisture analysis system for the operational ECMWF Integrated Forecast System*. Geophysical Research Letters, vol. 36, 2009.
- [Ducharne *et al.* 2000] Ducharne A., R. D. Koster, M. J. Suarez, M. Stieglitz and P. Kumar. *A catchment-based approach to modeling land surface processes in a general circulation model: 2. Parameter estimation and model demonstration*. Journal of Geophysical Research, vol. 105, no. D20, page 24823, 2000.
- [Ducharne *et al.* 2003] Ducharne A., C. Golaz, E. Leblois, K. Laval, J. Polcher, E. Ledoux and G. de Marsily. *Development of a high resolution runoff routing model, calibration and application to assess runoff from the LMD GCM*. Journal of Hydrology, vol. 280, no. 1-4, pages 207–228, 2003.
- [Dunn *et al.* 2003] Dunn C., W. Bertiger, Y. Bar-Sever, S. Desai, B. Haines, D. Kuang, G. Franklin, I. Harris, G. Kruizinga, T. Meehan, S. Nandi, D. Nguyen, T. Rogstad, J. Thomas, J. Tien, L. Romans, M. Watkins, S. Wu, S. Bettadpur and J. Kim. *Application challenge: instrument of GRACE GPS augments gravity measurements*. GPS World, vol. 14, pages 16–28, 2003.
- [Durand *et al.* 2008] Durand M., K. M. Andreadis, D. E. Alsdorf, D. P. Lettenmaier, D. Moller and M. Wilson. *Estimation of bathymetric depth and slope from data assimilation of swath altimetry into a hydrodynamic model*. Geophysical Research Letters, vol. 35, no. 20, 2008.

- [Durand *et al.* 2010] Durand M., E. Rodriguez, D. E. Alsdorf and M. Trigg. *Estimating River Depth From Remote Sensing Swath Interferometry Measurements of River Height, Slope, and Width*. IEEE Journal of Selected Topics in Applied Earth Observations and Remote Sensing, vol. 3, no. 1, pages 20–31, 2010.
- [Dümenil & Todini 1992] Dümenil L. and E. Todini. *A rainfall-runoff scheme for use in the Hamburg climate model*. In Advances in Theoretical Hydrology: A Tribute to James Dooge, volume 1 of *European Geophysical Society Series on Hydrological Sciences*, pages 129–157. Elsevier Science, Amsterdam, J.P. O’Kane édition, 1992.
- [d’Orgeval & Polcher 2007] d’Orgeval T. and J. Polcher. *Impacts of precipitation events and land-use changes on West African river discharges during the years 1951–2000*. Climate Dynamics, vol. 31, no. 2-3, pages 249–262, 2007.
- [Enjolras & Rodriguez 2009] Enjolras V. and E. Rodriguez. *Using Altimetry Waveform Data and Ancillary Information From SRTM, Landsat, and MODIS to Retrieve River Characteristics*. IEEE Transactions on Geoscience and Remote Sensing, vol. 47, no. 6, pages 1869–1881, 2009.
- [Entekhabi & Eagleson 1989] Entekhabi D. and P. S. Eagleson. *Land Surface Hydrology Parameterization for Atmospheric General Circulation models Including Subgrid Scale Spatial Variability*. Journal of Climate, vol. 2, no. 8, pages 816–831, 1989.
- [Essery *et al.* 2003] Essery R. L. H., M. J. Best, R. A. Betts, P. M. Cox and C. M. Taylor. *Explicit Representation of Subgrid Heterogeneity in a GCM Land Surface Scheme*. Journal of Hydrometeorology, vol. 4, no. 3, pages 530–543, 2003.
- [Etchevers *et al.* 2001] Etchevers P., Y. Durand, F. Habets, E. Martin and J. Noilhan. *Impact of spatial resolution on the hydrological simulation of the Durance high-Alpine catchment, France*. Annals of Glaciology, vol. 32, no. 1, pages 87–92, 2001.
- [Evensen 2004] Evensen G. *Sampling strategies and square root analysis schemes for the EnKF*. Ocean Dynamics, vol. 54, no. 6, pages 539–560, 2004.
- [Famiglietti & Wood 1994a] Famiglietti J. S. and E. F. Wood. *Application of multiscale water and energy balance models on a tallgrass prairie*. Water Resources Research, vol. 30, no. 11, page 3079, 1994.

- [Famiglietti & Wood 1994b] Famiglietti J. S. and E. F. Wood. *Multiscale modeling of spatially variable water and energy balance processes*. Water Resources Research, vol. 30, no. 11, page 3061, 1994.
- [Fan *et al.* 1996] Fan Y., E. E. Wood, M. L. Baeck and J. A. Smith. *Fractional Coverage of Rainfall Over a Grid: Analyses of NEXRAD Data Over the Southern Plains*. Water Resources Research, vol. 32, no. 9, page 2787, 1996.
- [Farr *et al.* 2007] Farr T. G., P. A. Rosen, E. Caro, R. Crippen, R. Duren, S. Hensley, M. Kobrick, M. Paller, E. Rodriguez, L. Roth, D. Seal, S. Shaffer, J. Shimada, J. Umland, M. Werner, M. Oskin, D. Burbank and D. Alsdorf. *The Shuttle Radar Topography Mission*. Reviews of Geophysics, vol. 45, no. 2, 2007.
- [Foley *et al.* 1996] Foley J. A., I. C. Prentice, N. Ramankutty, S. Levis, D. Pollard, S. Sitch and A. Haxeltine. *An integrated biosphere model of land surface processes, terrestrial carbon balance, and vegetation dynamics*. Global Biogeochemical Cycles, vol. 10, no. 4, page 603, 1996.
- [Fontes *et al.* 1991] Fontes J.-C., J. N. Andrews, W. M. Edmunds, A. Guerre and Y. Travi. *Paleorecharge by the Niger River (Mali) Deduced From Groundwater Geochemistry*. Water Resources Research, vol. 27, no. 2, pages 199–214, 1991.
- [Fouilloux & Piacentini 1999] Fouilloux A. and A. Piacentini. *The PALM project: MPMD paradigm for an oceanic data assimilation software*. In Amestoy P., P. Berger, M. Dayde, I. Duff, V. Frayssé, L. Giraud and D. Ruiz, editeurs, Euro-Par'99: Parallel Processing, volume 1685, pages 1423–1430. Springer-Verlag Berlin, Berlin, 1999.
- [Frey & Smith 2007] Frey K. E. and L. C. Smith. *How well do we know northern land cover? Comparison of four global vegetation and wetland products with a new ground-truth database for West Siberia*. Global Biogeochemical Cycles, vol. 21, no. 1, 2007.
- [Fritsch 1992] Fritsch J.-M. *Les effets du défrichement de la forêt amazonienne et de la mise en culture sur l'hydrologie de petits bassins versants : opération ECEREX [écoulements, érosion, expérimentation] en Guyane française*. PhD thesis, Ed. de l'ORSTOM, Paris, 1992.
- [Fu & Rodriguez 2004] Fu L.-L. and E. Rodriguez. *High-resolution measurement of ocean surface topography by radar interferometry for oceanographic and*

- geophysical applications*. In Sparks R. S. J. and C. J. Hawkesworth, editors, Geophysical Monograph Series, volume 150, pages 209–224. American Geophysical Union, Washington, D. C., 2004.
- [Gadd & Keers 1970] Gadd A. J. and J. F. Keers. *Surface exchanges of sensible and latent heat in a 10-level model atmosphere*. Quarterly Journal of the Royal Meteorological Society, vol. 96, no. 408, pages 297–308, 1970.
- [Garratt 1993] Garratt J. R. *Sensitivity of Climate Simulations to Land-Surface and Atmospheric Boundary-Layer Treatments-A Review*. Journal of Climate, vol. 6, no. 3, pages 419–448, 1993.
- [Gedney & Cox 2003] Gedney N. and P. M. Cox. *The Sensitivity of Global Climate Model Simulations to the Representation of Soil Moisture Heterogeneity*. Journal of Hydrometeorology, vol. 4, no. 6, pages 1265–1275, 2003.
- [Gedney *et al.* 2000] Gedney N., P. M. Cox, H. Douville, J. Polcher and P. J. Valdes. *Characterizing GCM Land Surface Schemes to Understand Their Responses to Climate Change*. Journal of Climate, vol. 13, no. 17, pages 3066–3079, 2000.
- [Geiger *et al.* 2008] Geiger B., C. Meurey, D. Lajas, L. Franchistéguy, D. Carrer and J.-L. Roujean. *Near real-time provision of downwelling shortwave radiation estimates derived from satellite observations*. Meteorological Applications, vol. 15, no. 3, pages 411–420, 2008.
- [Gelb 1974] Gelb A. Applied optimal estimation. The MIT Press, 1974.
- [Getirana *et al.* 2010] Getirana A. C. V., M.-P. Bonnet, O. C. Rotunno Filho, W. Collischonn, J.-L. Guyot, F. Seyler and W. J. Mansur. *Hydrological modelling and water balance of the Negro River basin: evaluation based on in situ and spatial altimetry data*. Hydrological Processes, vol. 24, no. 22, pages 3219–3236, 2010.
- [Getirana 2010] Getirana A. C. *Integrating spatial altimetry data into the automatic calibration of hydrological models*. Journal of Hydrology, vol. 387, no. 3–4, pages 244–255, 2010.
- [Giard & Bazile 2000] Giard D. and E. Bazile. *Implementation of a New Assimilation Scheme for Soil and Surface Variables in a Global NWP Model*. Monthly Weather Review, vol. 128, no. 4, pages 997–1015, 2000.

- [Giordani *et al.* 1996] Giordani H., J. Noilhan, P. Lacarrère, P. Bessemoulin and P. Mascart. *Modelling the surface processes and the atmospheric boundary layer for semi-arid conditions*. Agricultural and Forest Meteorology, vol. 80, no. 2-4, pages 263–287, 1996.
- [Gounou *et al.* 2012] Gounou A., F. Guichard and F. Couvreux. *Observations of Diurnal Cycles Over a West African Meridional Transect: Pre-Monsoon and Full-Monsoon Seasons*. Boundary-Layer Meteorology, vol. 144, no. 3, pages 329–357, 2012.
- [Goutorbe *et al.* 1997] Goutorbe J. P., J. Noilhan, P. Lacarrere and I. Braud. *Modelling of the atmospheric column over the central sites during HAPEX-Sahel*. Journal of Hydrology, vol. 189, no. 1-4, pages 1017–1039, 1997.
- [Grippa *et al.* 2004] Grippa M., N. Mognard, T. Le Toan and E. Josberger. *Siberia snow depth climatology derived from SSM/I data using a combined dynamic and static algorithm*. Remote Sensing of Environment, vol. 93, no. 1-2, pages 30–41, 2004.
- [Grippa *et al.* 2011] Grippa M., L. Kergoat, F. Frappart, Q. Araud, A. Boone, P. de Rosnay, J.-M. Lemoine, S. Gascoin, G. Balsamo, C. Ottlé, B. Decharme, S. Saux-Picart and G. Ramillien. *Land water storage variability over West Africa estimated by Gravity Recovery and Climate Experiment (GRACE) and land surface models*. Water Resources Research, vol. 47, no. 5, 2011.
- [Habets & Saulnier 2001] Habets F. and G. Saulnier. *Subgrid runoff parameterization*. Physics and Chemistry of the Earth, Part B: Hydrology, Oceans and Atmosphere, vol. 26, no. 5-6, pages 455–459, 2001.
- [Habets *et al.* 1999a] Habets F., J. Noilhan, C. Golaz, J. Goutorbe, P. Lacarrère, E. Leblois, E. Ledoux, E. Martin, C. Ottlé and D. Vidal-Madjar. *The ISBA surface scheme in a macroscale hydrological model applied to the Hapex-Mobilhy area - Part I: Model and database*. Journal of Hydrology, vol. 217, no. 1-2, pages 75–96, 1999.
- [Habets *et al.* 1999b] Habets F., J. Noilhan, C. Golaz, J. Goutorbe, P. Lacarrère, E. Leblois, E. Ledoux, E. Martin, C. Ottlé and D. Vidal-Madjar. *The ISBA surface scheme in a macroscale hydrological model applied to the Hapex-Mobilhy area - Part II: Simulation of streamflows and annual*. Journal of Hydrology, vol. 217, no. 1-2, pages 97–118, 1999.

- [Habets *et al.* 2003] Habets F., A. Boone and J. Noilhan. *Simulation of a Scandinavian basin using the diffusion transfer version of ISBA*. Global and Planetary Change, vol. 38, no. 1-2, pages 137–149, 2003.
- [Habets *et al.* 2008] Habets F., A. Boone, J. L. Champeaux, P. Etchevers, L. Franchistéguy, E. Leblois, E. Ledoux, P. Le Moigne, E. Martin, S. Morel, J. Noilhan, P. Quintana Seguí, F. Rousset-Regimbeau and P. Vienneot. *The SAFRAN-ISBA-MODCOU hydrometeorological model applied over France*. Journal of Geophysical Research, vol. 113, no. D6, 2008.
- [Haines *et al.* 2003] Haines B., C. Dunn, J. Kim, Y. Bar-Sever, S. Desai, D. Kuang, G. Franklin, I. Harris, G. Kruizinga, T. Meehan, S. Nandi, D. Nguyen, T. Rogstad, J. Thomas, J. Tien, L. Romans, M. Watkins, S. Wu, S. Bettadpur and W. Bertiger. *Application challenge: instrument of GRACE GPS augments gravity measurements*. GPS World, 2003.
- [Henderson-Sellers *et al.* 1993] Henderson-Sellers A., Z.-L. Yang and R. E. Dickinson. *The Project for Intercomparison of Land-surface Parameterization Schemes*. Bulletin of the American Meteorological Society, vol. 74, no. 7, pages 1335–1349, 1993.
- [Henderson-Sellers *et al.* 1995] Henderson-Sellers A., A. J. Pitman, P. K. Love, P. Irannejad and T. H. Chen. *The Project for Intercomparison of Land Surface Parameterization Schemes (PILPS): Phases 2 and 3*. Bulletin of the American Meteorological Society, vol. 76, no. 4, pages 489–503, 1995.
- [Henderson-Sellers *et al.* 1996] Henderson-Sellers A., K. McGuffie and A. J. Pitman. *The Project for Intercomparison of Land-surface Parameterization Schemes (PILPS): 1992 to 1995*. Climate Dynamics, vol. 12, no. 12, pages 849–859, 1996.
- [Hourdin *et al.* 2010] Hourdin F., I. Musat, J.-Y. Grandpeix, J. Polcher, F. Guichard, F. Favot, P. Marquet, A. Boone, J.-P. Lafore, J.-L. Redelsperger, P. M. Ruti, A. Dell’aquila, M.-A. Filiberti\*, M. Pham, T. L. Doval, A. K. Traore and H. Gallée. *AMMA-Model Intercomparison Project*. Bulletin of the American Meteorological Society, vol. 91, no. 1, pages 95–104, 2010.
- [Houweling *et al.* 1999] Houweling S., T. Kaminski, F. Dentener, J. Lelieveld and M. Heimann. *Inverse modeling of methane sources and sinks using the adjoint of a global transport model*. Journal of Geophysical Research, vol. 104, no. D21, page 26137, 1999.

- [Huffman *et al.* 2007] Huffman G. J., D. T. Bolvin, E. J. Nelkin, D. B. Wolff, R. F. Adler, G. Gu, Y. Hong, K. P. Bowman and E. F. Stocker. *The TRMM Multisatellite Precipitation Analysis (TMPA): Quasi-Global, Multiyear, Combined-Sensor Precipitation Estimates at Fine Scales*. Journal of Hydrometeorology, vol. 8, no. 1, pages 38–55, 2007.
- [Huneau *et al.* 2011] Huneau F., D. Dakoure, H. Celle-Jeanton, T. Vitvar, M. Ito, S. Traore, N. Compaore, H. Jirakova and P. Le Coustumer. *Flow pattern and residence time of groundwater within the south-eastern Taoudeni sedimentary basin (Burkina Faso, Mali)*. Journal of Hydrology, vol. 409, no. 1-2, pages 423–439, 2011.
- [Jacob 1999] Jacob F. *Utilisation de la teledetection courtes longueurs d'onde et infrarouge thermique a haute resolution spatiale pour l'estimation des flux d'energie a l'echelle de la parcelle agricole*. PhD thesis, Univ. Paul Sabatier - Toulouse III, Toulouse, 1999.
- [Jacobs *et al.* 1996] Jacobs C., B. van den Hurk and H. de Bruin. *Stomatal behaviour and photosynthetic rate of unstressed grapevines in semi-arid conditions*. Agricultural and Forest Meteorology, vol. 80, no. 2-4, pages 111–134, 1996.
- [Jacquemin & Noilhan 1990] Jacquemin B. and J. Noilhan. *Sensitivity study and validation of a land surface parameterization using the HAPEX-MOBILHY data set*. Boundary-Layer Meteorology, vol. 52, no. 1-2, pages 93–134, 1990.
- [Jarvis 1976] Jarvis P. G. *The Interpretation of the Variations in Leaf Water Potential and Stomatal Conductance Found in Canopies in the Field*. Philosophical Transactions of the Royal Society B: Biological Sciences, vol. 273, no. 927, pages 593–610, 1976.
- [Kasahara & Washington 1971] Kasahara A. and W. M. Washington. *General Circulation Experiments with a Six-Layer NCAR Model, Including Orography, Cloudiness and Surface Temperature Calculations*. Journal of the Atmospheric Sciences, vol. 28, no. 5, pages 657–701, 1971.
- [Kasei *et al.* 2009a] Kasei R., B. Diekkrüger and C. Leemhuis. *Drought frequency in the Volta Basin of West Africa*. Sustainability Science, vol. 5, no. 1, pages 89–97, 2009.
- [Kasei *et al.* 2009b] Kasei R., B. Diekkrüger and C. Leemhuis. *Drought frequency in the Volta Basin of West Africa*. Sustainability Science, vol. 5, no. 1, pages 89–97, 2009.

- [Kerr *et al.* 2000] Kerr Y., J. Wigneron, P. Ferrazzoli and P. Waldteufel. *Soil moisture and vegetation biomass retrievals using L band, dual polarised and multi angular radiometric data in preparation of the SMOS mission*. In IGARSS 2000. IEEE 2000 International, volume 3, pages 1244–1246, Honolulu, 2000. IEEE.
- [Kerr *et al.* 2010] Kerr Y., P. Waldteufel, J.-P. Wigneron, S. Delwart, F. Cabot, J. Boutin, M.-J. Escorihuela, J. Font, N. Reul, C. Gruhier, S. Juglea, M. Drinkwater, A. Hahne, M. Martin-Neira and S. Mecklenburg. *The SMOS Mission: New Tool for Monitoring Key Elements of the Global Water Cycle*. Proceedings of the IEEE, vol. 98, no. 5, pages 666–687, 2010.
- [Kim *et al.* 2009] Kim H., P. J.-F. Yeh, T. Oki and S. Kanae. *Role of rivers in the seasonal variations of terrestrial water storage over global basins*. Geophysical Research Letters, vol. 36, no. 17, 2009.
- [Knighton 1998] Knighton D. *Fluvial forms and processes : A new perspective*. Arnold ; Oxford University Press, London; New York, 1998.
- [Kocha *et al.* 2012] Kocha C., J.-P. Lafore, P. Tulet and Y. Seity. *High-resolution simulation of a major West African dust-storm: comparison with observations and investigation of dust impact*. Quarterly Journal of the Royal Meteorological Society, vol. 138, no. 663, pages 455–470, 2012.
- [Koster & Suarez 1992] Koster R. and M. Suarez. *Modeling the Land Surface Boundary in Climate Models as a Composite of Independent Vegetation Stands*. Journal of Geophysical Research-Atmospheres, vol. 97, no. D3, pages 2697–2715, 1992.
- [Koster *et al.* 2000a] Koster R. D., M. J. Suarez, A. Ducharne, M. Stieglitz and P. Kumar. *A catchment-based approach to modeling land surface processes in a general circulation model. Part 1: Model structure*. Journal of Geophysical Research, vol. 105, no. D20, page 24809, 2000.
- [Koster *et al.* 2000b] Koster R. D., M. J. Suarez and M. Heiser. *Variance and Predictability of Precipitation at Seasonal-to-Interannual Timescales*. Journal of Hydrometeorology, vol. 1, no. 1, pages 26–46, 2000.
- [Koster *et al.* 2002] Koster R. D., P. A. Dirmeyer, A. N. Hahmann, R. Ijpelaar, L. Tyahla, P. Cox and M. J. Suarez. *Comparing the Degree of Land-Atmosphere Interaction in Four Atmospheric General Circulation Models*. Journal of Hydrometeorology, vol. 3, no. 3, pages 363–375, 2002.

- [Koster *et al.* 2004] Koster R. D., M. J. Suarez, P. Liu, U. Jambor, A. Berg, M. Kistler, R. Reichle, M. Rodell and J. Famiglietti. *Realistic Initialization of Land Surface States: Impacts on Subseasonal Forecast Skill*. Journal of Hydrometeorology, vol. 5, no. 6, pages 1049–1063, 2004.
- [Lawrence & Slater 2007] Lawrence D. M. and A. G. Slater. *Incorporating organic soil into a global climate model*. Climate Dynamics, vol. 30, no. 2-3, pages 145–160, 2007.
- [Laws *et al.* 2004] Laws K., J. Janowiak and J. Huffman. *Verification of rainfall estimates over Africa using RFE, NASA MPA-RT and CMORPH*. In American Meteorological Society Annual Conference, Seattle, Washington, 2004.
- [Le Gal La Salle *et al.* 2001] Le Gal La Salle C., C. Marlin, C. Leduc, J. Taupin, M. Massault and G. Favreau. *Renewal rate estimation of groundwater based on radioactive tracers  $^3H$ ,  $^{14}C$  in an unconfined aquifer in a semi-arid area, Iullemeden Basin, Niger*. Journal of Hydrology, vol. 254, no. 1-4, pages 145–156, 2001.
- [Lebel *et al.* 2005] Lebel T., J.-L. Redelsperger and C. D. Thorncroft. *AMMA international science plan. Technical report*. Rapport technique, 2005.
- [Lebel *et al.* 2009] Lebel T., B. Cappelaere, S. Galle, N. Hanan, L. Kergoat, S. Levis, B. Vieux, L. Descroix, M. Gosset, E. Mougin, C. Peugeot and L. Seguis. *AMMA-CATCH studies in the Sahelian region of West-Africa: An overview*. Journal of Hydrology, vol. 375, no. 1-2, pages 3–13, 2009.
- [Lebel *et al.* 2010] Lebel T., D. J. Parker, C. Flamant, B. Bourlès, B. Marticorena, E. Mougin, C. Peugeot, A. Diedhiou, J. M. Haywood, J. B. Ngamini, J. Polcher, J.-L. Redelsperger and C. D. Thorncroft. *The AMMA field campaigns: multiscale and multidisciplinary observations in the West African region*. Quarterly Journal of the Royal Meteorological Society, vol. 136, no. S1, pages 8–33, 2010.
- [Leblanc *et al.* 2006] Leblanc M., G. Favreau, S. Tweed, C. Leduc, M. Razack and L. Mofor. *Remote sensing for groundwater modelling in large semiarid areas: Lake Chad Basin, Africa*. Hydrogeology Journal, vol. 15, no. 1, pages 97–100, 2006.
- [Leduc *et al.* 2000] Leduc C., G. Favreau, C. Marlin and M. Dray. *Comparison of recharge estimates for the two largest aquifers in Niger, based on hydrodynamic and isotopic data*. In Dassargues A., editeur, Tracers and

- Modelling in Hydrogeology, volume 262 of *IAHS PUBLICATION*, pages 391–399, Liege, 2000. Int Assoc Hydrological Sciences.
- [Lee *et al.* 2010] Lee H., M. Durand, H. C. Jung, D. Alsdorf, C. K. Shum and Y. Sheng. *Characterization of surface water storage changes in Arctic lakes using simulated SWOT measurements*. International Journal of Remote Sensing, vol. 31, no. 14, pages 3931–3953, 2010.
- [Lehner & Döll 2004] Lehner B. and P. Döll. *Development and validation of a global database of lakes, reservoirs and wetlands*. Journal of Hydrology, vol. 296, no. 1-4, pages 1–22, 2004.
- [Leon *et al.* 2006] Leon J., S. Calmant, F. Seyler, M.-P. Bonnet, M. Cauhopé, F. Frappart, N. Filizola and P. Fraizy. *Rating curves and estimation of average water depth at the upper Negro River based on satellite altimeter data and modeled discharges*. Journal of Hydrology, vol. 328, no. 3–4, pages 481–496, 2006.
- [Leopold *et al.* 1964] Leopold L. B., M. G. Wolman and J. P. Miller. *Fluvial processes in geomorphology*. W.H. Freeman, San Francisco, 1964.
- [Liang & Xie 2001] Liang X. and Z. Xie. *A new surface runoff parameterization with subgrid-scale soil heterogeneity for land surface models*. Advances in Water Resources, vol. 24, no. 9-10, pages 1173–1193, 2001.
- [Liang *et al.* 1994] Liang X., D. P. Lettenmaier, E. F. Wood and S. J. Burges. *A simple hydrologically based model of land surface water and energy fluxes for general circulation models*. Journal of Geophysical Research, vol. 99, no. D7, page 14415, 1994.
- [Liang *et al.* 1996] Liang X., D. P. Lettenmaier and E. F. Wood. *One-dimensional statistical dynamic representation of subgrid spatial variability of precipitation in the two-layer variable infiltration capacity model*. Journal of Geophysical Research, vol. 101, no. D16, page 21403, 1996.
- [Lion 2012] Lion C. *Simulation des données SWOT haute résolution et applications à l'étude de l'estuaire de l'Amazone*. PhD thesis, 2012.
- [Lohmann *et al.* 1998] Lohmann D., D. P. Lettenmaier, X. Liang, E. F. Wood, A. Boone, S. Chang, F. Chen, Y. Dai, C. Desborough, R. E. Dickinson, Q. Duan, M. Ek, Y. M. Gusev, F. Habets, P. Irannejad, R. Koster, K. E. Mitchell, O. N. Nasonova, J. Noilhan, J. Schaake, A. Schlosser, Y. Shao, A. B. Shmakin, D. Verseghy, K. Warrach, P. Wetzler, Y. Xue, Z.-L. Yang

- and Q.-c. Zeng. *The Project for Intercomparison of Land-surface Parameterization Schemes (PILPS) phase 2(c) Red–Arkansas River basin experiment:: 3. Spatial and temporal analysis of water fluxes*. *Global and Planetary Change*, vol. 19, no. 1–4, pages 161–179, 1998.
- [Lu *et al.* 2007] Lu Z., O. Kwoun and R. Rykhus. *Interferometric synthetic aperture radar (InSAR): Its past, present and future*. *Photogrammetric Engineering and Remote Sensing*, vol. 73, no. 3, pages 217–221, 2007.
- [Lunetta *et al.* 2006] Lunetta R. S., J. F. Knight, J. Ediriwickrema, J. G. Lyon and L. D. Worthy. *Land-cover change detection using multi-temporal MODIS NDVI data*. *Remote Sensing of Environment*, vol. 105, no. 2, pages 142–154, 2006.
- [Lutz *et al.* 2009] Lutz A., J. M. Thomas, G. Pohll, M. Keita and W. A. McKay. *Sustainability of groundwater in Mali, West Africa*. *Environmental Geology*, vol. 58, no. 7, pages 1441–1450, 2009.
- [Lyon *et al.* 1998] Lyon J. G., D. Yuan, R. S. Lunetta and C. D. Elvidge. *A change detection experiment using vegetation indices*. *Photogrammetric Engineering and Remote Sensing*, vol. 64, no. 2, pages 143–150, 1998.
- [Mahfouf & Noilhan 1991] Mahfouf J. F. and J. Noilhan. *Comparative Study of Various Formulations of Evaporations from Bare Soil Using In Situ Data*. *Journal of Applied Meteorology*, vol. 30, no. 9, pages 1354–1365, 1991.
- [Mahfouf & Noilhan 1996] Mahfouf J.-F. and J. Noilhan. *Inclusion of Gravitational Drainage in a Land Surface Scheme Based on the Force-Restore Method*. *Journal of Applied Meteorology*, vol. 35, no. 6, pages 987–992, 1996.
- [Mahé *et al.* 2009] Mahé G., F. Bamba, A. Soumaguel, D. Orange and J. C. Olivry. *Water losses in the inner delta of the River Niger: Water balance and flooded area*. *Hydrological Processes*, vol. 23, no. 22, pages 3157–3160, 2009.
- [Maidment 1993] Maidment D. R. *Handbook of hydrology*. McGraw-Hill, New York, 1993.
- [Manabe 1969] Manabe S. *Climate and the Ocean Circulation 1: The Atmospheric Circulation and the Hydrology of the Earth's Surface*. *Monthly Weather Review*, vol. 97, no. 11, pages 739–774, 1969.

- [Mathon *et al.* 2002] Mathon V., H. Laurent and T. Lebel. *Mesoscale convective system rainfall in the Sahel*. Journal of Applied Meteorology, vol. 41, no. 11, pages 1081–1092, 2002.
- [Matthews 2000] Matthews E. Wetlands, in atmospheric methane: Its role in the global environment. M.A.K. Khalil, Springer Verlag, 2000.
- [McCumber & Pielke 1981] McCumber M. C. and R. A. Pielke. *Simulation of the effects of surface fluxes of heat and moisture in a mesoscale numerical model: 1. Soil layer*. Journal of Geophysical Research, vol. 86, no. C10, page 9929, 1981.
- [Meidner & Mansfield 1966] Meidner H. and T. A. Mansfield. *Rates of Photosynthesis and Respiration in Relation to Stomatal Movements in Leaves Treated with -Hydroxysulphonate and Glycollate*. Journal of Experimental Botany, vol. 17, no. 3, pages 502–509, 1966.
- [Meynadier *et al.* 2010] Meynadier R., O. Bock, F. Guichard, A. Boone, P. Roucou and J.-L. Redelsperger. *The West African Monsoon water cycle. Part 1: A hybrid water budget data set*. Journal of Geophysical Research, vol. 115, no. D19, 2010.
- [Milford *et al.* 1996] Milford J., V. McDougall and G. Dugdale. *Rainfall estimation from cold cloud duration : experience of the TAMSAT group in West Africa*. In Guillot B. and Problèmes de Validation des Méthodes d'Estimation des Précipitations par Satellite en Afrique Intertropicale : Atelier = Validation Problems of Rainfall Estimation Methods by Satellite in Intertropical Africa : Workshop, Niamey (NER), 1994/12/01-03, éditeurs, Problèmes de validation des méthodes d'estimation des précipitations par satellite en Afrique intertropicale, Colloques et Séminaires, pages 13–29. ORSTOM, Paris, 1996.
- [Miller *et al.* 1994] Miller J. R., G. L. Russell and G. Caliri. *Continental-Scale River Flow in Climate Models*. Journal of Climate, vol. 7, no. 6, pages 914–928, 1994.
- [Milzow *et al.* 2011] Milzow C., P. E. Krogh and P. Bauer-Gottwein. *Combining satellite radar altimetry, SAR surface soil moisture and GRACE total storage changes for hydrological model calibration in a large poorly gauged catchment*. Hydrology and Earth System Sciences, vol. 15, no. 6, pages 1729–1743, 2011.

- [Mognard 2005] Mognard N. *WatER: The Water Elevation Recovery mission, a proposal to the Earth Explorer program of the European Space Agency*, 2005.
- [Molod *et al.* 2004] Molod A., H. Salmun and D. W. Waugh. *The Impact on a GCM Climate of an Extended Mosaic Technique for the Land-Atmosphere Coupling*. *Journal of Climate*, vol. 17, no. 20, pages 3877–3891, 2004.
- [Montanari *et al.* 2009] Montanari M., R. Hostache, P. Matgen, G. Schumann, L. Pfister and L. Hoffmann. *Calibration and sequential updating of a coupled hydrologic-hydraulic model using remote sensing-derived water stages*. *Hydrology and Earth System Sciences*, vol. 13, no. 3, pages 367–380, 2009.
- [Moody & Troutman 2002] Moody J. A. and B. M. Troutman. *Characterization of the spatial variability of channel morphology*. *Earth Surface Processes and Landforms*, vol. 27, no. 12, pages 1251–1266, 2002.
- [Namias 1985] Namias J. *Some Empirical Evidence for the Influence of Snow Cover on Temperature and Precipitation*. *Monthly Weather Review*, vol. 113, no. 9, pages 1542–1553, 1985.
- [Neal *et al.* 2009] Neal J., G. Schumann, P. Bates, W. Buytaert, P. Matgen and F. Pappenberger. *A data assimilation approach to discharge estimation from space*. *Hydrological Processes*, vol. 23, no. 25, pages 3641–3649, 2009.
- [Nicholson 1980] Nicholson S. E. *The Nature of Rainfall Fluctuations in Sub-tropical West Africa*. *Monthly Weather Review*, vol. 108, no. 4, pages 473–487, 1980.
- [Nicholson 2001] Nicholson S. *Climatic and environmental change in Africa during the last two centuries*. *Climate Research*, vol. 17, pages 123–144, 2001.
- [Nickerson & Smiley 1975] Nickerson E. C. and V. E. Smiley. *Surface Layer and Energy Budget Parameterizations for Mesoscale Models*. *Journal of Applied Meteorology*, vol. 14, no. 3, pages 297–300, 1975.
- [Niu & Yang 2003] Niu G.-Y. and Z.-L. Yang. *The versatile integrator of surface atmospheric processes - Part 2: evaluation of three topography-based runoff schemes*. *Global and Planetary Change*, vol. 38, no. 1-2, pages 191–208, 2003.

- [Niyogi & Raman 1997] Niyogi D. S. and S. Raman. *Comparison of Four Different Stomatal Resistance Schemes Using FIFE Observations*. Journal of Applied Meteorology, vol. 36, no. 7, pages 903–917, 1997.
- [Noilhan & Lacarrère 1995] Noilhan J. and P. Lacarrère. *GCM Grid-Scale Evaporation from Mesoscale Modeling*. Journal of Climate, vol. 8, no. 2, pages 206–223, 1995.
- [Noilhan & Mahfouf 1996] Noilhan J. and J.-F. Mahfouf. *The ISBA land surface parameterisation scheme*. Global and Planetary Change, vol. 13, no. 1-4, pages 145–159, 1996.
- [Noilhan & Planton 1989] Noilhan J. and S. Planton. *A Simple Parameterization of Land Surface Processes for Meteorological Models*. Monthly Weather Review, vol. 117, no. 3, pages 536–549, 1989.
- [Oki & Sud 1998] Oki T. and Y. C. Sud. *Design of Total Runoff Integrating Pathways (TRIP) - A Global River Channel Network*. Earth Interactions, vol. 2, no. 1, pages 1–37, 1998.
- [Oki *et al.* 1999] Oki T., T. Nishimura and P. Dirmeyer. *Assessment of annual runoff from land surface models using Total Runoff Integrating Pathways (TRIP)*. Journal of the Meteorological Society of Japan, vol. 77, no. 1B, pages 235–255, 1999.
- [Olivry *et al.* 1998] Olivry J.-C., J.-P. Bricquet, G. Mahé and Water Resources Variability in Africa during the 20th Century : International Conference, Abidjan (CIV), 1998/11/16-19. *Variabilité de la puissance des crues des grands cours d'eau d'Afrique intertropicale et incidence de la baisse des écoulements de base au cours des deux dernières décennies*. In Servat E., D. Hughes, J.-M. Fritsch and M. Hulme, editeurs, Water resources variability in Africa during the 20th century = Variabilité des ressources en eau en Afrique au 20ème siècle, numéro 252 de Publication - AISH, pages 189–195. AISH, Wallingford, 1998.
- [Orsolini & Kvamstø 2009] Orsolini Y. J. and N. G. Kvamstø. *Role of Eurasian snow cover in wintertime circulation: Decadal simulations forced with satellite observations*. Journal of Geophysical Research, vol. 114, no. D19, 2009.
- [Papa *et al.* 2008] Papa F., A. Güntner, F. Frappart, C. Prigent and W. B. Rossow. *Variations of surface water extent and water storage in large river basins: A comparison of different global data sources*. Geophysical Research Letters, vol. 35, no. 11, 2008.

- [Papa *et al.* 2010a] Papa F., C. Prigent, F. Aires, C. Jimenez, W. B. Rossow and E. Matthews. *Interannual variability of surface water extent at the global scale, 1993–2004*. Journal of Geophysical Research, vol. 115, no. D12, 2010.
- [Papa *et al.* 2010b] Papa F., F. Durand, W. B. Rossow, A. Rahman and S. K. Bala. *Satellite altimeter-derived monthly discharge of the Ganga-Brahmaputra River and its seasonal to interannual variations from 1993 to 2008*. Journal of Geophysical Research, vol. 115, no. C12, 2010.
- [Pauwels & De Lannoy 2006] Pauwels V. R. N. and G. J. M. De Lannoy. *Improvement of Modeled Soil Wetness Conditions and Turbulent Fluxes through the Assimilation of Observed Discharge*. Journal of Hydrometeorology, vol. 7, no. 3, pages 458–477, 2006.
- [Pedinotti *et al.* 2012] Pedinotti V., A. Boone, B. Decharme, J. F. Crétaux, N. Mognard, G. Panthou, F. Papa and B. A. Tanimoun. *Evaluation of the ISBA-TRIP continental hydrologic system over the Niger basin using in situ and satellite derived datasets*. Hydrology and Earth System Sciences, vol. 16, no. 6, pages 1745–1773, 2012.
- [Pellenq 2002] Pellenq J. *Couplage de la modélisation hydrologique avec la modélisation des Transferts Sol-Végétation-Atmosphère Application à la spatialisation et l'assimilation des données du satellite SMOS*. PhD thesis, Univ. Paul Sabatier - Toulouse III, Toulouse, 2002.
- [Pereira-Cardenal *et al.* 2011] Pereira-Cardenal S. J., N. D. Riegels, P. A. M. Berry, R. G. Smith, A. Yakovlev, T. U. Siegfried and P. Bauer-Gottwein. *Real-time remote sensing driven river basin modeling using radar altimetry*. Hydrol. Earth Syst. Sci., vol. 15, no. 1, pages 241–254, 2011.
- [Peugeot *et al.* 2011] Peugeot C., F. Guichard, O. Bock, D. Bouniol, M. Chong, A. Boone, B. Cappelaere, M. Gosset, L. Besson, Y. Lemaitre, L. Seguis, A. Zannou, S. Galle and J.-L. Redelsperger. *Mesoscale water cycle within the West African Monsoon*. Atmospheric Science Letters, vol. 12, no. 1, pages 45–50, 2011.
- [Pielke 2001] Pielke R. A. *Commentary and analysis: Carbon Sequestration The Need for an Integrated Climate System Approach*. Bulletin of the American Meteorological Society, vol. 82, no. 9, pages 2021–2022, 2001.
- [Pierre *et al.* 2011] Pierre C., G. Bergametti, B. Marticorena, E. Mougin, T. Lebel and A. Ali. *Pluriannual comparisons of satellite-based rainfall*

- products over the Sahelian belt for seasonal vegetation modeling.* Journal of Geophysical Research, vol. 116, no. D18, 2011.
- [Pleim & Xiu 1995] Pleim J. E. and A. Xiu. *Development and Testing of a Surface Flux and Planetary Boundary Layer Model for Application in Mesoscale Models.* Journal of Applied Meteorology, vol. 34, no. 1, pages 16–32, 1995.
- [Polcher 1995] Polcher J. *Sensitivity of Tropical Convection to Land Surface Processes.* Journal of the Atmospheric Sciences, vol. 52, no. 17, pages 3143–3161, 1995.
- [Portmann *et al.* 2010] Portmann F. T., S. Siebert and P. Döll. *Global monthly irrigated and rainfed crop areas around the year 2000: A new high-resolution data set for agricultural and hydrological modeling.* Global Biogeochemical Cycles, vol. 24, no. 1, 2010.
- [Prigent *et al.* 2001] Prigent C., E. Matthews, F. Aires and W. B. Rossow. *Remote sensing of global wetland dynamics with multiple satellite data sets.* Geophysical Research Letters, vol. 28, no. 24, page 4631, 2001.
- [Prigent *et al.* 2007] Prigent C., F. Papa, F. Aires, W. B. Rossow and E. Matthews. *Global inundation dynamics inferred from multiple satellite observations, 1993–2000.* Journal of Geophysical Research, vol. 112, no. D12, 2007.
- [Pritchard *et al.* 1999] Pritchard S. G., H. H. Rogers, S. A. Prior and C. M. Peterson. *Elevated CO<sub>2</sub> and plant structure: a review.* Global Change Biology, vol. 5, no. 7, pages 807–837, 1999.
- [Redelsperger *et al.* 2006] Redelsperger J.-L., C. D. Thorncroft, A. Diedhiou, T. Lebel, D. J. Parker and J. Polcher. *African Monsoon Multidisciplinary Analysis: An International Research Project and Field Campaign.* Bulletin of the American Meteorological Society, vol. 87, no. 12, pages 1739–1746, 2006.
- [Reichle *et al.* 2002] Reichle R. H., J. P. Walker, R. D. Koster and P. R. Houser. *Extended versus ensemble Kalman filtering for land data assimilation.* Journal of Hydrometeorology, vol. 3, no. 6, pages 728–740, 2002.
- [Ricci 2004] Ricci S. *Assimilation variationnelle oceanique : modelisation multivariee de la matrice de covariance d’erreur d’ebauche.* PhD thesis, Paul Sabatier, Toulouse, France, 2004.

- [Richardson & University of California Libraries 1922] Richardson L. F. and University of California Libraries. *Weather prediction by numerical process*. Cambridge, The University press, 1922.
- [Richey *et al.* 2002] Richey J. E., J. M. Melack, A. K. Aufdenkampe, V. M. Ballester and L. L. Hess. *Outgassing from Amazonian rivers and wetlands as a large tropical source of atmospheric CO<sub>2</sub>*. *Nature*, vol. 416, no. 6881, pages 617–620, 2002.
- [Rodell *et al.* 2009] Rodell M., I. Velicogna and J. S. Famiglietti. *Satellite-based estimates of groundwater depletion in India*. *Nature*, vol. 460, no. 7258, pages 999–1002, 2009.
- [Rodriguez & Moller 2004] Rodriguez E. and D. Moller. *Measuring Surface Water From Space*. AGU Fall Meeting Abstracts, page 08, 2004.
- [Rodriguez 2009] Rodriguez E. *SWOT Science Requirements Document*, 2009.
- [Rodriguez 2012] Rodriguez E. *SWOT Science requirements document*, 2012.
- [Romanova 1954] Romanova E. *The Influence of Forest Belts on the Vertical Structure of Wind and on the Turbulent Exchange*. Study of the Central Geophysical Observatory, no. 44, pages 80–90, 1954.
- [Rosen *et al.* 2000] Rosen P., S. Hensley, I. Joughin, F. Li, S. Madsen, E. Rodriguez and R. Goldstein. *Synthetic aperture radar interferometry*. *Proceedings of the IEEE*, vol. 88, no. 3, pages 333–382, 2000.
- [Salamon & Feyen 2009] Salamon P. and L. Feyen. *Assessing parameter, precipitation, and predictive uncertainty in a distributed hydrological model using sequential data assimilation with the particle filter*. *Journal of Hydrology*, vol. 376, no. 3–4, pages 428–442, 2009.
- [Sausen *et al.* 1994] Sausen R., S. Schubert and L. Dümenil. *A model of river runoff for use in coupled atmosphere-ocean models*. *Journal of Hydrology*, vol. 155, no. 3-4, pages 337–352, 1994.
- [Scanlon *et al.* 2006] Scanlon B. R., K. E. Keese, A. L. Flint, L. E. Flint, C. B. Gaye, W. M. Edmunds and I. Simmers. *Global synthesis of groundwater recharge in semiarid and arid regions*. *Hydrological Processes*, vol. 20, no. 15, pages 3335–3370, 2006.
- [Sellers *et al.* 1996] Sellers P., D. Randall, G. Collatz, J. Berry, C. Field, D. Dalziel, C. Zhang, G. Collelo and L. Bounoua. *A Revised Land Surface Parameterization (SiB2) for Atmospheric GCMS. Part I: Model Formulation*. *Journal of Climate*, vol. 9, no. 4, pages 676–705, 1996.

- [Seth *et al.* 1994] Seth A., F. Giorgi and R. E. Dickinson. *Simulating fluxes from heterogeneous land surfaces: Explicit subgrid method employing the biosphere-atmosphere transfer scheme (BATS)*. Journal of Geophysical Research, vol. 99, no. D9, page 18651, 1994.
- [Seuffert *et al.* 2002] Seuffert G., P. Gross, C. Simmer and E. F. Wood. *The Influence of Hydrologic Modeling on the Predicted Local Weather: Two-Way Coupling of a Mesoscale Weather Prediction Model and a Land Surface Hydrologic Model*. Journal of Hydrometeorology, vol. 3, no. 5, pages 505–523, 2002.
- [Shaw & Doran 2001] Shaw W. J. and J. C. Doran. *Observations of Systematic Boundary Layer Divergence Patterns and Their Relationship to Land Use and Topography*. Journal of Climate, vol. 14, no. 8, pages 1753–1764, 2001.
- [Sheffield *et al.* 2006] Sheffield J., G. Goteti and E. F. Wood. *Development of a 50-Year High-Resolution Global Dataset of Meteorological Forcings for Land Surface Modeling*. Journal of Climate, vol. 19, no. 13, pages 3088–3111, 2006.
- [Shindell *et al.* 2004] Shindell D. T., B. P. Walter and G. Faluvegi. *Impacts of climate change on methane emissions from wetlands*. Geophysical Research Letters, vol. 31, no. 21, 2004.
- [Sivapalan *et al.* 1987] Sivapalan M., K. Beven and E. F. Wood. *On hydrologic similarity: 2. A scaled model of storm runoff production*. Water Resources Research, vol. 23, no. 12, page 2266, 1987.
- [Snelder & Bryan 1995] Snelder D. and R. Bryan. *The use of rainfall simulation tests to assess the influence of vegetation density on soil loss on degraded rangelands in the Baringo District, Kenya*. CATENA, vol. 25, no. 1–4, pages 105–116, 1995.
- [Stieglitz *et al.* 1997] Stieglitz M., D. Rind, J. Famiglietti and C. Rosenzweig. *An Efficient Approach to Modeling the Topographic Control of Surface Hydrology for Regional and Global Climate Modeling*. Journal of Climate, vol. 10, no. 1, pages 118–137, 1997.
- [Stisen *et al.* 2008] Stisen S., K. H. Jensen, I. Sandholt and D. I. F. Grimes. *A remote sensing driven distributed hydrological model of the Senegal River basin*. Journal of Hydrology, vol. 354, no. 1-4, pages 131–148, 2008.

- [Stisen 2007] Stisen S. *Geostationary Remote Sensing in Modelling of Land Surface Hydrology*. PhD thesis, Department of Geography and Geology, Faculty of Science, University of Copenhagen, 2007.
- [Swenson 2003] Swenson S. *Estimated accuracies of regional water storage variations inferred from the Gravity Recovery and Climate Experiment (GRACE)*. *Water Resources Research*, vol. 39, no. 8, 2003.
- [Séguis *et al.* 2011] Séguis L., B. Kamagaté, G. Favreau, M. Descloitres, J.-L. Seidel, S. Galle, C. Peugeot, M. Gosset, L. Le Barbé, F. Malinur, S. Van Exter, M. Arjounin, S. Boubkraoui and M. Wubda. *Origins of streamflow in a crystalline basement catchment in a sub-humid Sudanian zone: The Donga basin (Benin, West Africa)*. *Journal of Hydrology*, vol. 402, no. 1-2, pages 1–13, 2011.
- [Tapley *et al.* 2004] Tapley B. D., S. Bettadpur, J. C. Ries, P. F. Thompson and M. M. Watkins. *GRACE Measurements of Mass Variability in the Earth System*. *Science*, vol. 305, no. 5683, pages 503–505, 2004.
- [Taylor & Ellis 2006] Taylor C. M. and R. J. Ellis. *Satellite detection of soil moisture impacts on convection at the mesoscale*. *Geophysical Research Letters*, vol. 33, no. 3, 2006.
- [Taylor & Lebel 1998] Taylor C. M. and T. Lebel. *Observational Evidence of Persistent Convective-Scale Rainfall Patterns*. *Monthly Weather Review*, vol. 126, no. 6, pages 1597–1607, 1998.
- [Taylor *et al.* 2011] Taylor C. M., A. Gounou, F. Guichard, P. P. Harris, R. J. Ellis, F. Couvreur and M. De Kauwe. *Frequency of Sahelian storm initiation enhanced over mesoscale soil-moisture patterns*. *Nature Geoscience*, vol. 4, no. 7, pages 430–433, 2011.
- [Taylor 2010] Taylor C. M. *Feedbacks on convection from an African wetland*. *Geophysical Research Letters*, vol. 37, no. 5, 2010.
- [Verdin & Greenlee 1996] Verdin K. and S. Greenlee. *Development of continental scale digital elevation models and extraction of hydrographic features*. In *Third International Conference/Workshop on Integrating GIS and Environmental Modeling*, Santa Fe, New Mexico, 1996. National Center for Geographic Information and Analysis, Santa Barbara, California.
- [Vergnes *et al.* 2012] Vergnes J.-P., B. Decharme, R. Alkama, E. Martin, F. Habets and H. Douville. *A Simple Groundwater Scheme for Hydrological and Climate Applications: Description and Offline Evaluation over France*. *Journal of Hydrometeorology*, vol. 13, no. 4, pages 1149–1171, 2012.

- [Vermote *et al.* 2002] Vermote E. F., N. Z. El Saleous and C. O. Justice. *Atmospheric correction of MODIS data in the visible to middle infrared: first results*. Remote Sensing of Environment, vol. 83, no. 1-2, pages 97–111, 2002.
- [Vincendon *et al.* 2009] Vincendon B., V. Ducrocq, S. Dierer, V. Kotroni, M. Le Lay, M. Milelli, A. Quesney, G.-M. Saulnier, D. Rabuffetti, L. Bouilloud, K. Chancibault, S. Anquetin, K. Lagouvardos and P. Steiner. *Flash flood forecasting within the PREVIEW project: value of high-resolution hydrometeorological coupled forecast*. Meteorology and Atmospheric Physics, vol. 103, no. 1-4, pages 115–125, 2009.
- [Viterbo & Beljaars 1995] Viterbo P. and A. C. M. Beljaars. *An Improved Land Surface Parameterization Scheme in the ECMWF Model and Its Validation*. Journal of Climate, vol. 8, no. 11, pages 2716–2748, 1995.
- [Viterbo 2001] Viterbo P. *A review of parametrization schemes for land surface processes*, 2001.
- [Vorosmarty *et al.* 1989] Vorosmarty C. J., B. Moore, A. L. Grace, M. P. Gildea, J. M. Melillo, B. J. Peterson, E. B. Rastetter and P. A. Steudler. *Continental scale models of water balance and fluvial transport: An application to South America*. Global Biogeochemical Cycles, vol. 3, no. 3, page 241, 1989.
- [Vouillamoz *et al.* 2007] Vouillamoz J., B. Chatenoux, F. Mathieu, J. Baltassat and A. Legchenko. *Efficiency of joint use of MRS and VES to characterize coastal aquifer in Myanmar*. Journal of Applied Geophysics, vol. 61, no. 2, pages 142–154, 2007.
- [Wahr *et al.* 2004] Wahr J., S. Swenson, V. Zlotnicki and I. Velicogna. *Time-variable gravity from GRACE: First results*. Geophysical Research Letters, vol. 31, no. 11, page L11501, 2004.
- [Warrach *et al.* 2002] Warrach K., M. Stieglitz, H.-T. Mengelkamp and E. Raschke. *Advantages of a Topographically Controlled Runoff Simulation in a Soil-Vegetation-Atmosphere Transfer Model*. Journal of Hydrometeorology, vol. 3, no. 2, pages 131–148, 2002.
- [Wetzel & Chang 1987] Wetzel P. J. and J.-T. Chang. *Concerning the Relationship between Evapotranspiration and Soil Moisture*. Journal of Climate and Applied Meteorology, vol. 26, no. 1, pages 18–27, 1987.

- [Wetzel & Chang 1988] Wetzel P. J. and J.-T. Chang. *Evapotranspiration from Nonuniform Surfaces: A First Approach for Short-Term Numerical Weather Prediction*. Monthly Weather Review, vol. 116, no. 3, pages 600–621, 1988.
- [WHYCOS 2005] WHYCOS . Hydrological information systems for integrated water resources management: WHYCOS guidelines for development, implementation and governance. WMO, world meteorological organization (WMO) édition, 2005.
- [Wigneron *et al.* 2003] Wigneron J.-P., J.-C. Calvet, T. Pellarin, A. Van de Griend, M. Berger and P. Ferrazzoli. *Retrieving near-surface soil moisture from microwave radiometric observations: current status and future plans*. Remote Sensing of Environment, vol. 85, no. 4, pages 489–506, 2003.
- [Wood *et al.* 1992] Wood E., D. Lettenmaier and V. Zartarian. *A Land-Surface Hydrology Parameterization with Subgrid Variability for General-Circulation Models*. Journal of Geophysical Research-Atmospheres, vol. 97, no. D3, pages 2717–2728, 1992.
- [Wood *et al.* 1998] Wood E. F., D. P. Lettenmaier, X. Liang, D. Lohmann, A. Boone, S. Chang, F. Chen, Y. Dai, R. E. Dickinson, Q. Duan, M. Ek, Y. M. Gusev, F. Habets, P. Irannejad, R. Koster, K. E. Mitchel, O. N. Nasonova, J. Noilhan, J. Schaake, A. Schlosser, Y. Shao, A. B. Shmakin, D. Verseghy, K. Warrach, P. Wetzel, Y. Xue, Z.-L. Yang and Q.-c. Zeng. *The Project for Intercomparison of Land-surface Parameterization Schemes (PILPS) Phase 2(c) Red-Arkansas River basin experiment*. Global and Planetary Change, vol. 19, no. 1-4, pages 115–135, 1998.
- [Xue *et al.* 2010] Xue Y., F. Sales, W. K.-M. Lau, A. Boone, J. Feng, P. Dirmeyer, Z. Guo, K.-M. Kim, A. Kitoh, V. Kumar, I. Poccard-Leclercq, N. Mahowald, W. Moufouma-Okia, P. Pegion, D. P. Rowell, J. Schemm, S. D. Schubert, A. Sealy, W. M. Thiaw, A. Vintzileos, S. F. Williams and M.-L. C. Wu. *Intercomparison and analyses of the climatology of the West African Monsoon in the West African Monsoon Modeling and Evaluation project (WAMME) first model intercomparison experiment*. Climate Dynamics, vol. 35, no. 1, pages 3–27, 2010.
- [Yamazaki *et al.* 2009] Yamazaki D., T. Oki and S. Kanae. *Deriving a global river network map and its sub-grid topographic characteristics from a fine-resolution flow direction map*. Hydrology and Earth System Sciences, vol. 13, no. 11, pages 2241–2251, 2009.

- [Yamazaki *et al.* 2011] Yamazaki D., S. Kanae, H. Kim and T. Oki. *A physically based description of floodplain inundation dynamics in a global river routing model*. *Water Resources Research*, vol. 47, no. 4, 2011.
- [Yang & Niu 2003] Yang Z.-L. and G.-Y. Niu. *The Versatile Integrator of Surface and Atmosphere processes*. *Global and Planetary Change*, vol. 38, no. 1-2, pages 175–189, 2003.
- [Zagona *et al.* 2001] Zagona E. A., T. J. Fulp, R. Shane, T. Magee and H. M. Goranflo. *Riverware: a Generalized Tool for Complex Reservoir System Modeling*. *JAWRA Journal of the American Water Resources Association*, vol. 37, no. 4, pages 913–929, 2001.
- [Zaitchik *et al.* 2008] Zaitchik B. F., M. Rodell and R. H. Reichle. *Assimilation of GRACE Terrestrial Water Storage Data into a Land Surface Model: Results for the Mississippi River Basin*. *Journal of Hydrometeorology*, vol. 9, no. 3, pages 535–548, 2008.
- [Zhao 1992] Zhao R. *The Xinanjiang Model Applied in China*. *Journal of Hydrology*, vol. 135, no. 1-4, pages 371–381, 1992.



# Résumé

**Auteur :** Vanessa Pedinotti

**Titre :** Préparation à la mission SWOT (Surface Water Ocean Topography) : apport de l'altimétrie à large fauchée à la modélisation à grande échelle des processus hydrodynamiques en Afrique de l'Ouest.

**Date de soutenance :**

---

Le bassin versant du fleuve Niger est directement influencé par les fluctuations de la mousson africaine, qui impactent les ressources en eau et entraînent des événements extrêmes tels que des inondations ou des sécheresses. En retour, les forts taux d'évaporation observés dans le Delta intérieur du Niger, large région annuellement inondée, impactent le climat, au moins à l'échelle régionale. Une meilleure compréhension des processus hydrodynamiques de ce bassin ne peut cependant être obtenue sans un réseau d'observations ayant une couverture spatiale et temporelle suffisante. La mission SWOT fournira des cartes 2D de hauteurs et pente des eaux de surface avec une résolution encore jamais atteinte en altimétrie (50 à 100 mètres).

Cette thèse s'inscrit dans le cadre de la phase de préparation à la mission SWOT et se propose d'offrir des perspectives d'utilisation de ces données satellites pour l'amélioration des modèles d'hydrologie globale. Dans un premier temps, le modèle hydrologique du CNRM, ISBA-TRIP, incluant un schéma d'inondations et un réservoir simple d'aquifères ajouté durant cette thèse est évalué sur le bassin du Niger à l'aide de multiples observations in-situ et satellites. L'étude montre que le modèle simule de façon cohérente l'évolution des eaux de surface, des zones inondées, et les anomalies de stock d'eau sur le bassin.

Ensuite, un schéma d'assimilation de données est mis en place afin d'optimiser un des paramètres clés en hydrologie, le coefficient de Manning. Ce coefficient, décrivant la propriété du sol à 'retenir' les flux d'eau, influence fortement la dynamique des eaux de surface, et notamment les hauteurs d'eau et le débit. L'assimilation des données SWOT est appliquée dans le cadre d'une expérience jumelle, qui consiste à considérer une simulation de référence, appelée 'vérité', de laquelle sont issues les observations virtuelles de hauteur d'eau SWOT. L'étude montre que l'assimilation des hauteurs d'eau SWOT permet l'optimisation du coefficient de Manning, distribué spatialement, malgré l'hypothèse d'équifinalité. Les hauteurs d'eau et les débits sont considérablement améliorés, et on obtient une meilleure simulation des anomalies de stocks d'eau sur le bassin ainsi que des zones inondées sur le Delta intérieur du Niger (occurrence, intensité). Enfin, le potentiel des données SWOT pour améliorer les prévisions hydrologiques sur des périodes plus longues que celle de la phase d'assimilation est mis en évidence.

---

**Mots clés :** Niger, cycle hydrologique, inondations, modélisation, ISBA, TRIP, assimilation de données, fleuve, débit, altimétrie à large fauchée, SWOT



# Summary

**Author :** Vanessa Pedinotti

**Title :** The Surface Water Ocean Topography (SWOT) mission : contribution of large swath altimetry to the improvement of large scale hydrologic and hydrodynamic modeling in West Africa.

**Directors:** PhD directors : Aaron Boone and Nelly Mognard.

**Date de soutenance :**

---

The hydrologic and hydrodynamic processes of the Niger basin are largely influenced by the West African monsoon variability. In the last 3 decades these variations have resulted in an increase of extreme events such as floods and droughts. Retrospectively, the climate might be impacted by the evaporation fluxes from the inner Delta flooded region, at least regionally. A better understanding of the Niger basin water cycle is a crucial issue for water resources management but requires observation datasets with a large spatial and temporal coverage. The SWOT satellite mission will provide 2D global maps of water level and slope at an unprecedented resolution (50 to 100 meters). Within the framework of the preparation of the SWOT mission, this thesis aims at proposing a SWOT data assimilation strategy for the improvement of global scale hydrological models. First, the ISBA-TRIP hydrological model from CNRM is evaluated over the Niger basin. This model includes an inundation scheme and simple aquifer reservoir. The model diagnostics are compared to an extensive set of in-situ and satellite observations. According to its relative simple physics, the model is able to simulate in a realistic manner, the continental water dynamics : discharge, water levels, floods, total water storage variations. Sensitivity tests are also performed to determine the most sensitive ISBA-TRIP parameters. Among them, the Manning coefficient has a key role in the flow dynamics but its estimation is difficult and usually based on geomorphologic relationships.

The second part of this work consists in setting up a SWOT data assimilation strategy for the optimization of the ISBA-TRIP parameters. Since the SWOT observations are not available yet and also to assess the skills of the assimilation method, the study is carried out in the framework of an Observing System Simulation Experiment (OSSE). The corrected parameter is the Manning coefficient, spatially distributed over the river. The assimilation allows a good improvement of the relative bias of discharge and water level over the river. The Manning coefficient is also globally improved and tends to an optimal value. Moreover, the water storage anomalies and flooded fraction are also better simulated. Finally, the study shows that the method is useful for hydrological forecasting over longer time periods than those of the calibration.

---

**Key words :** modeling, hydrology, SWOT, river, Niger, water budget, global scale, water resources, flood

